Explosion safety of biomass and torrefied biomass powders

Clara Huéscar Medina

Submitted in accordance with the requirements for the degree of
Doctor of Philosophy

The University of Leeds
School of Chemical and Process Engineering

October, 2014

The candidate confirms that the work submitted is her own, except where work which has formed part of jointly-authored publications has been included. The contribution of the candidate and the other authors to this work has been explicitly indicated below. The candidate confirms that appropriate credit has been given within the thesis where reference has been made to the work of others.

List of Publications

This section contains a list of publications which are part of the present study. Where the work formed part of jointly-authored publications between researchers, the contribution of the candidate and other researchers towards the work has been explicitly explained.

- *Calibration of a 10 L volume dust holding pot for the 1 m^3 standard vessel, for use in low-bulk-density biomass explosibility testing. Sattar, H., Huéscar Medina, C., Phylaktou, H.N,. Andrews, G.E., Gibbs B.M. 7th International Symposium on Fire and Explosion Hazards. Providence, USA. May 2013*

The candidate participated in carrying out the experiments presented by the main author (Hamed Sattar) who led the experimental procedures and writing up of the publication. Dr. Phylaktou, Prof. Andrews and Prof. Gibbs were co-supervisors of the research work, participated in the analysis of results and proof-read the publication.

- *The development of an experimental method for the determination of the minimum explosible concentration of biomass powders. Huéscar Medina, C., Phylaktou, H.N., Sattar, H., Andrews G.E., Gibbs B.M. Biomass and Bioenergy (53) 95-104, 2013*

The candidate led the experimental procedures, development of techniques and writing up of the publication. H. Sattar participated in carrying out the experiments. Dr. Phylaktou, Prof. Andrews and Prof. Gibbs were co-supervisors of the research work, participated in the analysis of results and proof-read the publication.

(Contents of both the above publications are part of **Chapter 3)**

- *Torrefaction effects on the reactivity and explosibility of woody biomass. Huéscar Medina, C., Phylaktou, H.N., Sattar, H., Andrews, G.E., Gibbs, B.M. 7th International Symposium on Fire and Explosion Hazards. Providence, USA. May 2013*

The candidate led the experimental procedures, development of experimental techniques and writing up of the publication. H. Sattar participated in carrying out the experiments. Dr. Phylaktou, Prof. Andrews and Prof. Gibbs were co-supervisors of the research work, participated in the analysis of results and proof-read the publication.

(Contents of this publication are part of **Chapter 4**)

- *Explosion reactivity characterisation of pulverised torrefied spruce wood. Huéscar Medina, C., Sattar, H., Phylaktou, H.N., Andrews, G.E., Gibbs, B.M. X International*

Symposium of Hazards, Prevention and Mitigation of Industrial Explosions 10-14 June 2014, Bergen (Norway)

The candidate led the experimental procedures and writing up of the publication. H. Sattar designed and calibrated the 1 m^3 vessel set-up used for testing of fibrous biomass. Dr. Phylaktou, Prof. Andrews and Prof. Gibbs were co-supervisors of the research work, participated in the analysis of results and proof-read the publication.

- *Explosibility of torrefied biomass compared to their raw parent biomass material. Huéscar Medina, C., Phylaktou H.N., Andrews G.E., Gibbs, B.M., European Biomass Conference and Exhibition 2014 (Hamburg, Germany)*

The candidate led the experimental procedures and writing up of the publication. Dr. Phylaktou, Prof. Andrews and Prof. Gibbs were co-supervisors of the research work, participated in the analysis of results and proof-read the publication.

(Contents of both the above publications are part of **Chapter 5**)

Acknowledgements

I am extremely grateful to my supervisors, Dr. Herodotos Phylaktou and Prof. Gordon Andrews for their guidance during the course of the past years, for many hours of discussions and for trusting me and giving me confidence to undertake this research. Special thanks to Prof. Bernard Gibbs for his valuable contributions.

I am also grateful to the Energy Program (EPSRC, ESCR, NERC, BBSRC and STFC, Grant EP/H048839/1) for financial support in this project, and to all sample suppliers: ECN, RWE, Sea2Sky Energy UK Ltd., New Biomass Energy, ESB International and Umeå University.

I would also like to thank all of my colleagues: Hamed Sattar, Bala Fakandu, Abdul Na'Inna, Dave Slatter, Azam Saeed, Aziz Alarifi and Aysha Irshad. I wish them all the best for the future.

I am also most grateful to Bob Boreham, Adrian Cunliffe, Sara Dona, Ed Woodhouse and Susanne Patel for their patience, help and advice with all technical issues, which were numerous.

Very special thanks to my parents who have given me every opportunity in life and who, together with my sister, have been an endless source of encouragement. I am also grateful to the rest of my family and friends both in Spain and the UK. The best reward is to spend time with all them.

Last but not least I would like to thank Craig who tolerated my occasional bad temperament and always put a smile in my face. I hope I can repay him with the same affection over the course of many years to come.

Abstract

The use of pulverised biomass for electrical power generation is of growing importance in the UK as a route to low carbon electricity. It can be used in existing power stations co-fired with coal or 100% biomass firing. However, this use of biomass has led to several major biomass storage or burner feed explosions in recent years. There is minimal information in the open literature on the explosion risks of pulverised biomass, as the fibrous nature of pulverised biomass results in it blocking the injection system of the standard ISO 1 m^3 and 20 L spheres. New injection systems for fibrous biomass developed and calibrated for the ISO 1 m^3 spherical explosion vessel were used in this research. In addition to the explosion safety data, the experimental methods enabled the measurement of the turbulent spherical flame speed, from which the fundamental laminar burning velocity of the pulverised biomass could be determined, this data is relevant to practical burner design and flame stability.

In dust explosion research the dust concentration has always been reported as g/m^3 and not converted to equivalence ratio, Ø. An important feature of the present work was the presentation of the flame propagation properties as a function of equivalence ratio, Ø. This enabled comparison to be made with equivalent burner operating conditions and gas explosions data.

A feature of dust explosions was found, that has rarely been reported elsewhere, and this was that around 50% of the dust that was injected was left as a debris in the vessel after an explosion test. This debris was vacuumed out of the vessel, collected, weighed and analysed. The debris was composed of ash from the biomass that did burn, completely unreacted biomass and partially pyrolysed particles. The mass of the debris was deducted from the mass injected and the actual Ø that the flame propagated through was determined.

Torrefaction is a process involving heating the biomass in an inert atmosphere at about 200°C-300°C, which breaks up the biomass fibres and makes it easier to handle and pulverise. The present work presents the first measurements of the explosion and flame propagation properties of these new biomass materials. The results are compared with the raw biomass from which the torrefied material was derived.

Research was undertaken on the explosion and flame propagation characteristics of a range of raw biomass, torrefied biomass, coal and mixtures of biomass with coal. Fuel characteristics (chemical composition, particle morphology, size distribution) were compared in order to assess the most influential parameters on the reactivity of

torrefied and raw biomass. The experimental evidence suggests that pulverised biomass flame propagation occurred in the gas phase, leaving no char residue, indicating that for the biomass that participated in the flame propagation all the mass was burned. Evidence suggested that coal and torrefied biomass flames did result in enhanced char in the debris and that surface reactions through the diffusion of oxygen were part of the flame propagation process.

For minimum explosion concentration measurements the Hartmann tube explosion technique was modified to work repeatably for fibrous biomass and to determine flame speeds. This enabled the most reactive mixture to be determined. The MEC of biomass and torrefied biomass were found to be leaner (Ø=0.2-0.3) than for coal or gaseous hydrocarbons. This supports the conclusion that for the Hartmann equipment all the mass injected must burn, as if only part burned the MEC would be richer. The current methods for determining the MEC in the ISO 1 m^3 and 20 L sphere were shown to be invalid as they were based on the injected concentration of dust, with no account taken of the fact that most of it did not burn, so the actual concentration at the lean limit was unknown. More work is required on the reliable determination of MEC.

Torrefied biomass was found to be more reactive than the raw biomass due to the presence of finer particles in the torrefied biomass samples and not due to the material being inherently more reactive. Torrefied, raw biomass and coal samples were found to have K_{St} values ranging from 60 to 150 barm/s and the maximum explosion pressure ranged between 8 and 9 bar. The mixtures that gave these peak reactivities and pressures was around Ø = 2 – 3, quite different from the peak reactivity of gases at Ø=1.05. The reason for peak reactivity occurring at richer mixtures was addressed as part of the research. Biomass and coal were found to have a similar range of reactivity and peak pressures. Synergistic effects in the reactivity of biomass/coal mixtures were observed with certain fuels and blend ratios. TGA analysis gave indication of such synergistic effects which are likely to occur due to interaction of the fuels during the devolatilisation step. However, no synergistic effects were detected for a mixture containing 50% torrefied biomass.

Table of Contents

List of Tables

List of Figures

Nomenclature

Abbreviations

A	Area (m^2)
A/F	Air to fuel ratio
ATEX	Directive on equipment for use in explosive atmospheres
CHP	Combined heat and power
daf	Dry ash free basis
d	Particle diameter
D	Vessel diameter
D_f	Flame diameter
DSEAR	Dangerous Substances and Explosive Atmospheres Regulations
dP/dt	Rate of pressure rise (bar/s)
E	Expansion factor
E_p	Expansion factor at constant pressure
F/A	Fuel to air ratio
FC	Fixed carbon
FIT	Feed in tariff
fps	frames per second
GCV	Gross calorific value (MJ/kg)
GHG	Greenhouse gases
GHRR	Global heat release rate (MW/m^2)
HFC	Hydrofluorocarbon
HR	Heating rate
K_G	cubic-law gas constant
K_{St}	cubic-law dust constant
LFL	Lean flammability limit
LOC	Limiting Oxygen Concentration
MEC	Minimum Explosible Concentration
MIE	Minimum Ignition Energy
Ø	equivalence ratio
P	Pressure
P_{air}	Pressure due to air injection
P_{ex}	Explosion pressure
P_i	Initial pressure
$P_{ignitor}$	Pressure due to ignitor
P_{inj}	Pressure of injected air
P_{max}	Maximum explosion pressure
P_{max}/P_i	Maximum explosion pressure normalised
P_{red}	Reduced pressure
P_{stat}	Static activation pressure
PFC	Perfluorocarbon
RHI	Renewable Heat Incentive
RHPP	Renewable Heat Premium Payment
RO	Renewable Obligation

ROC	Renewable Obligation Certificate
S_F	Flame speed (m/s)
S_L	Laminar burning velocity (m/s)
S_T	Turbulent burning velocity (m/s)
SEM	Scanning Electron Microscopy
STD	standard
t	time
T	Temperature
T_{max}	maximum mass loss temperature (°C)
TGA	Thermogravimetric analysis
UFL	Upper Flammability Limit
V	Volume
VM	Volatile Matter
V.Y	Volatile Yield

Greek symbols

β	Turbulent factor
λ	layer thickness
ρ	density

Subscripts

b	burnt
c	corrected
i	initial
Inj	injected
L	laminar
T	turbulent
u	unburnt

Chapter 1 INTRODUCTION

CONTENTS

1.1. UK Energy sector characteristics, emissions, targets and policies

The energy sector in the UK is characterised by a heavy reliance on fossil fuels. In 2012, the consumption of primary energy reached 206.3 million tonnes of oil equivalent (toe) [1]. 87% of the total energy supply came from fossil fuels, (mainly coal, gas and oil). Furthermore, the UK is a net importer of energy which often results in uncertainty of prices and supply. Around 38% of the energy consumed was used in 2012 for the generation of 375.9 TWh of electricity. The main fuels used for generation of electricity were coal and gas, accounting for 39% and 28% of the share respectively [2].

The combustion of fossil fuels results in the emission of carbon dioxide (CO_2) to the atmosphere. In industrialised countries CO_2 emissions account for an average of 92%

of the greenhouse gases (GHG) produced [3]. In 2012, the UK emitted 479.1 million tonnes of CO_2, the main contributors by fuel were gas (39%), oil (30%) and coal (27%).

Under the Kyoto protocol agreement, signed by the European Union in 1998, the UK committed to reducing the emission of six anthropogenic GHG: carbon dioxide (CO_2), methane (CH_4), nitrous oxide (N_2O), hydrofluorocarbons (HFCs), perfluorocarbons (PFCs) and sulphur hexafluoride (SF_6). Additionally the UK set domestic targets by means of the Climate Change Act 2008 and Carbon Budgets, and from 2013 onwards the UK adhered to the European Union 2020 target. The current targets for GHG emissions reductions are [2]:

- Under Kyoto Protocol:

From 2013 to 2020, reduction of emissions by 20% below base year levels, on average over the period

- Under EU 2020 target:

Reduction of emissions by 20% by 2020 (rather than on average)

- Under Climate Change Act 2008:

Annual average reduction of 28% over the period 2013-2017, which corresponds to a limit of GHG emissions of 2782 $MtCO_2e$ over the five year period.

In 2012 finalised the previous five year period, in which, under the Kyoto protocol the UK had committed to a 12.5% reduction below base year levels. Under the Climate Change Act 2008, the emissions were limited to 3018 $MtCO_2e$ over the five year period.

EU member states therefore agreed under the Kyoto Protocol to implement and introduce new policies in order to enhance and improve the energy efficiency of fossil fuel to energy conversion technologies; protect natural sinks of GHG (forests), promote sustainable agriculture; develop and increase the use of renewable sources of energy or carbon capture technologies. Consequently, the UK has taken a series of actions which include: setting a national policy and strategy [4], reducing the demand for energy, increasing energy efficiency and investing in low-carbon technologies.

1.2. De-carbonisation of the Energy sector

In order to increase the use of low-carbon technologies, the UK introduced a series of initiatives to incentivise renewable sources of electricity, heat and transport fuels (Renewables Obligation (RO), Feed-in Tariffs (FITs) scheme, Renewable Heat

Incentive (RHI), Renewable Heat Premium Payment (RHPP) or Renewable Transport Fuel Obligation) and released the first UK Renewable Energy Roadmap in 2011 [5]. This document set a target to achieve that 15% of UK's energy demand is met from renewable sources in 2020; this corresponds to approximately 234 TWh of renewable energy by 2020. This amount of energy would be sourced by 8 existing renewable technologies: onshore and offshore wind, biomass electricity, marine energy, biomass heat, heat pumps, renewable transport and others (including geothermal, solar, hydro and domestic heat). The level of deployment of these technologies will depend on the future energy demand, the cost of technologies and the level of renewable energy deployment the industry believes can be achieved.
In 2012, 4.1% of the total energy consumption came from renewable sources, whilst renewable electricity contribution grew during the period 2011-2012, renewable heat contribution remained constant and renewable transport contribution fell.

1.2.1. Renewable power generation

The main contributors to renewable electricity generation in 2012 were biomass fuels, see Figure 1-1.

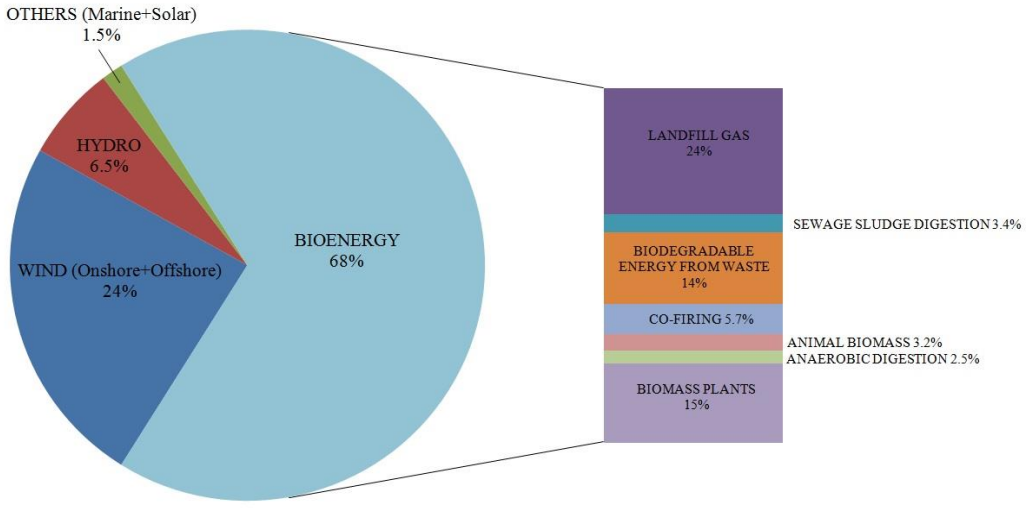

Figure 1-1. Main contributors to renewable electricity generation in 2012 [2]

Biomass fuels also contributed in the greatest measure to renewable transport and heat. Presently, biomass fuels account for 3% of the UK's primary energy consumption and the major part of it (65%) is used for power generation. The advantages of biomass fuels over other renewable sources are [6]:

- Versatility and continuity. It is the only source that can contribute to all the sectors (electricity, heat and power) and provides a constant flow of energy.

- Variety of fuel types. Contributes to a diverse energy mix and therefore to more energy security.
- Boost to agriculture, forestry and waste management sectors.
- Potential reduction of landfill waste.
- Good cost effectiveness in comparison to other renewable sources.

However drawbacks are:

- Not directly low carbon, renewable or sustainable
- Competition with other uses.

Authorities have been incentivising large-scale electricity generation from biomass since 2002 by means of the Renewables Obligation scheme. The scheme requires power generators to supply a proportion of the electricity generated from renewable sources. The "obligation" or proportion of renewable sourced electricity is set and increased annually. Renewable Obligation Certificates (ROCs) are issued to generators depending on the amount of renewable sources exploited. ROCs are then sold to suppliers, and suppliers use them to comply with RO. If the obligation is not met, suppliers must pay a penalty. The number of ROCs issued depend on the type of technology used (each type of technology falls in a "banding level", these levels are reviewed every 4 years) and the amount of electricity generated.

In 2012, electricity generated from biomass reached 15 TWh. Under the UK's renewable energy strategy projections are to generate 32 to 50 TWh by 2020 to meet the targets (16-22 million tonnes of dry biomass/year). Therefore it is expected that the proportion of biomass used for power generation will continue to increase.

In the short term, due to the low costs associated, biomass power generation will be focused on co-firing and on conversion of existing coal power plant to biomass rather than on lower cost effective dedicated biomass plants. However, most of coal-to-biomass plants will stop operating by the late 2020s when they reach the end of their lifetime. Still, the main concern that could limit the use of bioenergy is the sustainability of feedstock. As a result authorities elaborated a Bioenergy Strategy with an account of fuel availability and best uses.

1.2.2. Supply and sustainability of biomass

Assessing the amount of resources available, especially imports, is subject to uncertainties: global demand, land productivity, technological development, competing uses of the land and prices of biomass are some examples. The total supply projected for the UK is between 200 to 650 TWh in 2020, and imports are expected to account for the majority of the supply available. Most of the domestic

supplies will come from agricultural wastes and energy crops which hopefully, will not compete with food production, as this would incur in higher carbon impacts.

Most of the criticism on the use of biomass resources comes from sustainability issues and accounting of emissions in lifecycle analysis [7]. However, Lamers et al. [8] concluded that the risks related to biomass for energy outtake are feedstock specific and vary in terms of scientific certainty.

In the UK, however, under the RO, over 50 kWe power plants need to comply with sustainability requirements [9]. It is required to provide a minimum of 60% reduction in GHG emissions relative to fossil fuels. Furthermore, there are restrictions applied to fuels supplied from land with high biodiversity value or high carbon stock. In addition, generators have been implementing their own sustainability policies even when regulations were not in place [10].

1.3. Biomass to energy conversion

Currently, the major contributors to biomass electricity generation are landfill gas (33%), followed by dedicated biomass plants (15%), biodegradable waste (14%) and co-firing plants (5.7%). Dedicated biomass plants can be new built or converted from coal fired power plants [2]. A list of existing plants is given in Table 1-1.

Table 1-1. Biomass fuelled plants operational by the end of May 2013

Owner	Plant Name	Fuel	Capacity (MW)
E. On UK	Ironbridge	Biomass	900
E. On UK	Steven's Croft	Biomass	50
RWE Npower Plc	Tilbury B	Biomass	750
Sembcorp Utilities (UK) Ltd	Wilton 10	Biomass	38
Drax Power Ltd	Drax	Coal/Biomass	3870
Scottish & Southern Energy Plc	Ferrybridge C	Coal/Biomass	1960
Scottish & Southern Energy Plc	Fiddler's Ferry	Coal/Biomass	1961
Scottish & Southern Energy Plc	Uskmouth	Coal/Biomass	363
Scottish & Southern Energy Plc	Slough	Coal/biomass/gas/waste derived fuel	61
EPR Ely Limited	Elean	Straw/Gas	38

The UK's Bioenergy Strategy set the potential for electricity generated from biomass by 2020 in 6 GW, equivalent to around 50 TWh, and anticipates that such increase will be achieved from conversion of coal plants to biomass, dedicated biomass plants

as well as biomass waste combustion and anaerobic digestion. Co-firing is likely to continue its level of deployment, if not more, since it is the least expensive option (followed by conversions and dedicated plants). The conversion of coal plants to biomass plants extends the life of the existing assets and sources flexible low carbon electricity. However authorities pointed out that this option should only be seen as a short term solution, since they are considered to be less efficient than new built plants, and unlikely to become CHP. Nevertheless, for the period 2013-2017 conversion of coal plants to biomass plants is encouraged with a level of support of 1 ROC/MWh.

Co-firing is also supported with different levels of support depending on the percentage of biomass by energy content, in order to reflect both the level of investment required and the risks that exists between conversion and co-firing (Table 1-2).

Table 1-2. ROC/MWh support level for co-firing ranges [11]

Percentage of biomass by energy content	ROC's/ MWh	Title of support
At least 85% but less than 100%	0.7 (2013/2014) 0.9 (from 2014/2015)	High-range co-firing
At least 50% but less than 85%	0.6	Mid-range co-firing
Under 50%	0.3 (2013/14, 2014/15) 0.5 (from 2015/16)	Standard (low range) co-firing

New built dedicated biomass plants are also subsidised by ROC's, the support levels are set for the period 2013-2017 as: 1.5 ROC's/MWh from April 2013 to March 2016, and 1.4 ROC's/MWh. However, a cap on the total new built dedicated biomass generating capacity of 400 MW is in place from December 2012, to avoid deploying more than initially predicted, which could risk both the RO budget and the Government's policy intentions. As a result a number of projects to build new dedicated biomass plants have been shelved [12].

1.4. Challenges of biomass fuels

There are many different methods to convert biomass into energy but combustion is the most commonly used [13]. Biomass properties, like high moisture and ash contents cause problems for combustion and also, its main advantages, such as high volatility and high reactivity pose safety concerns during handling, storage, and combustion operations.

1.4.1. Biomass fuels

The term “biomass” incorporates many different types of fuels, not only plant based materials, but also any animal or human organic waste. The biomass resources most commonly used in power generation can be divided into:

- Agricultural residues by-products of food production (straw, husks, shells)
- Forestry products and residues: managed forests and forestry residues can supply biomass such as bark, thinning, tree tops and branches.
- Energy crops: crops dedicated specifically to supply fuel for energy generation, including short rotation coppice willow or miscanthus.

Some of the challenges related to the use of biomass for power generation include seasonal variations on different biomass types and reliability of supply. In comparison to coal, biomass contains less carbon, sulphur and ash, but more oxygen, lower heating values and higher moisture. In addition, biomass has lower bulk density and it is more heterogeneous in terms of shape and size, which influences storage, transportation and handling [14].

In order to improve these characteristics, densification or upgrading processes have been developed, these can be mechanical (e.g. pelletising) or chemical, through torrefaction or pyrolysis [15].

1.4.2. Torrefaction

Torrefaction is especially attractive for power generation through co-firing or in converted dedicated biomass plants. Torrefaction is a thermal pre-treatment in which biomass is subjected to temperatures of 200°C-300°C during a certain amount of time. During torrefaction biomass losses moisture and releases volatiles and the end solid product is similar to low rank coals. As a result torrefied biomass has higher carbon content and calorific value, and lower moisture, volatile, and oxygen contents. The product acquires hydrophobic properties and better grindability [16]. Torrefied biomass pellets are predicted to be competitive with traditional wood pellets once torrefaction reactors have been optimised and scaled-up [17]. Therefore, in the future torrefied biomass has the potential to be used in power generation systems.

1.4.3. Technical issues

Existing solid fuel power generation plants where biomass can be used to replace fossil fuels and consequently reduce GHG emissions are optimised to burn fuels such as coal. Although the cost of retrofitting the plants to be used with biomass fuels is considered to be low compared to building 100% biomass new plants, there

are a few challenges to overcome. The technical issues are related to the high moisture content of biomass which impacts the general utilisation and handling of fuels. Furthermore, moisture decreases flame temperature and consequently the efficiency of the boiler. The high contents of alkali on the ash can lead to corrosion in the boilers (slagging, fouling). Also, since biomass has lower calorific values, more fuel is needed to maintain the thermal output. Another significant cost is related to the poor grindability of biomass which requires dedicated mills for pulverised fuel (pf) combustion. Some of these issues could be easily avoided or alleviated in the future by using torrefied fuels, since these have characteristics which approach those of low rank coals. This coupled with potential savings in transportation costs present very attractive advantages for torrefied fuels.

1.5. Safety concerns

In addition to the technical issues already mentioned, there is a potential for new or intensified safety concerns when using biomass in large quantities for power generation or when replacing traditional solid fossil fuels (coal) with biomass and torrefied biomass [18]. In general, the use of potentially degradable, highly reactive and finely divided fuels, poses major fire and explosion hazards.

Fundamental properties of biomass which differ from those of coal require alterations to the way fuels are transported, stored and handled from harvesting to final utilisation (combustion) in power plants. Therefore adjustments should also be considered in the safety aspects.

1.5.1. Fire and explosion hazards

Potentially, dust explosions in power generation can occur in several areas: during unloading and handling [19-21], in silos, in bunkers, during the milling process, as well as when pulverised fuel is blown into the burners [22].

Fires can take place providing three factors are present: fuel, oxidant and an ignition source. For an explosion to occur two more factors are necessary: confinement and mixing. Both phenomena (fire and explosion) are essentially combustion reactions with different combustion rates. The rate of combustion increases when the solid is finely divided, and it increases even more when it is suspended in air, such as when biomass and coal are pulverised and pneumatically conveyed in power stations, or when “dropped” into storage silos.

There are many sources of ignition in power plants such as rotating devices, electrostatic discharges, mechanical sparks or even a stone transported with the fuel.

All of these can cause smouldering fires that can migrate undetected in conveyor systems leading to fires and explosions.

Self-heating can occur when oxidation or microorganism activity produce heat, for a sufficient time, capable of raising the temperature of the surrounding material. It occurs more frequently in large piles of fuels during storage. Self-ignition temperatures decrease with pile size, whereas the necessary time for self-ignition to occur increases with pile size. Both coals and biomass fuels can self-ignite at temperatures lower than 200°C in a few hours [23, 24]. Self-ignition can lead not only to fires but also to dust explosions.

1.5.2. Fire and explosion incidents

Table 1-3, shows a summary of the most recent incidents occurred around the world in the last few years in plants or industries where biomass materials are used. Dust explosion and fire incidents are included.

Table 1-3. Recent incidents occurred due to biomass dust

Date	Facility	Location	Details	Casualties
06/05/2014	Landskrona port wood pellet storage	Landskrona, Sweden	Small fire reported. In 9 minutes fire spread via a conveyor to 20,000 m^2 storage building escalating to large fire. 10,000 tons of pellets lost	None
26/04/2014	Georgia Pacific Plywood plant	Corrigan, TX, USA	Sawdust collector malfunction led to dust explosion	7 injured
17/03/2014	Exmouth Wood Processing plant	Exmouth, UK	Fire at dust compactor unit	None
27/02/2014	Resolute forest products mill	Fort Frances, Ontario, Canada	Dust explosion and fire	1 injured
18/02/2014	Chips Inc. Wood processing plant	Troy, VA, USA	Fire provoked by ignition of chips and sawdust due to a rupture in hydraulic line within conveyor system in a silo	None
14/02/2014	Hibbing Public Utilities (HPU) biomass plant	Hibbing, USA	Fire in exterior wall of structure housing wood chip boiler. Cause of the fire unknown	None

Date	Facility	Location	Details	Casualties
05/02/2014	Heilongjiang Longfeng Corn Development	Qinggang, China	Explosion in a corn and agricultural products plant	9 injured
30/01/2014	Buchanan Hardwoods	Aliceville, AL, USA	Explosion ignited a silo fire	None
21/01/2014	Biomasa Forestal pellet Plant	A Coruña, Spain	Fire caused by ignition of wood dust due to some mechanical element	None
09/01/2014	UK Wood Recycling	Middlesbrough, UK	Fire of stored biomass that supplies Wilton Power Station	None
13/11/2013	Bay State Pellet Mill	Fitchburg, Massachusetts, USA	Smouldering ember ignited accumulated wood dust, causing a dust explosion and subsequent fire	None
27/10/2013	Atlantic Veneer Corp facility	Beaufort NC, USA	Fire and explosion of wood chip and sawdust silo	1 injured
16/09/2013	Anderson Hardwood Pellets Company	Louisville, Kentucky, USA	Spark inside the system provoked sawdust explosion and fire. Explosion vented.	1 injured
04/09/2013	Nature's Flame Pellet Factory	Rotokawa, New Zealand	Wood dust explosion, two sawdust hoppers caught alight	None
20/08/2013	Inferno Pellets	Rumford, RI, USA	Dust explosion and fire	1 injured
24/06/2013	LaPorte County Union Mills Grain Elevator and Storage Facility	Union Mills, Indiana, USA	Grain dust explosion	1 dead
02/06/2013	Hexham Egger UK chipboard plant	Northumberland, UK	Fire in a biomass to heat unit. Cause yet not known.	None
30/05/2013	Buena Vista Biomass Power Plant	Amador county, California, USA	Boiler ruptured due to mechanical failure. Limited information	2 injured
27/02/2012	Tilbury Power Station	Essex, UK	Most likely caused by increased levels of oxygen causing ignition of smouldering dust	None

Date	Facility	Location	Details	Casualties
20/01/2012	Babine Forest Products Sawmill	Burns Lake, BC, Canada	Wood dust explosion and subsequent fire travelled through mill, disturbing and dispersing accumulated wood dust setting off secondary deflagrating explosions	2 dead, 20 injured
19/10/2011	South Shields, Port of Tyne	Northumberland, UK	Wood pellets spontaneously combusted inside a concrete storage unit	None
11/07/2011	Essex Wood recycling site	Essex, UK	Fire of stored biomass. 21,000 tonnes of material destroyed	None
20/06/2011	Georgia Biomass	Waycross, Georgia, USA	Overheated roller/ bearing assembly in a pelletiser sparked a wood dust cloud. The explosion caused three weeks shut down.	None

1.5.3. Dust explosion safety legislation

Dust explosion hazards exist for a large number of industries, and incidents have occurred during the years which have led to the development of safety requirements [25]. In order to avoid incidents, protect property and personnel, and in order to comply with safety regulations it is necessary to identify the hazards present and consequently design suitable safety systems.

The European legislation in this matter consists of two regulations for Dangerous Substances and Explosive Atmospheres (DSEAR), which place duties on employers to eliminate and control the risks from explosive atmospheres and the ATEX framework, consisting of two European directives (99/92/EC and 94/9/EC) [26-28] that set the requirements for improving the health and safety of workers at risk from explosive atmospheres and for the equipment and protective systems used in potentially explosive atmospheres. The European regulations are somewhat restrictive in the definition of explosive atmosphere, since only mixtures with air at atmospheric conditions are considered, and they also fail to differentiate between gases and dusts [29].

According to the principles of ATEX regulations, the hierarchy of risk control measures consists in:

- Elimination of hazardous substances or conditions or substitution by less hazardous substances or conditions during the design of operations. This would include keeping flammable mixtures outside of the flammable range, limitation of ignition sources, or avoiding oxidative atmospheres.
- Reduction of risks through measures which are functioning all the time (e.g. enclosures are designed to withstand explosion overpressures; avoid expansion of the explosion to other enclosures by isolating the affected unit
- Control measures which can be built into the design and start working when an event initiates: venting or suppression
    - Venting: The overpressure created by the explosion is relieved by opening a weak cover or vent that bursts at a certain pressure. This way, the impact of the explosion can be minimised. However, important hazards have to be addressed, like the emission of toxic products from combustion, the release of solid objects (e.g. vent covers), the emission of blast waves from the explosion, the expulsion of strong flame jets or the reaction forces as a result of the venting process. The area of the vent cover depends on the volume of the enclosure, the strength of the enclosure, the strength of the vent cover and the burning rate of the dust cloud. The burning rate of a dust cloud is not a property of the dust; it will depend on the turbulence and the degree of dispersion of the dust. The theories and standard methods for the design of venting systems are given by the NFPA 68 (US Standard) and EN 14797:2007 and EN 14491:2006 (European Standards), and require knowledge of explosion characteristics (K_{St}, P_{max}).
    - Suppression: Consists on putting in place a system that is capable of quenching the explosion by adding an inert stone dust capable of cooling the flame front. The injection of suppressant occurs at a certain pressure and the pressure is reduced. Suppression systems need higher maintenance. The European standard for explosion suppression is the EN 14373:2005 Explosion suppression systems.
- Mitigation of the impacts of an incident when prevention and control measures fail (firefighting arrangements, evacuation, etc)

Therefore in order to design safety systems that protect property and personnel from dust explosions it is necessary to have knowledge of the explosibility of the specific fuel used. Standard methods exist for the measurement of explosion characteristics; however these have limitations when testing certain types of dusts. The difficulties are related to the fibrous nature of some dusts that impede proper dust dispersion. Many biomass materials are fibrous and fall in the category of "difficult dusts". In addition, most biomass materials have very low bulk density which limits the amounts of dust that can be tested.

In conclusion, as a result of the increasing use of biomass for power generation and the limited data and knowledge about the explosibility of biomass materials for adequate design of safety systems, serious incidents are proliferating.

1.6. Objectives

Biomass dust explosion incidents in power generation and in other related industries can be avoided if precise explosion characterisation of fuels is available and applied in the design of safety systems. Explosibility data for biomass fuels and their mixtures with coal are very scarce in the literature and in cases there are doubts about their reliability. More importantly data is inexistent for biomass fuels upgraded through torrefaction. Therefore the present work provides fundamental explosibility and combustion data for torrefied biomass, biomass and mixtures with coal using the Leeds ISO 1 m^3 dust explosion vessel, suitably modified and calibrated to allow measurement of explosion characteristics of fibrous and low bulk density biomass materials. The results were compared to the reactivity of corresponding parent biomass materials and to samples of coal. Additionally combustion properties such as flame speeds and approximate burning velocities were also derived and offer additional data for burner design. Further analysis of residual deposits of dust remaining in the explosion chamber after explosion tests was carried out to understand their origin and nature.

An alternative technique for the measurement of minimum explosible concentrations (MEC) was also devised and partially developed. The method proposed is set to allow a faster and more accurate determination of lean flammability limits in comparison to the standard techniques.

Chapter 2 LITERATURE REVIEW

CONTENTS

2.1. Dust explosions - General

2.1.1. Definitions

A dust explosion is the rapid combustion of a finely divided combustible solid material with a subsequent increase in temperature and pressure. There is lack of agreement on an exact definition of how fine a material must be to be referred to as a "dust" as opposed to a "powder", values often quoted in the standards are less than 500 μm [30]. Explosion characteristics are required to be measured for dusts of <60μm by the standards as these will provide the worst case scenarios [31]. However, these sizes are often artificial and not representative of the size distributions used in some industries.

2.1.2. Differences between gas and dust explosions

The main differences between gas and dust explosions are related to the heterogeneous character of dust explosions and the need of a dispersive medium to suspend the powder into the oxidising atmosphere (usually air) and to prevent particles from depositing, before ignition. Dispersion can also be the mechanism for gaseous fuels mixing with oxidants but they can also mix by diffusion and the

mixing is at a molecular level therefore can remain stable (and flammable) even in a quiescent mixture (unlike dust clouds). These differences and the lower frequency of occurrence of dust explosion incidents have resulted in more research in gas explosions and hence better understanding of gas rather than dust explosions. Fundamentally, gas and dust explosions have the same propagation mechanisms (deflagration or detonation). The damage produced is also similar and therefore safety systems use similar principles [32].

Other observed differences between gases and dusts are that when the reactivity of gases is investigated for different mixtures, the most reactive concentration is always found for mixtures slightly richer than stoichiometric. However, the peak reactivity for dusts occurs at much richer mixtures. This fact has been usually overlooked because concentrations of dusts are expressed as grams of dust per m^3 of air and gases as the volume %. However, if concentrations are expressed as equivalence ratios (Ø), that is, as the ratio of actual to stoichiometric concentrations these differences become clear. In addition this method of expressing mixture concentrations allows direct comparison between fuels with different stoichiometry. Illustrative examples of gas peak reactivity are methane, propane, ethylene and hydrogen gases, for which their respective most reactive mixtures are found at equivalence ratios of 1.06, 1.13, 1.30, 1.60 [33]. However for dusts, most reactive mixtures are often found for very rich mixtures (Ø~2) [34]. Another difference between gases and dusts is related to the upper flammability limits. UFL of the previously listed gases are measurable at equivalence ratios of 1.7, 2.6, 5.8 and 7.2 [33] whereas for dusts, the reactivity decays very slowly and in many cases the standard methods cannot measure upper explosible limits.

Slatter et al. [35] postulated reasons for dusts having such rich upper limits in comparison to gases: in a closed vessel a fixed mass of air is available, therefore there is a fixed heat release of 3.68 MJ per m^3 of air irrespective of the fuel. For rich mixtures of gases air is displaced and therefore the energy available to be released is lower in an equivalent gas system. This is illustrated in Figure 2-1 for methane, propane, ethylene and hydrogen gases and for two different types of dusts, a coal and a biomass dust. Another given explanation for the pressure to remain high at rich concentrations is that although the initial mixture pressure is 1 atm, this increases when the dust particles pyrolyse in the preheat zone of the flame. Very few other hypotheses have been published; however this matter should be taken into account as many processes, such as milling in pulverised fuel power plants, operate with very rich mixtures on the premise that such rich mixtures are not flammable.

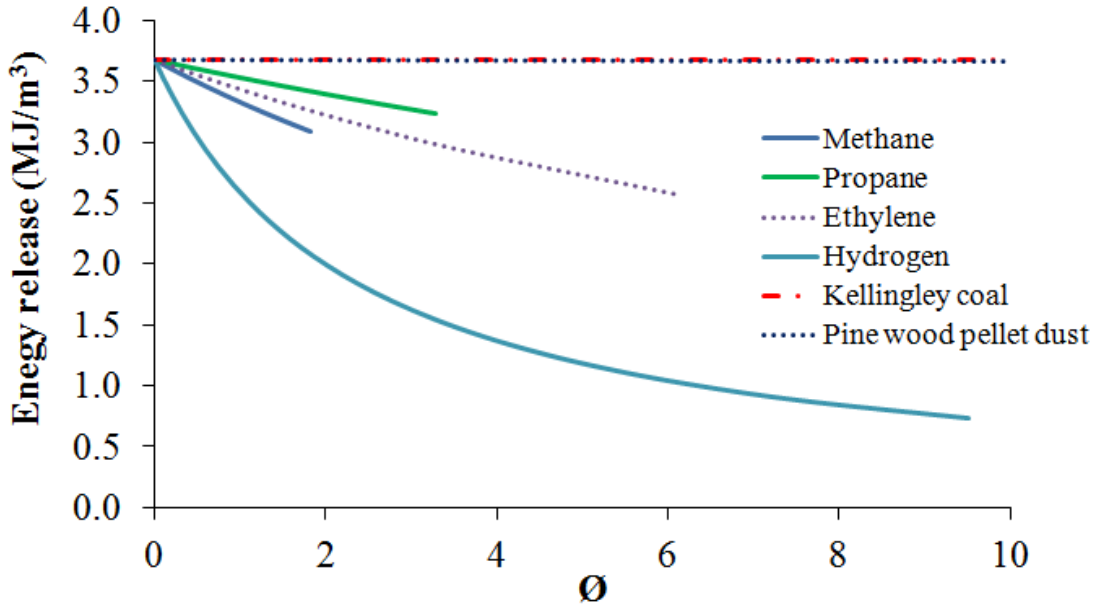

Figure 2-1. Comparison of fixed heat release due to the mass of air available for gas and dust fuels

Hertzberg et al. [36] did recognise that measured explosion pressures did not parallel adiabatic predictions for pressures and flame temperatures at rich mixtures. Predictions indicated that pressures and flame temperatures decreased at rich mixtures (see Figure 2-2 and Figure 2-3).

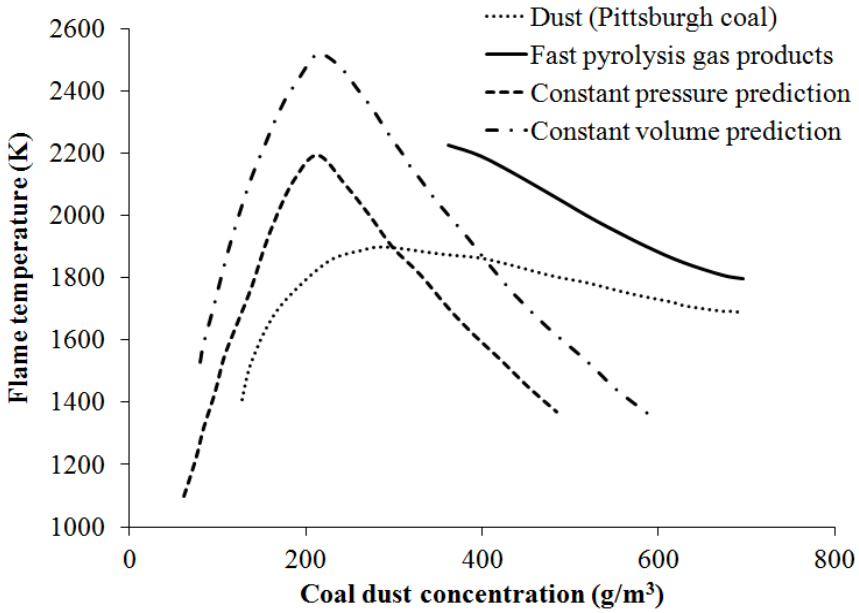

Figure 2-2. Calculated adiabatic flame temperatures for constant volume and pressure combustion compared to measured temperature at constant volume [36]

The unparallel difference between predicted and experimental curves for rich mixtures could not be explained by nonadiabaticities in the system. They instead proposed that the aforementioned differences between predicted and experimental data were due to “limitations on the rate of devolatilisation”. Although rich mixtures generate more volatiles these are emitted too late to dilute the flame front with excess fuel vapour. As the fuel loading is very high it continues to reach high explosion pressures and temperatures. However, due to the presence of excess coal which did not contribute to flame propagation, heat from the flame front is absorbed slowly reducing flame temperatures and explosion pressures.

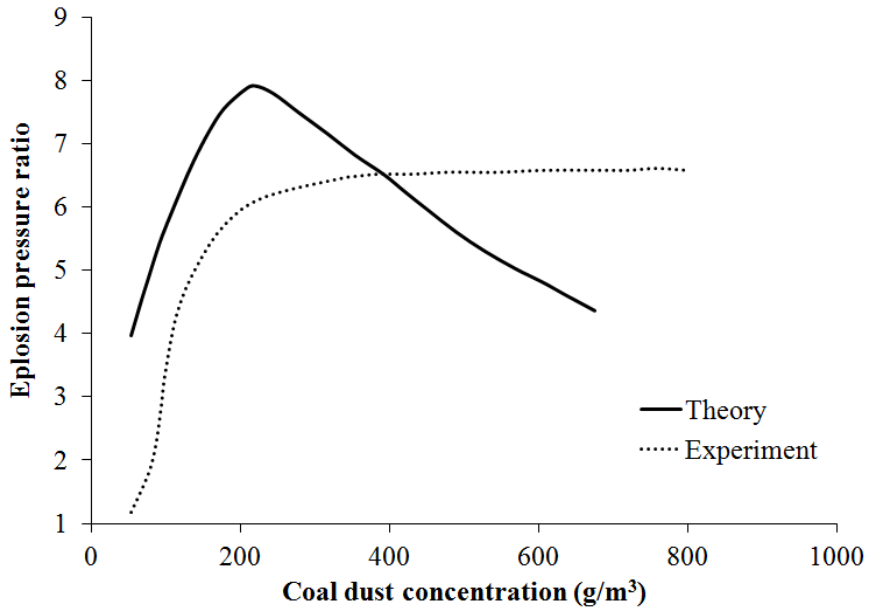

Figure 2-3. Calculated adiabatic explosion pressure ratio for constant volume compared to experimental result [36]

2.2. Dust explosibility parameters and assessment

2.2.1. Explosion characteristics

A number of parameters or properties are used to characterise the explosibility and reactivity of dusts. The following definitions correspond to European standards [30] or NFPA 68 [37]:

1. Flammability limits

a) Lower flammability limit (LFL) or minimum explosible concentration (MEC): “Lowest concentration of a combustible dust in mixture with air at which an explosion occurs”

b) Upper flammability limit (UFL): "highest concentration of a combustible substance in a gaseous oxidiser that will propagate a flame"

2. Maximum explosion pressure (P_{max}): "Highest overpressure occurring during an explosion of a dust cloud in a closed vessel".

3. Maximum rate of pressure rise $(dP/dt)_{max}$: "Maximum value of the pressure rise per unit time during explosions of all explosive atmospheres in the explosion range of a combustible substance in a closed vessel under specified test conditions and standard atmospheric conditions"

4. Deflagration index, (K_{St} or K_{max}): "dust specific, volume independent characteristic which is calculated using the cubic law equation", given in Eq.(2.1):

$$K_{St} = \left(dP/dt\right)_{max} \cdot V^{1/3} \tag{2.1}$$

Where V is the volume of the explosion vessel used for the determination of maximum rates of pressure rise. This formula is only valid for vessels where the flame thickness is negligible compared to vessel radius and if the burning velocity as a function of temperature and pressure is identical in all volumes.

According to their K_{St} dusts can be classified as:

Group St-1	$0<K_{St}<200$	Moderately explosible
Group St-2	$200<K_{St}<300$	Strongly explosible
Group St-3	$K_{St}>300$	Very strongly explosible

K_{St} and maximum explosion pressures are parameters which are used for instance in the design of explosion venting protection systems. For example the American standard for venting of deflagrations of dusts and hybrid mixtures [37] recommends determining the minimum vent area required to protect an enclosure using the correlation below:

$$A_{vo} = 1 \cdot 10^{-4} \cdot \left(1 + 1.54 \cdot P_{stat}^{4/3}\right) \cdot K_{St} \cdot V^{3/4} \cdot \sqrt{\frac{P_{max}}{P_{red}} - 1} \tag{2.2}$$

The parameters K_{St} and P_{max} are determined as a function of concentration, as shown in Figure 2-4, the maximum values for each dust are used in design calculations, since they represent the worst case scenario.

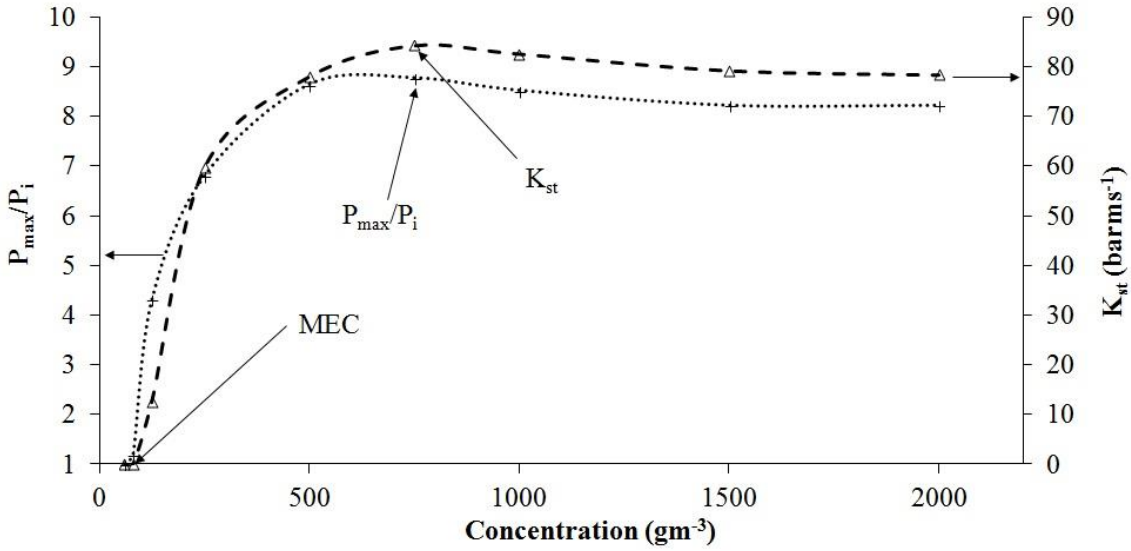

Figure 2-4. Example derivation of explosion characteristics of pine wood dust mixture

There are other parameters related to the explosibility of dusts which are not determined as part of this research project. These are the Minimum Ignition Energy (MIE) and the Limiting Oxygen Concentration (LOC). The MIE is the "minimum amount of energy released at a point in a combustible mixture that causes flame propagation away from the point, under specified test conditions". The ignition source used in this research is sufficiently strong to ensure ignition of mixtures inside the flammable range. The LOC is the "maximum oxygen concentration in mixture of a combustible dust and air and an inert gas, in which an explosion will not occur, determined under test conditions" [38]. These parameters and the LFL are relevant when it is possible to apply prevention measures to avoid explosions from happening at all.

Other important parameters related to explosions are flame speed (S_F) and burning velocity (S_L). Laminar burning velocities are fundamental property of the fuel and it is used in the NFPA68 as a reactivity parameter for gases instead of the deflagration index.

The burning velocity is the rate of flame propagation relative to the velocity of the unburnt gas that is ahead of it. It is possible to define a turbulent burning velocity (S_T) when the conditions in which flame propagates are turbulent, in which case, the flame front wrinkles increasing the surface area. Locally, the combustion is still governed by the laminar burning velocity but the flame advances with a higher velocity than the laminar. Turbulent and laminar burning velocities are related as follows:

$$\beta = \frac{S_T}{S_L} \tag{2.3}$$

Where β is the turbulence factor that accounts for the turbulence induced.

Deflagration indexes are not a good measurement of reactivity when different vessels to the standard vessels are used for its measurement as the cube root law is not valid [39]. In addition, deflagration indexes do not account for the induced turbulence due to dispersion and therefore a lot of effort is being devoted by researchers to establish a method of measuring the reactivity of dusts through burning velocities [39-44]. Silvestrini et al. [45] give good account of the methods used for measurement of laminar burning velocities of dust flames and of the inadequacies of each method which are mainly related to: residual turbulence from dispersion, wake turbulence of settling particles, flame front instabilities, curvature effects, increased flame speed due to buoyancy of burnt gases or maldistribution of dust inside test equipment.

Flame speeds and burning velocities are related as follows due to the conservation of mass flow across a flame surface of area A:

$$\rho_u \cdot S_L \cdot A = \rho_b \cdot S_F \cdot A \tag{2.4}$$

$$S_F = \frac{\rho_u}{\rho_b} S_L \tag{2.5}$$

The ratio of unburnt to burnt gases is also expressed as the expansion factor E, and therefore:

$$S_F = E \cdot S_L \tag{2.6}$$

This relationship is only valid if the flame is planar, hemispherical or spherical and if the burnt gases remain behind the expanding flame front [46].

In addition flame speed data is relevant to practical burner applications and flame stability and provides valuable information to prevent blow-off and flash-back issues.

2.2.2. Flame propagation

Combustion in dust explosions can occur through different mechanisms. Typically for metal dusts the reaction takes place at the surface of the solid and therefore the rate of reaction is proportional to the surface area available for reaction. Other dusts such as polyethylene or lycopodium react in the gas phase [42]; particles vaporise

and the gases react with the surrounding oxygen. But in most cases the reaction occurs as a combination of the two [32].

There are many factors that affect dust flame propagation such as: heat conductivity, temperature of unburnt and burnt masses, emissivity of particles surface, radiation of combustion products, flame thickness, specific heats of gases and dusts present as well as their density and concentration and particle radius. The main experimental challenge is to produce uniformly dispersed dust clouds that can be maintained for long enough periods as to allow observations of a stationary dust flame [47]. As a result of researcher's efforts, laminar burning velocities, flame thicknesses and flame temperatures have been measured for some dusts such as coal, corn flour or lycopodium [48-51]. Corn flour and lycopodium results should be comparable to biomass samples as they present similar elemental composition and stoichiometry. Corn flour is regarded as a dust where both homogeneous and heterogeneous combustion mechanisms take place. A laminar flame front of corn starch has shown a perceptible, continuous and apparently smooth structure which suggests a marginal contribution to flame propagation of heat exchange by radiation, in which case the contribution of heterogeneous combustion can be disregarded. Therefore researchers concluded that when dust particles are capable of gasifying at low temperatures (such as biomass), flame propagation is similar to that of premixed gases where the preheat zone is dominated by heat conduction. Maximum laminar burning velocities were found around 0.2 m/s, and maximum temperatures of 1300°C [52].

2.2.3. Experimental measurement of explosion characteristics

2.2.3.1. Hartmann Bomb/Tube

The Hartmann tube and Hartmann bomb were the first widely used laboratory scale apparatuses for explosion characterisation of dusts. Developed by the US Bureau of Mines, the Hartmann bomb consisted of a closed steel tube (69 mm internal diameter, 325 mm long, 1.2 L volume in total) whereas the Hartmann open tube was made of Lucite and its top was covered with a paper vent. The Hartmann bomb used a 50 mL reservoir for the dispersing air, pressurised at 7 bar, whereas the Hartmann tube used a 1310 mL volume, with air pressurised to 1 bar [53]. Although the Hartmann bomb was used for the measurement of rates of pressure rise and maximum explosion pressure and the open tube for lean flammability limits and minimum ignition energy, the principle of operation was invariable: a deposit of known mass was dispersed in the volume using a blast of air from an internal reservoir. The dust cloud was ignited by a continuous spark source of around 4 J [53]. Extensive data was produced by the Bureau of Mines on many types of dusts using the Hartmann bomb [54-61].

The current European standard for the determination of minimum ignition energy (MIE) [62] recommends the use of Hartmann tube as the test vessel. In addition, this experimental set up is used as A/B Classification apparatus to classify dusts as type A, “explosible” or type B, “not explosible”.

Hartmann tubes are no longer used for determination of MEC as they were reported to produce improperly mixed dust suspensions (with higher concentrations near the walls) by a number of authors [63-66]. Other issues were summarised by Makris and Lee [67] including: difficulty of ignition for dusts with quenching diameters larger than the vessel diameter or unrealistic results relative to open space events. Additionally, being a tube, the flame touches the vessel walls before burning the entire mixture. The heat losses through the walls prevent measurement of maximum peak pressures and rates of pressure rise. However, vertical cylindrical tubes are used for the measurement of lean flammability limits of gases and it was accepted that this effect would be small for tubes of diameter higher than 50 mm, also limits should best be taken as those for upward propagation since these are wider [33, 68]. As a result one of the recommended experimental vessels for the determination of LFL of gases is a cylindrical tube, very similar to the Hartmann tube. The reason why the standard method for MEC determination for dusts is different is unclear.

In this work the Hartmann tube was modified in order to measure MEC of biomass and torrefied biomass dusts as well as flame speeds. Details are given in Chapters 3 and 4.

The Hartmann tube has been modified by other researchers in order to improve the distribution of dust clouds by altering the shape of the dispersion cup [64]. Similar equipment has been developed (e.g. MIKE 3) for MIE measurement with different ignition source circuit design [69, 70].

Bigger vessels are believed to achieve more comparable results to the industrial case [71], therefore, despite the efforts to improve the Hartmann tube, bigger and close to spherical vessels were designed, such as the 20 L sphere, the 1 m^3 vessel or the Nordtest Fire 011 [58] and eventually the 1 m^3 and more recently the 20 L sphere were adopted as the ISO standards.

2.2.3.2. 1 m^3 ISO vessel

The 1m^3 vessel was developed by Bartcknecht [72] and it is considered to yield the most reliable results. Smaller vessels such as the 20 L sphere should give comparable results using the same ignition energy (10 kJ). The standard set up (see Figure 2-5) consists of a 5 L dust/air container pressurised to 20 bar. The dust/air container is connected to the explosion vessel through a pipe, and a fast acting valve (10 ms).

Inside the vessel a dispersion system consisting of a perforated C-ring disperses the dust. Chemical igniters providing 10 kJ ignition energy and situated in the geometrical centre of the vessel are used to ignite the dust cloud. The explosion vessel is not a sphere but a cylinder with round edges with L/D of unity.

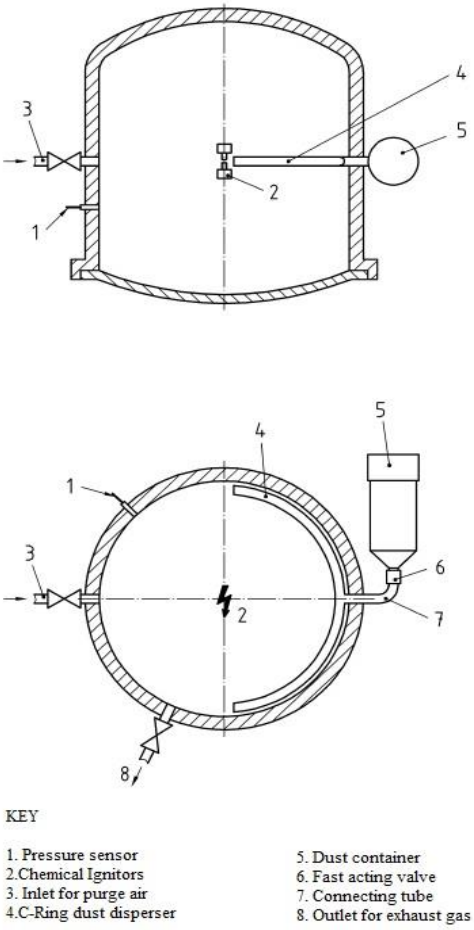

Figure 2-5. ISO 1 m^3 vessel [30, 73, 74]

A number of features in the 1 m^3 vessel are empirical and greatly affect the results: the design of the C-ring (tube size, number, location and orientation of holes), the volume of the dust holder and its level of pressurisation, the time of dust injection and the ignition energy and ignition delay time. Other vessels such as the 20 L sphere have different features and in turn this affects turbulence levels, therefore in order to achieve similar results the ignition delay is adjusted accordingly.

Many studies have been presented comparing the results from 1 m^3 vessels and 20 L spheres [75-78]. Some of this studies show contradictory results as for example Siwek affirmed that lean flammability limit results were comparable whereas other researchers found that the high ignition source in the 20 L sphere would overdrive the reaction and widen the limits [77-79]. Where K_{St} and P_{max} measured through both

methods have been compared [76], lower K_{St} and P_{max} were found in the 20 L sphere, whereas Siwek found good agreement (see Figure 2-6).

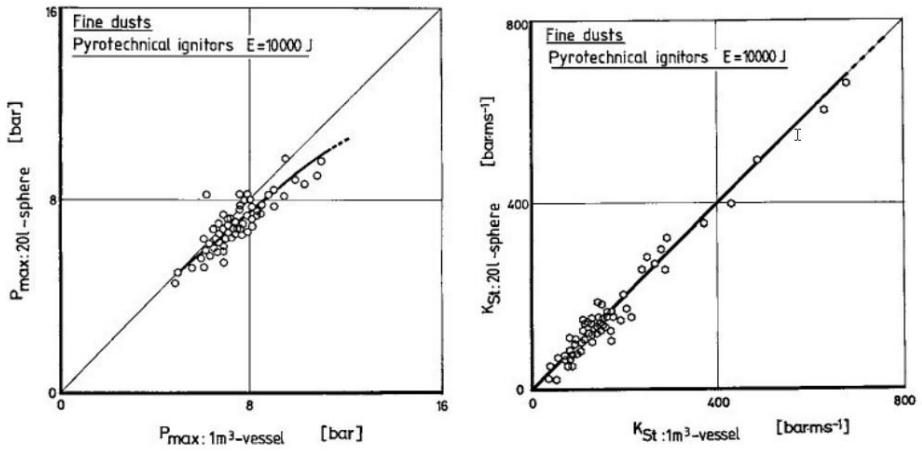

Figure 2-6. Correlations of maximum explosion pressure and K_{St} from 20 L sphere and 1 m^3 vessel (Source: [58], original work from Siwek)

2.2.3.3. 20 L sphere

The 20 L sphere is a reduced size version of the 1 m^3, cheaper, and more suitable for routine testing of dusts. The principle of operation is similar since the dust is dispersed from an external reservoir or dust holder, central ignition is supplied generally with 10 kJ igniters. There are different types of 20 L spheres. They mainly differ on the dispersion system used.

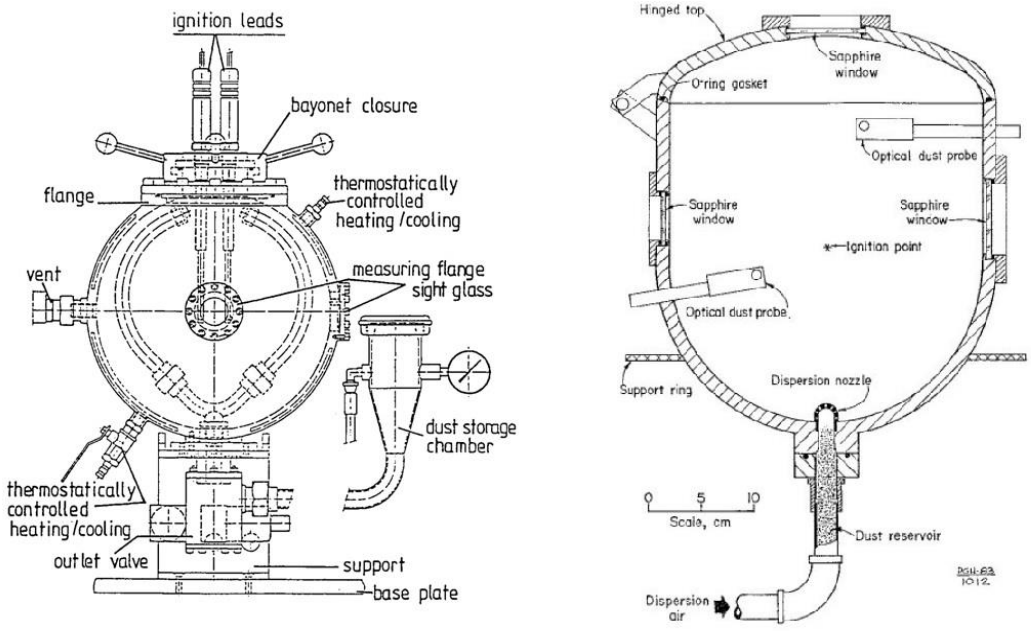

Figure 2-7. Left: Siwek 20 L sphere (Source: [80]) and Right: US Bureau of Mines 20 L sphere (Source: [81])

The 20 L sphere developed by the Bureau of Mines in the USA used a dispersion nozzle, an example is shown in Figure 2-7 (right), The 20 L sphere developed by Siwek in Ciba Geigy (Switzerland) used a dispersion tube similar to the 1 m^3 C-ring (see Figure 2-7 (left)).

The Siwek 20 L sphere has been known to use a rebound nozzle as well for poor flowing dusts, such as fibrous dusts. The rebound nozzle is shown in Figure 2-8. The same geometry is recommended in the current European standards for poor flowing dusts. This nozzle has been tested with biomass dusts in the 1 m^3 vessel by the Leeds group and others [82], more details will be given in section 2.3 of the present Chapter.

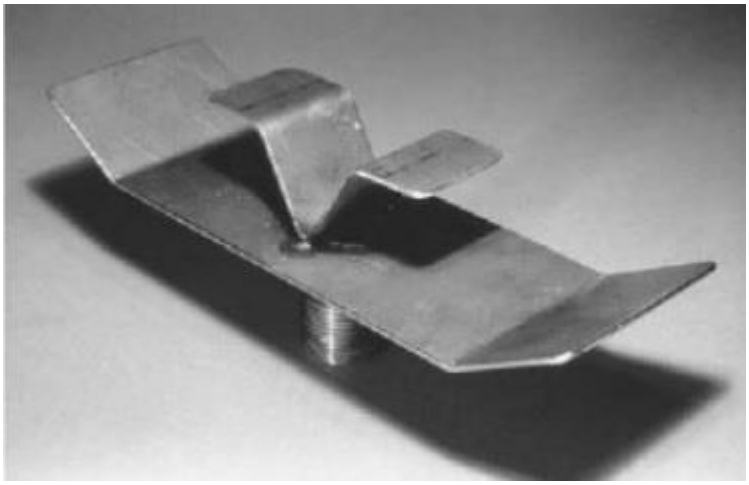

Figure 2-8. 20 L sphere Siwek rebound nozzle

It could be due to the disparity of 20 L sphere designs, that comparison of results from 20 L spheres and 1 m^3 vessels provide discrepant results, and therefore it would appear that the Siwek 20 L sphere design is more successful in reproducing the 1 m^3 vessel results than the instrument used by Proust, which differed with Siwek in the position of the perforated ring disperser.

Apart from the already discussed issue of the large ignition source in the 20 L sphere that affects the ambient conditions at the time of ignition, therefore extending the flammability limit; the pressure rise due to the igniters is 1.1±0.1 barg therefore, rates of pressure rise and potential measurements of burning velocity would be over predicted. Although this issue is recognised by the standards for the measurement of flammability limits, the standard for measurement of $(dP/dt)_{max}$ and P_{max} still uses 10 kJ ignition source.

The 20 L sphere has also been found to provide non-uniform distribution of dust at the moment of ignition [83-85]. Concentrations are richer closer to the vessel walls and it has also been found that as the diameter of particles increase the distribution is

less uniform. Conversely, Kalejaiye et al [71] used optical dust probes to test the dispersion uniformity of three different dusts and different nozzles (C-ring) in a 20 L sphere and compared the results with other available for other 20 L spheres and one 1 m^3 vessel. The results showed that both nozzles achieved similar dispersion uniformity. It was also detected that particle size was reduced after injection in the Siwek 20 L sphere due to the design of the outlet valve rather than the nozzle geometry, which did not occur in the 1 m^3 vessel but could have an effect over the K_{St} measurements.

Researches using both the 1 m^3 vessel, and smaller dust explosion vessels such as the 20 L sphere or an 8 L sphere have reported large residues of dust remaining inside the explosion chambers after explosion [86-88]. Some of these researchers analysed the residues morphology as a means of understanding the combustion mechanisms. The dust holder was also reported to retain some dust residue [86, 89], which could be weighted and used to correct for the amount of dust that actually entered the explosion chamber.

2.2.4. Factors influencing dust explosion test results

Explosion test results (maximum pressures and rates of pressure rise) are influenced by a number of parameters. These are either related to dust properties or to test conditions. The maximum explosion pressure depends on the energy content of the mix and on any potential heat losses. The rate of pressure rise and therefore K_{St} is affected by parameters or conditions that influence the area of the flame and the mass burning rate.

2.2.4.1. Test conditions

2.2.4.1.1. Turbulence: Ignition delay

Turbulence is a key parameter in dust explosions. In order to create a dust cloud a degree of turbulence is needed. In existing experimental set ups the necessary turbulence for dust dispersion is introduced through a flow of air. The strength of the dispersion air as well as the geometry of the dispersion system will affect turbulence levels. The turbulence level at the time of ignition is regulated through the ignition delay [90]. A short ignition delay results in high turbulence, whereas after a long ignition delay turbulence decays and particles start falling from suspension due to gravity.

Ignition delay, as defined in the standards, is the time between the initiation of the dust dispersion and the activation of the ignition source. Standard ignition delay in the 1 m^3 vessel is 600 ms. A 60 ms ignition delay was empirically determined to give

comparable results in the 20 L sphere. The effect of turbulence on K_{St} and P_{max} has been researched very thoroughly over the years in different vessels [59, 72, 90, 91], and has been found to affect the rates of pressure rise in a greater measure than the maximum explosion pressures. Turbulence encourages faster heat transfer rates and therefore the higher the turbulence the higher the K_{St}. Although pressure is less influenced, faster flames are created at high turbulence levels, allowing less time for heat losses which results in an increase of peak pressure. Furthermore, highly turbulent dust clouds are more difficult to ignite, and as a consequence the MIE increases with turbulence intensity [92].

By increasing the ignition delay, it is possible to measure reactivity parameters in near laminar conditions [32, 93].

The turbulence factor (β) is defined as the ratio of turbulent to laminar burning velocities and is typically used in pressure relief vent calculations to allow for induced turbulence due to obstacles encountered in the path of the flame [94]. If a laminar gas explosion is performed and then the same mixture is made turbulent (by using a rotating fan for example) the measurements of K_G or burning velocities can be used to determine the turbulence factor β. It is then possible to find the turbulence factor in closed explosion vessels such as the 1 m^3 ISO vessel by performing laminar gas explosions and turbulent gas explosions where the turbulence is induced by the dispersion air flow.

2.2.4.1.2. Ignition energy

In general, dusts need stronger ignition energy than gases (10-100 mJ), but due to the turbulence induced from dust dispersion, higher ignition energy is normally used. 10 kJ was the energy proposed by Bartknecht [72] to ensure ignition of more difficult to ignite dusts. Chemical igniters are conventionally used rather than spark ignition sources. The ignition energy though can influence K_{St}, P_{max} and explosion limits, especially when it becomes too strong relative to the explosion chamber size [95]. Explosions initiate by instantaneous jet like volumetric ignition and/or multipoint ignition depending on the orientation of the ignitor cups, which results in a source of imprecision for the standard systems [93]. It is recommended [30] to place igniters facing each other, however spherical flame propagation is still difficult to achieve.

2.2.4.1.3. Concentration of reactants

The concentration of dust and oxidiser also affect the explosion parameters. Within the flammable range the reactivity increases from the lower explosible concentration to reach the most reactive mixture and, in the case of dusts, slowly decrease. As briefly discussed earlier the most reactive concentration for gases is found usually

for slightly richer than stoichiometric mixtures, whereas for many dusts the most reactive mixture is generally richer, this is shown in Figure 2-9. [81]. This has not been typically noted in the literature, probably because concentrations, except in very rare occasions [96], are reported in g/m^3, not taking into account the stoichiometry of each dust. Mapping reactivity against equivalence ratio is a more informative approach; however, ideally, reactivity should be mapped against the equivalence ratio of the composition of the pyrolysed gases through which the flame actually propagates [35, 96].

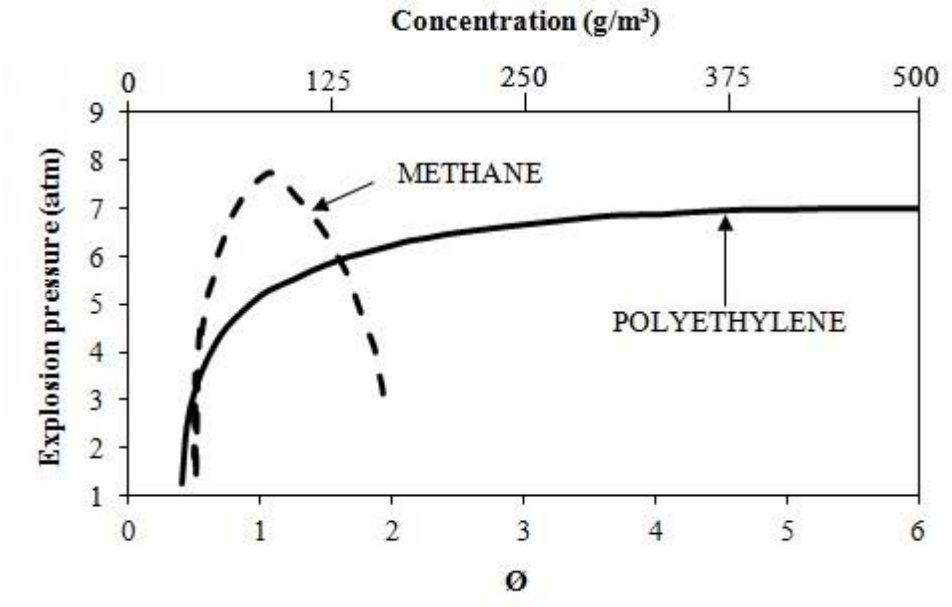

Figure 2-9. Comparison of the reactivity of gases and dusts [97]

2.2.4.1.4. Temperature, pressure and humidity conditions

The initial temperature and pressure conditions can affect the reactivity of dusts. In particular higher than ambient initial temperatures result in a decrease of MEC, an increase in rates of pressure rise and a decrease of peak pressure [72]. Burning velocities increase with the square of temperature and decrease with the square root of pressure. It should be noted that at elevated temperature the density of air decreases and therefore it would be preferable to express concentrations in grams of dust/grams of air when varying both pressure and temperature. Increased initial pressure increases peak pressure [72, 98, 99] and pressure rises should be expressed as the ratio of maximum pressure to initial pressure. Characterisation of explosible dusts is carried out at 1 atm (1.013 bara) and ambient temperature, but this could be unrealistic in some industrial processes as well.

The effect of ambient humidity is generally to decrease the reactivity of dusts, as shown by Traore et al. [100].

2.2.4.2. Dust properties

2.2.4.2.1. Dust chemical composition

Materials that can cause explosions include organic materials (sugar, grain, plastics, pesticides), coal and peat and metals [58]. Except with metals, the combustion reaction occurs mainly in the gas phase, and therefore the ideal gas law applies. In a constant volume explosion (closed vessel), pressure is proportional to temperature and the number of gas molecules in the volume.

When considering the chemistry of a dust in dust explosion, two factors are key: the amount of heat that can be liberated and how fast that heat is liberated. Therefore, the heat of combustion of a material is important, Eckhoff [58] showed that metals have the highest heats of combustion per mol of oxygen and they produce typically high rates of pressure rise in an explosion.

Other influential factor is the moisture content. High moisture content reduces the flame temperature and therefore P_{max}. In addition moisture can increase inter-particle cohesion and prevent dispersion into primary particles [58]. Also, the flammability limit is narrowed and MIE increases for high moisture content, however, some dusts are more sensitive to moisture than others [72].

The volatile content of the dust is also an important parameter. Dusts containing high percentage of volatiles are more reactive, but particle size plays a role on the overall reactivity as dusts with high volatile content see a rapid increase in reactivity when particle size becomes small, due to faster combustion rates [101].

The ash content can also affect the reactivity of dusts, decreasing K_{St} and P_{max} and increasing MEC and MIE. This is due to ash acting as an inert and acting as a heat sink although the effect is likely to be smaller than moisture or volatile content.

2.2.4.2.2. Particle size distribution

The particle size and surface area available for the combustion reaction to occur have an effect over dust explosibility, especially over how easily the dust can ignit, the rate of reaction and the rate of pressure rise, and therefore over K_{St}. In contrast the maximum explosion pressure has lower sensitivity to particle size [102].

The MEC of dusts is affected by particle size [103], studies with coal dust showed that particles of 250-841 μm did not explode. With increased presence of small particles the MEC decreased until about 150 μm when the MEC was constant [104]. This behaviour has been found for other dusts such as polyethylene dust, corn flour, magnesium [58, 72, 105, 106].

Standards for determination of K_{St}, P_{max}, MEC of dusts recommend testing fine particles of typically <60 μm to protect against worst case scenario explosions. However this particle size is often unrealistic in regards to the real hazards. In many occasions it has been found that bigger particles do not ignite when narrow distributions of large particles are tested, however, wide distributions that still contain fine particles can ignite very readily [107]. Particle size has also been found to affect the structure of the flame front and the propagation mechanisms [108].

In recent years, researchers have also been concerned with dusts of nano-size particles [70, 109]. In previous studies [110] it had been found that particles smaller than a few microns tend to agglomerate and therefore the hazard would remain in a similar level. However, nano-particles present smaller minimum ignition energies [111].

2.3. Biomass and torrefied biomass explosibility

Wood dust hazards are considered tolerable risks in traditional operations such as sawmills but the unprecedented amounts of solid biomass resulting from the intensification and scaling up in power generation requires an improvement of the knowledge of the risks associated to these materials [112]. In this section characteristics of biomass and torrefied biomass powders used in power generation are presented and compared to coal. Secondly an account of the main difficulties encountered in the measurement of explosion characteristics for biomass dusts is given. To conclude data available in the literature involving biomass and biomass/coal mixtures are revised.

2.3.1. Biomass and torrefied biomass powders

Many researchers have investigated the composition of biomass fuels [113, 114]. The chemical composition of biomass is very variable and these are variations of moisture, ash and inorganic matter depending on the nature of the biomass [115]. Typical composition of biomass used in power generation and coal are shown in Table 2-1. Biomass generally contain more volatile content and moisture, as well as more oxygen. However calorific values and bulk densities are lower than for coal.

Table 2-1. Typical composition of biomass and coal fuels

	Wood/Woody biomass (chips, bark, sawdust)	Herbaceous and agricultural biomass (grasses, straw, nut shells)	Coal
Proximate analysis (wt%, dry basis) [115]			
Volatile Matter	69.5-86.3	59.3-85.5	12.4-51.8
Fixed Carbon	12.3-26.3	12.4-37.9	20.0-71.8
Ash	0.1-16.5	0.9-20.1	5.7-52.0
Moisture	4.7-62.9	4.4-47.9	0.4-20.2
Elemental analysis (wt%, dry, ash free basis) [115]			
C	48.7-57.0	42.2-58.4	62.9-86.9
O	32.0-45.3	34.2-49.0	4.4-29.9
H	5.4-10.2	3.2-9.2	3.5-6.3
N	0.1-0.7	0.1-3.4	0.5-2.9
S	0.01-0.42	0.01-0.60	0.2-9.8
GCV (MJ/kg)	15.0-20.8 [116]	14.0-20.0 [117]	23-28 [13]
Bulk density (kg/m^3)	200-800	100-300	400-1000

The calorific values of biomass and coal can be either measured experimentally or calculated through multiple correlations found in the literature by means of their elemental or proximate composition [117-122]. Specific correlations for torrefied biomass have not been found in the literature but researchers have previously used the existing correlations for biomass [123].

Figure 2-10 is known as the Van Krevelen diagram, it plots the hydrogen to carbon atomic ratio as a function of the oxygen to carbon atomic ratio. This graph is typically used to classify coals according to their rank. Higher rank coals are positioned at low H:C and O:C ratios due to the high carbon content and low oxygen contents. Biomass materials included in the plot are situated in a wide area with higher H:C ratios and O:C ratios. Torrefied biomass materials are not depicted in this particular graph, but torrefied materials tend to move towards the “lignite” or low rank coal area as a result of the increase of carbon content and decrease of oxygen content [124].

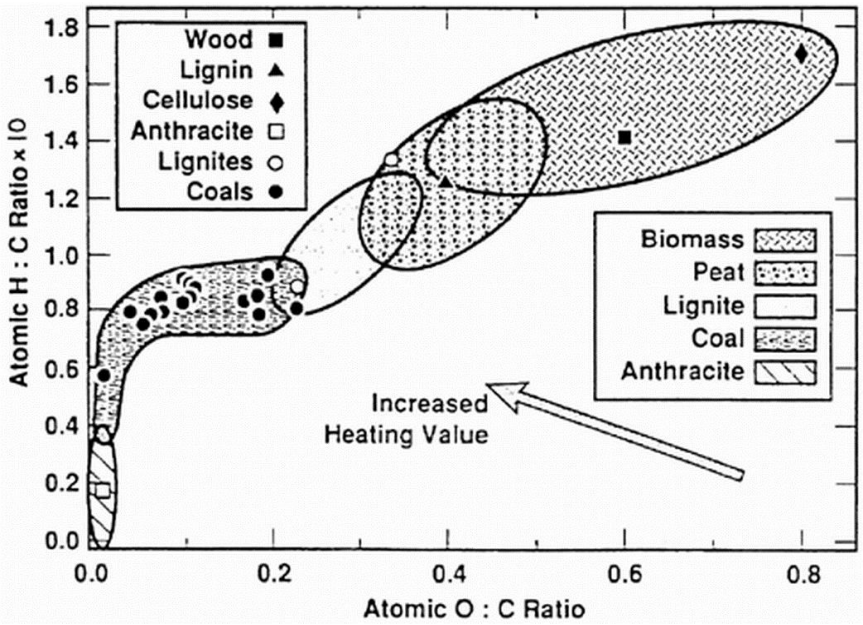

Figure 2-10. Van Krevelen diagram. Source: [125]

2.3.1.1. Biomass-to-energy conversion

Although currently there is not a standard for fuels quality for industrial uses most power stations buy biomass to a specification of their own, often avoiding "difficult fuels" such as olive residue, which is hard to mill, PKE (palm kernel expeller) since it is an aggressive irritant or straw and miscanthus with high chlorine content which leads to corrosion and slagging in the boiler. Others use fuels according to the specifications from the industrial pellet buyers associations [126]. These specifications put restrictions over the moisture, ash, nitrogen, sulphur, chlorine contents as well as calorific values, bulk density or content of fines [127].

Energy stored in plants is contained in its three main cell-wall components: cellulose, hemicellulose and lignin, the proportions of which vary with the type of plant and are key factors in establishing the best energy conversion path for each biomass type [128].

In biomass combustion the release of volatiles can overlap with the drying stage, therefore immediately releasing combustible gaseous compounds. These stages are separated for coal. The release of volatiles is also slower for coal which results in heterogeneous gas-solid reactions. Differences in volatility for different fuels are due to the "architecture" of the fuel. As already mentioned wood is composed by cellulose, hemicellulose, lignin and extractives, and cellulose is the dominant polysaccharide. Coal molecular structure consists of clusters of aromatic components fused to each other. The oxygen contained in coal is also present in less reactive groups. Therefore aromaticity and the way in which oxygen is present in the fuel determine the fuel reactivity. These characteristics affect the combustion typically

promoting early ignition and increasing the overall rate of combustion depending on the technology used [129].

The main technologies used in biomass power generation include combustion in fixed and moving grate, suspension fired boilers where biomass particles of 1-2 mm burn satisfactorily, fluidised beds with biomass fuel size ranges of 5-50 mm and gasification [22]. Van den Broek et al. [130] discussed the major advantages and disadvantages of these technologies and found that no one technology is comparatively better, and that the suitability of technologies depends on local circumstances such as fuel price, emission standard and revenues from electricity sales.

Many of the technologies used with biomass were originally optimised for combustion of coals. However biomass properties affect the performance of traditional combustion systems, i.e. the amount of primary and secondary air, the temperature gradients in the furnace, gas emissions, burnout times and efficiency, flame stability and extinction. The ignition behaviour also influences the location of fuel injection and the inlet air temperature.

Other concerns in power generation are related to handling issues. During storage moisture content, calorific value and flow properties can be affected by microbiological activity. Decomposition of biomass can increase the temperature of the stockpile and lead to auto ignition and fires [23, 24, 131-133]. Biomass is usually milled in purpose built milling plants using existing or slightly modified hammer mills, vertical spindle mills, tube ball mills or fan beater mills depending on the biomass used. The mills are especially susceptible to dust explosions due to combustible volatiles being released at much lower temperatures for biomass than for coal. The safety precaution is normally inerting or keeping the amount of fuel well above the rich flammability limit during normal operation, and to keep the temperature of the mill low during start-up or shut down operations. Coal can propagate flames for concentrations 30 times fuel-rich [134]. However, other researchers were unable to find rich flammability limits of coal and other dusts and the possibility of dusts not having a rich limit has been proposed [81]. However, it has been observed that the devolatilisation rate is a limiting factor as concentration increases [135]. Researchers have constantly found flaws in experimental methods to determine rich limits, however, it has been established that high dust loading inhibit propagation and that the excess fuel does not take part in the exothermic combustion stage of the explosion and instead acts as a heat sink [136]. Due to the low bulk density of biomass and the limitations of the standard methods for explosion characterisations there is no data in the literature of the rich limits of biomass and

torrefied biomass powders used in power generation, and therefore the precaution of running the millers at rich mixtures could be insufficient and could lead to severe explosions.

2.3.1.2. Torrefaction

Many of the issues and challenges in the generation of power using biomass fuels discussed in the previous section can be mitigated by pre-treating materials through chemical processes. The process that has perhaps attracted more attention is "torrefaction". It consists on subjecting biomass to temperatures of 200-300°C in an inert atmosphere for a certain amount of time. Biomass therefore undergoes mild pyrolysis, during which moisture and volatiles are released. The target solid product should keep as much chemical energy as possible. Therefore the mass and energy yield are important parameters. Typical values are around 90% for energy yields and around 70% for mass yields. The main components of biomass (cellulose, hemicellulose and lignin) decompose depending on the torrefaction temperature and residence time. The degradation temperatures of hemicellulose, cellulose and lignin have been reported to be about 150°C-350°C, 275°C-350°C and 250°C-500°C, respectively [137-139]. The degree to which these components decompose determines the properties of the material produced. Generally, the end product has properties similar to those of low rank coals: the fuel becomes hydrophobic, more easily grounded, more energy dense, and less susceptible to degradation. The improvements have a positive impact on transport costs and storage performance [16, 123, 140, 141].

Batidzirai et al [17] examined the techno-economic features of torrefaction for power generation and found that torrefied pellets could be competitive with traditional pellets in the future. However, for reactors to be commercially available, these need to be optimised in order to achieve a consistent, fully hydrophobic and stable product, providing flexibility of feedstocks and optimum energy densities. In the nearer future torrefaction appears to be a viable option for the production of fuels for domestic use. A number of successful projects have been developed in Europe using a wide variety of feedstocks. In the UK there is a growing market for torrefied fuels due to the Renewable Heat Incentive which started a new scheme for domestic heat in 2014, which offers a potential for torrefaction up-scaling, saving on fuel bills and decreasing carbon emissions. This incentive covers biomass boilers where both biomass and torrefied biomass could be used as fuels (as long as they comply with sustainability requirements and are sourced from authorised suppliers available from a specially created "Biomass Supplier List"), and also solar panels and heat pumps.

A lot of the research on torrefaction has been devoted to investigate the characteristics of solid end products [123, 139, 140, 142-146]. Torrefaction usually increases the carbon, fixed carbon and ash contents and calorific value of biomass materials, whereas hydrogen and oxygen, moisture and volatiles are decreased with torrefaction severity [143, 146]. In addition, chlorine content, capable of heavily corroding boilers, can also be reduced with torrefaction [147]. The morphology of particles before and after torrefaction has also been studied. Structural changes depend on torrefaction temperatures. Cracks and fissures are formed as the biomass starts to lose its bound fibrous structure. At medium to high torrefaction temperatures surface area and pore volume decrease due to softening and plastic deformation of the pores and carbonisation of the particles. On the other hand, at lower temperatures both surface area and pore volume have been observed to increase as volatilisation of gas products results in the generation of large pores [144, 148].

After torrefaction, less energy is required for grinding [141, 142]. Particle size distributions of torrefied samples contain finer particles the more severe torrefaction gets. Bulk density has generally been found to remain similar as that of the raw biomass [145].

2.3.1.3. Co-firing

Both biomass and torrefied biomass can be mixed with coal to fuel existing plants. This practice is known as co-firing. Biomass co-firing is normally carried out in existing large pulverised coal power boilers [125]. It is a straightforward and cost-effective way of increasing the share of renewables in the energy mix and decreasing greenhouse gas emissions [10]. Plants using low proportions of biomass need little or no adjustments to operate without losing efficiency. Torrefaction allows large biomass proportion blends with minimal change to existing coal systems and important reductions in CO_2, SO_x and NO_x emissions [149, 150].

Additional benefits of co-firing include fuel cost decrease, minimisation of waste and solid and water pollution (depending on the chemical composition of the biomass used) and reduction of ash deposition and fouling issues normally encountered with biomass [151].

Co-firing of biomass and coal can take place in three different ways: using separate feed lines and separate burners for each fuel; separated feed lines but common burner or else using common feed lines and common burners with previously mixed biomass and coal blends [152]. Most UK co-fired plants adopted the co-milling approach (coal and biomass are milled simultaneously in existing coal mills). Both fuels are more commonly blended on site, which implies that fuel reception and

handling facilities, are separate [153]. It is therefore as important to know the explosion and combustion characteristics of the isolated fuels as well as those of the blends.

2.3.2. Reactivity of biomass, torrefied biomass and coal

The reactivity of coal, biomass and torrefied biomass has been investigated by many researchers using different methods [154]. These methods are flexible on their test conditions and gas atmospheres and can recreate combustion or pyrolysis conditions by using air or inert gases during the heating of samples. Some of these methods use low heating rates and the resulting weight loss and rate of weight loss curves can be used to derive reactivity parameters such as the activation energy (E_a) or the peak temperature (T_{max}), that is, the temperature at which the rate of mass loss is maximum during devolatilisation [155]. The lower the activation energy and peak temperature, the more reactive the material is.

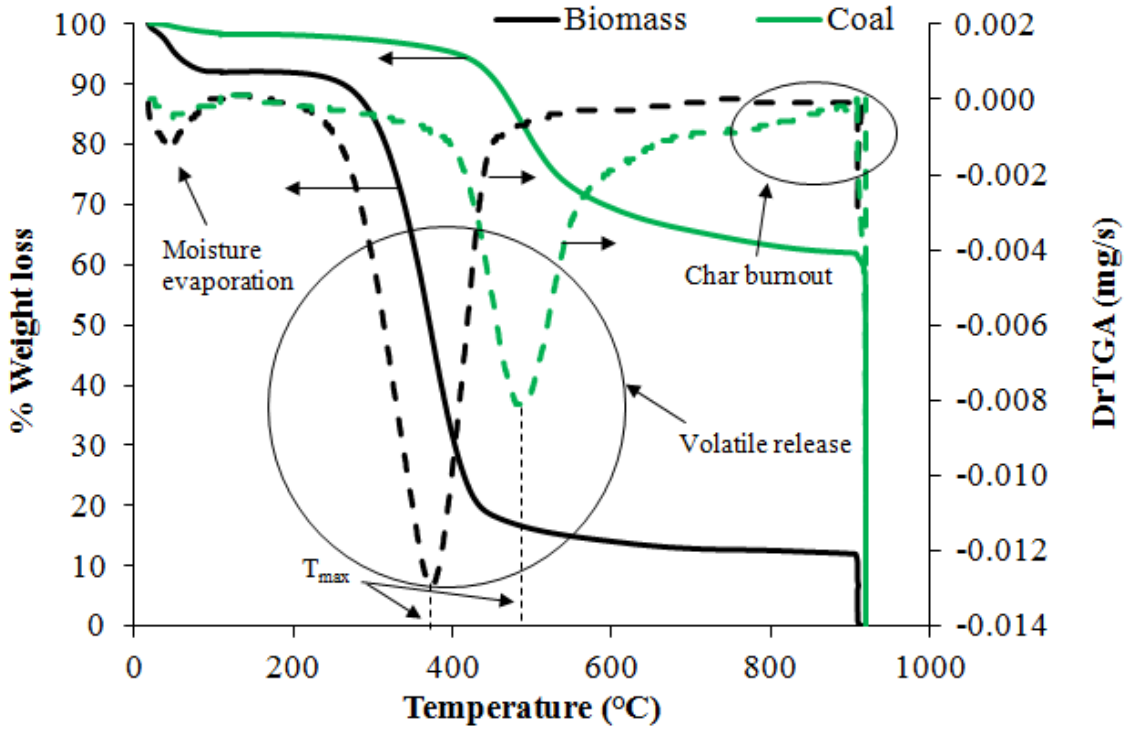

Figure 2-11. Weight loss and rate of weight loss curves during combustion of biomass and coal using TGA technique

Combustion of biomass is broadly separated into three stages which are depicted in TGA and DrTGA curves, these are shown in Figure 2-11: evaporation of moisture, release of volatiles and combustion of fixed carbon upon injection of oxygen at 900°C. In comparison to coal, biomass has a lower burnout and ignition temperature, higher combustion rates due to higher volatile content, and lower ash content. The burning rate and the products of combustion vary depending on the heating rate

[156]. It has been observed that faster temperature rise and higher final temperatures in pyrolysis of biomass promote the formation of gaseous yield and limit the char yield [157-159]. This occurs because the time available for primary volatile products to engage in secondary reactions (repolymerisation, cracking) that lead to char formation is heavily reduced. In the particular case of pure cellulose, no char is produced at all at high heating rates and temperatures [160]. Back in 1973, Palmer suggested that cellulosic materials are likely to devolatilise completely at high heating rates typical of dust explosion flames (10^4 to 10^5 °C/s) [161].

It has also been pointed out that upon rapid heating (flash pyrolysis) of coal, a greater quantity of volatile material is produced above the proximate volatile matter obtained through TGA analysis [162-164]. This has also been found even for torrefied wood [165].

In summary, the yield and composition of the volatiles evolved strongly depends on the material, heating rate and ultimate temperature. This is relevant to the case of explosions, as during these events the heating rates are much faster than the ones used in TGA and therefore, reactivity parameters are not necessarily related to volatile matter measured by the TGA proximate method. This is depicted in Figure 2-12, where the K_{St} values published for a few different coals are plotted against their corresponding volatile matter content measured through TGA techniques. There is hardly a correlation between them.

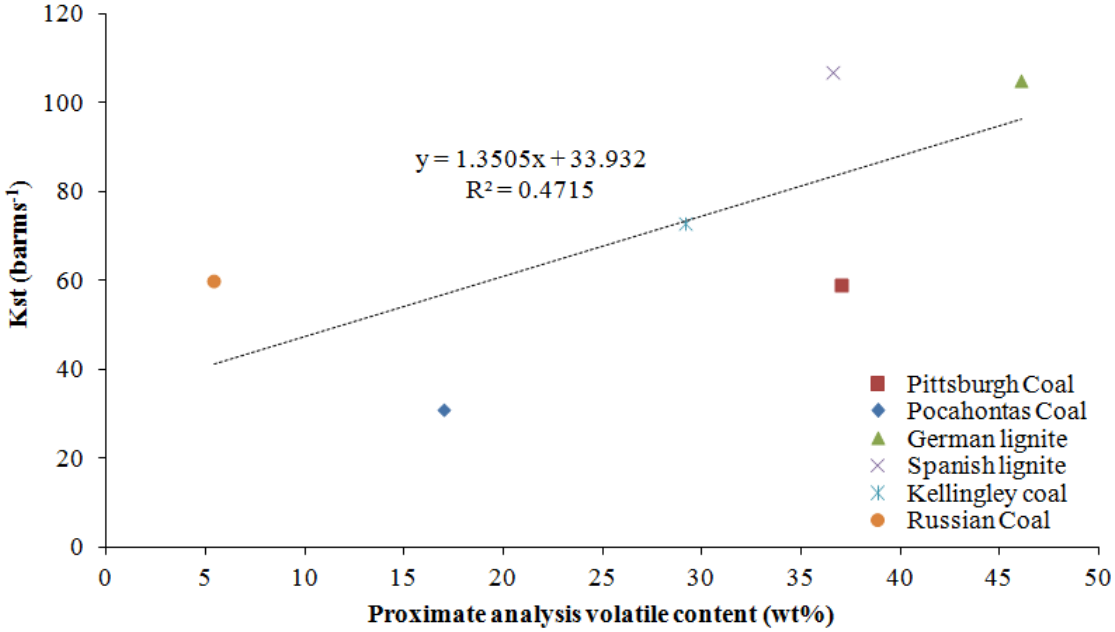

Figure 2-12. Correlation between K_{St} and volatile content determined by TGA [82, 86, 107, 166]

Neoh et al [167] measured and correlated the total volatile release for a number of coals at high heating rates (10^5 K/s) and high temperatures (1600-2400 K) with the elemental composition of a range of coals. The best correlations are shown in the following equations:

$$V.Y_{1600K} = 48.1\left(\frac{H+2O}{C+S}\right) - 1.41 \tag{2.7}$$

$$V.Y_{2400K} = 52.6\left(\frac{H+2O}{C+S}\right) + 6.89 \tag{2.8}$$

Where H, O, C and S are the atomic ratios to carbon of hydrogen, oxygen carbon and sulphur obtained from the ultimate analysis.

Figure 2-13, shows the correlation for K_{St} and the volatile yield obtained from Eq.(2.8) at high heating rate and 2400 K. It is appreciated that there is a much better correlation with the volatile yield at high temperature and heating rate than between K_{St} and the volatile matter obtained through TGA techniques.

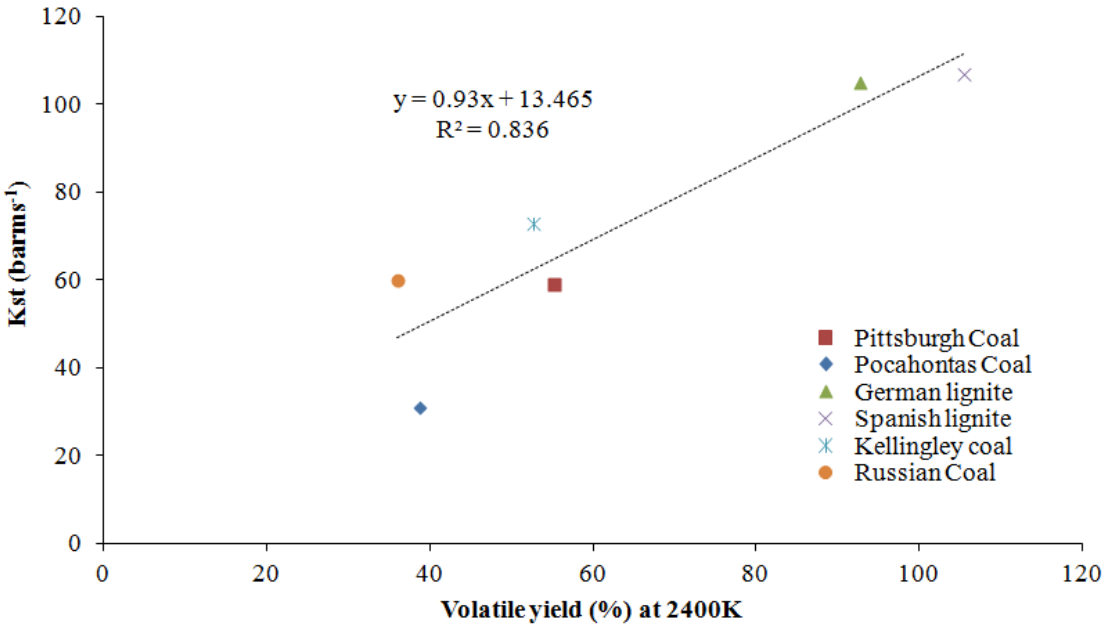

Figure 2-13. Correlation K_{St} and volatile yield at high heating rate and high temperature (2400K) [82, 86, 107, 166]

Di Benedetto et al [168] created a model in order to estimate K_{St} and laminar burning velocity appropriately using fast pyrolysis data (gas products obtained at high temperatures and heating rates) for cornstarch, cellulose and polyethylene. The results differed from the experimental measurements however this was largely due to the effect of turbulence in experimental measurements.

Slow pyrolysis (TGA) techniques have been used to compare the reactivity of biomass and torrefied biomass fuels [142, 143, 169]. Results have shown that torrefied materials present higher activation energies (E_a) which increase with torrefaction severity, and therefore the more severe is torrefaction, the less reactive the materials appear to be. Fast pyrolysis experiments conducted by Li et al [170] also found torrefied biomass to become less reactive (increased E_a) with torrefaction severity. It was similarly found as for coal that the volatile yields increased above the proximate analysis volatile yields. The increase was greater for the raw biomass. It is suggested that this behaviour is due to more torrefied samples containing less cellulose [170].

Li et al [170] also studied the gaseous species produced from biomass at high heating rates and high temperatures. CO and H_2 were found to be the main components released, followed by small quantities of CH_4 and CO_2. The composition of volatiles is said to be more dependent on the final temperature and residence time than on the heating rate [171]. H_2 presence in the reacting gaseous products could be affecting the flammability of dusts since H_2 has a very lean lower flammability limit (Ø=0.14).

Similar studies are present in the literature for the flash pyrolysis or combustion of coal [164, 172], the gas yields depend on the type of coal and heating rate. At high heating rates the presence of hydrocarbons decrease and CO_2 and CO are produced in greater amounts. The lean limit of CO is found at Ø=0.67 [33], and CO_2 is non-flammable which could lead to coals having richer flammability limits.

Biagini et al. [173] investigated the chars obtained from high temperature and high heating rate pyrolysis of ligno-cellulosic materials. The chars were different from the parent materials showing fissures, holes and bubbles formed during devolatilisation (Figure 2-14). Particles also seemed to swell during pyrolysis. Similar results were found for chars formed during combustion [174].

Coal chars have also been investigated in numerous occasions under combustion atmospheres, and these have been found to present rounded hollow or cellular structures with cenospheres [88, 164, 172].

Devolatilisation of biomass is also affected by particle shape and size. Overall reaction rates and volatile yield especially for larger particles (>300μm) are affected. Near spherical particles lose mass more slowly and yield less volatiles than cylinder or flake-like particles [175].

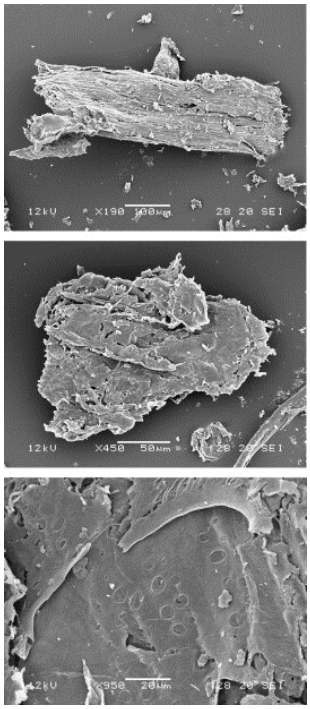

Figure 2-14. Wood char after fast pyrolysis (HR=20,000°C/s, T=1400°C). Source: [173]

Combustion characteristics of coal/biomass blends have been studied by Gil et al [176] and Haykiri-Acma et al. [151] using thermogravimetric methods (low heating rates) with oxidative environments. Results can vary from combustion to pyrolysis due to additional phenomena that occur in the presence of oxygen [177]. Haykiri-Acma et al. used blends of low proportion of biomass (hazelnut shells) and found that for blends with <10% biomass the combustion characteristics were dominated by the coal. Otherwise the effect of biomass presence was appreciable, promoting faster devolatilisation and early ignition at lower activation energies. Rates of devolatilisation were not higher than for biomass on its own. Gil et al. used blends with higher proportions of biomass and also found similar results where there were no interactions between the components of the blends or synergistic effects during combustion. However other studies have shown a synergistic behaviour of biomass/coal blends [178-180]. Similar studies under pyrolysis conditions are available for blends of torrefied biomass and coal. Lu et al [181] found an additive behaviour in the pyrolysis of torrefied wood and coal blends. Studies from Goldfarb et al. [182] using an oxidative environment and slightly higher heating rate (100°C/min rather than 20°C/min) found synergistic effects in terms of activation energies but notes that on a global reaction level the additive assumption is valid since the rate of devolatilisation can be modelled as a function of the individual contributions of coal and torrefied biomass.

In summary, results suggest that there could be dependence not only on the fuels used, but in the experimental conditions such as heating rates, or whether they are performed in oxidative or pyrolysis environments. All of which will be relevant when assessing the combustion behaviour in explosion conditions.

2.3.3. Difficulties in measuring biomass explosibility

As pointed out in Chapter 1, explosion data available in the literature for biomass are scarce and inexistent for torrefied biomass. The reason behind the lack of data for these materials lays on the challenges that characterising the explosibility of these types of dusts pose to the current explosion characterisation methods (1 m^3, 20 L sphere). Many biomass materials are fibrous and have low bulk density (~200 kg/m^3) and these cause problems with the dispersion system and dust holder.

2.3.3.1. The dispersion system

Fibrous materials tend to choke the delivery system when the dust is placed in a dust holder external to the explosion chamber (Figure 2-15); this is recognised by the standards [30, 183] and examples of special dispersers are proposed. The so called "rebound nozzle" is similar to the one used in the Siwek 20 L sphere. An in-vessel dispersion cup is another proposed option (Figure 2-16). These are meant to yield identical results to the standard system. Previous work by the Leeds group was concerned with the calibration of new dispersers for biomass powders. This work tested the dispersers proposed in the standard plus a wall mounted spherical perforated grid nozzle.

A turbulence factor β, analogous to the one used in venting correlations, in order to account for turbulence induced by obstacles in the path of the flame, was determined to account for the turbulence induced by the dispersion of dust in the explosion vessel. Explosion tests using 10% methane in laminar and turbulent conditions were performed. Turbulence was introduced by dispersing air from the dust holder. The turbulence factor β was found as the ratio of K_G in turbulent condition to K_G in laminar condition. Comparable ratios were also found for other reactivity parameters such as maximum pressures and flame speeds. All dispersers were tested with 10% methane gas in turbulent and laminar conditions at different ignition delays. This way the dispersers were calibrated to provide the same β factor as the standard C-ring injector at the standard ignition delay of 0.6 s. However it was found that the dispersion cup failed to provide spherical flame propagation due to non-uniform dispersion of dust within the vessel. The rebound nozzle provided higher MEC measurements. In addition at high dust loadings (500-1500 g/m^3) a lot of dust remained in the dust holder undelivered. The spherical nozzle provided good agreement with the results from the standard system and therefore this design has

been used in the present work for the characterisation of fibrous biomass and torrefied biomass, more details are given in the Chapter 3.

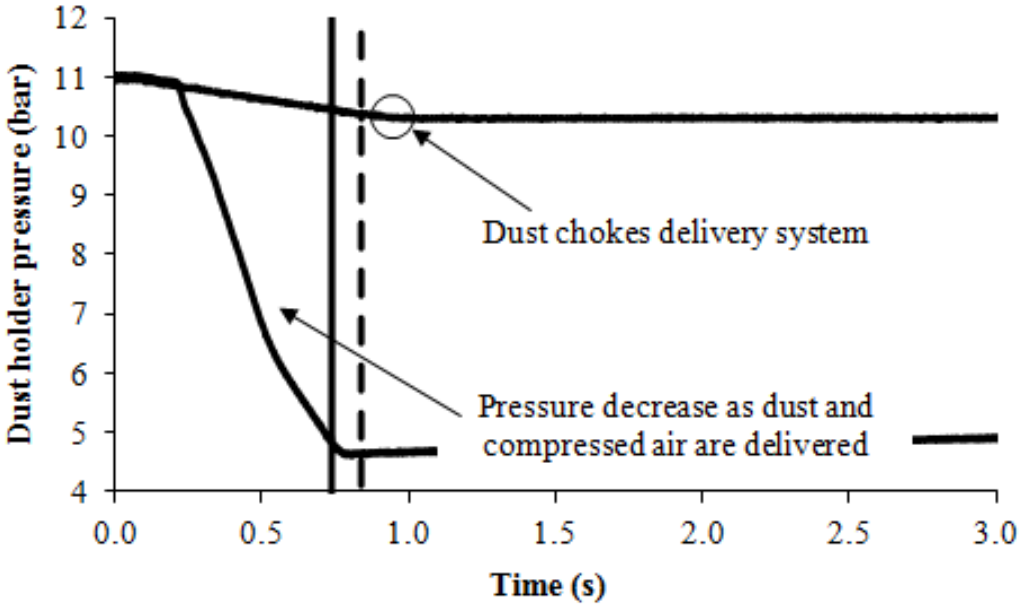

Figure 2-15. Dust holder pressure traces with fibrous dust delivered and undelivered due to system choking

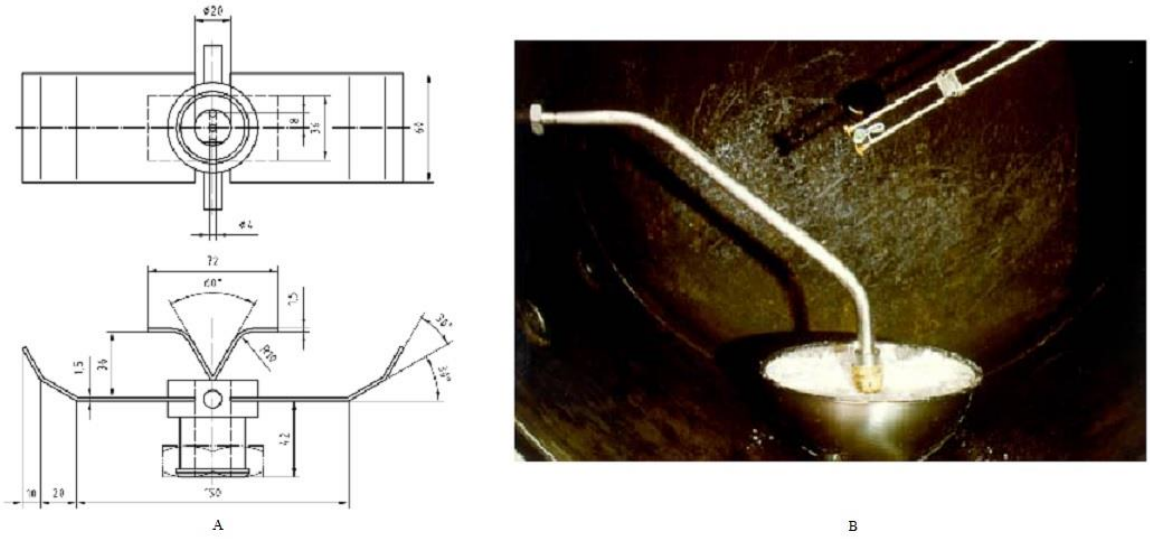

Figure 2-16. Special dispersers proposed in European standard: rebound nozzle (left) and hemispherical disperser (right). Source: BS14034

Other researchers have faced the problem of delivering fibrous dust into explosion chambers, and therefore different dispersion nozzles were tested [184] with the aim to achieve comparable results with the standard system. However, it was only ensured that K_{St} values were comparable whereas other parameters such as maximum pressure or the most reactive concentrations failed to match the results with the standard system.

2.3.3.2. Dust holder for low bulk density dusts

In addition to the delivery problems with fibrous woody biomass, due to their low bulk density, the dust holder cannot hold enough quantities of biomass dust to allow full characterisation of materials. The standard dust holder consists of a volume of 5 L in which the dust sample shall not exceed ¾ of the dust container in order to allow correct pressurisation. According to the European standard if this cannot be achieved, two holders of 5.4 dm^3 shall be fitted in parallel. In order to characterise samples of biomass materials of low bulk densities an extended dust holder is needed. The extended volume suggested by the standards could only hold 1215 g/m^3 of a sample with a bulk density as low as 150 kg/m^3. Authors encountering this problem when using the 20 L sphere method opted for placing part of the sample in the dust holder and placing the rest of the dust in the bottom of the vessel [82, 185]. Unfortunately, none of these solutions allows measurements of upper flammability of most dusts, which have been reported to be generally around 2000-3000 g/m^3 but also as high as 13000 g/m^3 [186].

When the dust holder volume, or pressure, suffer modifications the velocity of fuel delivery changes. Therefore the turbulence levels change as well. This was investigated by Sattar et al. [187] and concluded that if the new 10 L volume was pressurised at 20 bar (like the standard 5 L holder) the dispersion time increased, whereas, if the volume was pressurised to 10 bar then the delivery time was equal as the standard system. Ignition delays and the time at which the valve started closing were varied as well and it was found that the optimum ignition delay was 0.6 s (like the standard) whereas the valve needed to remain open for a longer time (0.65 s) in order to allow all dust sample to flow into the vessel. Sattar et al. recognised that the longer opening of the valve could result in explosion pressure going into the dust holder which could in turn result in pressure piling and violent explosions in the dust holder. Results for different dusts showed good agreement with the standard 5 L system. Barknecht [72] had previously used an extended dust holder, and recommended a longer ignition delay for the extended volume (900 ms), however, the maximum rate of pressure rise was found at different concentrations and therefore the results were not comparable to the standard.

2.3.4. Explosion characteristics of biomass

Despite the aforementioned difficulty in the measurement of explosibility data for biomass, wood and agricultural products dusts have been known to be explosive for more than a hundred years [188]. Early studies even showed that the hazards posed by some biomass materials could be higher than that of coal [189]. Most of the early studies investigated the explosion characteristics and the effects of dust properties

and test conditions, and were conducted using the Hartmann tube. Table 2-2 shows the more recent explosion characteristics for biomass type materials published in the literature. The validity of some of these results is questionable as in some cases there is no reference to the practical issues mentioned in section 2.3.3. Furthermore, where the issues were recognised, calibrations were only provided for K_{St} values.

Table 2-2. Literature data on explosion characteristics of biomass dusts

Fuel	K_{St} (barm/s)	P_{max} (bar)	MEC (g/m^3)	Method	Reference
Cork	179	7.2	40	20 L	[87]
Walnut shells dust	105	9.4	70		
Pine nut shells dust	61	8.9	-	1 m^3	[86]
Pistachio shells dust	82	9.3	90		
Wood	115	8.6	30		
Bark	132	9.0	30		
Forest residue	87	8.6	60		
Spanish pine	44	7.7	90	20 L	[82]
Barley straw	72	7.9	90		
Miscanthus	53	7.8	120		
Sorghum	41	7.3	120		
Rape seed straw	23	6.7	210		
Wood dust (beech and oak mix)	136	7.7	-	20 L	[190]
Forest residue (bark and wood)	92	9.1	20	20 L	[89]
Wood dust	87	7.8	-	20 L	[191]
Wood dust, chipboard	102	8.7	60	20 L/1 m^3	[58]
Wheat grain dust	112	9.3	60	20 L/1 m^3	[58]
Olive pellets	74	10.4	125	20 L/1 m^3	[58]
Cellulose	66	9.3	60	20 L/1 m^3	[58]
British Columbia wood pellets	146	8.1	70		
Nova Scotia wood pellets	162	8.4	70	ASTM E1226	[192]
Southern yellow pine wood pellets (USA)	98	7.7	25		
Wood dusts	208	9.4	-	1 m^3	[72]
Fibrous wood	149	8.2	20	20 L	[102]
Sawdust	115	9.0	-	1 m^3	[76]

There is no data available in the open literature for torrefied biomass. There is also very scarce data for the explosibility of biomass-coal mixtures, and none for mixtures of torrefied biomass and coal. Wilen et al. [82] tested a mixture of wood dust and German lignite and a mixture of barley straw and Spanish lignite in ratios of 25% biomass, 75% lignite. The results, summarised in Table 2-3 , show that the mixtures remained less reactive than the most reactive of the pair used for the mixture in terms of K_{St} and only in one specific case [191] the maximum explosion pressure was higher than either biomass and coal.

It is therefore not clear if the reactivity of a mixture of coal and biomass could be more reactive than either of the components of the mixture. Although co-firing mostly takes place in low proportion of biomass, since there are more attractive economic incentives the more biomass is used, samples of different proportions of biomass should also be assessed to establish whether there could be synergistic effects on the reactivity of the mixture.

Table 2-3. Literature data on explosion characteristics of biomass-coal mixtures

Fuel	K_{St} (barm/s)	P_{max} (bar)	MEC (g/m^3)	Method	Reference
Wood dust	115	8.6	30	20L	[82]
German Lignite	146	8.6	60		
Mixture (25/75)	111	8.4	90		
Barley straw	72	7.9	90		
Spanish lignite	164	8.6	90		
Mixture (25/75)	137	8.4	150		
Wood dust	87	7.8	-	20L	[191]
Black lignite	105	7.7	-		
Mixture (25/75)	104	8.8	-		

The main issues with characterisation of fibrous dusts in the 1 m^3, described in detail in sections 2.3.3.1 and 2.3.3.2 are only described in some of the publications included in Table 2-2. Wilen et al. [82] calibrated new dispersion systems by adjusting the ignition delay until the set-up was found to yield the same K_{St} value as the standard system, however it was not investigated if the changes altered the rest of properties, such as the maximum pressure. Garcia-Torrent et al. and Conde Lazaro et al. [89, 191] used extended dust holders of 25 L only for high dust loadings in their hyperbaric explosion tests. The ignition delay was also modified as well as the dispersion pressure. In turn, it was illustrated that using different ignition delay and dust holder volume yielded results that were not comparable to the standard system

due to varied turbulence levels. The issue of dust deposits after the explosion in both the explosion chamber and dust holder was recognised and even the concentrations were corrected for the dust that remained undelivered in the dust holder. Large dust deposits in the explosion chamber after explosions were suggested to be due to a fast quenching of the flame produced by the depletion of available oxygen. However, if this was true maximum pressures should be lower than expected which was not shown in this case.

Sattar et al. [86] realised that MEC for CHO dusts happened at lower equivalence ratios than for typical hydrocarbon dusts and gases (Table 2-4).

Table 2-4. Explosion characteristics and corresponding equivalence ratios for various dusts

Fuel	Ø=1 (g/m^3)	P_{max} Concentration (g/m^3)	P_{max} Ø	MEC ($Ø_{MEC}$)	Reference
		K_{St} Concentration (g/m^3)	K_{St} Ø		
Cellulose $(C_6H_{1.67}O_5)_n$	235	500	2.13	60(0.26)	[58, 72]
		500	2.13		
Lycopodium $(CH_{1.65}O_{0.22})$	115	427	3.71	42(0.37)	[77, 96]
		427	3.71		
Corn flour $(CH_{2.01}O_{0.80})$	212	635	2.99	67(0.32)	[193, 194]
		635	2.99		
Forest residue $(CH_{1.53}O_{0.56})$	177	683	3.86	30(0.17)	[89]
		1367	7.72		
Cork dust $(CH_{1.62}O_{0.70})$	204	378	1.86	40(0.20)	[195]
		426	2.09		
Polyethylene $(C_2H_4)_n$	81	500	6.17	20(0.25)	[61, 107]
		500	6.17		
Bituminous coal $(CH_{0.84}O_{0.66})$	102	253	2.48	80(0.78)	[98]
		368	3.61		
Methane (CH_4)	70	74	1.06	32(0.46)	[37, 196]
		74	1.06		
Propane (C_3H_8)	77	86	1.13	32(0.42)	[37, 196]
		86	1.13		

These works concluded that the model of dust flame propagation for coal through devolatilisation and burning of volatiles, if these are mainly CH_4, mixed with air is not compatible with biomass having such low MEC (Ø~0.3). In addition, the methodology used allowed the derivation of flame speeds and burning velocities of nut dusts which were found to be between 2.5 and 4.5 times higher than those for coal. Flame speed and laminar burning velocity data are summarised in Table 2-5.

Table 2-5. Literature values for biomass flame speeds and burning velocity

	$(S_F)_T$ (m/s)	$(S_F)_L$ (m/s)	S_L(m/s)	Ref.
Kellingley coal	1.2	0.3	0.04	[86]
Walnut shells	5.1	1.26	0.13	[86]
Pine nut shells	3.8	0.94	0.11	[86]
Pistachio nut shells	3.7	0.91	0.1	[86]
Lycopodium	-	-	0.47	[51]
Corn starch	-	-	0.24	[197]

Previous work [86-88, 107, 195] investigated the residual dust found inside the explosion chamber after a test. The particle size of original and residue samples was compared, and in some cases bigger particles were present. Researchers concluded that there was preferential burning of fines. SEM images showed burnt particles (char) with the presence of blow out holes for the release of volatiles.

Further work into the residual deposits matter by the Leeds group [35] postulated that the residue found after explosion is formed from dust blown ahead of the flame by the explosion wind, therefore creating a layer of dust in the walls. This was confirmed by comparing the rate of pressure losses for dust and gas explosions in the 1 m^3 vessel. The pressure loss in dust explosions was much slower which suggests that the layer of dust acted as an insulation layer.

Amyotte et al [102] resolved the delivery issues of fibrous dust by simply placing part of the dust directly inside the vessel when high dust loadings of large size flocculent samples were tested. However, using this method dispersion patterns could be different in each test and it is actually shown that the results vary for maximum pressure. The variability for K_{St} is unfortunately not shown, but as K_{St} is more susceptible to dissimilar dispersion patterns the variability of this parameter

could be even larger. However Amyotte's work already showed that biomass samples containing large fraction of big particles (59% by weight of particles >500μm) were still explosible reaching 7.2 bar maximum explosion pressure and a K_{St} of 41 barm/s. This is noteworthy as most dusts usually show much more reduced pressures at those particle size ranges. This can also be observed in Figure 2-17 where maximum explosion pressures rapidly decrease for particles of dust of around 500 μm, for all dusts except for cork dust.

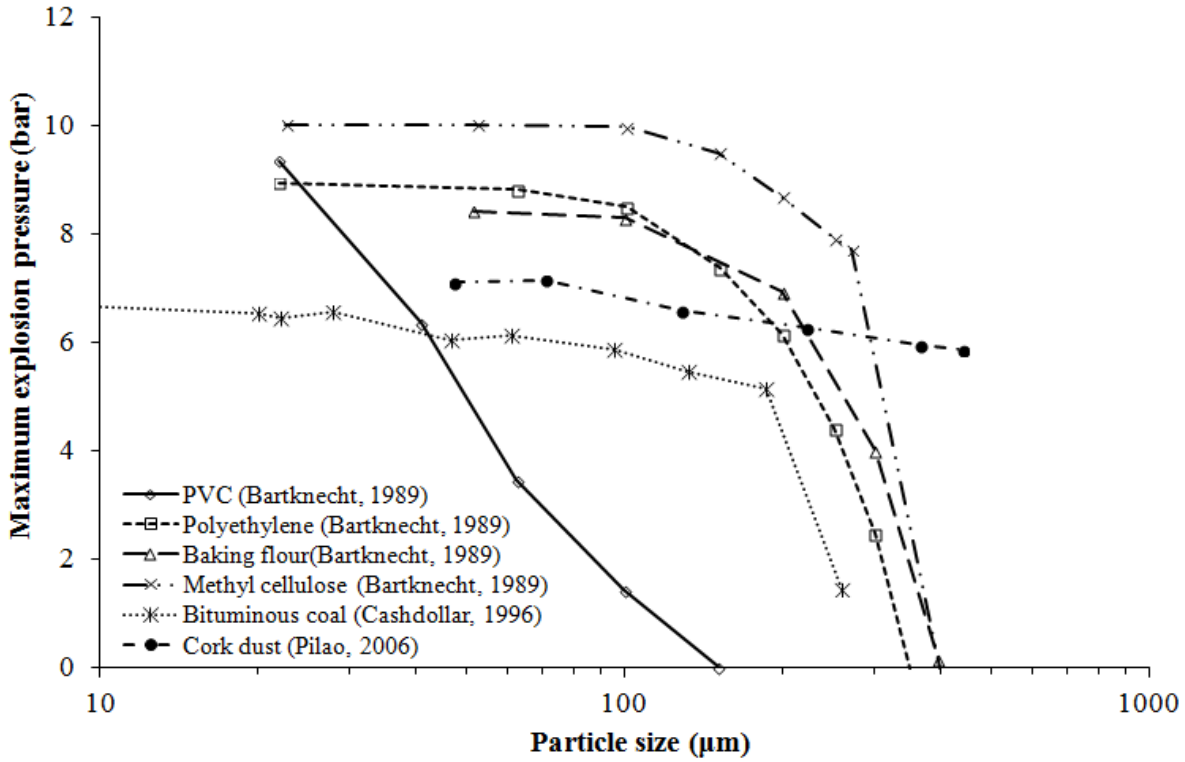

Figure 2-17. Maximum explosion pressure as a function of particle size

Particle size has been thoroughly investigated also with wood and agricultural products and it has become clear that particle size affects the K_{St} and MEC of biomass samples specially. Slatter et al. [198] found, using a Hartmann tube and pulverised pine wood pellets in different size ranges, that the presence of fine particles widens the flammability limits. However, samples of narrow particle sizes such as 300-500 μm still could ignite at rich mixtures, which is not typical of any other dust, or aerosol droplets [199].

MEC for biomass have been found at equivalence ratios with respect to the solid stoichiometry which were unusually lean. For a more correct approach the stoichiometry of the actual gaseous mixture in the flame should be used. Both hydrogen and ethylene have their flammability limits between Ø=0.12-0.14 and Ø=0.38-0.48 respectively (depending on the measurement method used). These equivalence ratios are more similar to CHO dusts and has been suggested in the

literature that biomass dusts [34, 86, 200] could be yielding high amounts of these gases upon heating in the flame front.

In summary, biomass materials are different from other dusts in that they burn at leaner mixtures and large particles still burn with little effect on maximum pressure and lean flammability limits.

The data available in the literature for biomass is scarce and present doubts as to their reliability. The explosion characteristics of torrefied biomass and mixtures of coal and biomass are unknown. The following chapters provide details on the adjustments and calibrations necessary for producing valid data on the explosibility of biomass materials and contain series of results on the explosibility of torrefied biomass and biomass-coal mixtures, as well as MEC measurements from a developed method using a modified Hartmann tube.

Chapter 3 EXPERIMENTAL METHODS

CONTENTS

3.1. Fuels and sample preparation

Biomass, torrefied biomass and coal samples were used for this work. A number of samples were used for Minimum Explosible Concentration (MEC) determination in the Modified Hartmann tube (Chapter 4). Samples used in the Hartmann tube were materials that could flow through the standard injection system in the 1m^3 ISO vessel to allow comparison of MEC results in the Hartmann and 1 m^3 vessel, and included: reference dusts (corn flour, supplied from Tesco's supermarket and lycopodium supplied from Sigma Aldrich), brittle biomass dusts (walnut shells, pistachio nut dusts, both shipped from Pakistan), one raw fibrous biomass (pine wood mixture dust, supplied by Drax), one torrefied biomass (torrefied Norway spruce, supplied by Sea2Sky Energy UK Ltd.), and off-spec torrefied wood pellets with its corresponding parent material. Furthermore, the modified Hartmann tube was used for a study on the effect of torrefaction severity in explosibility and reactivity. In this study a series of torrefied Norway spruce, torrefied to different degrees, supplied by the University of Umeå (Sweden) were used.

Fibrous biomass, torrefied biomass and coal samples were used for explosion characterisation in the 1 m^3 ISO vessel (Chapters 5 and 6). Where possible, torrefied

biomass samples and their corresponding untreated material were sourced. Due to commercial sensitivities it was not possible in most cases to source materials of known origin and torrefaction conditions. Also, due to the big quantities of sample required (20 kg) it was not possible to source enough quantities for full explosion characterisation. However, in these cases the samples were used for establishing trends for comparison. Kellingley coal (supplied by Drax) and Colombian coal (supplied by ESB Energy International) were also used for comparison. A list of biomass samples used for explosion characterisation with specifications (when available) is shown in Table 3-1.

Table 3-1. Biomass samples tested in the 1 m^3 ISO vessel

Sample Name	Supplier	Specifications
ECNR	ECN	Raw "whole tree" wood
ECNT	ECN	Torrefied (T=250°C) "whole tree" wood
RWER	Topell through RWE	Raw wood
RWET	Topell through RWE	Off specification torrefied wood pellets
S2SR	Sea2Sky Energy UK Ltd.	Raw Norway spruce wood
S2STS	Sea2Sky Energy UK Ltd.	Torrefied Norway Spruce (T=260°C, t=13 min). Milled to <75µm (ABT Reactor, Gotland, Sweden)
S2STA	Sea2Sky Energy UK Ltd.	Torrefied Norway Spruce (T=260°C, t=13 min). Milled to <60µm (ABT Reactor, Gotland, Sweden)
S2STB	Sea2Sky Energy UK Ltd.	Torrefied Norway Spruce. Milled to <60µm (River Basin Enegy Reactor, Wyoming, USA)
NBER	New Biomass Energy (USA)	Southern pine harvested in Mississippi (USA)
NBET	New Biomass Energy (USA)	Torrefied wood pellets (T~300°C). Torrefaction details not disclosed by supplier.
Pine Wood Pellets	ESB Energy International	Ground pellets

Samples of all residues found after explosion were collected and quantified. Residual samples collected after most reactive tests were analysed in the same way as the original samples prior to explosion.

Most samples were supplied either in wood chips or in pellets. All samples were ground to a particle size that would allow free flowing through the 1 m^3 dispersion

system. This proved to be possible with particle size distributions in which 90% of the particles were smaller than 150 μm. Otherwise, for large concentrations, too much powder remained in the dust holder undispersed. Milling of chips and pellets required using different grinding devices in stages. In the first stage a Retsch Cutting Mill SM100 or a Retsch Rotor Beater Mill SR200 were used to mill samples down to <500 μm. Then samples were further milled in a Retsch Ultra Centrifugal Grinding mill ZM100 to <60 μm, which is also the requirement for explosion characterisation according to the standard procedure [31]. It was found that the milling process could affect the sample's properties and therefore, where one of the same sample was more finely ground it was regarded as a different sample. The mills were thoroughly cleaned prior to use to avoid contamination. All sample analysis was conducted after milling. Samples were homogeneous as has been proved by good repeatability of results. Samples were stored in sealed containers.

3.2. Fuels Characterisation

All samples and residue samples were analysed for their chemical composition as well as for their surface morphology, surface area and porosity, particle size distribution and density.

3.2.1. Elemental Analysis

The percentage by weight of carbon, hydrogen, nitrogen and sulphur was measured using a CE Instruments Flash EA 2000 instrument. Biomass samples required less than 4 mg, whereas coal and torrefied biomass required less than 3 mg of sample. This difference was due to coal and torrefied samples burning slower than biomass and needing a longer oxygen injection time. Vanadium pentoxide (V_2O_5) was added in coal and torrefied biomass samples to avoid high sulphur contents (>0.5 wt%) inhibiting combustion. Powdered samples were placed in a tin capsule of 3 mm diameter, which was then crushed in order to remove any air. Samples were placed in the auto sampler and fed automatically to the combustion reactor at a temperature of 900-1000°C. The required amount of oxygen for optimum combustion was delivered into the reactor. The system increased the temperature to 1800°C. At this temperature, organic and inorganic substances are converted into oxidised gases which were later separated in a chromatographic column and detected by a thermal conductivity detector (for carbon, hydrogen and nitrogen) and by a flame photometric detector (for sulphur). The calibration of the instrument was routinely verified by running two tin capsules containing standard materials (C, H, N, S contents known) that were selected depending on the samples to analyse. For biomass, coal and torrefied biomass, BBOT and oatmeal were used. Blank capsules

containing V_2O_5 only, were also run prior to analysis to ensure that no unexpected peaks or disturbed baseline were produced in the chromatogram. The results were taken as the average of two measurements providing the variation of results was <5%. Results obtained were therefore expressed on an as received basis. The oxygen content could then be calculated by subtraction according to Eq.(3.1):

$$\%O = 100 - (\%C + \%H + \%N + \%S + \%Moisture + \%Ash) \quad (3.1)$$

3.2.2. TGA-proximate analysis

Proximate analysis for the determination of moisture, volatiles and fixed carbon was performed for all samples in a TGA-50 Shimadzu analyser. The instrument consisted of a furnace and a balance with vibration resistance and was capable of taking high precision weight measurements. Computer software controlled data collection and gas supplies. 4-6 mg of sample were weighted into the balance in an alumina crucible, the instrument was then programmed to increase the temperature from ambient temperature to 110°C under a flow of nitrogen at a rate of 10 °C/min. This temperature was held for 10 min. During this time samples lost all their moisture content. Next, the temperature was further increased to 910°C at a rate of 25 °C/min, when 910 °C were reached the temperature was held for 10 minutes until all volatiles were released. At that point, a flow of air was added in order to burn the remaining carbon. The weight lost in this step corresponded to the amount of fixed carbon in the sample. The remaining weight corresponded to the ash content and was calculated by subtraction, according to Eq.(3.2):

$$Ash\ (wt\%) = 100 - (\%Moisture + \%VM + \%FC) \quad (3.2)$$

All gases (nitrogen and air) flowed at a fixed rate of 50 mL/min. The weight of sample in the crucible was continuously measured throughout the test. Figure 3-1 shows a typical TGA plot, in which the loss of mass over time or with respect to the temperature programme can be observed. Also, it was possible to obtain a plot for the first derivative (DTG) of the weight loss curve, where any change in the rate of weight loss can be appreciated in the form of peaks or shoulders (which represent simultaneous reactions).

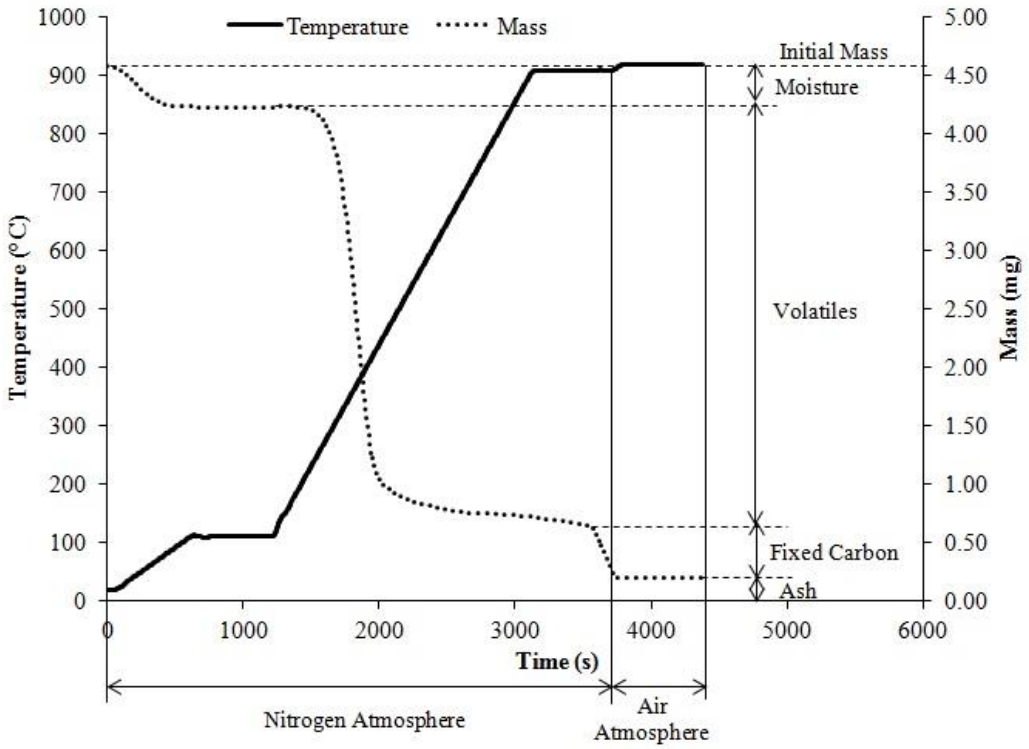

Figure 3-1. Thermogravimetric analysis. Temperature programme and mass loss.

3.2.3. Gross Calorific Value: Bomb calorimetry and formulae

The calorific value of samples could be measured or calculated. Measured values were obtained using a Parr 6200 Oxygen Bomb Calorimeter. For this method, if powdered samples were explosible, a pellet had to be formed using approximately 0.5 g of sample in a Specac Hydraulic Manual press, with a load of 10 tonnes. The pellet was then placed in the centre of a crucible. The crucible was then placed in the head of the bomb, and a loop of fuse wire was formed above the sample. The fuse wire should not touch the sample or the crucible being placed 1 mm above the pellet. The head of the bomb could then be loaded into the bomb cylinder. The cap was screwed to close the bomb cylinder and then the bomb was filled with oxygen. A bucket containing exactly 2 kg of water was placed inside the calorimeter. The cylinder bomb was placed inside the bucket making sure that there were no leakages of oxygen from the bomb and the ignitor wires were attached to the head of the cylinder bomb. The lid of the bomb calorimeter was then closed making sure the stirrer and thermistor did not touch the bomb or the bucket. The measurement proceeded automatically after the weight of sample and the spike were specified to the program. After the test, the valve in the bomb head was opened under a fume cupboard to release the combustion gases. Samples of coal and torrefied biomass proved difficult to ignite and therefore a smaller mass of sample of around 0.3 g and

a few drops of spike (0.06 g of kerosene) were added to the pellet, which had been pelletised slightly less packed by applying no more than 2 or 3 tonnes of pressure with the hydraulic press. The calorimeter was calibrated with 10 benzoic acid pellets of known gross calorific value supplied by the manufacturer. The results were obtained in an as received basis in MJ/kg.

Alternatively, the gross calorific value of biomass and coal samples could be calculated from a series of formulas using the chemical composition of the samples that have shown good agreement with measured values in the literature [118-122, 201]. The gross calorific value in a dry, ash free basis for coals is given by the Dulong formula [120] shown in Eq.(3.3):

$$GCV\left({}^{BTU}/_{lb}\right) = 144.4(\%C) + 610.2(\%H) - 65.9(\%O) - 0.39(\%O)^2 \quad (3.3)$$

where the contents of C, H and O are given on a dry ash free basis.

For this work the equation given by Friedl et al. [119] was used for biomass and torrefied biomass samples as shown in Eq.(3.4):

$$HHV\left({}^{kJ}/_{kg}\right) = 1.87(\%C)^2 - 144(\%C) - 2820(\%H) + 63.8(\%C)(\%H) + 129(\%N) + 20147 \quad (3.4)$$

Where the contents of C, H and N are given on a dry basis.

3.2.4. Bulk density

The bulk density of fuels affects transportation and storage costs [128] and it is a key parameter in this investigation due to the limitation that low bulk density fuels (like biomass) pose to the standard explosion characterisation methods. The bulk density of a material is the density of a large volume of material in air and is dependent on the level of compaction of the solid.

Bulk densities of all samples were measured in powder form. A 25 mL graduated cylinder with a resolution of 0.5 mL and a weighting balance with a resolution of 0.1 g were used. The graduated cylinder was filled gradually with increasing masses of powder. Ten measurements of weight and volume were taken and the “tapped” bulk density was calculated as the average of 10 mass to volume ratios. The average error for the measurements was 15 kg/m^3, i.e. <10%.

3.2.5. True density

The true density or particle density is regarded as a better defined property than the bulk density because it does not depend on the degree of compaction of the material. A Micrometrics AccuPyc 1330 gas displacement pycnometer was used.

The system comprised two cells of calibrated volumes separated by a valve, one cell containing a known mass of sample at ambient pressure. The sample cell was then pressurised to an elevated value measured with a gauge pressure transducer. Then the valve opened, and the pressure fell to an intermediate value. A mass balance equation was used by the instrument to calculate the volume of the sample. The result expressed in g/cm^3 was the average of 5 measurements and the average coefficient of variation was 0.09%. The calibration of the cell volumes followed the same procedure as the actual measurement of true density but used a calibration volume supplied by the manufacturers.

3.2.6. Particle size distribution

The particle size distribution of all the samples was measured using a Malvern Mastersizer 2000 capable of measuring particle sizes in the range of 0.1-1000 μm. The instrument measured the intensity of light scattered when a laser beam passed through the sample dispersed in deionised water. The analysis method used by the instrument is known as the Mie and Fraunhofer scattering model that assumed all particles were spherical. The intensity of the light scattered was a function of the wavelength, the scattering angle, the particle size and the relative index of refraction of the material and the medium. Mie theory is capable of calculating particle size if the refractive index is known. Refractive index of 1.386 was used for all biomass samples [202] and 1.680 was used for coal [203]. The instrument consists of a sample dispersion unit, and an optical unit connected to a computer. A few grams of sample were mixed with deionised water and a few drops of IGEPAL (a detergent that helped samples get wet and mix well with water without changing the nature of the sample), forming a paste. This paste was then added to the dispersion unit where deionised water was flowing through the lens. The optical unit had a stirrer rotating at around 2000 rpm to allow a better dispersion of particles and avoid bigger particles depositing in the bottom of the unit. Particle size results were expressed as the average of 30 measurements. The instrument was calibrated in a monthly basis using calibration samples provided by the manufacturer. A number of parameters are automatically generated by the software. These include the mean diameter (d_{50}) or the surface and volume weighted mean diameters. D50 indicates that 50% of the particles in the sample have a diameter less than D50. The surface and volume

weighted mean diameters however, are the mean diameters whenever the results are displayed as a surface and volume distributions respectively.

3.2.7. Particle morphology: Scanning Electron Microscopy

The morphology of particles was assessed with a Carl Zeiss EVO MA15 Scanning Electron Microscope. Samples for the microscope were prepared by fixing dust particles in a standard carbon conductive adhesive tab, previously attached to a sample stub. An air duster was used to remove any loose particles. Samples were then coated with gold in an Emscope SC 500 coating unit. Samples were placed in the sample holder and the sample chamber was evacuated. An electron beam was then directed towards the sample. The intensity of interactions between the beam and the sample were measured and stored in the computer. The stored values were mapped as brightness variations on an image. Still images of the samples could be stored at different magnifications.

3.2.8. Surface area and porosity: BET analysis

Surface area is a property of solids that typically affects combustion rates. Surface area of all samples was determined in a Micrometrics Tristar 3000 Surface Area and Porosity analyser. Samples of approximately 0.5 g were loaded into a clean sample tube ensuring minimal sample deposition on the walls. Samples were then degassed at 120 °C for 4 hours in a FlowPrep 060 unit with flowing nitrogen gas. Samples tubes incorporated a filler rod and necessary fittings in order to attach the tubes to the analyser ports. The 4 L Dewar was filled with liquid nitrogen prior to analysis. Automatically, the instrument analysed the sample by decreasing the temperature of the sample using liquid nitrogen and allowing a flow of adsorbing gas in incremental doses. The quantity of gas adsorbed could then be plotted against the ratio of actual pressure of gas adsorbed to the saturation pressure of the gas, creating a curve called the adsorption isotherm. The instrument used the BET calculation method, and therefore, from the adsorption isotherm, a series of terms could be derived to create the BET plot, a linear plot from which the BET surface area can be calculated in units of m^2/g. Simultaneously, the pore size in terms of pore diameter and the volume of pores could also be measured according to the BJH method [204].

3.3. Explosion characterisation

Two explosion vessels were used for the explosion characterisation of samples. The modified Hartmann was developed as part of this research for the determination of minimum explosible concentrations (MEC) and evaluation of most reactive mixtures. The modification of the Hartmann method attempted to provide an

accurate determination of the mentioned parameters to facilitate and reduce the number of tests required in the 1 m^3. Results obtained through this method are presented in Chapter 4. In order to validate the results from the Modified Hartmann, a set-up that allowed gas propane explosions to be performed was also developed.

The 1 m^3 is the standard vessel used for the measurement of maximum explosion pressure (P_{max}), deflagration index (K_{St}) and MEC. In the present work it was used for the study of those properties, once suitable modifications were in place in order to test fibrous and low bulk density fuels and the calibration of the system ensured comparable results with the standard method.

3.3.1. Modified Hartmann tube

3.3.1.1. Apparatus

A Chilworth technology A/B Screening apparatus (Figure 3-2) originally used to classify dusts as Group A (explosible) or Group B (non explosible), was used to visually determine the presence of a propagating flame. The apparatus consisted of a polished stainless steel dispersion base with a dispersion air pressure indicator, dispersion cup and mushroom; a Perspex Hartmann tube 322 mm long with 61 mm internal diameter fitted with end rings and bayonet base fitting; a pair of brass electrodes; a remote handset for arc and air dispersion control and a constant arc power source 10 kV 25 mA s/c for generating 4-5 J of discharge energy across the electrodes. The electrodes, placed at 12.5 cm above the bottom of the tube were activated with a remote control prior to dust dispersion. The top of the tube was initially covered with paper rupture discs secured with a locking ring.

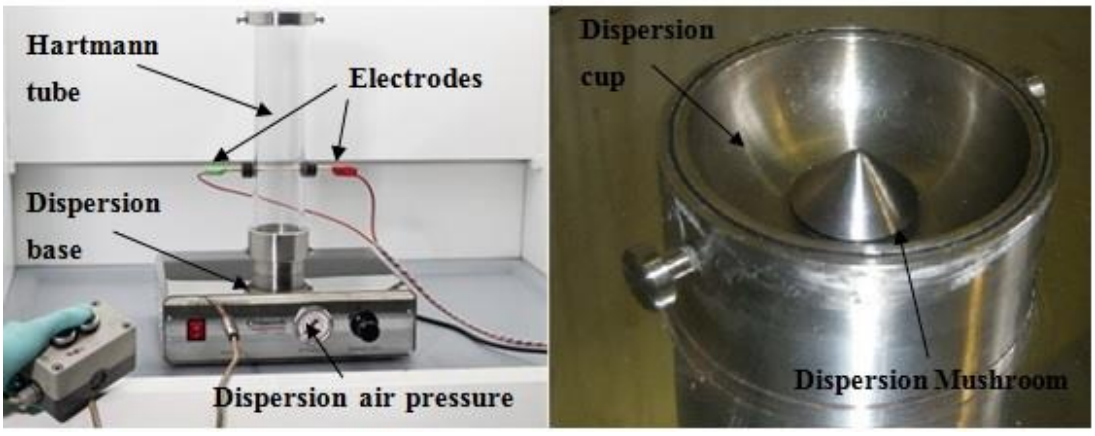

Figure 3-2. A/B Screening apparatus

Decreasing masses of dusts were placed in the dispersion cup and dispersed by a blast of compressed air in the presence of a constant arc. The dispersion base contained a 50 mL reservoir of air connected through the rear of the base with a 6

mm outside diameter nylon tube to a compressed air bottle. On activation of the ignition source and air reservoir valve using the remote control, the air, pressurised to 4 barg, was released through the bottom of the dispersion cup. The dust placed in the dispersion cup impinged against the mushroom and dispersed throughout the tube.

Using this original set up, it was found that different observers would conclude differently on the existence of a flame when the concentrations approached the limit. The lower explosible limits measured were also extremely low and not repeatable. Therefore, it was decided that, in order to clearly identify a flame, some modifications were required.

In line with the method for determination of LFL of gases it was decided to incorporate three thermocouples above the ignition arc at 50, 100 and 150 mm in order to establish a flame propagation criterion. In addition, a pressure transducer mounted in the wall of the tube was used to record the pressure-time history inside the tube. Subsequently, thermocouples and pressure transducers could be used to derive flame speeds and initial rates of pressure rise, and therefore map out the reactivity of different dust/air mixtures (see Figure 3-3).

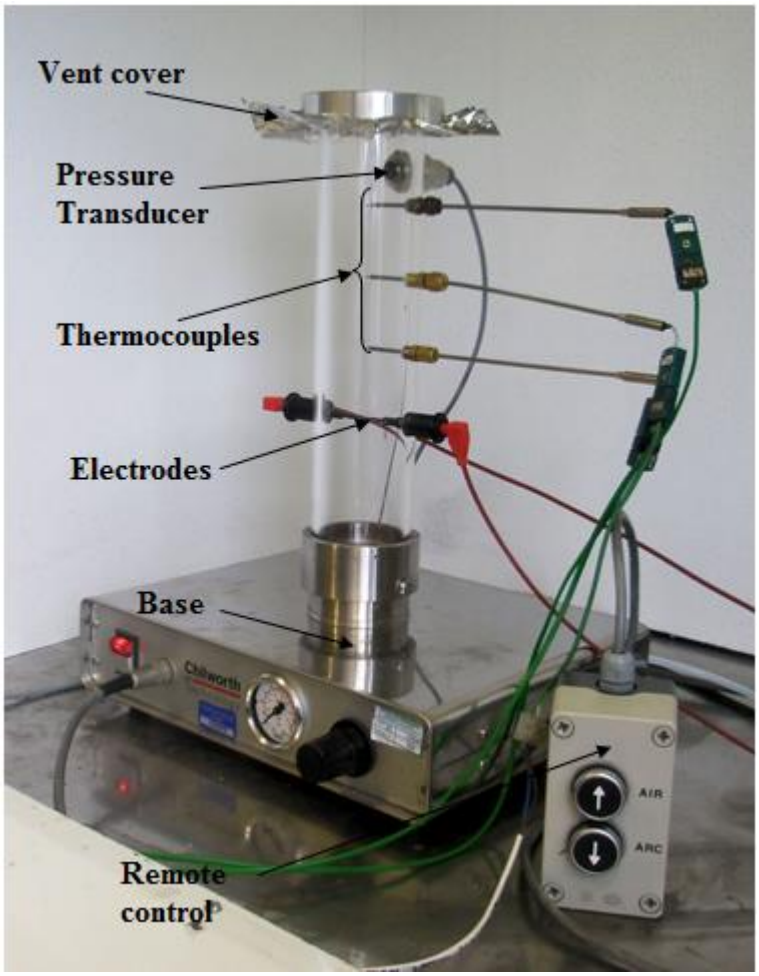

Figure 3-3. Modified Hartmann tube

3.3.1.2. New instrumentation and data collection

A piezoelectric Keller PAA-11 pressure transducer was fitted through a threaded hole drilled in the upper part of the tube to record the pressure histories during each test. The pressure transducer required a power supply unit (PSU) to be connected in-line with the data logging card to convert the signal into a signal compatible with the computer data logging system. This required a calibration of the pressure transducer. Three bare bead type-K thermocouples (mounted at 50 mm, 100 mm and 150 mm, also through threaded drilled holes with Swagelock compression fittings situated on the side of the tube above the ignitor) to record the time at which the flame arrived to each of the thermocouples. Thermocouples were earthed to avoid proliferation of noise in the signal due to interactions with the Hartmann's high voltage power supply. As depicted in Figure 3-4 the addition of this measure improved significantly the recorded thermocouple signal and allowed for an accurate determination of the time of flame arrival to the thermocouple.

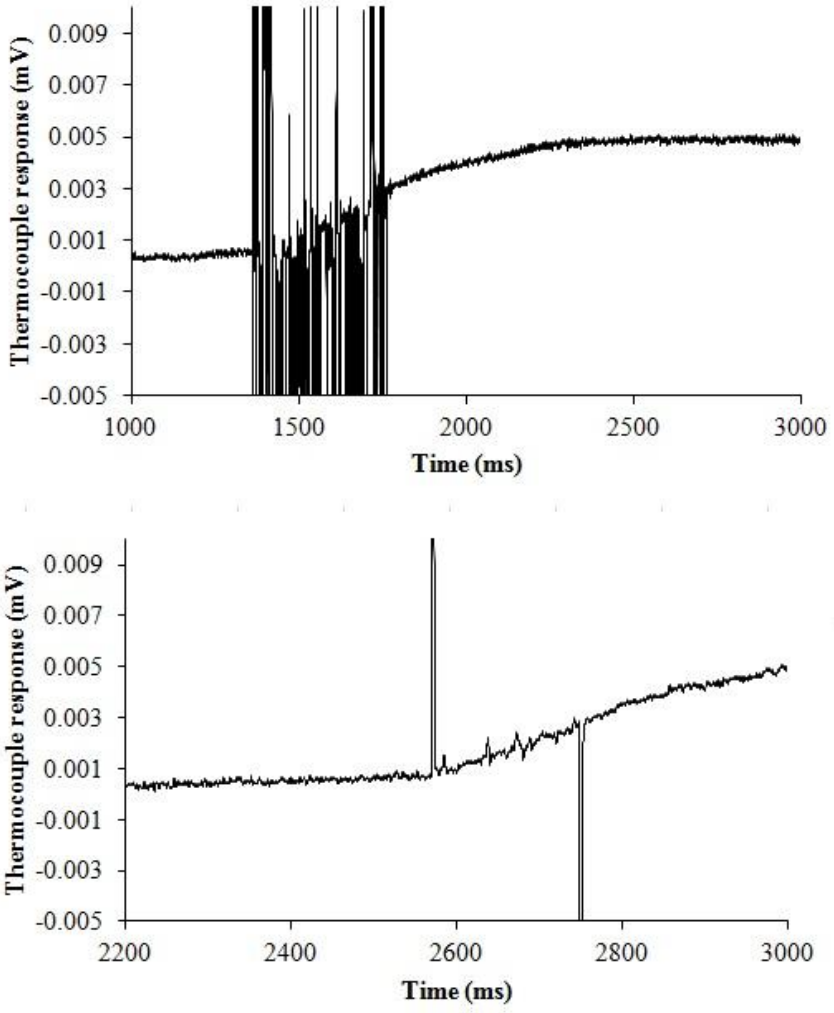

Figure 3-4. Improvement of thermocouple signal noise

All modifications facilitated the determination of ignition of the powder at near limit mixtures rather than relying on a visual observation of flame travel beyond a critical distance, and allowed the measurement of rates of pressure rise, and the determination of flame speeds between thermocouples. These additional data, in turn, allowed the charting of reactivity with concentration and determination of most reactive mixtures for different samples, for further assessment in the 1 m^3 vessel. Thermocouples and pressure transducers cables were welded onto a DBK200 adapter board for analogue inputs. The data collected was then transferred through a CA195 connector to the DaqBoard2000 Series board installed in the computer. Daqview 9.0.3 Real time data Acquisition System was the software used for data analysis. Data logging was triggered manually and the event consisted on 50,000 scans at a rate of 10,000 scans per second.

3.3.1.3. Vent cover

The rupture paper vent cover used in the original system was found to be a source of inconsistency in the results since bursting pressures varied from test to test. Figure 3-5 shows the pressure trace for 5 repeat tests with 75 g/m^3 of dust. It can be seen that in some tests the cover vent did not burst, and when it did, the bursting pressure varied. As a result it was decided to test other vent cover materials.

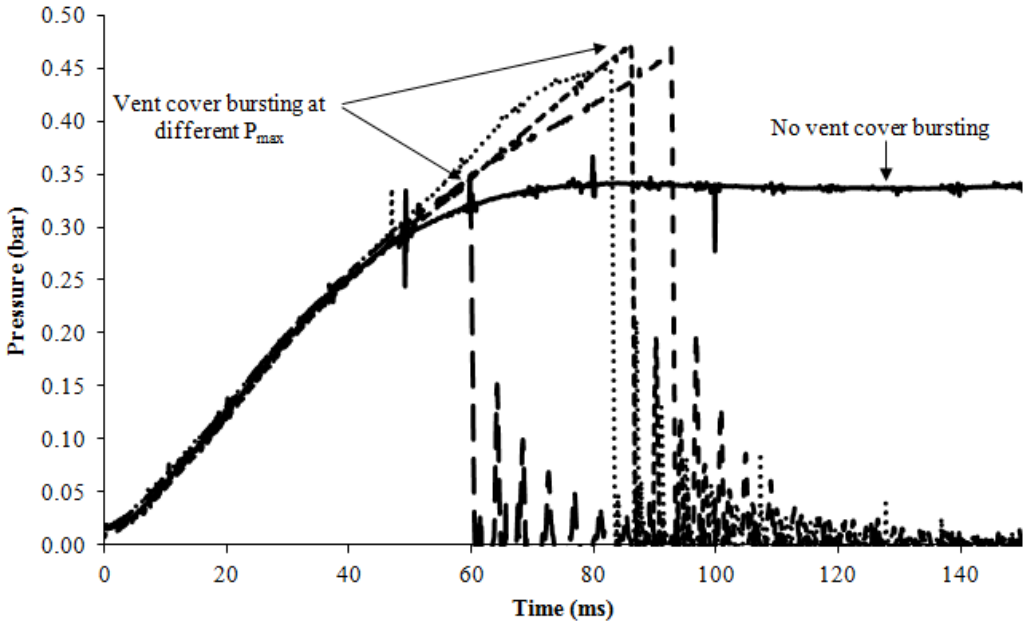

Figure 3-5. Inconsistencies of vent cover bursting

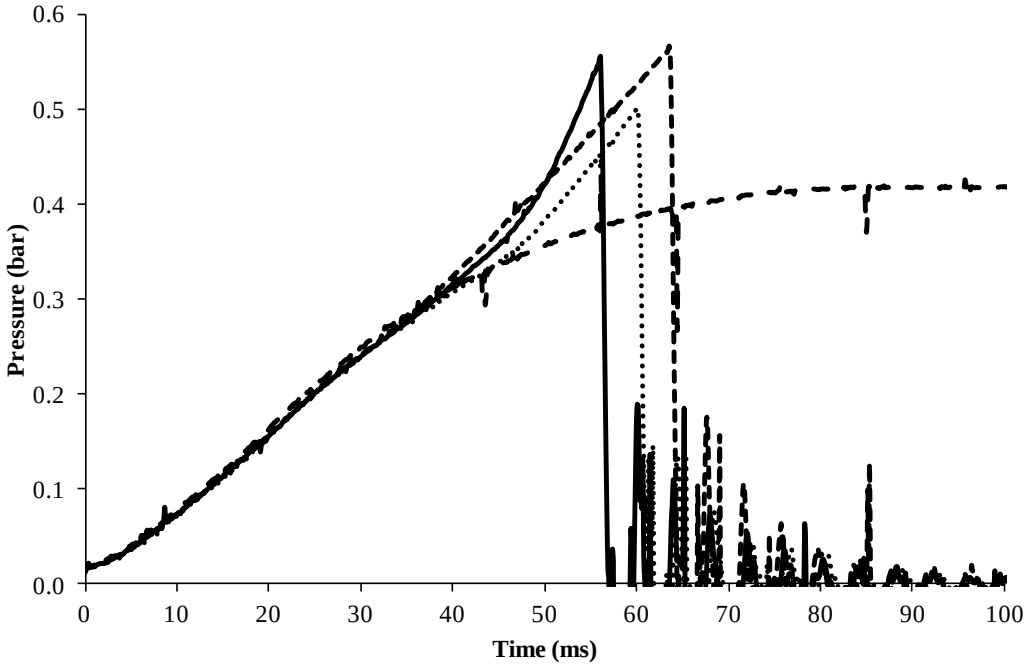

Figure 3-6. Repeatability of tests with 20 μm thickness aluminium foil

The most suitable vent cover would be that which provided consistency on maximum bursting pressure (P_{max}), and in the time between injection of compressed air (t_0) and the time (t_{Pmax}) at which the pressure reached P_{max}.

The burst cover materials used were: commercial aluminium foil (single and double layers), thin and transparent melamine paper and aluminium foil of increased and specific thickness (20 μm). Also it was desirable that the bursting pressure was as high as possible, in order to appreciate a longer pressure history before the vent cover burst. Best results were achieved with the 20 μm thick aluminium foil with an average bursting pressure of 1.53 bara (See Figure 3-6). Ten tests with 75 g/m^3 of dust were performed to assess the variability of bursting pressures, rates of pressure rise and time to achieve bursting pressure (t_{Pmax}-t_0), see Table 3-2.

Although the repeatability of tests was found to be acceptable using 20 μm aluminium foil, it was observed that possibly, due to variations in the dispersion of the dust the initial rates of pressure rise varied from test to test. As a result it was decided that every test should be repeated three times.

Table 3-2. Statistical study on repeatability of results for 20 µm aluminium foil

Test	Mass (g)	Concentration (g/m^3)	P_{max} (bar)	dP/dt (bar/s)	t_{Pmax}-t_0 (s)
1	0.1	74.1	1.540	24.12	0.056
2	0.1	74.1	1.483	12.56	0.060
3	0.1	74.1	1.550	12.27	0.064
4	0.1	74.1	1.499	19.66	0.054
5	0.1	74.1	1.547	33.20	0.051
6	0.1	74.1	1.549	30.96	0.050
7	0.1	74.1	1.545	20.31	0.060
8	0.1	74.1	1.516	15.64	0.056
9	0.1	74.1	1.527	27.52	0.050
10	0.1	74.1	1.542	24.17	0.055
AVERAGE			1.530	22.0	0.055
STD. DEVIATION			0.023	7.3	0.005
Variation Coefficient (%)			**1.5**	**33.1**	**8.2**

3.3.1.4. Dispersion pressure

The manufacturers of the original A/B group classification apparatus recommended a dispersion pressure of 4 barg. It was found that near the limit, using a dispersion pressure of 4 barg, there was a large range of concentrations near the limit for which explosion happened only sometimes. It was therefore decided to increase the dispersion pressure to 6 barg and 7 barg to assess if this improved the uncertainty in the probability of explosion near the limit. For this study, lycopodium dust was used. Figure 3-7 shows that increasing the dispersion pressure narrowed the range for which explosions happened only sometimes, which implied that dust mixing was improved and allowed clear identification of MECs. The lean limit was pushed to a lower concentration with 6 barg, but the same MEC was found with 7 barg, which implied that MEC would not be pushed to even lower concentration if the dispersion pressure was increased. It was decided to use 7 barg as the dispersion pressure since it was the maximum recommended by the manufacturers.

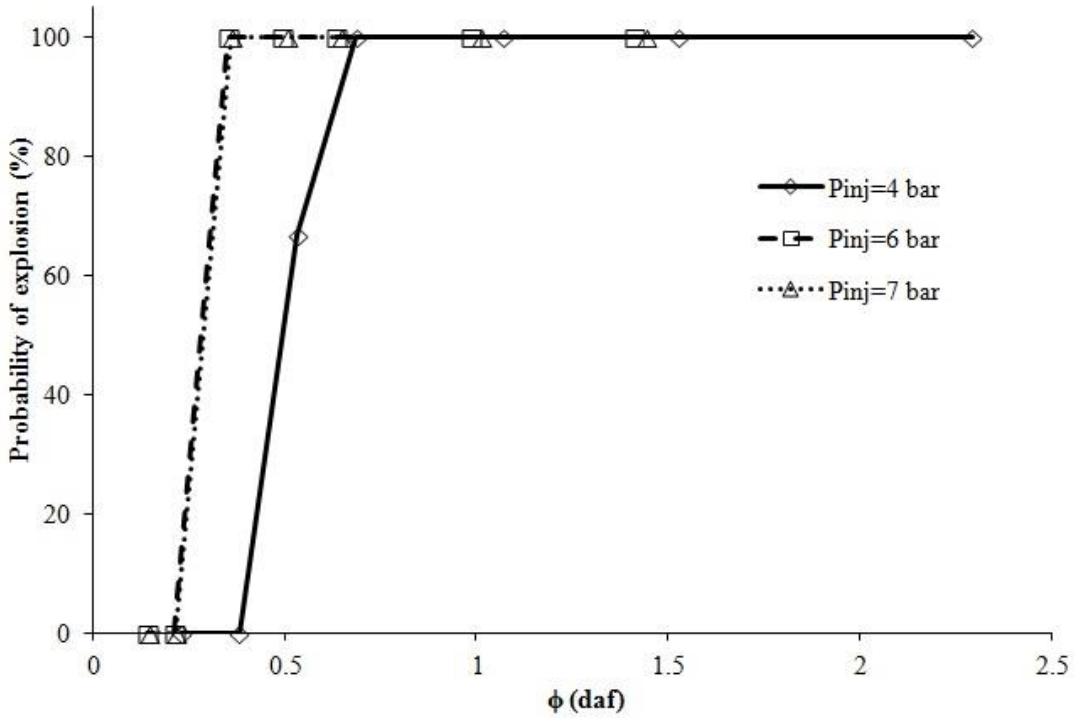

Figure 3-7. Experimental probability of explosion occurrence as a function of equivalence ratio and dispersion reservoir pressure.

3.3.1.5. Explosion criteria

The explosion criteria were established in terms of flame detachment and pressure rise to resemble the explosion criteria used in the determination of LFL of gases. In order to do so, high speed videos were recorded. The videos showed clearly if the flame detached from the spark and reached the thermocouples, and since pressure histories were recorded it was possible to associate the pressure rise achieved for clearly propagating flames. It was found that the ignition source produced a slight increase in response of the thermocouple situated 50 mm above the spark; however thermocouples 2 and 3, situated at 100 mm and 150 mm remained undisturbed. It was also observed that flames that reached thermocouple 2 at 100 mm produced a clear pressure rise of 100 mbar. As a result an explosion would be considered if the flame reached thermocouple 2 at 100 mm above the spark and/or if the pressure rise due to the explosion was equal or higher than 100 mbar: $P_{ex} \geq P_i + \Delta P_{air} + 0.1\text{bar}$

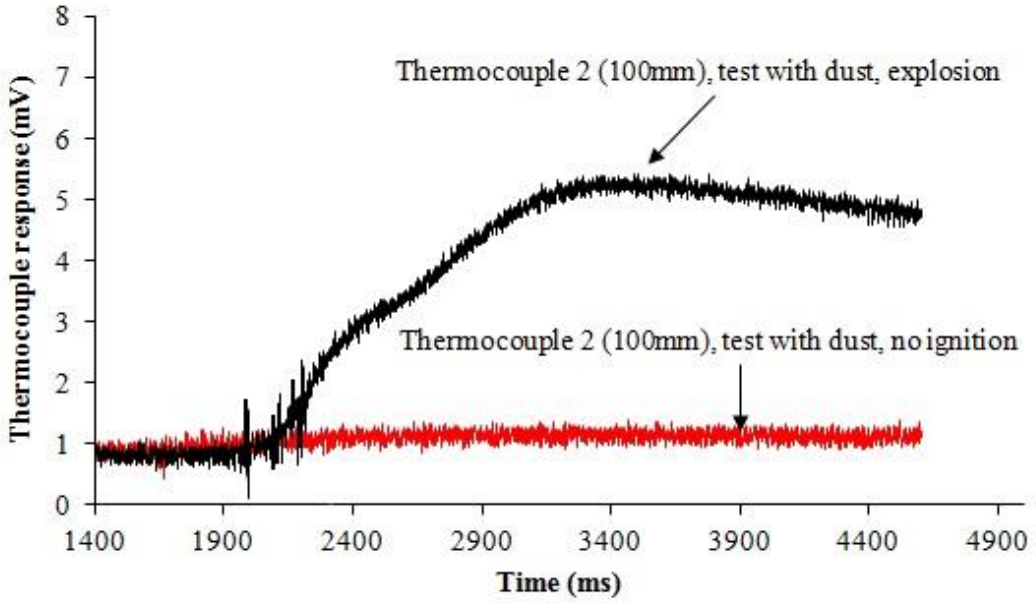

Figure 3-8. Examples of thermocouple response at 100 mm for tests with and without ignition

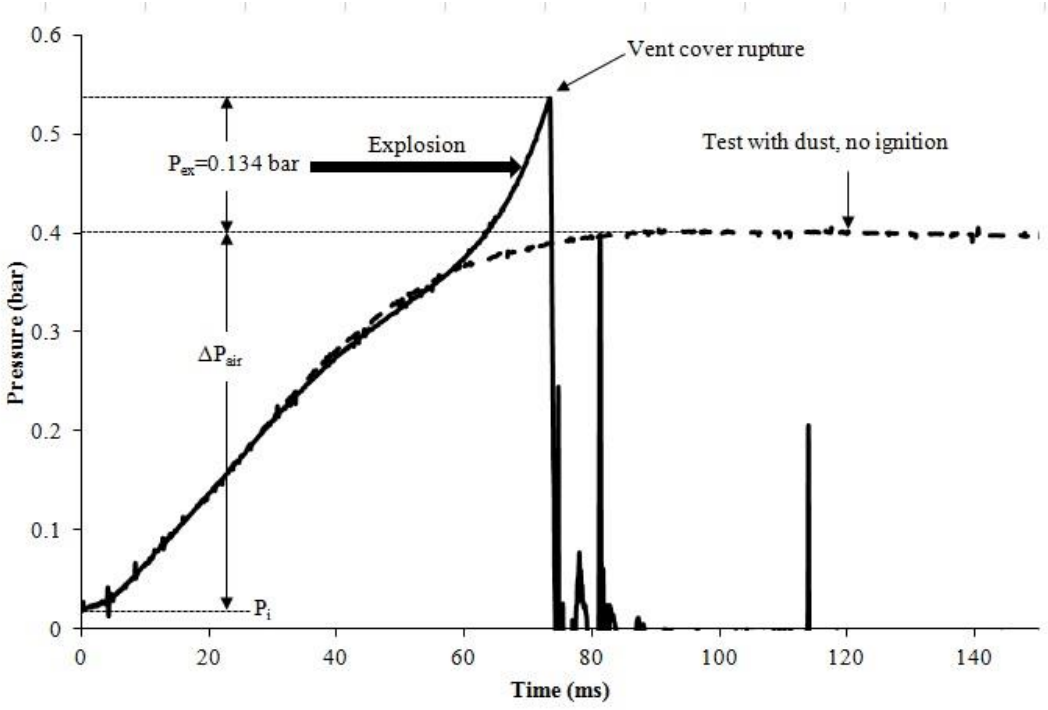

Figure 3-9. Pressure traces for tests with ignition and with no ignition in the modified Hartmann tube

Figure 3-8 and Figure 3-9 show example traces of two tests: one where ignition took place and other where it did not take place. The thermocouple response at 100 mm above the spark shown in Figure 3-8 corresponds to the overpressure due to explosion of 134 mbar shown in Figure 3-9. On the other hand, for the test where

there was no explosion, it can be appreciated how there was no change in thermocouple response and no pressure increase due to explosion.

3.3.1.6. MEC determination

The procedure for the determination of MECs with the modified Hartmann tube involved testing decreasing masses of dust in triplicate until a concentration was found not ignitable in all three tests, normally starting with rich mixtures (1-0.5 g) and in decreasing steps of 50% or smaller. When a concentration was found not to ignite in any of the 3 tests, 10% less mass than the preceding mass was tested rounding to the nearest whole number. The curve of probability of explosion versus concentration (or its equivalence ratio) could be plotted. The MEC could then be expressed as the highest concentration that would not explode (MEC_0), in agreement to the European definition for gases and dusts, or else, the lowest concentration that exploded in all cases (MEC_{100}) or the point in concentration between the two (MEC_{50}), in line with the American definition for dusts and gases respectively (Figure 3-10).

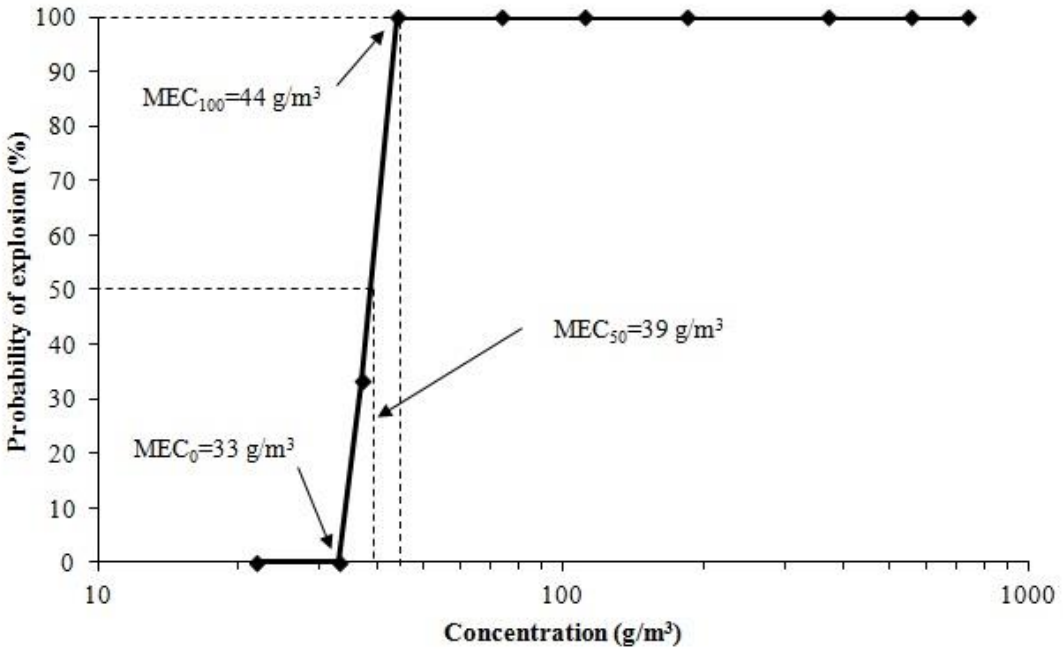

Figure 3-10. Example determination of MEC

3.3.1.7. Flame speed measurements

A sudden increase in the thermocouple trace gave the indication of the flame having arrived to the thermocouple as shown in Figure 3-8. Therefore the distance between thermocouples could be plotted against the time of flame arrival identified in the thermocouple traces. An example is shown in Figure 3-11.

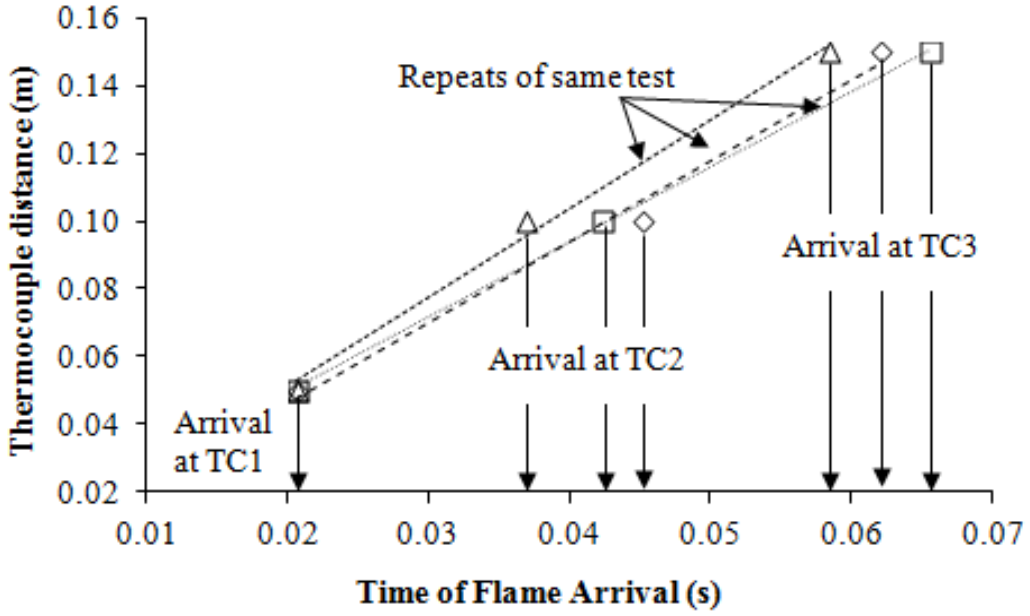

Figure 3-11. Flame speeds measurement method for Hartmann tube

The slope of each line was the average flame speed for that specific test. The average flame speed for a certain composition is expressed as the average of three slopes obtained for each repeated test. In the particular case of Figure 3-11 the results varied within 8%.

High speed videos taken to aid in the establishment of the explosion criteria showed that on activation of the ignition spark and dispersion of the dust, a flame kernel formed. When the pressure build-up was sufficient, the vent cover burst and the initial flame observed quickly travelled through the tube. Then it was noted that momentarily the flame became extinct and re-ignited almost instantly (See Figure 3-12).

The measured rate of pressure rise, therefore, undoubtedly corresponded to the rise of pressure due to the mass burnt in the initial fast flame prior to the vent burst.

It was then noted that the thermocouples failed to capture any disturbance as a result of the faster flame and that the flame speed that was actually measured was the secondary slower flame. This is shown in Figure 3-13 where the increase in the thermocouple signal occurs after the venting of the explosion.

When the vent cover burst it was likely that some dust particles were ejected, also there could be air entrainment into the tube, therefore the corresponding concentration at which flame speeds were measured was unknown.

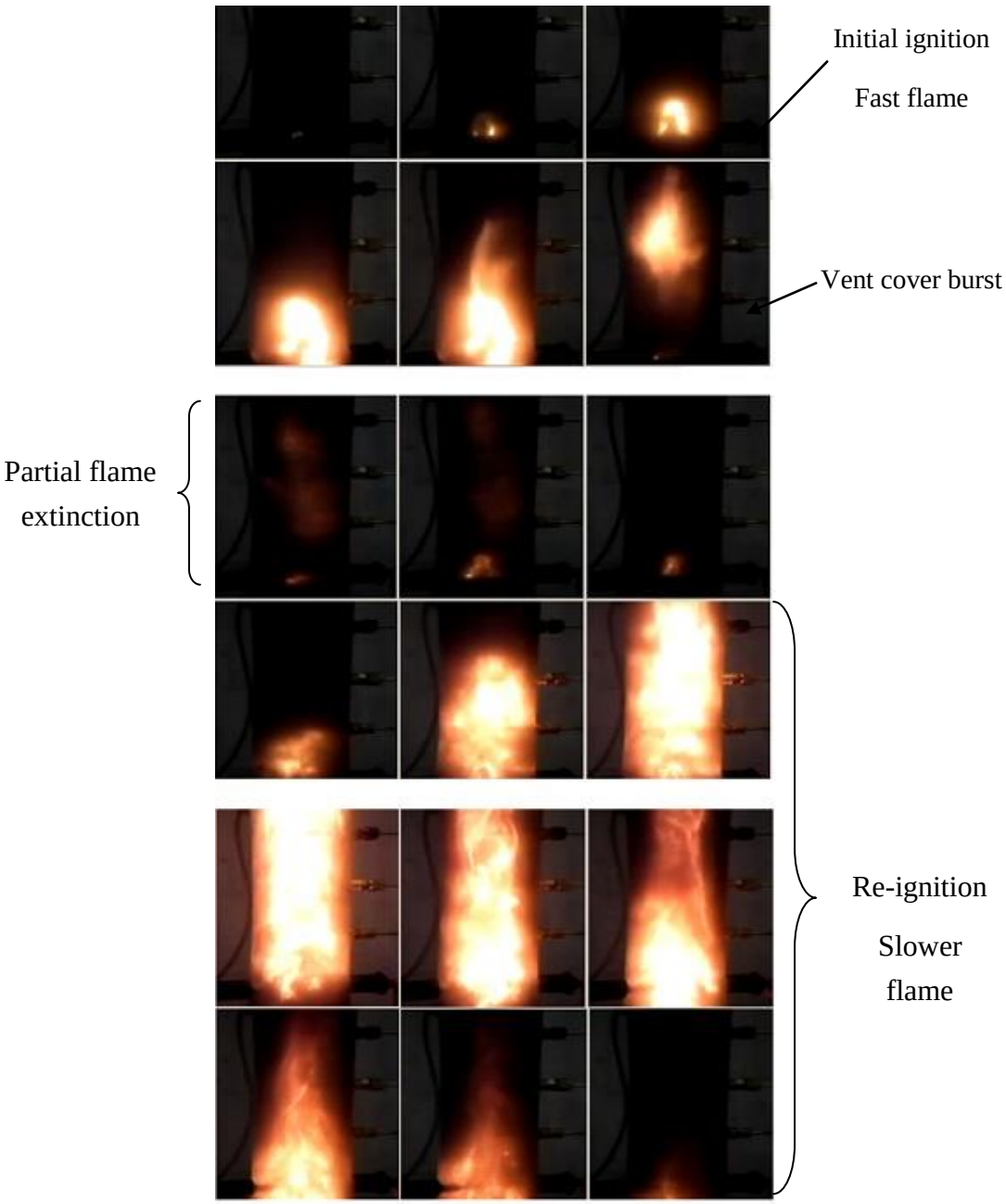

Figure 3-12. High speed video (1000 fps) of a modified Hartmann test with 250 g/m^3 of biomass of <75 µm

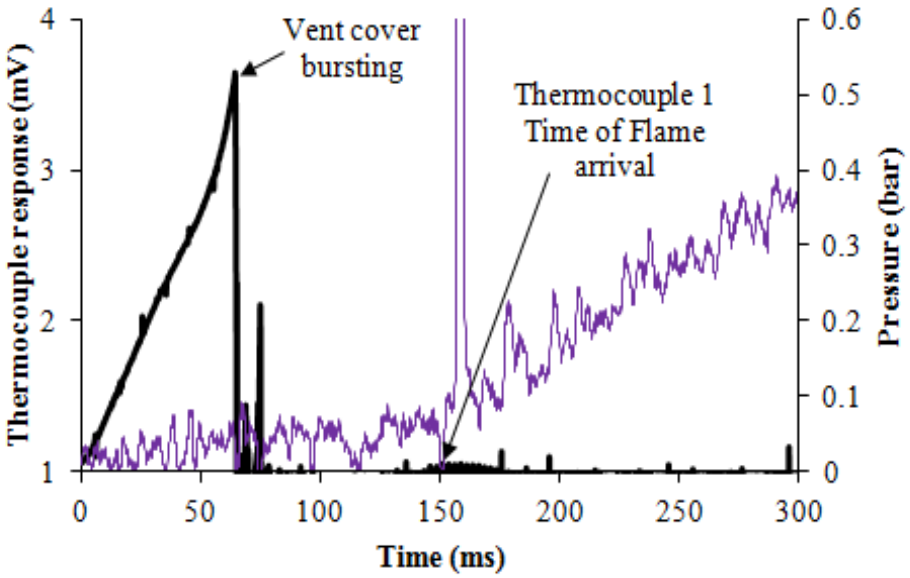

Figure 3-13. Location of time of flame arrival

3.3.1.8. Modified Hartmann set up for propane explosions

Despite improvements in dust distribution mentioned earlier, it was unclear whether the distribution of dust throughout the tube was satisfactory. It was decided to test propane gas to check if it was possible to find its limit, as propane lean flammability limit is well known.

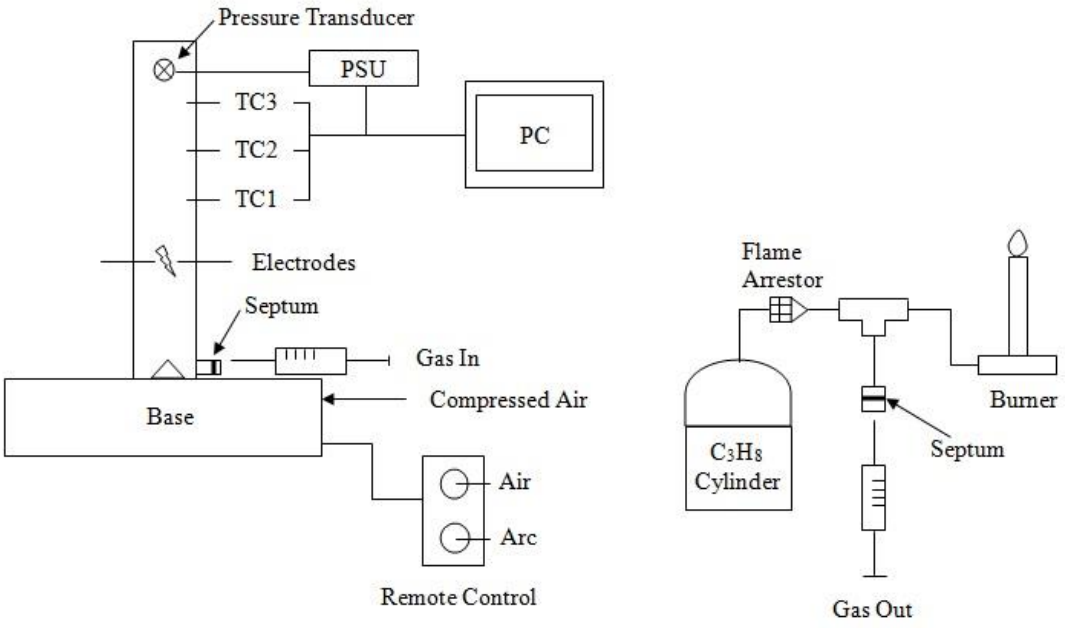

Figure 3-14. Hartmann set up for propane explosions

In order to allow testing of gas propane in the Hartmann test vessel, a gas syringing method was devised. Gas propane/air mixtures were tested using a SGE 50 mL gas-tight syringe to syringe gas from the gas propane cylinder line, fitted with a flame arrestor, to the Hartmann tube. Both fittings to the propane cylinder and Hartmann tube were fitted with a septum. The propane cylinder line was connected to a burner to ensure that only propane and not a mixture of propane and air was syringed.

First the propane bottle was opened and the burner lit. After a minute the sample was syringed through the septum in the gas line and injected inside the tube through the septum fitting. Once syringed into the tube from a point 10 cm below the spark, the propane gas diffused at its diffusion velocity in air of 0.34 cm/s [205], therefore, to avoid ignition of the sample prior to air dispersion, no later than 30 seconds the remote control handset was activated to allow the continuous arc and to disperse the air in the 50 mL reservoir. The same set-up and instrumentation was used for gas and dust explosions, except for the data acquisition in which, for gas, at the end of the event, acquisition was manually stopped.

3.3.1.9. Gas propane LFL tests in the modified Hartmann tube.

Only near flammability limit (1.7-2.1%) tests were conducted. It was observed that a concentration of 2.3% propane (Ø=0.55) reacted faster than a rich mixture (Ø=3.80) of 740 g/m^3 torrefied biomass dust in the Hartmann tube (Figure 3-15).

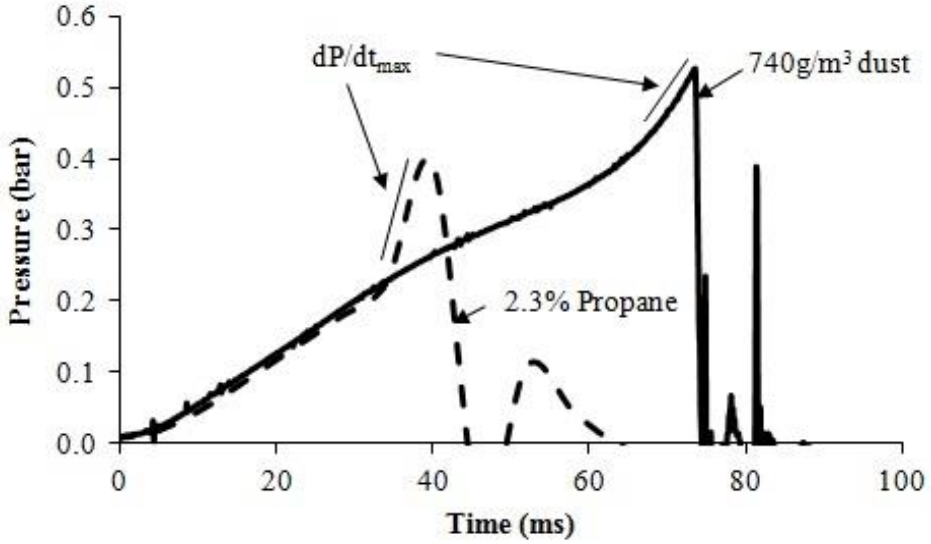

Figure 3-15. Comparison of pressure traces for gas propane and biomass dust in the modified Hartmann tube

Decreasing concentrations of propane were therefore tested until it was found that the limit using the Hartmann method with propane was 1.1% which is much lower than any published value for LFL of propane. It was decided then to alter the normal

procedure by allowing the blast of air to disperse the gas prior to ignition and allowing a random time before igniting the mixture. Using this procedure the lean limit found was 1.9% which is within 10% of the accepted value of 2.1% for LFL of propane. It was therefore concluded that the original method would not disperse the gas properly and rich pockets of propane were formed resulting in much higher concentrations of propane and in much higher rates of pressure rise than expected as shown in Figure 3-15.

Although this could be intrinsic to gas and could just point to the Hartmann method being unsuitable for testing LFL of gases, it was decided that further work would be required to devise if including an ignition delay would provide better dust mixing. Due to time constrains in the research project further modifications to the Hartmann tube have been conducted by other Leeds researchers and will not be presented in this work. However, some results using the method described are presented in Chapter 4.

3.3.1.10. Modified Hartmann procedures

The procedure for dust explosions in the modified Hartmann followed the following steps:

1. Turn on fume cupboard and apparatus
2. Ensure Hartmann tube and dispersion cup are clean.
3. Ensure dispersion cup mushroom is approximately 2 turns open
4. Clamp aluminium foil cover to the top of the Hartmann tube
5. Attach electrodes to power supply
6. Weight the initial mass of sample required, each mass of sample will be tested 3 times.
7. Load powder uniformly around the dispersion cup
8. Place the Hartmann tube onto dispersion base bayonet fitting and ensure that the base pins are securely in place. Note that it is anti-clockwise to tighten the tube in place and clockwise to remove the tube.
9. Earth thermocouples
10. Open compressed air cylinder or air line
11. Set compression to dispersion cup at 7 barg
12. Ensure fume cupboard door is properly closed
13. Switch on the transformer to enable constant arc ignition source

14. Allow acquisition of data from data logger
15. Operate solenoid to disperse powder
16. After the test, close air feed, clean dispersion cup and tube and replace aluminium vent.
17. Record how many of the three tests show an explosion, if the 3 test showed an explosion decrease the sample mass by 30%, if no test showed ignition increase mass by 30%. A graph of probability of explosion vs. concentration should be produced where a series of concentrations show increasing probability of explosion from 0% to 100%, in which case, the concentration with 0% probability of explosion will be determined as the MEC.

Alternatively, the procedure for gas explosions differed in a few steps:

1. Turn on fume cupboard and apparatus
2. Ensure Hartmann tube and dispersion cup are clean.
3. Ensure dispersion cup mushroom is approximately 2 turns open
4. Clamp aluminium foil cover to the top of the Hartmann tube
5. Place the Hartmann tube onto dispersion base bayonet fitting and ensure that the base pins are securely in place. Note that it is anti-clockwise to tighten the tube in place and clockwise to remove the tube.
6. Attach electrodes to power supply
7. Earth thermocouples
8. Operator 1 open propane bottle
9. Operator 2 light propane flame in the burner
10. After 1 minute, Operator 1 fill syringe
11. Operator 1, purge syringe under fume cupboard
12. Repeat steps 9 to 11
13. Operator 2 light propane flame in the burner
14. Operator 1 fill syringe
15. Operator 2 manually star data acquisition
16. Operator 1, slowly inject gas into tube and close fume cupboard door
17. Operator 2 open compressed air line set compression to dispersion cup at 7 barg

18. Switch on the transformer to enable constant arc ignition source
19. Operator 2 operate solenoid to disperse gas/air mixture
20. After the test, close air feed and replace aluminium vent.

Safety precautions and risk assessments were provided for tests performed in the modified Hartmann tube. Tick sheets were used to ensure all steps were taken for safe operation.

3.3.2. 1 m^3 ISO test vessel

The 1 m^3 vessel was constructed to the specifications of the ISO 6184 [31]. However, it was necessary to introduce some changes to allow testing of fibrous biomass materials. These changes are contemplated by the standard providing results are comparable to the standard system, and they affected the volume of the external dust holder and the dust dispersion system.

The steel vessel was a 1.2 m diameter cylinder with round edges constructed according to the Specification for unfired fusion welded pressure vessels (BS 5500:1997, now replaced by the PD 5500:2012+A2:2013). Although here and later in the text it is referred to as 1 m^3 vessel, the volume of the vessel was 1.138 m^3. The design pressure was 25 bar, with a certified hydraulic pressure of 31.25 bar (see Figure 3-16)

Known masses of dust were placed in an external dust holder. The dust holder was connected to the explosion chamber through a delivery pipe, and both were isolated by an electro pneumatic valve. The dust holder was then pressurised to allow that, on activation of the valve the dust could be dispersed inside the explosion chamber, the delivery pipe was connected to a disperser inside the explosion chamber that evenly distributed the dust. Ignition of the evenly distributed dust cloud was by means of centrally positioned chemical igniters firing into a perforated hemispherical cup to ensure central ignition and spherical propagation as far as possible. After explosion dust residues were found both in the dust holder and in the explosion vessel. The main parameters monitored were pressure over time and flame position. Detailed information is given in the following sections. The door of the vessel was a blank plate, drilled and tapped to fit valves. Other blank plates were fitted in different positions of the vessel to allow for electrodes, valves and instrumentation to be fixed.

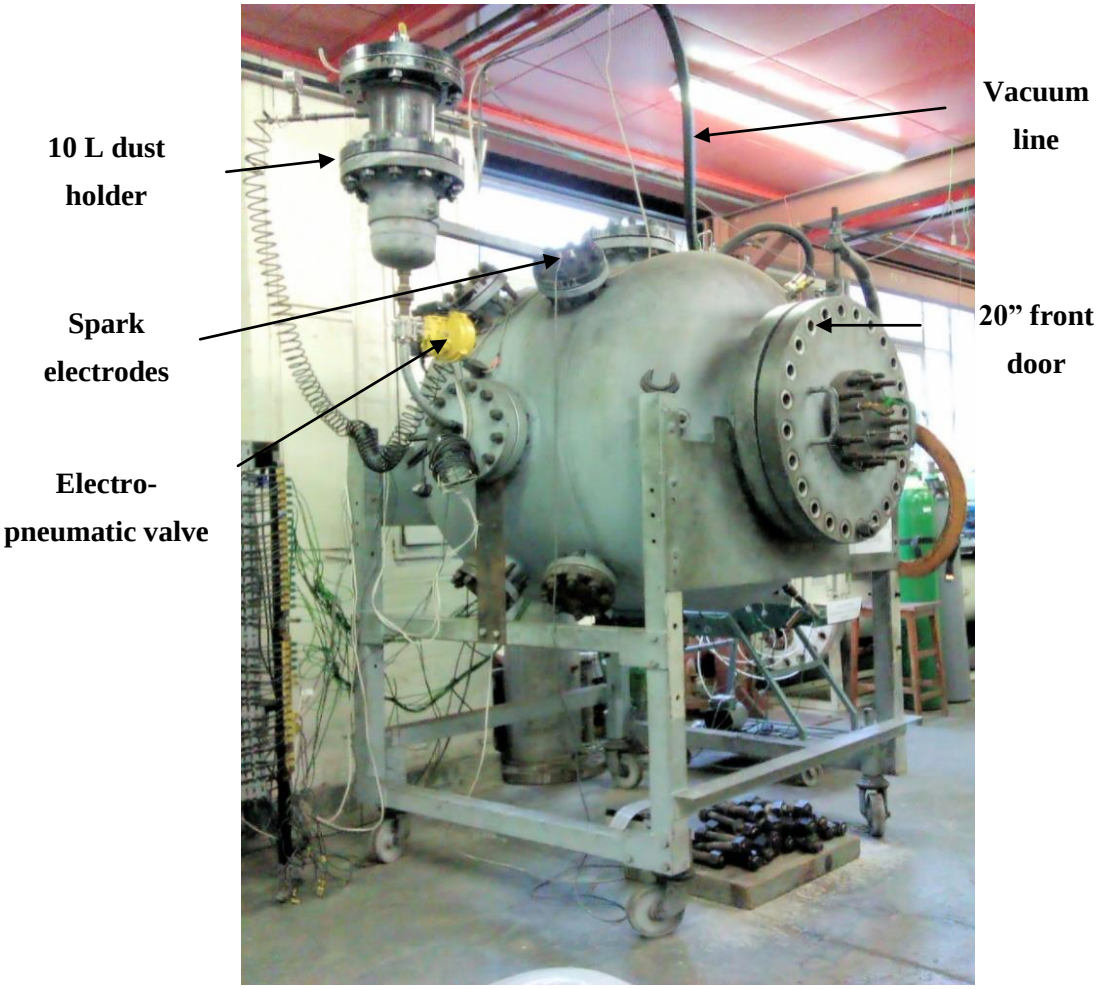

Figure 3-16. 1 m^3 Leeds ISO vessel

3.3.2.1. Dust holder and delivery pipe

The standard system used a 5 L (actually 4.6 L, 290 mm long and 162 internal diameter with round edges). This dust holder was pressurised to 20 bar to disperse the dust into the explosion chamber by operating the electro-pneumatic valve situated in the delivery pipe. This system was used for coal and other non-fibrous dusts. However, the 10 L dust holder setting, shown in Figure 3-17, which consisted of the standard 5 L holder and a 5 L cylindrical extension volume was used when fibrous biomass dusts were tested.

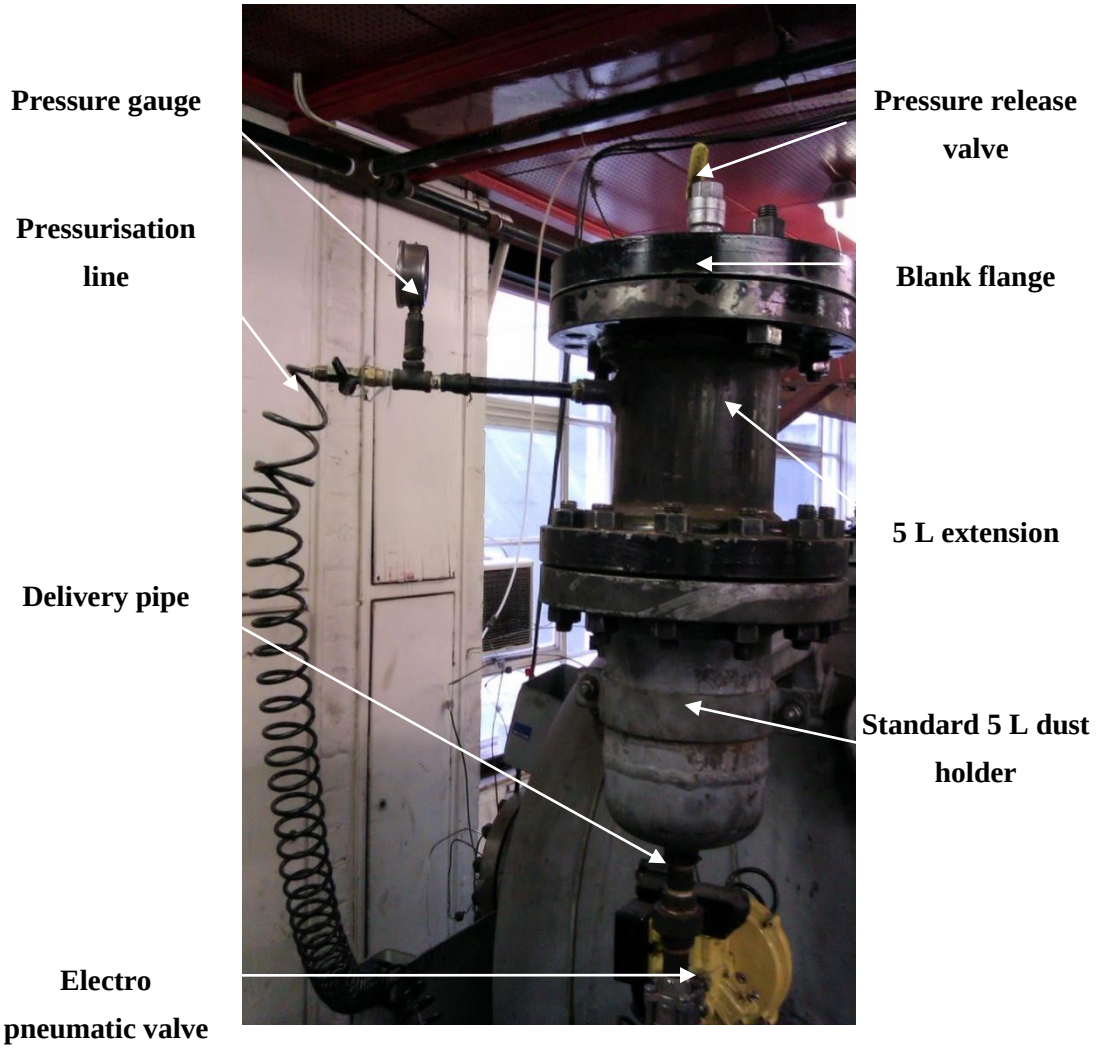

Figure 3-17. 10 L dust holder for fibrous biomass

The bottom volume was connected through the 19 mm diameter delivery pipe to the explosion chamber. A blind flange was bolted to the dust holder to seal the enclosure. The blind flange was fitted with a ball valve that allowed releasing any residual pressure after the explosion event. Lines of compressed air were used to pressurise the dust holder to the required pressure and to action the electro-pneumatic valve. A pressure gauge was fitted in the line to the upper volume of the dust holder to monitor the pressure inside. The 10 L dust holder setting for biomass dusts was calibrated to deliver the dust in the same way as the 5 L dust when this was pressurised to the standard 20 bar pressure. This calibration consisted on pressurising the 10 L dust holder to 10 bar, rather than 20 bar. This was justified in previous work by the Leeds research group [187].

The Leeds ISO vessel differed from the standard vessel in two features: the delivery pipe was longer and the electro-pneumatic valve used here takes a longer time in

opening and closing. These timing differences are contemplated and accepted by the standard; however these need to be taken into account for the purposes of introducing the right ignition delay. Figure 3-18 shows that the valve actually took 90 ms to fully open and close and that the effect of the longer delivery pipe supposed a further 50 ms delay.

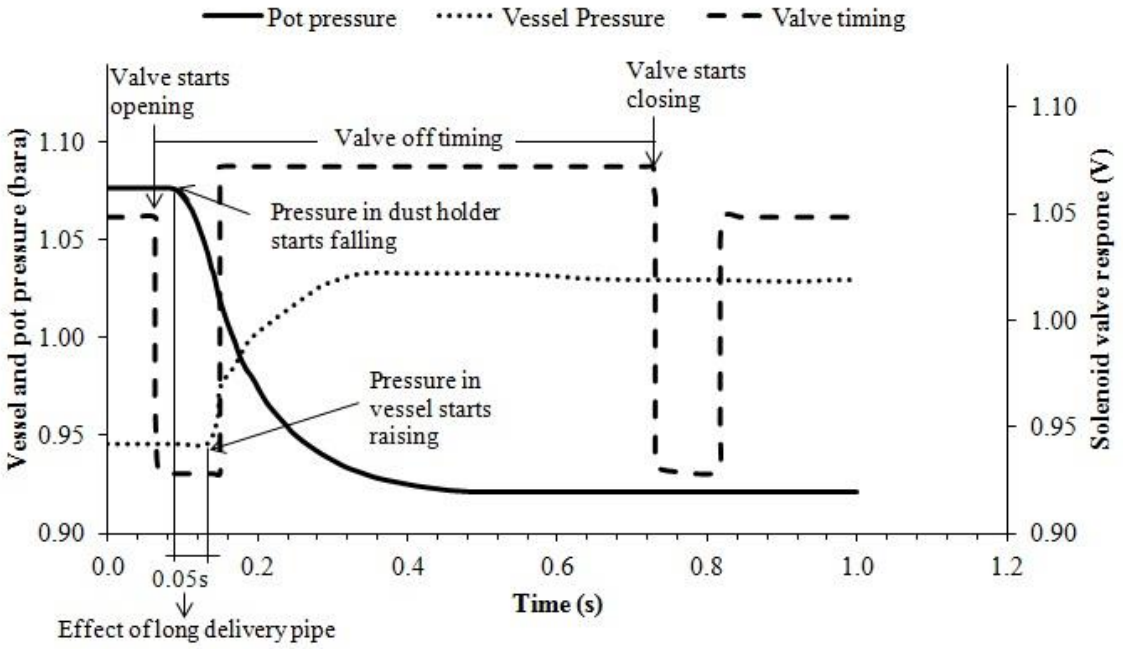

Figure 3-18. Timing sequence in 1 m^3 vessel

As a result the actual time of ignition after the activation of data logging was 0.74 s, in order to achieve the standard 0.6 s ignition delay. The valve off timing is also important because if the valve remained opened after ignition, the transmission of the explosion into the dust holder could result in potentially violent explosion, particularly since the transmission would be from a large to a small volume with consequent pressure piling [206] (See section 3.3.2.3).

3.3.2.2. Dispersion system

The standard dispersion system (Figure 3-19) was a C-tube placed in the vessel wall made up of two curved and perforated branches joint together to the delivery pipe by a T-piece screwed at the end of the delivery pipe. The C-tube was constructed according to the standard specifications given in [30] with each branch containing 6 holes of 5 mm diameter and 1 perforation at the end of the pipe of 6 mm diameter. The joining T-piece had a 5 mm diameter perforation. This provides a total hole area of 331 mm^2 (equal to the total cross sectional area of the pipe). Therefore, the ratio of flow to hole area was equal to unity. The standard allows for C-tube holes of 5-6 mm diameter and different number of holes arguing historical reasons; however this

is an unnecessary source of variability in results from different laboratories that could be eliminated, since such differences affect the mixing of dust and air and the turbulence created. The C-tube failed to deliver fibrous biomass inside the explosion chamber and therefore, a new disperser was designed and calibrated. Different designs were tested, as shown in Figure 3-20.

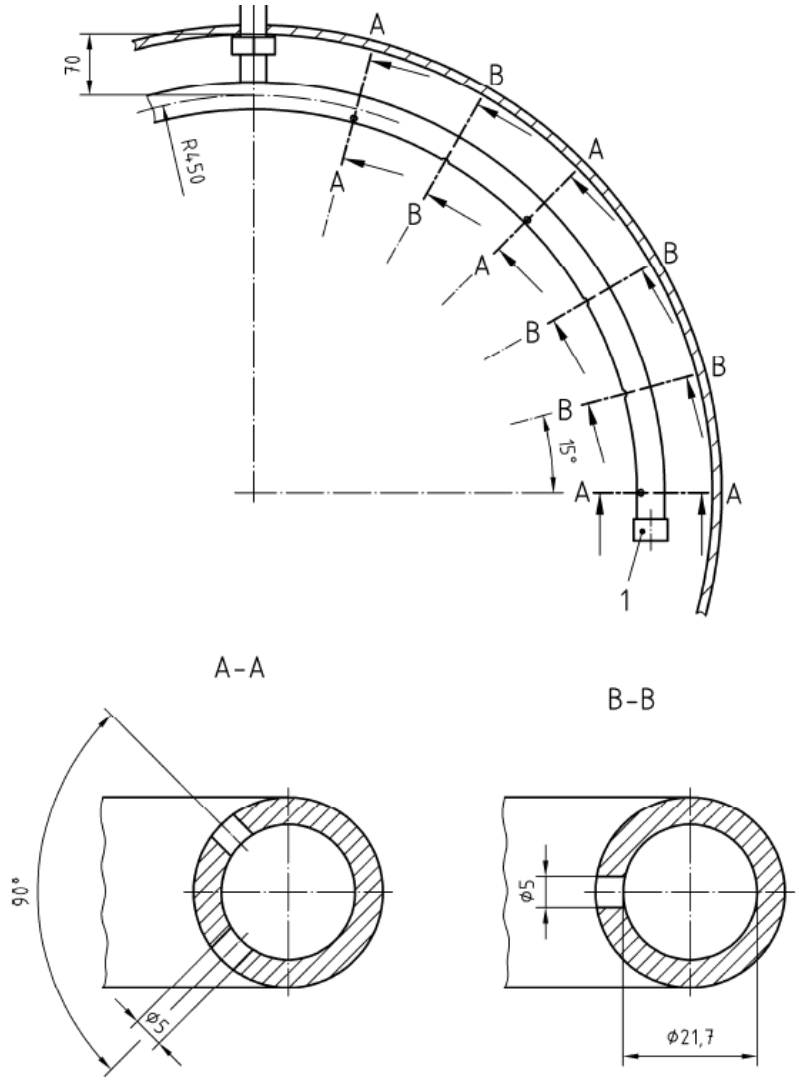

Key

1 end cap with 5 mm hole

Figure 3-19. C-tube design guideline [30]

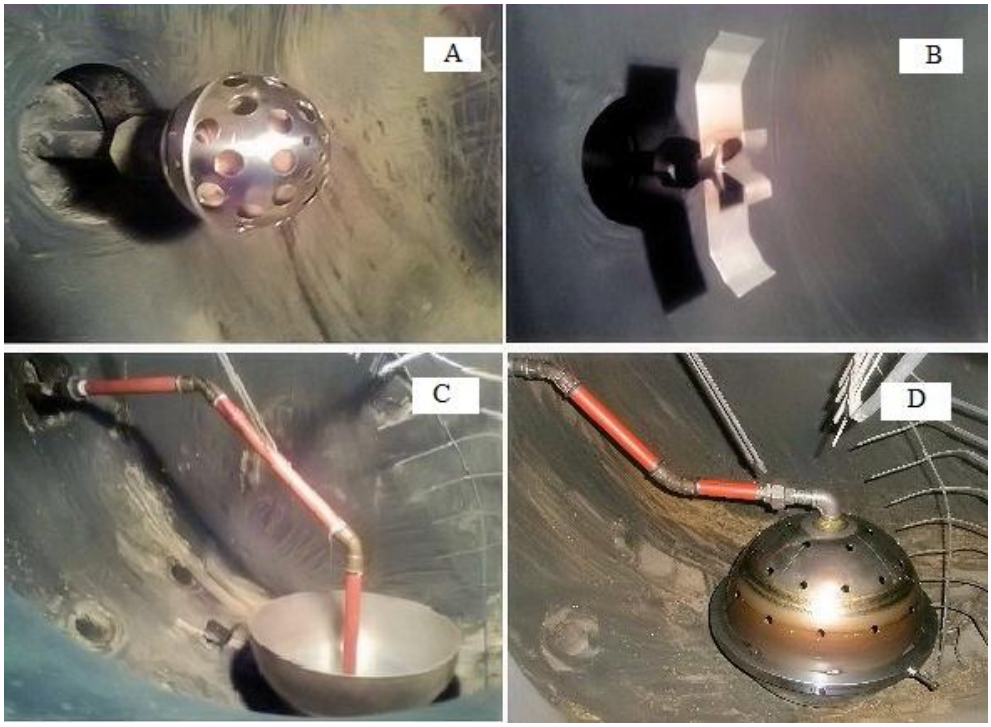

Figure 3-20. Dust dispersers designed by Leeds group: A-spherical nozzle, B-rebound nozzle, C-Hemispherical in-vessel dispersion cup, D-Spherical in-vessel disperser

All tests with coal dust were performed with the standard C-ring in place. However, for fibrous biomass, the spherical wall mounted perforated nozzle was the preferred design (Figure 3-20, A). In previous work by the Leeds research group, all the dispersers were tested and calibrated by performing laminar and turbulent gas explosions. The aim was to quantify the turbulent factor β when the standard system was in place, with the standard 0.6 s ignition delay. Deflagration indexes (K_G) were determined in turbulent (injecting air from the dust pot) and laminar conditions with 10% methane gas mixture in air. Eq.(3.5) was used to derive the turbulent factor:

$$\beta = \frac{K_{G\,turbulent}}{K_{G\,Laminar}} \tag{3.5}$$

Following this calculation the turbulent factor for the vessel was found to be 4.03. Therefore, the requirement for any new dispersion system was to provide the same turbulent factor as the C-ring at the standard ignition delay (0.6 s). The spherical nozzle was found to give the same turbulent factor with an ignition delay of 0.50 s with 10% methane (see Figure 3-21). This was then validated with a series of dust/air mixtures showing comparable results for K_{St}, P_{max}, flame speed, MEC and fraction of mass burnt.

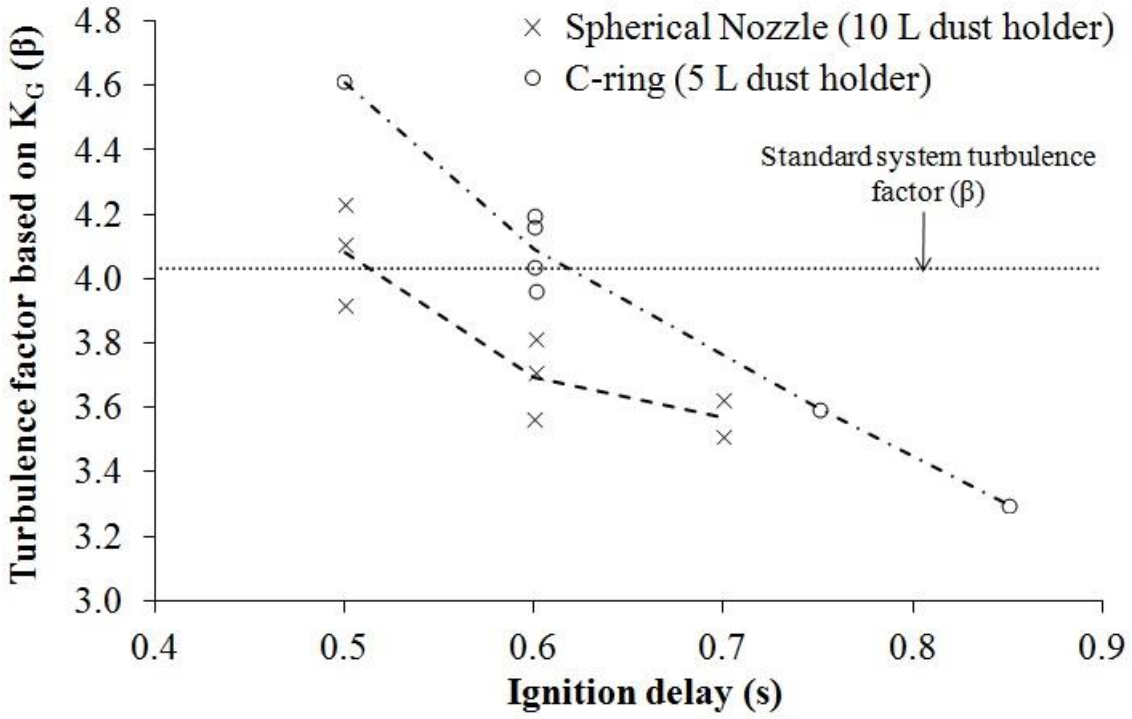

Figure 3-21. Turbulence factor for two dispersers as a function of ignition delay for 10% methane explosions

Other dust dispersers tests showed lower K_{St} and flame speed (hemispherical dispersion cup), or higher MEC (rebound nozzle) than the standard C-ring system. The spherical nozzle produced slightly lower K_{St} (with variation coefficient of 8%) and lower flame speed (with a variation coefficient of 5%), the same as for both fraction of mass burnt and P_{max}/P_i. Therefore, the spherical perforated wall mounted nozzle (spherical nozzle, here and later in the text) was the selected disperser for all biomass and torrefied biomass tests.

The spherical nozzle was designed with perforations just in the front half of the sphere (see Figure 3-22). The diameter of the sphere was 110 mm. The perforations consisted of 9 holes of 8 mm diameter, and 24 holes of 16 mm diameter, arranged in triangular pitch. The total flow area of the spherical nozzle was 5278 mm^2.

The spherical nozzle, however presented one limitation. The limitation was found for the testing of larger particle size dusts. It was found that when testing dusts with bigger particles, these would form blockages in the delivery pipe. Since all dusts tested in this research were milled down to <60 μm, the spherical nozzle was used. However, on-going work by the Leeds group includes the design of new in-vessel dispersers such as the one shown in Figure 3-20, D to overcome this problem.

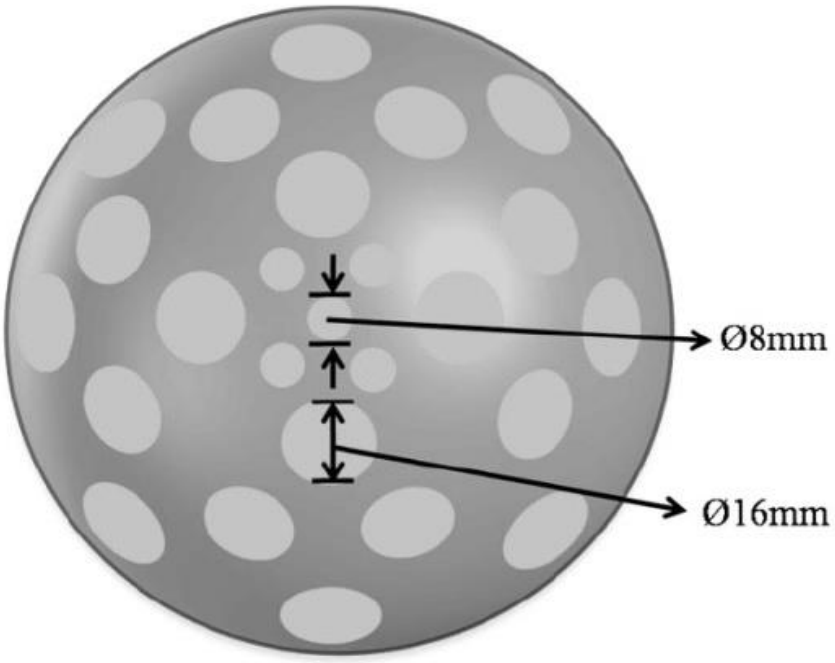

Figure 3-22. Spherical nozzle design schematic

3.3.2.3. Adjustment of valve off timing for biomass dust testing

When the dust holder and dispersion system were modified in order to allow testing of fibrous biomass materials (<60 μm), it was decided to use the spherical nozzle disperser and the 10 L extended dust holder pressurised to 10 bar. The valve off timing was unchanged. An example of traces found for this system with a biomass material is given in Figure 3-23. It was found that a considerable amount of explosion pressure (3.1 bar, in this particular case) was transmitting into the dust holder, increasing the risk of having a violent explosion that the dust holder could not withstand. Although the dust holder was pressure-rated to 25 bar, it was decided to modify the valve-off timing so that the valve would be completely closed by the onset of the pressure increase inside the dust holder due to the explosion (110 ms earlier). It was assumed that since the explosion pressure was already entering the dust holder, the change would not affect the amount of dust delivered into the explosion vessel. After the valve off timing was decreased by 110 ms, it was confirmed that the results were comparable, and that no explosion pressure was entering the dust holder.

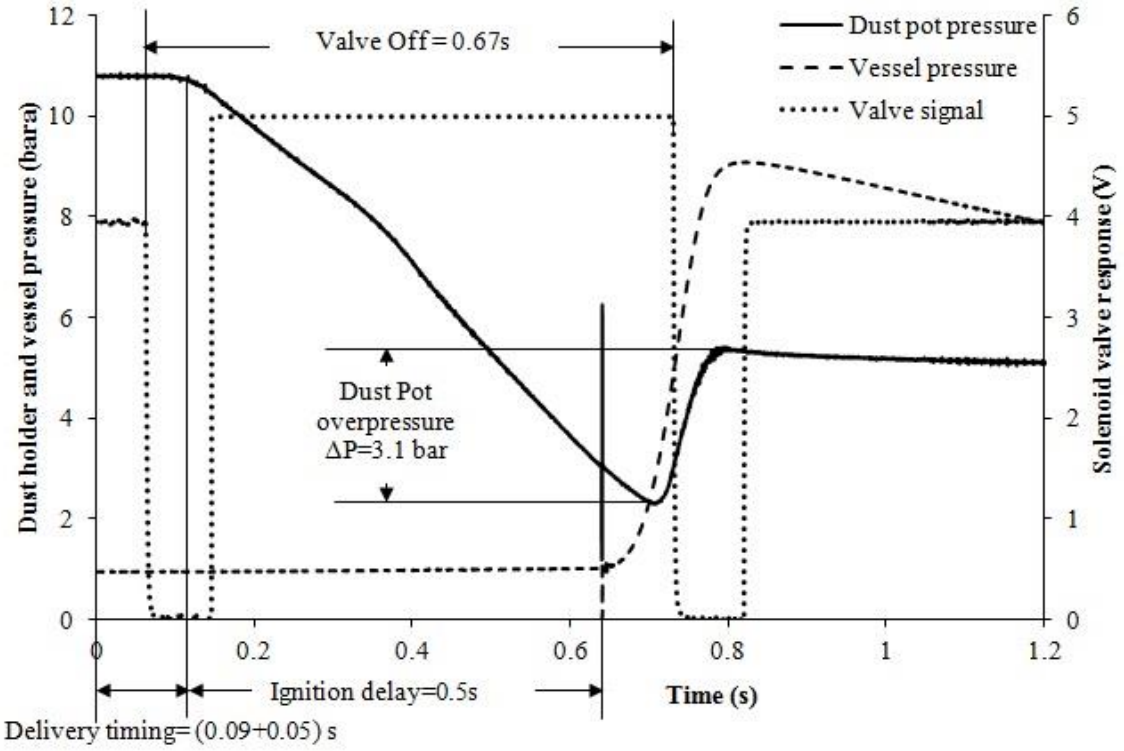

Figure 3-23. Transmission of explosion pressure into dust holder: pressure traces and solenoid valve response as a function of time

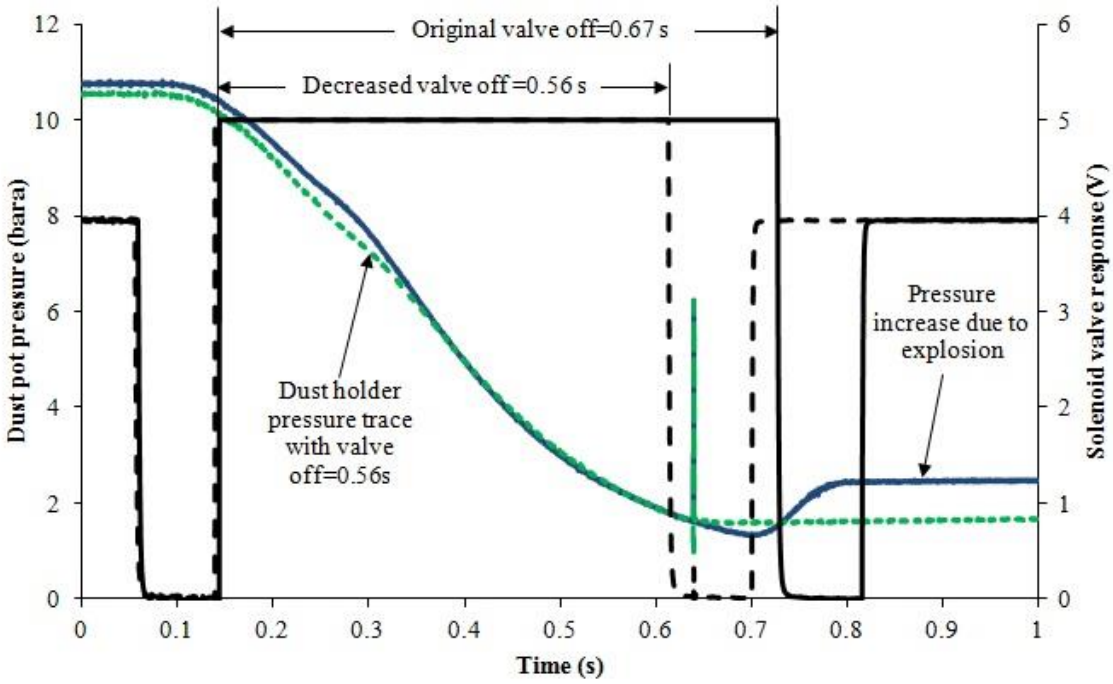

Figure 3-24. Modified valve off timing and pressure traces

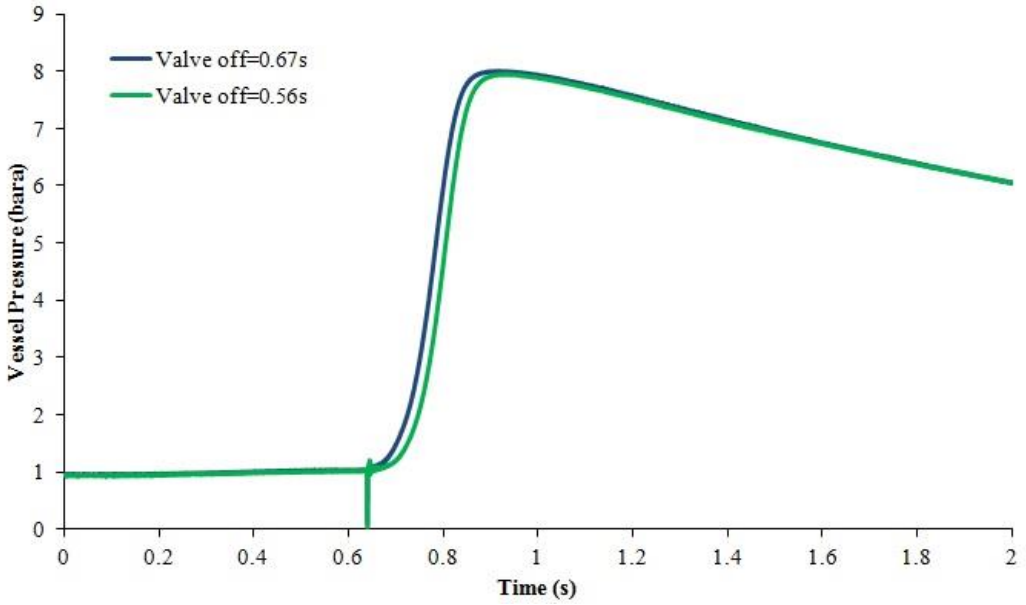

Figure 3-25. Repeat pressure traces before and after valve off timing modification

As depicted in Figure 3-24 the change of valve off timing was effective, and no explosion pressure was entering the dust holder eliminating the risk of violent explosion inside the dust pot. Also Figure 3-25 shows the effect of the change on the pressure trace.

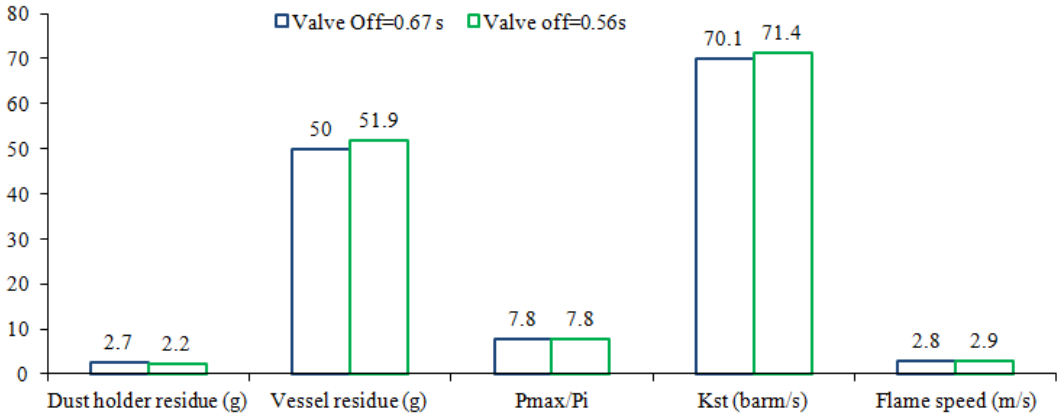

Figure 3-26. Comparison of explosion characterisation parameters before and after valve off timing modification

As shown in Figure 3-26 all values were comparable. The coefficients of variation were smaller than 3% for maximum pressure, K_{St}, flame speed and vessel residue. The coefficient of variation for the amount of residue left in the dust holder was 14%. It was therefore concluded that the change of settings did not affect the results.

3.3.2.4. Ignition circuit

Ignition of an explosible dust cloud inside the explosion chamber was achieved with two 5 KJ chemical igniters supplied by Fr. Sobbe GmbH. The igniters consisted of two insulated wires of 0.18 m length and a cap containing 40% zirconium metal, 30% barium nitrate and 30% barium peroxide. The igniters were connected in parallel with two extended electrodes mounted on a blind flange and placed in a perforated hemispherical cup in the geometric centre of the vessel (see Figure 3-31). This cup ensured no directional ignition effects that could disturb the formation of spherical flames. The chemical igniters were activated by a current discharge coming from an external spark box.

3.3.2.5. Evacuation system

Prior to explosion, in accordance to the standards, the explosion chamber was evacuated so that in addition of the pressure coming from the dust holder, the pressure at the time of explosion was 1.013 bara. Therefore the vessel was evacuated using an Edwards two stage high vacuum pump E2M175 (Figure 3-27). The vacuum pump was also used for purging the combustion gases generated in the explosion, which after particulates collection in a dust filter, were expelled to the ambient through an exhaust pipe. This method had to be modified when coal explosions were performed due to the formation of high concentration of H_2S. The devised system for the exhaust of gases from coal explosions consisted on increasing the mixing of combustion gases with clean air from the laboratory by opening two valves in the purging line and by increasing the exhaust pipe length. A schematic of the modified system for coal explosions is shown in Figure 3-28.

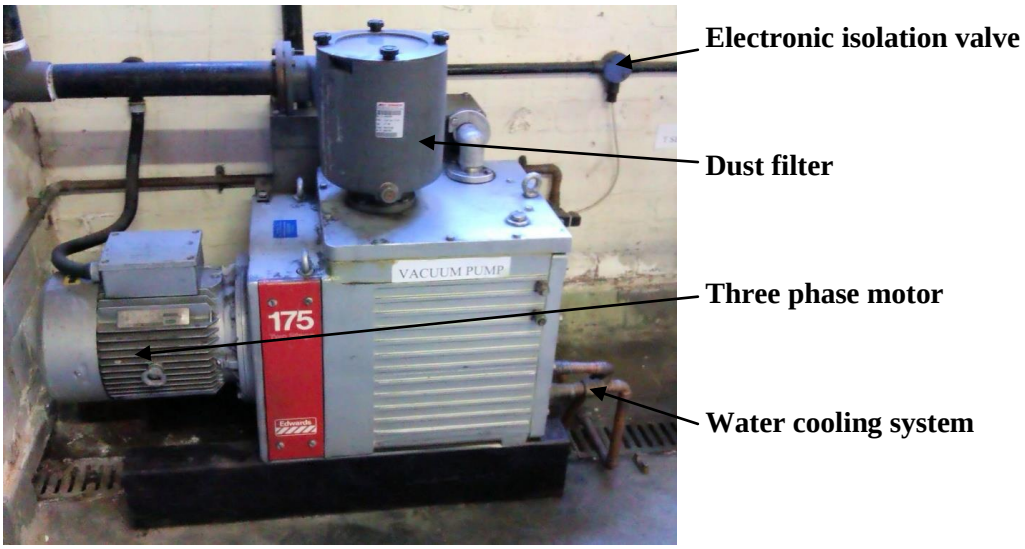

Figure 3-27. 1 m^3 Vacuum pump

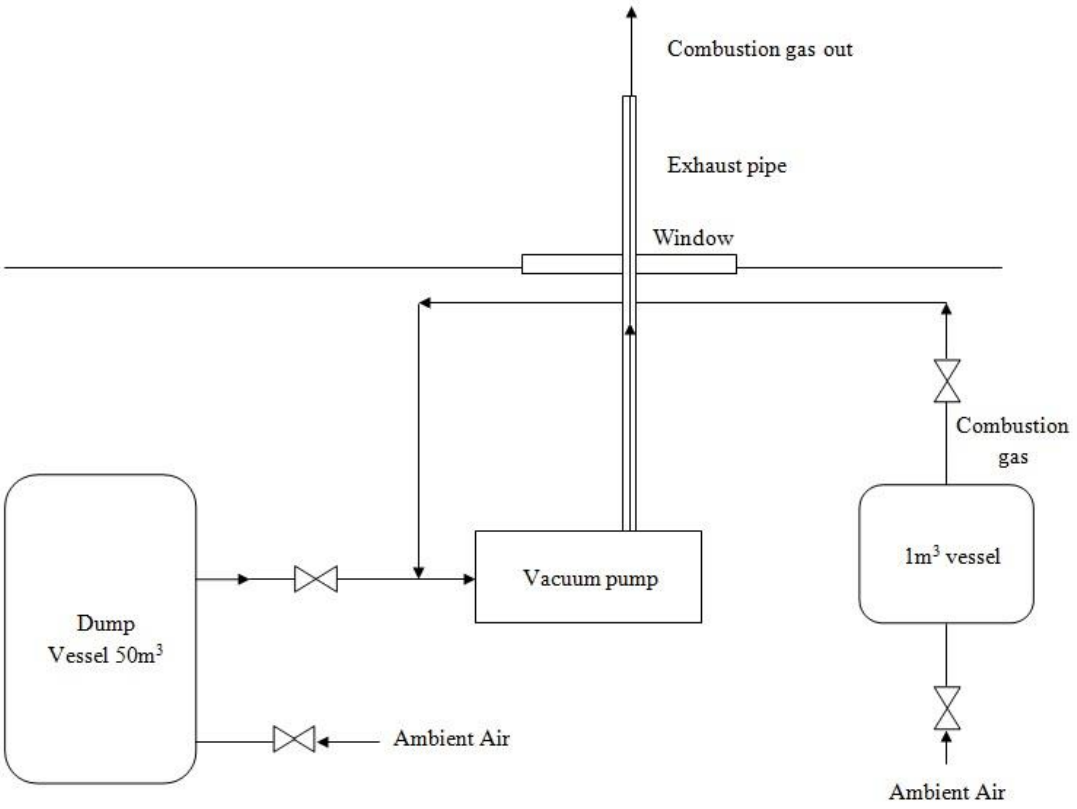

Figure 3-28. Coal dust explosion gas purging system

3.3.2.6. Residue collection

Residues found in the dust holder and explosion chamber after explosion were collected using a Numatic MFQ-372 vacuum cleaner fitted with NVM-1CH dust bags. Dust bags were weighted before and after collection to quantify the amount of dust remaining in each enclosure. Residues from the dust holder were not injected into the vessel and by quantifying this amount of dust it was possible to subtract such mass and have an accurate value of injected concentration. This has been usually disregarded in the literature and it is an unnecessary source of inaccuracy in the concentration that actually takes place in the combustion reaction.

Explosion residues found inside the explosion chamber were individually collected in a dust bag and stored in sample bottles. A greater challenge was posed by these residues since they were often a mixture of partially burnt and unburnt particles. However, it was possible to apply a series of corrections in order to improve the accuracy of concentrations. The nominal concentration refers to the concentration without taking into account any of the residues, that is, as expressed in Eq.(3.6):

$$Nominal\ Concentration\ \left({}^{g}/_{m^3}\right) = \frac{Mass\ placed\ in\ dust\ holder\ (g)}{Vessel\ Volume\ (m^3)} \qquad (3.6)$$

The dust holder residue did not participate in the reaction at all, and therefore, by weighing the amount of dust left in the dust holder it is possible to express the concentration as "Injected concentration", using Eq.(3.7) :

$$Injected\ Concentration\left(^{g}/_{m^3}\right) = \frac{Mass\ in\ dust\ holder\ (g) - Dust\ holder\ residue\ (g)}{Vessel\ volume\ (m^3)} \quad (3.7)$$

A 95% efficiency in the collection of vessel residue was considered, therefore;

$$Corrected\ vessel\ residue = \frac{Vessel\ residue}{0.95} \quad (3.8)$$

Now, considering the entire residue found in the vessel did not participate in the explosion flame front, the percentage of mass burnt is expressed as:

$$Mass\ burnt(\%) = \frac{Mass\ in\ dust\ holder - Dust\ holder\ residue - Corr.vessel\ residue}{Mass\ in\ dust\ holder - Dust\ hoder\ residue} \times 100 \quad (3.9)$$

Two corrections have been considered in this work, for the first, the actual concentration considers the % of mass burnt in each case, as shown in Eq.(3.10) :

$$Actual\ Concentration\ \left(^{g}/_{m^3}\right) = Injected\ concentration \times \frac{Mass\ burnt(\%)}{100} \quad (3.10)$$

The corrected concentration, in contrast, considers the maximum percentage of mass burnt for the sample, and therefore the corrected concentration is expressed as shown in Eq.(3.11):

$$Corrected\ Concentration\left(^{g}/_{m^3}\right) = Injected\ concentration \times \frac{Max\ mass\ burnt\ (\%)}{100} \quad (3.11)$$

The residues collected from the explosion chamber were characterised for their elemental and proximate composition as well as particles morphology, density and size distribution, following the same procedures as for original samples detailed in section 3.2.

It has been considered by Slatter et al. [35] that residues found inside the explosion chamber following an explosion test are a proportion of dust that is pushed by the explosion wind against the vessel walls. It was possible to derive the theoretical thickness (λ) of a layer formed uniformly in the vessel walls as follows:

$$Dust\ layer\ volume = 4\pi r^2 \lambda \tag{3.12}$$

$$\lambda = \frac{\frac{m_{residue}}{\rho_{dust}}}{4\pi r^2} \tag{3.13}$$

Where $m_{residue}$ is the corrected vessel residue, ρ_{dust} is the bulk density of the specific dust and r is the radius of the 1 m^3 vessel (0.65 m).

3.3.2.7. Instrumentation and data collection

3.3.2.7.1. Pressure Transducers: Pressure-time histories

Absolute pressures were measured inside the explosion chamber and dust holder. Two pressure transducers, as required by the standard, were centrally fitted in a blank plate through threaded drilled and tapped holes situated in the opposite flange to the vessel door. These were Keller PAA-11 piezo-resistive transducers with measurement ranges of 0-25 bara and 0-10 bara. There was an additional pressure transducer fitted in the dust holder with a range of 0-25 bar. Typical examples of pressure-time histories recorded are shown in Figure 3-29. From the pressure-time histories it was also possible to quantify the rate of pressure loss, taken as the reduction of 10% of the peak pressure divided by the time taken for such reduction to occur, as shown in Figure 3-29.

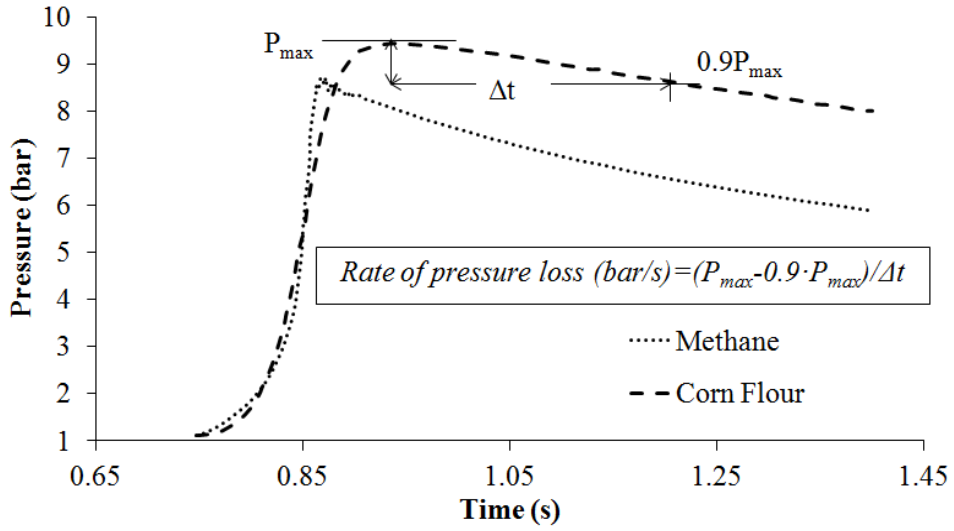

Figure 3-29. Rate of pressure loss determination method

3.3.2.7.2. Thermocouples: S_F, S_L and GHRR

An additional feature of the Leeds ISO 1 m^3 vessel not contemplated in the standard, was the addition of thermocouples to map flame position and derive flame speeds during the constant pressure period of the explosion. Arrays of exposed junction type-K thermocouples were fitted (using Swagelock compression fittings and PTFE ferrules with a total pressure rating of 69 bar) along the vertical and horizontal axis of the vessel. In the horizontal axis 12 thermocouples were positioned at both sides of the ignition point. These thermocouples provided the time of flame arrival in horizontal right and horizontal left directions. Another array of 8 thermocouples was fitted in vertical downwards direction (See Figure 3-30 and Figure 3-31).

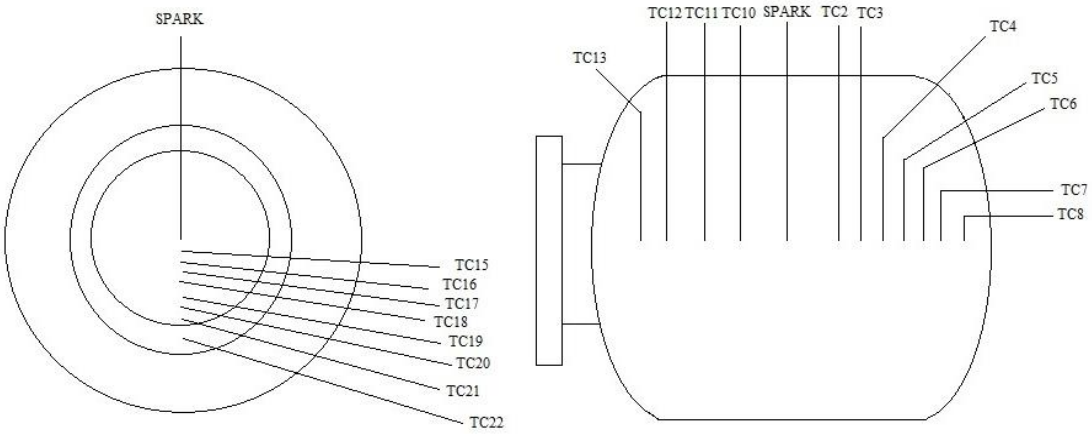

Figure 3-30. Thermocouple arrangement in 1 m^3 vessel schematic

Figure 3-31. Thermocouple arrangement and hemispherical cup

A flame travelling through the junction of the thermocouples registered a change in voltage potential across the junction; such change in voltage is then recorded in the output signal. The first point at which a thermocouple trace changes in voltage (Figure 3-32) is taken as the time of flame arrival.

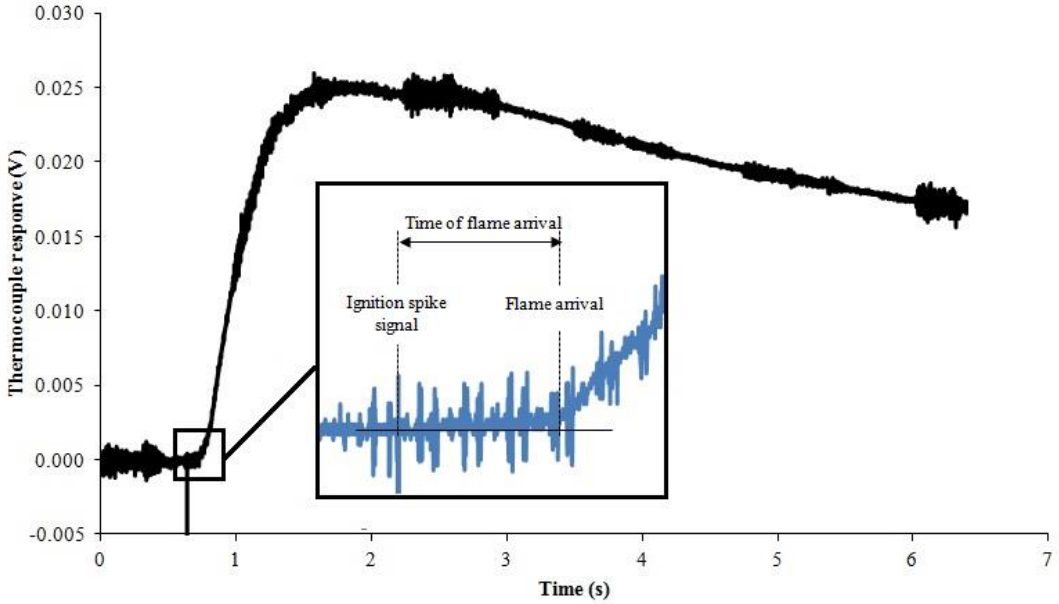

Figure 3-32. Typical thermocouple trace in 1 m^3 dust explosions

Table 3-3. Thermocouple distances

Horizontal Left		**Horizontal Right**		**Vertical downwards**	
Thermocouple	Distance from spark (mm)	Thermocouple	Distance from spark (mm)	Thermocouple	Distance from spark (mm)
2	135	**10**	74	**15**	140
3	200	**11**	135	**16**	200
4	267	**12**	199	**17**	267
5	332	**13**	260	**18**	315
6	393			**19**	372
7	460			**20**	431
8	527			**21**	483
				22	550

Measured distances for thermocouple to thermocouple, presented in Table 3-3, could be plotted against time of flame arrival. Each direction (horizontal right, horizontal left and vertical downwards) was plotted as separate series. The slope of the linear relationship between distance and time of flame arrival was the average flame speed in each direction (Figure 3-33).

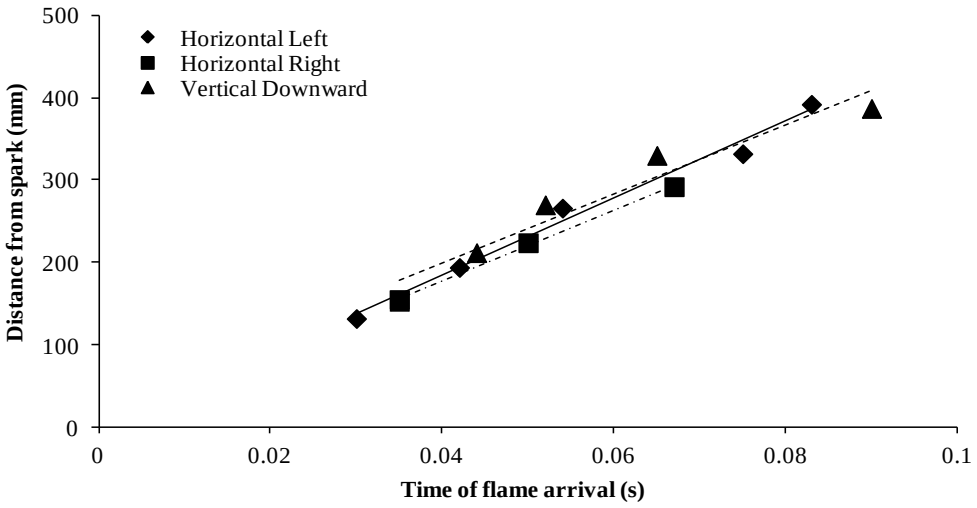

Figure 3-33. Flame speed measurement method

Flame speeds were measured in the constant pressure period, which takes place between 0.2 and 0.7 of the vessel radius. This is shown in Figure 3-34. The first 20% and last 70% of the flame travel is neglected due to ignitor and flame curvature effects in the early development of the flame and later due to wall effects.

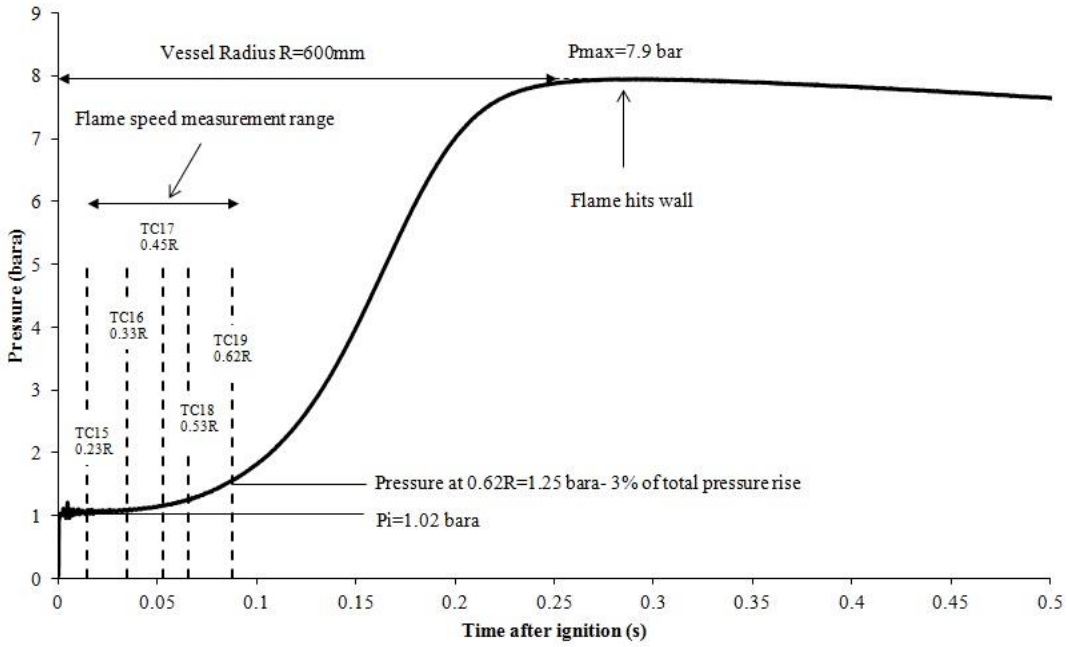

Figure 3-34. Flame travel and pressure rise

It is shown below that for 90% of the flame travel the fraction of mass burnt is negligible and therefore the pressure rise is too. The pressure rise in an enclosure is a linear function of initial mass [207]. Considering D as the diameter of a spherical vessel, D_f as the diameter of the flame and ρ_u and ρ_b as the density of unburnt and burnt gases:

$$Initial\ mass\ in\ volume\ V = \frac{1}{6}\pi D^3 \rho_u \tag{3.14}$$

$$Mass\ burnt = \frac{1}{6}\pi D_f^3 \rho_b \tag{3.15}$$

$$\%\ Mass\ burnt = \frac{\frac{1}{6}\pi D_f^3 \rho_b}{\frac{1}{6}\pi D^3 \rho_u} \times 100 = \left(\frac{D_f}{D}\right)^3 \frac{\rho_b}{\rho_u} \times 100 \tag{3.16}$$

the density ratio is inversely proportional to the temperature ratio, therefore:

$$\%\ Mass\ burnt = \left(\frac{D_f}{D}\right)^3 \frac{T_u}{T_b} \times 100 \tag{3.17}$$

Typical T_b for stoichiometric mixtures of hydrocarbons in air is about 2100 K and assuming T_u=300 K, for 90% of the flame travel 13% of mass is burnt.

Using flame speeds measured in the constant pressure period, it is possible to calculate burning velocities. Laminar burning velocity is a fundamental combustion property that is used in gas explosions as the explosion protection parameter instead of the deflagration index (K_G, equivalent to dusts K_{St}) [37]. However, for dusts K_{St} remains the preferred parameter. Turbulent flame speeds measured in the Leeds ISO 1 m^3 can be used for the calculation of laminar burning velocity. Turbulent flame speeds $(S_F)_T$ and turbulent burning velocity S_T are related as presented in Eq.(3.18),

$$(S_F)_T = E_p \cdot S_T \tag{3.18}$$

where E_p is the adiabatic expansion ratio at constant pressure. Laminar and turbulent burning velocity relate as follows,

$$S_T = \beta \cdot S_L \tag{3.19}$$

Where β is the turbulence factor of the vessel. Combining Eq.(3.18) and Eq.(3.19):

$$(S_F)_T = E_p \cdot \beta \cdot S_L \tag{3.20}$$

Knowing E_p the laminar burning velocity could be derived. It was found using in-house software FLAME that the E_p at constant pressure for solids was much lower than the expansion factor at constant volume. Using this E_p would produce burning velocities 2.5 times higher than those based on the measured peak pressure. Therefore, for this work it was decided to use P_{max}/P_i as the expansion factor for dusts as recommended by [208].

In addition global heat release rates can be derived from the flame speed measurements. The heat release rate was calculated as the fuel mass burn rate multiplied by the calorific value. The global heat release was given as the heat release rate per unit area of the flame front using the following equation:

$$GHRR\ \left({}^{MW}/_{m^2}\right) = \left(\frac{(S_F)_T}{\frac{Pmax}{Pi}}\right) \cdot \rho_u \cdot \frac{GCV}{\left(1 + \frac{A}{F}\right)} \tag{3.21}$$

The pressure ratio also substituted the expansion factor E_p here, and ρ_u was taken as 1.2 kg/m^3. Values derived from explosion tests could be compared to typical heat release rates of burners and provide realistic combustion parameters, which were an improvement over other small scale experimental techniques such as drop tube furnaces.

3.3.2.7.3. Barocel and control panel

The pressure inside the vessel was monitored using a diametric type 600 Barocel sensor and an absolute pressure gauge connected in series. The barocel, which was connected to a Datametrics type 1500 digital pressure display, transformed the absolute pressure into a DC output voltage. The resolution of this system provided a resolution of ±0.05 mbar. This circuit was fitted in the control panel, which is used for preparation of gas/air mixtures in the 1 m^3 and other vessels in the Leeds explosion test facility. The vessel and the pressure monitoring circuit were connected by means of a pressure line and Swagelock Quick Connect fittings.

3.3.2.7.4. Data logging and analysis

Pressure transducers, thermocouples, operating vale outputs and ignition system were connected to a 34-channel Microlink 4000 system. This data logger consisted of 3 modules capable of capturing high speed waveform at a sampling frequency of up to 100 KHz. For the present work the sampling frequency used was 5 KHz (or equivalently, the system collected data once every 0.0002 s).

The data logger was connected to a computer situated in the control room. The software used for initiation of control signals and storing the data capture was

Windmill Wavecap. Data capturing started through an external trigger. The external trigger consisted on pressing the "Start" button in the sequence generator unit. This unit also controlled the signals and timing of the opening and closing of the electro pneumatic valve and the ignition. It consisted of four time delay-programmable channels. Three of the channels were used to trigger the data logger, send the signal to a solid relay for activation of the electro pneumatic valve, and to send the signal to activate the spark box. After the event all data was stored in different channels which could be analysed using IMC FAMOS (Fast Analysis and Monitoring of Signals) software. This software also allowed manipulation of data such as smoothing or differentiation. Therefore the rate of pressure rise was calculated directly by the software through a sequence of smoothing, cropping and differentiation of the pressure trace. The smoothing complied with the normative given in BS EN 15967: 2011 (Annex C) [209].

3.3.2.8. Repeatability of results

The repeatability of results in the Leeds ISO 1 m^3 vessel has been confirmed in numerous occasions using dusts and gases. In previous work, 5 tests with 750 g/m^3 of corn flour were performed and results showed coefficient variations of 5.8% and 1.3% for K_{St} and P_{max}/P_i respectively. It was also found that the mass burnt and injected concentration was similar with variation coefficients of 1.5% and 0.1%. The explosion characteristics also showed good agreement with values found in the literature. In the present work, three tests were performed with 500 g/m^3 of fibrous biomass dust, using the spherical nozzle, and the 10 L dust pot pressurised to 10 bar, with a 0.5 s ignition delay. Table 3-4, shows the results obtained and the variation coefficient for a number of parameters. In all cases, values are within 10%, therefore, it was considered that the repeatability of the system was good.

Table 3-4. Repeatability of results in Leeds ISO 1 m^3 vessel adapted for fibrous biomass testing

	Injected concentration (g/m^3)	**Mass burned (%)**	**P_{max}/P_i**	**K_{St} (bar m/s)**	**$(S_F)_T$ (m/s)**
Fibrous biomass repeat tests	484	79	8.8	81	3.6
	468	69	8.6	74	3.4
	480	74	8.5	75	3.7
Mean	477	74	8.6	77	3.2
Standard Deviation	8.20	5.41	0.17	4.04	0.03
Variation Coefficient (%)	1.7	7.3	1.9	5.3	1.0

3.3.2.9. Stoichiometric fuel to air and equivalence ratio

Concentrations in the literature are often expressed as g of dust per m^3 of air. Explosion characteristics are therefore compared for different dusts in terms of concentrations. However, since all dusts have different chemical composition, the stoichiometry of the combustion reaction is different. Using equivalence ratios instead of concentrations allows direct comparison of characteristics for different dusts.

The elemental composition in terms of C,H, O, N and S was used to calculate the stoichiometric fuel to air ratio (F/A). The balanced combustion equation in air is shown in Eq.(3.22).

$$CH_yO_zN_wS_k + aO_2 \rightarrow bCO_2 + cH_2O + dNO_2 + eSO_2 \tag{3.22}$$

Where, y, z, w and k are the atomic ratios to carbon of H, O, N and S respectively. Substituting for a, b, c, d and e in terms of y, z, w and k the stoichiometric fuel to air mass ratio is given by:

$$Stoichiometric(F/A) = \frac{12 + y + 16z + 14w + 32k}{\left(1 + \frac{y}{4} - \frac{z}{2} + w + k\right)\frac{32}{0.232}} \tag{3.23}$$

Multiplying the fuel to air ratio by the density of air ρ_{air} (approximately 1.2 kg/m^3) expresses the stoichiometric fuel to air ratio in grams of fuel per cubic meter of air:

$$Stoichiometric\ (F/A)(g/m^3) = Stoichiometric\ (F/A) \cdot \rho_{air} \tag{3.24}$$

Concentrations of dust in air can be expressed in equivalence ratio (ratio of actual to stoichiometric fuel to air ratio), using Eq.(3.25):

$$\emptyset = \frac{Actual\ (F/A)\ (g/m^3)}{Stoichiometric\ (F/A)\ (g/m^3)} \tag{3.25}$$

3.3.2.10. 1 m^3 Procedures

Procedures for the operation of the Leeds ISO 1 m^3 vessel in this work followed a number of steps detailed as follows. Only a slightly different procedure for the evacuation of combustion gases was used when coal dust was tested.

1. Ensure all data logging connections are made.
2. Load software Wavecap program for dust explosion vessel
3. Ensure dust container, delivery pipe and explosion chamber are clean.
4. Check all instrumentation is in working order. This could be done by running the sequence, pressurising the dust holder but using no dust. The ignition circuit could be checked without wasting a chemical ignitor by using a conventional spark plug.
5. Ensure the right disperser was securely attached to the end of the delivery pipe.
6. Attach two chemical ignitors in parallel using the hemispherical cup in the centre of the vessel.
7. Close 20" explosion chamber door placing a non-asbestos jointing gasket, and tightening all bolts using the 4R Torque Wrench set to 500lb_f.ft. Opposite bolts should be tightened systematically.
8. Weigh required amount of dust and pour carefully into the dust holder.
9. Close blank flange to the dust holder using nuts and bolts, tighten with a torque wrench set to 150 kN/m^2
10. Check all valves in the dust holder and vessel are closed
11. Connect barocel pressure line to the vessel, open one of the ambient valves in the vessel (located in the front door) and record ambient pressure, temperature and humidity
12. Close valve and evacuate the vessel to <900 mbar. Allow pressure to settle. If pressure does not settle a specil procedure is required to check for leak forces and abandon test incase of not finding the leakage source.
13. Fill with air to a pre-ignition pressure of 933.3 mbar (the addiction of pressurised air and dust from the dust holder adds 80 mbar pressure to the vessel). Therefore, pressure at the time of ignition was always 1013.3 mbar.
14. Disconnect barocel pressure line.
15. Pressurise the dust holder to the required pressure.

16. Pressurise electro pneumatic valve for operation (10 bar)
17. Connect ignition lead and power spark box.
18. Leave test room.
19. Set time delay sequence in sequence generator
20. RUN and ARM data logger
21. Activate sequence in sequence generator (pressing START)
22. Reset sequence generator and save data.
23. Enter test room and disconnect: power to spark box, lead to spark box pressurisation to electro pneumatic valve.
24. Check dust holder residual pressure
25. Perform oxygen gas analysis
26. Purge the system:
    a. Biomass dust:
        i. Turn on vacuum pump
        ii. Open evacuating valve
        iii. After two minutes open ambient valve in the vessel for combustion gas and clean air mixing under vacuum (no combustion gases can be discharged into the test room)
        iv. After a few minutes (10-15), stop vacuum pump
    b. Coal dust:
        i. Turn on vacuum pump
        ii. Open evacuating valve
        iii. After two minutes open ambient valve in the vessel for combustion gas and clean air mixing under vacuum (no combustion gases can be discharged into the test room).
        iv. A dump vessel normally used for venting of gas explosions in the Leeds facility was used to increase the mixing of combustion gases purged from the $1m^3$ vessel. Two currents, the diluted gases from the $1m^3$ and ambient air flowing from the lab through the dumb vessel, mixed and passed through the vacuum pump. This mix of flows was subsequently vented

out through an extended exhaust pipe for increased dilution. See Figure 3-28.

27. After a few minutes (10-15), stop vacuum pump.
28. In a weighted vacuum cleaner bag, collect dust holder residue. Weight dust residue.
29. Open 20” vessel door. Discard fired igniters.
30. In a weighted vacuum cleaner bag, collect and weight vessel residue.

Tick sheets were used to ensure all steps were taken for safe operation.

Chapter 4 DETERMINATION OF MINIMUM EXPLOSIBLE CONCENTRATION AND REACTIVITY OF BIOMASS POWDERS USING A MODIFIED HARTMAN TUBE

CONTENTS

4.1. Introduction

The minimum explosible concentration (MEC) is the lowest concentration of a combustible dust in a mixture with air at which an explosion is able to propagate. This concept is equivalent to the lean flammability limit of a gas. Whereas LFL of gases are well defined and measured limits are widely accepted, MEC's of dusts often vary in great measure. Methods for the determination of MEC's have been criticised for a number of reasons, namely, small vessel sizes using diameters lower than the quenching diameter of some dusts, non-uniform distribution of dust, using closed vessels which are unrealistic when the aim is to find a concentration of dust that would propagate a flame in a large open space or use of large ignition sources [67, 186].

Presently, the methods recommended in the standards use the 20 L sphere or the 1 m^3 ISO vessel for the determination of MEC [74, 210]. Normally both methods use a strong ignition source (10 kJ) which is comparatively very large for the 20 L sphere and causes compression in the unburnt dust-air mixture and widens the flammability limits. Therefore weaker ignition energy (2 kJ, according to the European standard and 2.5 kJ or 5 kJ by the American standard) is recommended for the measurement of MEC in the 20 L sphere. Although this is recognised by the standard, it is recommended that if MEC's are suspected to be over predicted, a bigger vessel such as the 1 m^3 should be used. Another problem with both vessels is the issue of the residue remaining after explosion which prevents an accurate assessment of the dust concentration involved in an explosion. As described in Chapter 3, it was part of the methodology used throughout the present work to take into account the unburnt

powder left in the 1 m^3 vessel. However, it is not part of the procedures in the Standards to measure these unburnt residues.

Another controversial issue is the definition of MEC. The American standard uses the literal definition (MEC is the lowest concentration that explodes) whereas the European standard defines MEC as the first concentration that does not explode. Table 4-1 shows the main differences in the standards that can be contributing to the wide range of MEC values normally found for dusts.

Table 4-1. MEC measurement standard methods

	European Standard BS EN14034-3:2006+A1:2011		**ASTM E1515-07**
Vessel volume	1 m^3	20 L (0.02 m^3)	20 L (0.02 m^3)
Ignition Energy	10 kJ	2 kJ	2.5-5 kJ
Criteria	$P_{ex} \geq P_i + 0.3$ bar	$P_{ex} \geq P_i + 0.5$ bar	$P_{ex} \geq 2P_i + \Delta P_{ignitor}$
MEC resolution and repeats	• If MEC<500 g/m^3, resolution =50% • If MEC>500, resolution=250 g/m^3 • No repeats required	• If MEC<500 g/m3, resolution =50% • If MEC>500, resolution=250 g/m^3 • Three consecutive tests with no explosion required	• Resolution= 25% • Two repeats for concentrations near MEC
MEC definition	Highest concentration at which no ignition occurs	Highest concentration at which no ignition occurs	Lowest concentration that ignites

P_{ex}=explosion pressure
P_i=Pressure at the time of ignition
$\Delta P_{ignitor}$=Increase in pressure due to the igniters

Furthermore, none of the methods used for dusts is suitable for measuring the upper flammability limits of certain dusts. Upper flammability limits for dusts have been generally found to be around 2000 and 3000 g/m^3, but also as high as 13000 g/m^3 [186]. However, both standard methods use external 5 L dust holders that require ¼ of the volume to be empty to ensure a good pressurisation. That means that it would

be very difficult or impossible to determine the UFL of any dust with a bulk density lower than 500 kg/m^3.

As a result of the differences in vessels and criteria used, MEC's in the literature for corn flour vary in a range from 8 to 380 g/m^3 [186].

There is much more agreement on the flammability limits of gases, however there are also disagreements in the determination method of lean flammability limits of gases [211, 212].

For gases, the corresponding standard methods for the determination of the LFL and UFL are also given by the European and American standards. Recommended methods use either see-through vented vessels where visual flame propagation criteria are used (European standard BS-EN 1839-Method T, and American ASTM E681), or closed vessels using pressure criteria [211] (contained in European standard BS 1839 Method B and American rule ASTM E918). The American closed vessel method is designed to determine limits at elevated temperatures and pressures.

The American standard, based on the work of Brandes et al. [211], state that:

"There is a fundamental difference between the ASTM and European methods for flammability determination. The ASTM methods aim to produce the best representation of flammability parameters, and rely upon the safety margins imposed by the application standards, such as NFPA 69. On the other hand, European test methods aim to result in a conservative representation of flammability parameters. For example, in this standard, LFL is the calculated average of the lowest go and highest no-go concentrations while the European test methods report the LFL as the minimum of the 5 highest no-go concentrations"

As an illustration of these methods the European Method T and method B are explained below:

- Tube method (Method T): Uses a tube vessel of L≥300 mm and 80±2 mm internal diameter. With this method a flame detachment criterion is used, the upward movement of the flame from the spark gap should be of at least 100 mm for an explosion to be considered.
- Bomb method (Method B): Uses a spherical or cylindrical vessel of V≥0.005 m^3 or L/D between 1 and 1.5. The criterion is a pressure rise of $P_{ex} \geq \Delta P_{ignitor} + (5 \pm 0.1)\% Pi$.

The Tube method uses a vessel of similar dimensions to the Hartmann tube (described in Chapter 2, section 2.2.3.1).

The Hartmann tube which was initially used for dust MEC measurements [53] received a great deal of criticism when used for this purpose, as dust distributed unevenly with denser pockets of dust around the walls of the tube. In addition to this, the ignition source was activated prior to dust dispersion not allowing for dust to fill the entire volume of the vessel, and it was also considered as a weak ignition source. It was also claimed that the degree of turbulence was not reproducible for each test, and that only tests at ambient conditions could be performed [58]. However, literature values for MEC measured in the Hartmann tube are in cases not so different from those measured in the 1 m^3 or 20 L sphere results, as shown in Table 4-2.

Table 4-2. Comparison of MEC measurement in different vessels

Dust	Hartmann (g/m^3) [61]	1 m^3 or 20 L sphere (g/m^3) [58]	1 m^3 (g/m^3) [37]
Sugar	45	60	200
Milk Powder	50	60	60
Aluminium	30 (6μm)-40 (17μm)	30 (29-22 μm) 60 (10-43μm)	30 (29μm)
Cellulose	55	60	60
Wheat starch	45	60	30
Polypropylene	30-35	30-200	30
Sulphur	20	30	30
Peat	100	125	125

Moreover, the Hartmann tube is 1/800 of the volume of the 1 m^3 ISO vessel, which means that just a few grams of material are needed for each test. This is an important aspect in the present work due to the difficulty in sourcing enough materials for characterisation in the 1 m^3 vessel. An additional potential advantage of the Hartmann tube is that testing of high dust loadings is not limited by poor dispersion, which in turn could lead to the measurement of upper flammability limits.

For these reasons the Hartmann tube was modified according to the details given in Chapter 3 section 3.3.1 and a new method was developed for the measurements of minimum explosible concentrations and also initial rates of pressure rise and flame speeds. Although it was found that the set up could benefit from including an ignition delay for satisfactory dust dispersion and therefore further work was necessary, some example results of tests performed with the modified Hartmann tube are presented here.

MEC measurements for a series of biomass fuels are compared with measurements in the 1 m^3 vessel. The materials used for comparison of results with the standard 1

m^3 vessel were mainly selected so that such materials would easily disperse a cloud in the 1 m^3 and included:

- corn flour and lycopodium dusts
- two brittle biomass dusts: walnut shells, pistachio nut dusts (<63μm)
- one raw fibrous biomass: pine wood mixture dust
- One torrefied biomass: torrefied Norway spruce (T=260°C, 13min, <75μm)
- Off-spec torrefied pellets (<63μm)

Rates of pressure rise and flame speeds were also compared to those found in the 1 m^3 vessel for the same fuels.

To conclude, the effect of torrefaction severity on reactivity was studied using the modified Hartmann. For such study samples of Norway spruce torrefied to different degrees, ranging from lightly to severely torrefied, were used to measure minimum explosible concentrations, initial rates of pressure rise and flame speeds. The torrefaction conditions for these samples were:

- A: T=260°C, t=8min
- B: T=260°C, t=25min
- C: T=285°C, t=16.5min
- D: T=310°C, t=8min
- E: T=310°C, t=25min

These samples were sieved in a Retsch Sieve Shaker to obtain different size fractions such as: <63μm, <500 μm and 63-500μm. Characterisation of fuels was performed for all samples as described in Chapter 3, section 3.2.

This study was of importance since it was not possible to supply enough materials for a study of the same characteristics in the 1 m^3 vessel.

The aim of this work was not to provide yet another method yielding different values of MEC for dusts, but to propose a set up similar to the gas LFL measurement method, that is fast, repeatable, and uses small samples, which can also offer results on flame speeds and most reactive concentrations. The development of the experimental techniques and validation efforts for this method were presented in Chapter 3, section 3.3.1.

4.2. MEC measurements

The European standard for MEC determination notes that other methods different to those recommended (1 m^3 and 20 L sphere) can be used if it is proved that such methods yield comparable results to the methods recommended. It is also specified that the so called Hartmann tube can be used however, if the dust is not explosible in the Hartmann tube it should not be considered that the dust is not explosible or that it does not have a lean limit, presumably due to the low ignition source. In the present work difficulties were experienced to ignite Kellingley coal in the modified Hartmann tube. Seven readily explosible biomass dusts were tested in the Hartmann tube and 1 m^3 vessel, Table 4-3 shows their characteristics.

All the samples used were CHO type dusts, although certain differences exist between them. In general cornflour presented lower carbon content whereas torrefied fuels contained more carbon. Lycopodium contained significantly less oxygen than any of the other fuels.

Table 4-4 shows the comparison of MEC values found using both the modified Hartmann and the 1 m^3 vessel. The MEC shown for the Hartmann method corresponds to the concentration for which the probability of explosion was 0% in agreement with the European standard definition of MEC in the 1 m^3 vessel.

The nominal MEC concentrations from the 1 m^3 correspond to the mass loaded in the dust holder divided by the volume of the 1 m^3 vessel. On the other hand, the corrected concentration takes into account the residues left in the pot and in the vessel, and the maximum mass burnt for the sample, as explained in Chapter 3, section 3.3.2.6. Corrections for the residues from the Hartmann tube were not calculated due to the impossibility of accurately collecting residues in this equipment as part of the dust is ejected from the tube and other particles remained stuck to the walls. The corresponding equivalence ratios for all MECs are also given. In general, the values for MEC found in the Hartmann were lower than those found in the 1 m^3 (both expressed as nominal or corrected MEC). The MEC's measured in the Hartmann tube varied an average of 36% from the corrected MEC's measured in the 1 m^3 vessel. However, values are in good agreement with those found in the literature for lycopodium and corn flour (see Table 4-5).

Table 4-3. Characterisation of fuels used for MEC comparison in modified Hartmann and 1 m^3 vessel

	Corn Flour	Lycopodium	Walnut shell	Pistachio nut shell	Pine wood mixture	Torrefied Norway spruce	Off-spec Torrefied pellets
Elemental Analysis(wt%), as received							
C	37.7	64.3	47.0	44.0	43.9	51.6	49.1
H	6.3	8.9	6.0	5.6	6.2	5.2	5.3
O	40.5	19.3	35.4	37.4	37.6	35.4	30.9
N	0.1	1.9	0.5	2.3	0.6	0.7	2.4
S	0.0	0.0	0.1	0.0	0.0	0.0	0.0
TGA-proximate (wt%), as received							
Moisture	11.6	1.6	4.9	2.7	3.5	2.8	3.9
Volatile Matter	77.8	89.2	74.5	78.4	79.5	77.0	68.9
Fixed Carbon	6.8	5.1	14.5	10.7	8.7	15.9	18.8
Ash	3.8	4.1	6.1	8.3	8.2	4.2	8.4
Ø=1 F/A ratio (g/m^3), as received	212	115	178	194	190	178	165
GCV (MJ/kg) dry, ash free	17.5	32.5	21.2	19.9	19.8	21.9	22.4

In view of the results from the present work and the literature, biomass dusts appear to burn at leaner mixtures than other dusts. It should be noted that the stoichiometric F/A concentration used for the calculation of equivalence ratios corresponds to the solid fuel composition. It is likely that biomass particles burn by releasing volatiles that then burn mixed with air, therefore the stoichiometry of the mixture of gases should be used instead.

Table 4-4. Comparison of MEC determined in the modified Hartmann tube and the 1m^3 vessel

Fuel	MEC Hartmann (g/m^3)	Hartamnn $Ø_{MEC}$	Nominal MEC 1m^3 (g/m^3)	1 m^3 Nominal $Ø_{MEC}$	Corrected MEC 1 m^3 (g/m^3)	1 m^3 Corrected $Ø_{MEC}$
Corn flour	67	0.32	115	0.54	85	0.40
Lycopodium	22	0.19	30	0.26	13	0.12
Walnut dust	30	0.17	75	0.40	49	0.27
Pistachio nut dust	30	0.15	90	0.46	38	0.20
Pine wood mix	44	0.23	40	0.21	30	0.16
S2STS	37	0.21	63	0.35	49	0.28
RWET	37	0.22	89	0.54	55	0.32

Table 4-5. Literature MEC values for CHO and pure hydrocarbon dusts

Material	Ø=1 (g/m^3)	MEC (g/m^3)	$Ø_{MEC}$	MEC Ref.
Cellulose ($CH_{1.67}O_{0.83}$)	234	55 60	0.24 0.26	[61] [58]
Pitch Pine ($CH_{1.46}O_{0.42}$)	148	30-60	~0.3 (0.20 – 0.40)	[58]
Spruce ($CH_{3.58}O_{1.55}$)	313	20 – 70	~0.14 (0.06-0.22)	[60]
Carbon (C)	104	60	0.55	[37] [58]
Bituminous Coal ($CH_{0.78}O_{0.67}$)	94.5	55	0.58	[61]
Corn flour ($CH_{0.06}O_{0.4}$)	212	75 55	0.35 0.26	[58] [61]
Lycopodium ($CH_{1.65}O_{0.22}$)	115	20 25	0.17 0.22	[58] [61]
Polypropylene (CH_2)	81	35	0.43	[61] [58]

The results presented here suggest that the gases evolved from biomass particles are different than those evolved from coal, pure carbon or polypropylene and that they are more reactive. It was discussed in Chapter 2 that the main gases found to evolve at high heating rates and high temperatures from torrefied biomass are CO and H_2. H_2 lean flammability limit is found at Ø=0.14, and therefore it is suspected that hydrogen mixed with other gases evolving from biomass and torrefied biomass result in lower flammability limits than for coal where volatiles are mainly composed by CO (Ø=0.67) and CO_2 (non-flammable).

4.3. Rates of pressure rise and flame speeds

The modified Hartmann tube allowed measurement of incipient rates of pressure rise prior to venting of an explosion. As three tests were performed for each mass of dust, an average rate of pressure rise was obtained. Examples of rates of pressure rise measured within the flammable range in the modified Hartmann and the average values obtained for Norway spruce and pine wood dust are shown in Figure 4-1. The scatter of measurements was usually wider near the limits.

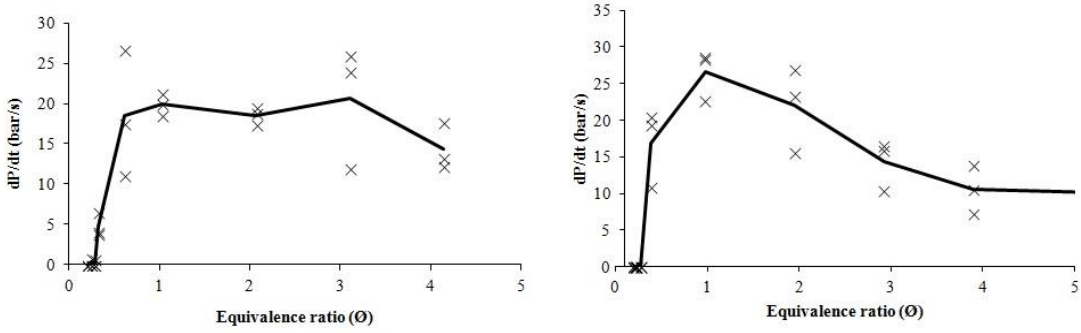

Figure 4-1. Initial rates of pressure rise in Hartmann tube for torrefied Norway spruce (left) and pine wood mixture (right).

In addition to rates of pressure rise, it was possible to measure flame speeds in the modified Hartmann using the array of thermocouples placed in the path of the flame above the ignition point. It was shown in Chapter 3 that the flame speeds measured in the Hartmann tube corresponded to a secondary slower flame observed after the vent cover burst. Figure 4-2 shows that there was a fairly linear relationship between flame speeds and rates of pressure rise for torrefied Norway spruce and pine wood pellet dusts.

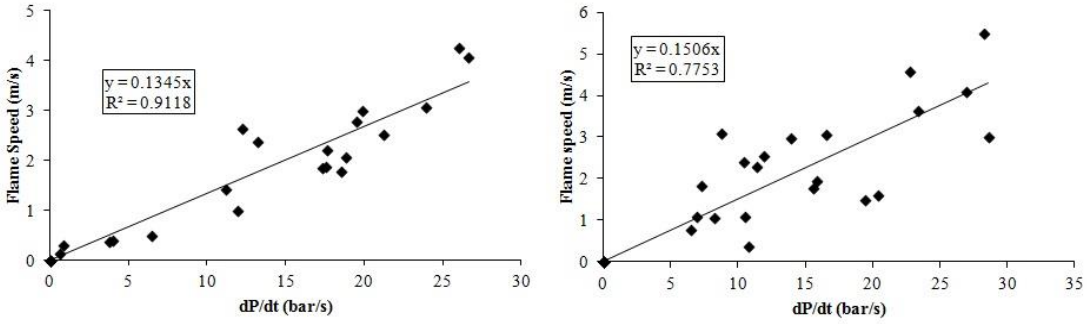

Figure 4-2. Relationship between flame speeds and rates of pressure rise in Hartmann tube for torrefied Norway spruce (left) and pine wood mixture (right)

However, the flame speeds measured in the Hartmann tube were different to those measured in the 1 m^3. As the Hartmann tube flame speeds were measured when the vent burst the corresponding concentration was uncertain (see Figure 4-3).

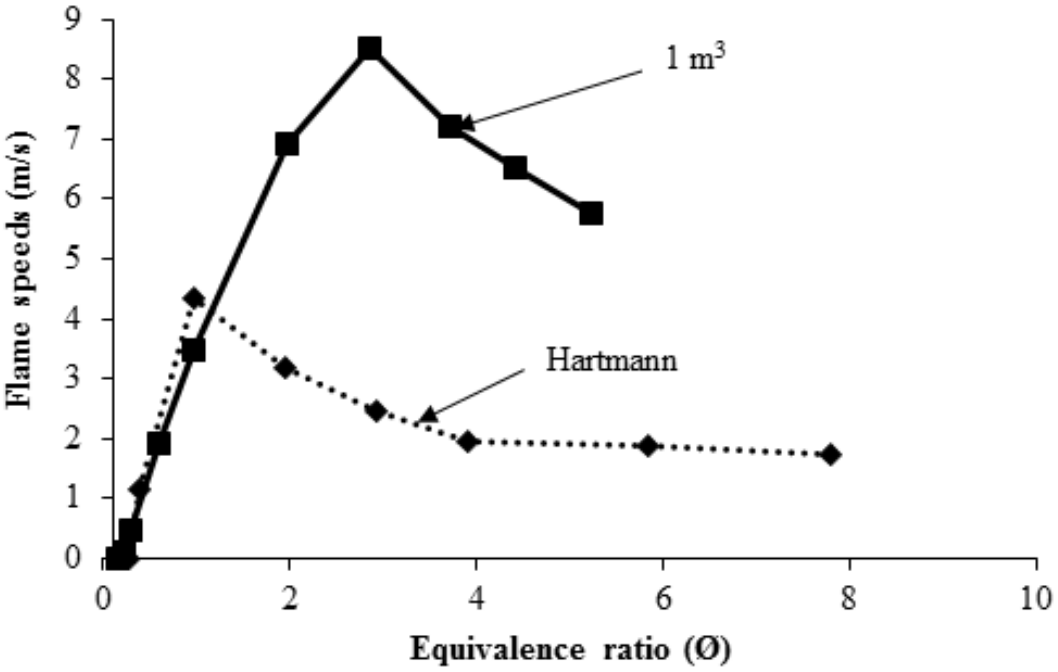

Figure 4-3. Comparison of flame speeds measured in 1 m^3 vessel and modified Hartmann for pine wood mixture dust

Flame speeds measured in the Hartmann tube were considerably slower than those measured in the 1 m^3 vessel. In fact, 1m^3 flame speeds were more than twice as fast for pine wood dust.

Figure 4-4 contains additional data for corn flour, walnut shells, pine wood mixture, torrefied Norway spruce and off-spec torrefied pellets in terms of rates of pressure rise.

Maximum rates of pressure rise measured in the 1 m^3 and modified Hartmann did not correlate either (see Figure 4-4). This could be due to the fact that in the Hartmann tube, the pressure is not allowed to develop completely and it is vented at 1.53 bara. Therefore the maximum rate of pressure rise corresponds to the initial stages of pressure rise, whereas in the 1 m^3 the pressure can develop fully until it touches the vessel wall and starts decreasing. However, both pressure rises (in the Hartmann and in the 1 m^3) provided a measurement of dust reactivity.

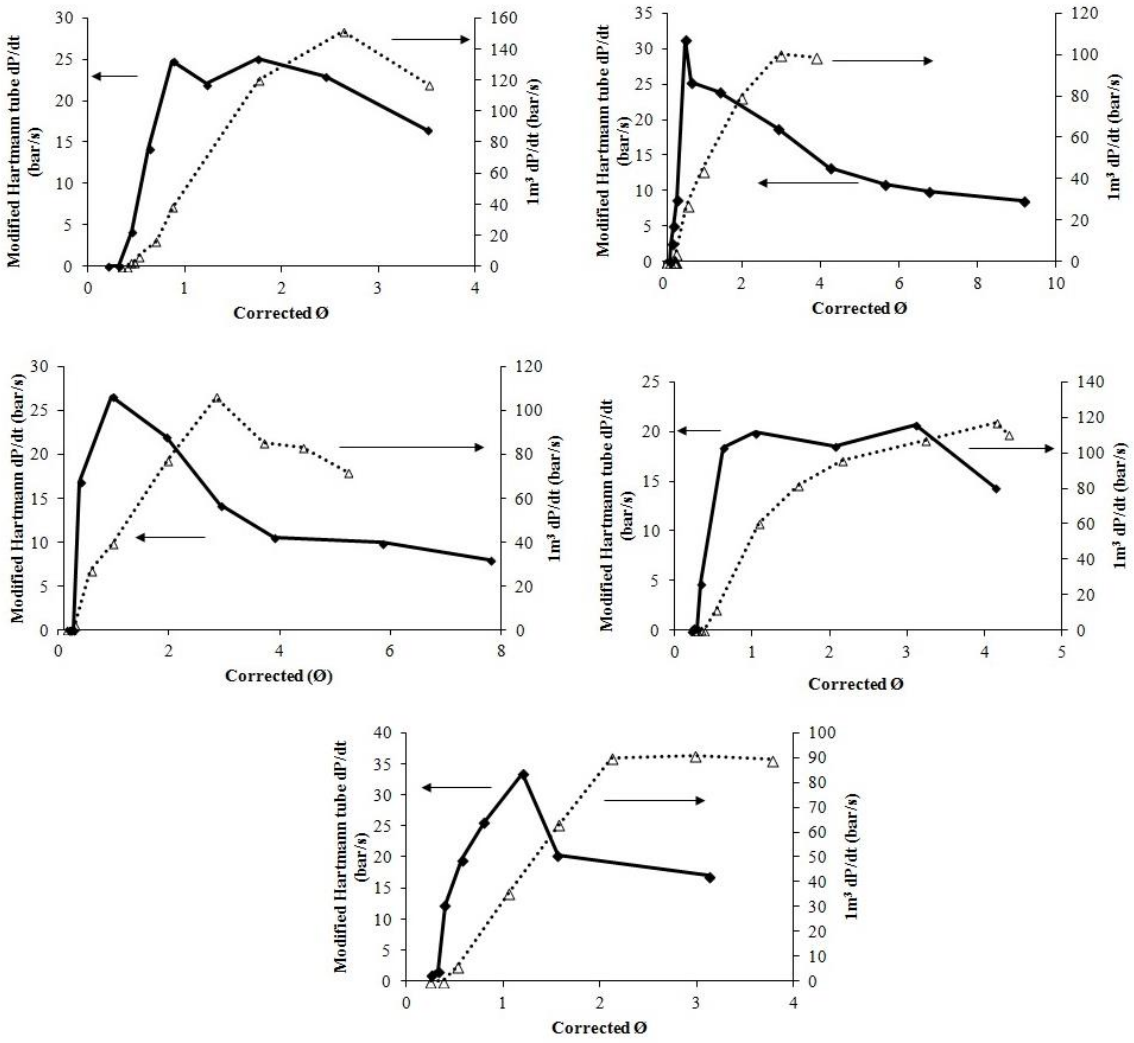

Figure 4-4. Reactivity map for corn flour (top left), walnut shells (top right), pine wood mixture (middle left), torrefied Norway spruce (middle right) and off spec torrefied pellets (bottom).

For gases, most reactive concentrations are usually found for mixtures slightly richer than stoichiometric, as illustrated earlier in Figure 2-9. However, for dusts most reactive mixtures are typically found for very rich mixtures in the 1 m^3. This was the case for all dusts tested in the Leeds 1 m^3, however, the most reactive concentrations found in the Hartmann were for mixtures around stoichiometric, as it is usually found for gases. It is suspected that this happened due to the different vessel geometry leading to differences in heat losses, but also to the Hartmann vent cover bursting half way into the event. Another difference between the Hartmann and the 1m^3 was that the reactivity of dusts seemed to decrease much faster for rich mixtures in the Hartmann than in the 1 m^3. It is likely that increased heat losses in the Hartmann tube promoted this behaviour.

In its current shape the modified Hartmann showed a discrepancy in results to those of the 1m^3 vessel, mainly in terms of rates of pressure rise and flame speeds.

However it has been shown that vessel shape differences and experimental conditions (the Hartmann tube was opened during part on the explosion event) can be accounted for these differences. In terms of MEC measurements, results obtained with the modified Hartmann were on average 34% different from corrected MEC's measured in the $1m^3$ and from MEC values found in the public literature.

4.4. Effects of torrefaction severity on reactivity

Five samples of stem wood of Norway spruce, torrefied to different degrees, were used for this study. The samples were supplied and torrefied by and according to [143]. Samples were also sived in different size fractions (<63μm, <500 μm, 63 μm-500 μm) to assess the effect of particle size. Samples of <63 μm are shown in Figure 4-5.

Figure 4-5. From left to right, samples of torrefied Norway spruce (<63 μm) in order of increasing torrefaction severity, A-E.

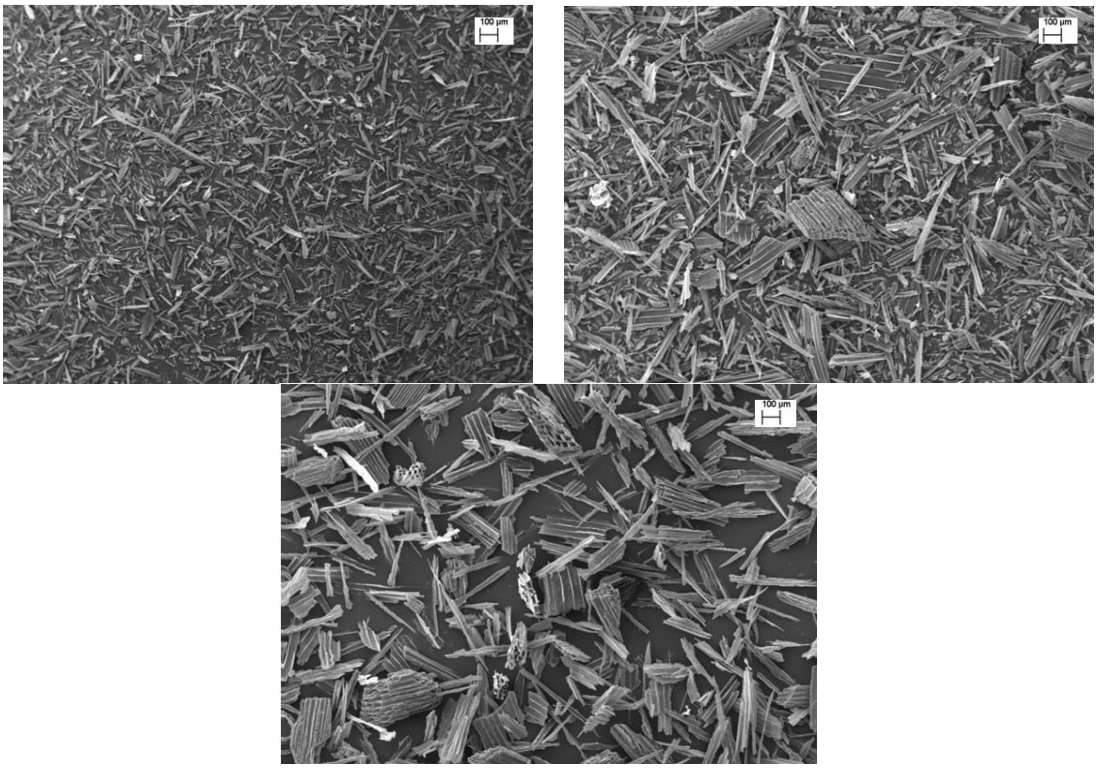

Figure 4-6. SEM images (x100) of the separated size fractions: <63 μm (top left), <500μm (top right) and 63 μm-500μm (bottom)

SEM images were taken for the different size fractions and are shown in Figure 4-6. The <63 μm sample contained smaller needle shaped particles of variable length. The <500 μm sample was a mixture of these and bigger brick-like shaped particles, whereas the size fraction where fines were removed is mainly conformed by the wider and thicker brick-like shaped particles.

The elemental and proximate analyses of the samples used in this work were reported by the samples supplier [143] and included in Appendix A. It is shown that when torrefaction characteristics are more severe (longer residence time and higher temperature), the product has lower H:C and O:C ratios (since the compounds liberated during torrefaction have high contents of hydrogen and oxygen). Table 4-6 gives the torrefaction conditions, the elemental formula (in a dry, ash free basis), the particle size analyses for the samples with size fraction <63 μm, the stoichiometric fuel to air ratios and the volatile matter content of the 5 samples tested.

Table 4-6. Fuel characteristics (<63 μm)

Sample	Particle Size (μm)			Stoichiometric F/A ratio (g m^{-3})	Volatile Matter (%)
	d(0.1)	d(0.5)	d(0.9)		
A: T=260°, t=8min ($CH_{1.377}O_{0.617}$)	20.6	60.5	186.1	195	84.0
B: T=260°, t=25min ($CH_{1.321}O_{0.560}$)	17.4	51.9	153.3	184	80.3
C: T=285°, t=16.5min ($CH_{1.217}O_{0.526}$)	18.8	58.3	186.6	181	77.3
D: T=310°, t=8min ($CH_{1.247}O_{0.509}$)	18.1	51.1	136.8	176	76.2
E: T=310°, t=25min ($CH_{0.867}O_{0.271}$)	16.4	44.3	115.9	138	51.5

The size distribution of the samples shows that the more severely torrefied samples contained smaller particles. Even though all samples were sieved through a 63 μm sieve, it can be seen that bigger particles were present, this is because woody biomass particles were not round but elongated and long particles with small diameters could pass through the sieve mesh. These long thin particles were interpreted by the particle analyser as equivalent spherical particles with a larger diameter.

Figure 4-7 shows the flame speeds and rates of pressure rise for different mixtures, each point is the average of three repeat tests. The 46% increase in flame speed between the sample with the lowest maximum speed and the sample with the highest value, was in very close agreement with the corresponding increase on rate of pressure rise which was 48%. The decrease in reactivity represented by the flame speeds and rate of pressure rise, corresponded to the increase in torrefaction severity.

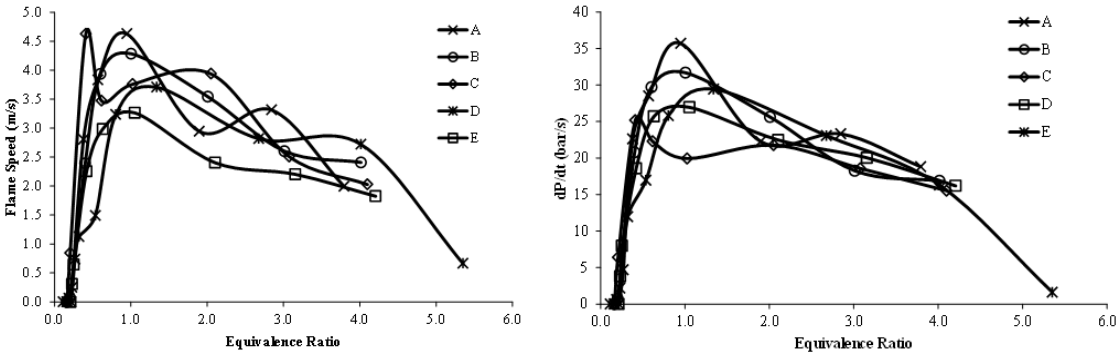

Figure 4-7. Flame speeds and rates of pressure rise over a range of concentrations for samples A-E as in Table 4-6.

Figure 4-8 shows the results of MEC expressed as an equivalence ratio ($Ø_{MEC}$) in order to account for the differences in elemental compositions, and therefore stoichiometry, of the samples, as well as the peak rate of pressure rise for each sample. All samples were explosible between 0.15 and 0.25 equivalence ratio (~30 g/m^3), which indicated a very high explosibility in comparison to coal samples and quite similar in comparison to raw biomass.

The data for samples <63 μm suggested that as the volatile content decreased due to torrefaction severity the sample peak reactivity (as indicated by the rate of pressure rise) also initially decreased. However, for samples D and E the peak rate of pressure rise increased despite the decrease in volatile content particularly for sample E.

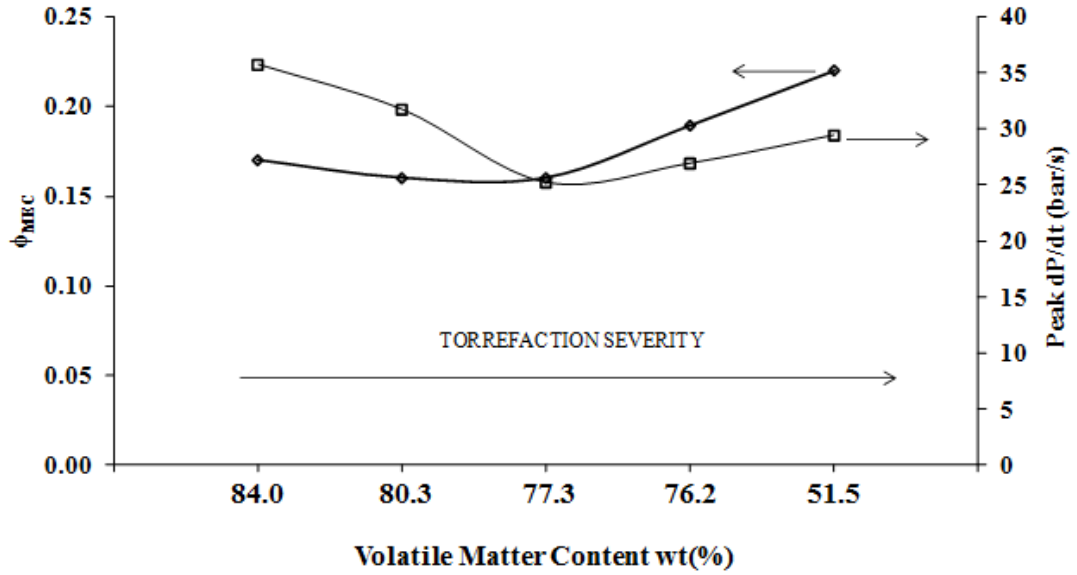

Figure 4-8. MEC expressed as equivalence ratio (Ø) and peak rates of pressure rise as a function of volatile matter content for samples <63 μm

It is noted from Table 4-6 and Figure 4-9 that the more torrefied samples D and E were made up of smaller particles – see for example d(0.9) – which was most likely due to these samples being more brittle resulting in higher fraction of smaller particles through the milling process. It is plausible that the presence of more powder fines counter-balanced the reduction of volatiles.

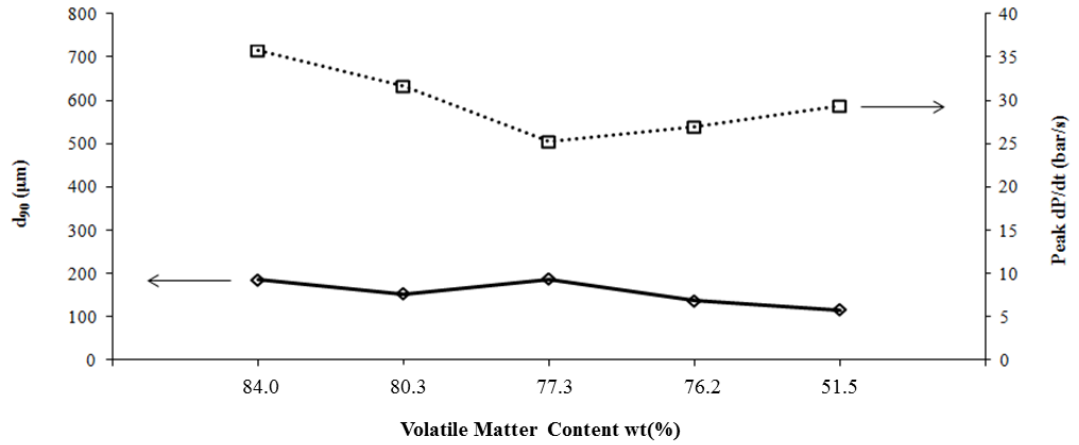

Figure 4-9. Peak rates of pressure rise and particle size as a function of volatile matter content for samples <63 µm

This effect was also found for the samples of <500µm, as shown in Figure 4-10,

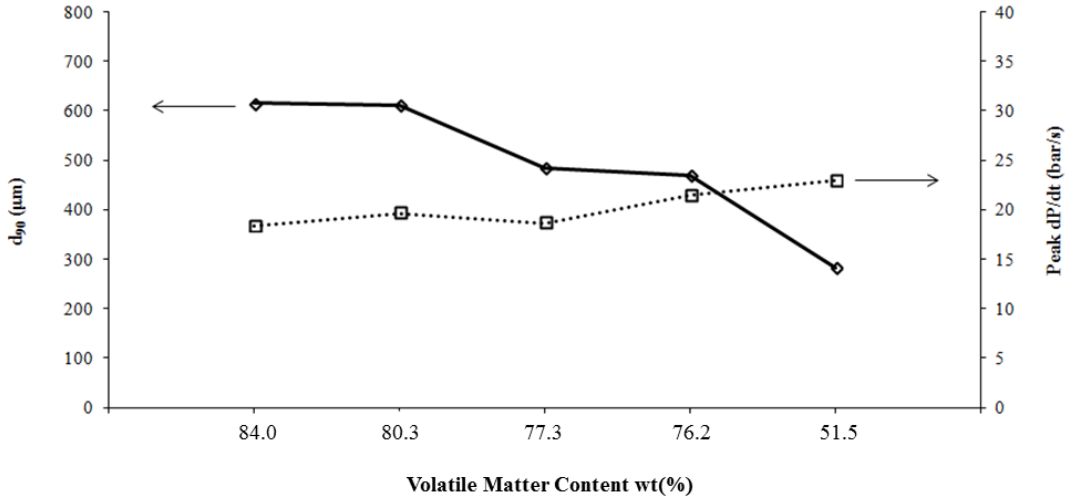

Figure 4-10. Peak rates of pressure rise and particle size as a function of volatile matter content for samples <500 µm

but not for the narrow size distribution (see Figure 4-11). For this sample the fines had been removed.

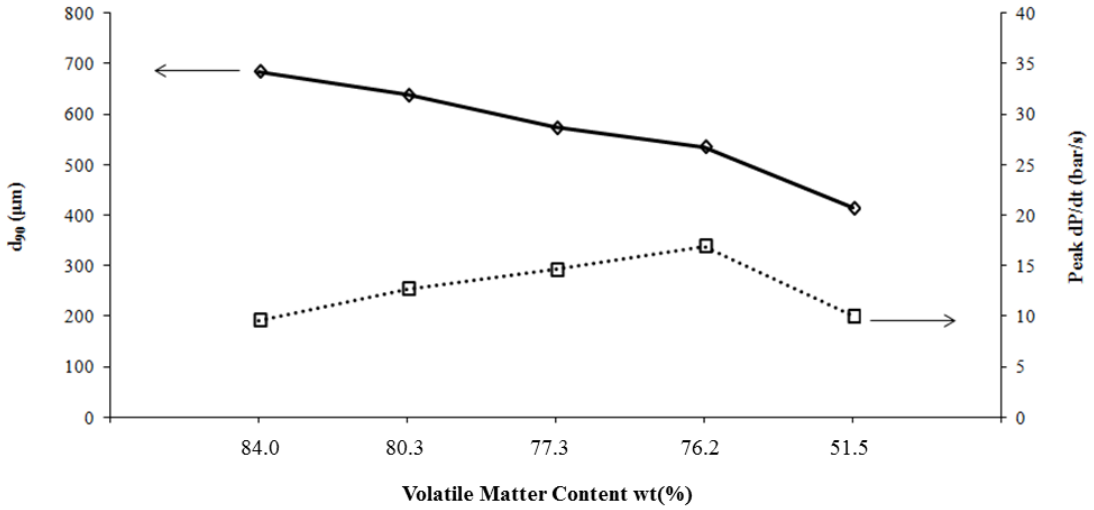

Figure 4-11. Peak rates of pressure rise and particle size in relation to torrefaction severity for samples 63-500 µm

For samples containing between 70 and 90% volatile (A-D) it was observed that the more torrefied samples contained smaller particles and the peak reactivity increased. However, when the volatile content was reduced down to around 50% (E) the presence of smaller particles ceased to promote higher peak rates of pressure rise. This suggests that the reactivity of torrefied samples is dependent on a balance between the size of particles and the volatile content. If particles were sufficiently small, the reactivity increases despite the lower volatiles. Conversely, if particles are not as fine (like in the 63-500 µm sample) and volatiles are low the reactivity decreases.

Figure 4-12 shows the average rates of pressure rise and flame speeds measured at different mixtures for sample B (T=260°C, t=25 min), on the same plot. Similar graphs were found for the other samples.

In Figure 4-13, the maximum rates of pressure rise, for all samples from all size fractions, and the particle size expressed as d_{90} have been plotted . As particles become bigger the peak reactivity had the tendency to decrease, as would be expected.

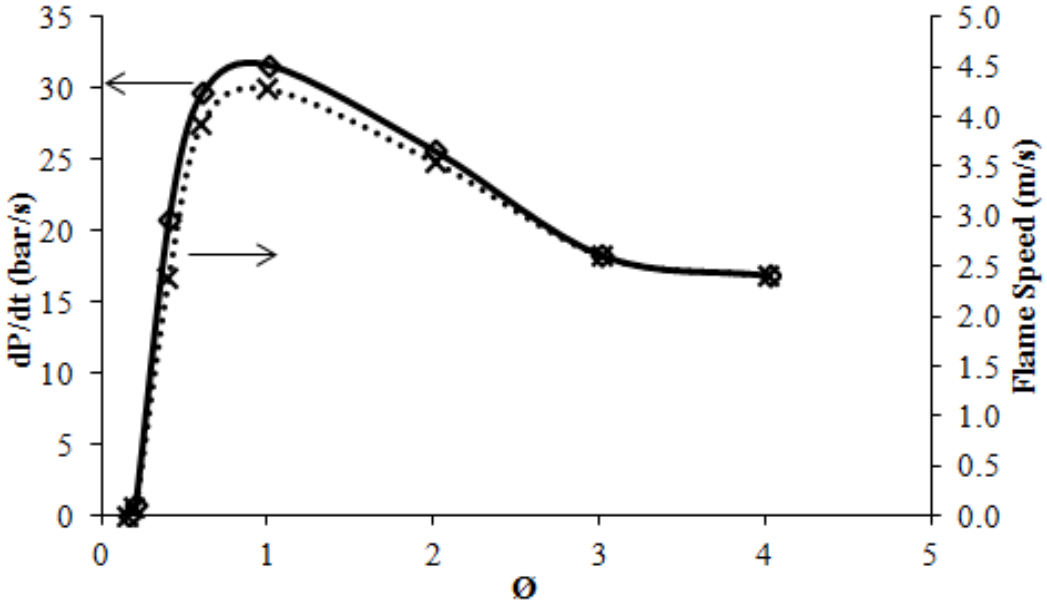

Figure 4-12. Rates of pressure rise and flame spends for a range of mixtures

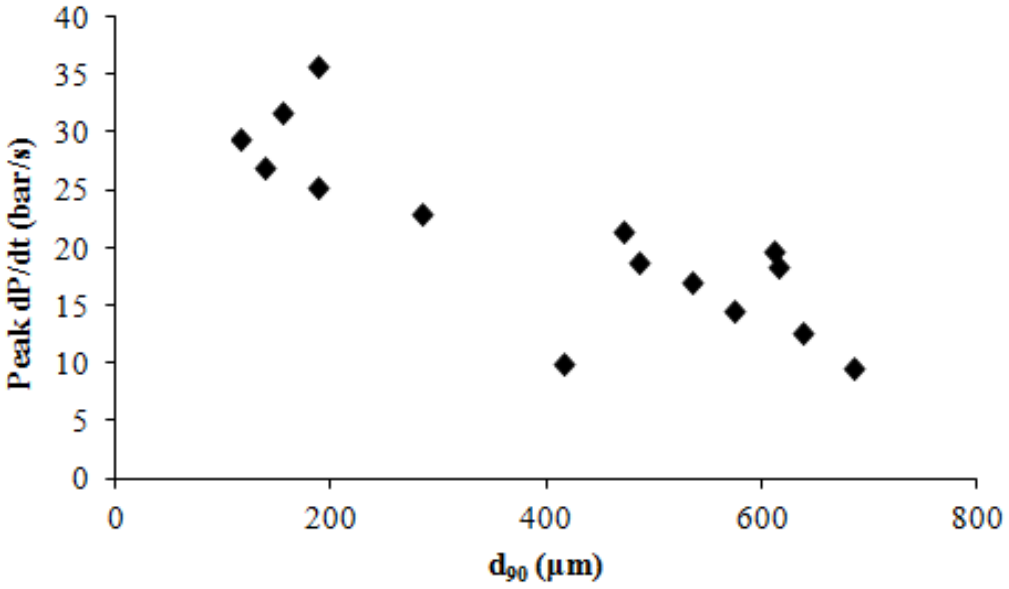

Figure 4-13. Peak rates of pressure rise as a function of particle size

Figure 4-14 also demonstrated that there was a good correlation between the flame speeds and the rate of pressure rise. This confirmed the trends of reactivity and is illustrated by the correlation of rates of pressure rise and flame speeds shown in Figure 4-14.

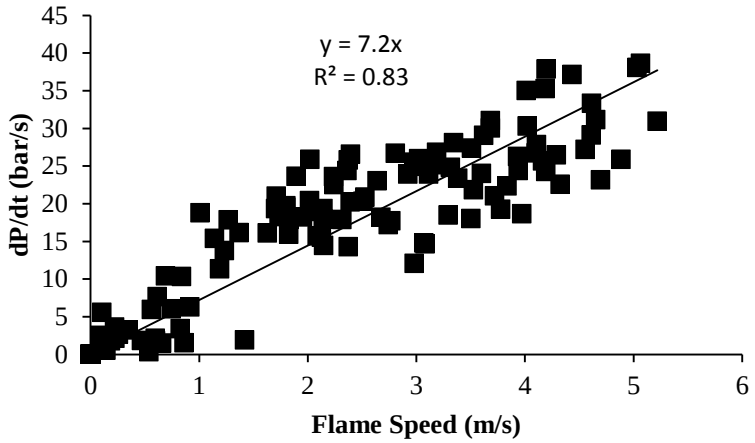

Figure 4-14. Correlation between rates of pressure rise and flame speeds

The values for the explosibility characteristics reported here for the torrefied biomass materials are in the same order as the raw biomass reported by our group and other literature data also cited in [200].

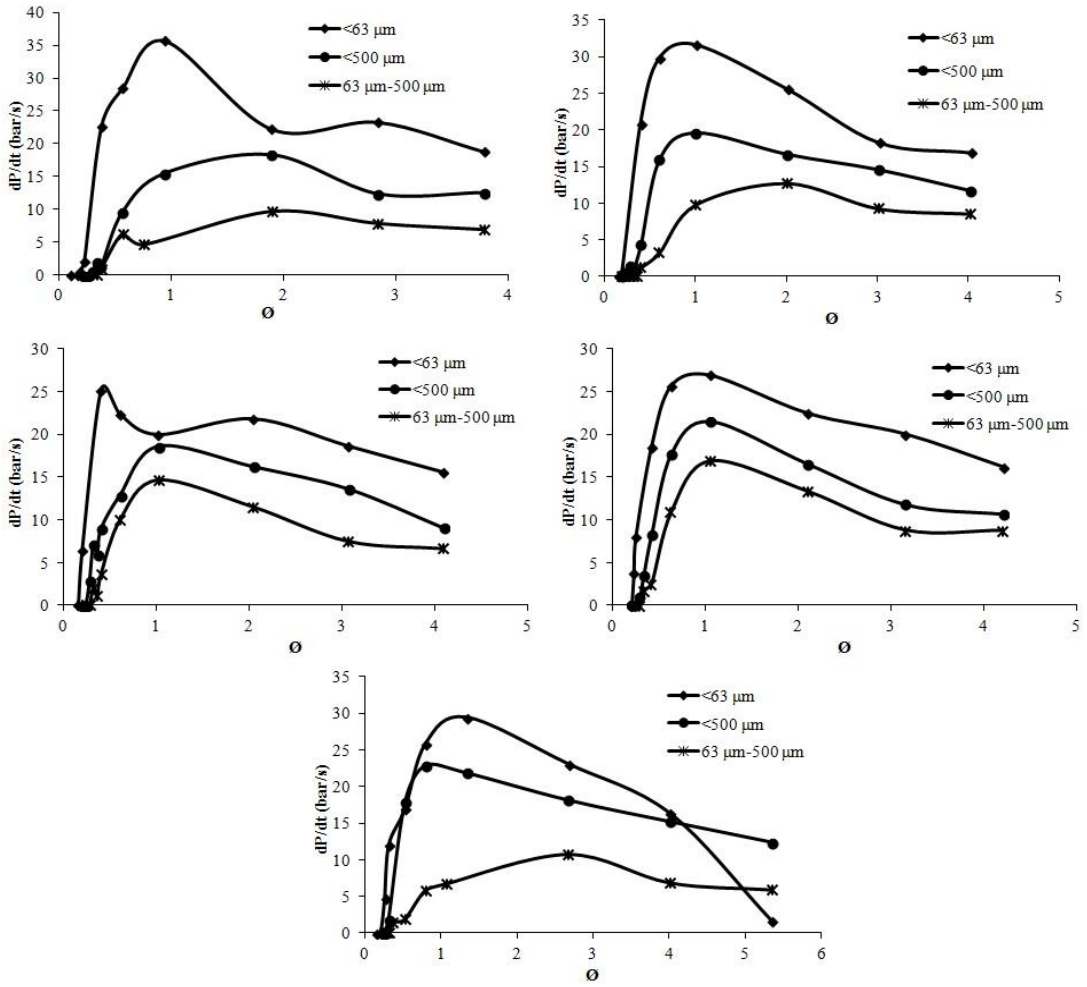

Figure 4-15. Effect of particle size on reactivity in terms of rates of pressure rise for samples A-E, left to right, top to bottom

It was found for all samples that the samples of smaller size fraction (<63 μm), provoked the highest rates of pressure rise, followed by the samples with size fraction of <500 μm, where fine particles were still present, and finally by the 63-500 μm sample fractions, where the finer size fraction particles had been removed. This is illustrated in Figure 4-15 for all samples A-E. Similar graphs were found when flame speeds were plotted against equivalent ratio.

The presence of fine particles clearly increased the reactivity of the samples, but in the absence of fine particles the samples were still very explosible. In terms of minimum explosible concentrations it was found that samples containing bigger particles would have a higher MEC. For the two least torrefied samples, the minimum explosible equivalence ratio was two times richer for the samples of 63-500 μm, whereas for the three more severely torrefied samples, the increase in MEC was slightly smaller (~1.6 times higher). Nevertheless, the samples with larger particles had lean limits at very lean mixtures of around Ø=0.3. It can be observed in Figure 4-16 that the lean limit of torrefied samples for big particle sizes (e.g. >200 μm) was no higher than Ø=0.35, whereas at such particle size the limit for other fuels such as polyethylene [81], bituminous coal [213] and corn flour [103] was well above Ø=0.5.

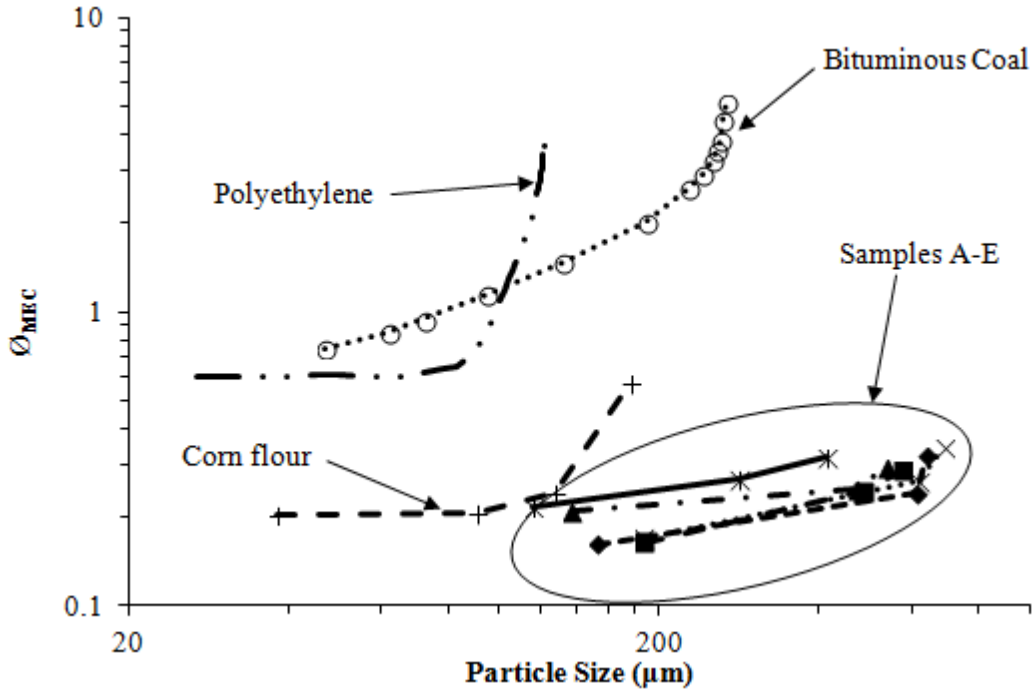

Figure 4-16. Lean limit as a function of particle size for torrefied Norway spruce in comparison to other dusts from the literature

4.5. Conclusions

A new technique for the measurement of minimum explosible concentration was developed. The aim was to provide a reliable and fast technique avoiding the problem of accurately knowing the concentration that reacts in both a 20 L sphere and the 1 m^3 vessel, and similar to the method agreed for the measurements of LFL of gases. Thermocouples and a pressure transducer were fitted to assess the existence of an explosion and to measure initial rates of pressure rise and flame speeds. The results show that the new instrumentation allowed fast recognition of propagating flames near the limit. Repeated tests confirmed similar turbulence levels in the vessel.

MEC measured in the modified Hartmann tube were in good agreement with values in the literature for reference dusts. Rates of pressure rise and flame speeds could be measured for a range of concentrations to find most reactive mixtures, although these have been found to be different to the most reactive mixtures found with the 1 m^3 vessel. Measured peak flame speeds are lower in the modified Hartmann in comparison to the flame speeds measured in the 1 m^3, this was due to the fact that flame speeds were measured in the Hartmann after the vent cover was open.

However, a number of improvements and verifications could be made to the modified Hartmann method. The addition of a timer and ignition delay, to avoid dust mixtures igniting prior to complete dispersion and high speed video study could clarify if the low measurements of MEC in the Hartmann are actually due to poor mixing. A variable ignition source could be used to assess the adequacy of ignition energy and ensure that reactions are not over or under driven. Further modifications to measure the initial flame speeds before the vent cover burst rather than after would allow direct comparison of flame speeds from the 1 m^3 and the modified Hartmann.

The explosibility and reactivity of 5 samples of Norway spruce wood, torrefied to different degrees, was investigated by measuring their MEC, rates of pressure rise and flame speeds in the modified Hartman apparatus. Despite the improvements that the Hartmann method needed, this study was important as it was not possible to supply fuels for a similar study in the 1 m^3. The aim was to assess the effect of torrefaction severity taking into account the differences in particle sizes. All samples <63 μm showed that they were explosible at very low concentrations – between 0.15 to 0.20 equivalence ratio (~30 g/m^3), i.e. in the same range of values previously found for raw wood, however, it was found that more severely torrefied samples showed an increase in MEC, possibly due to the lower content of volatile matter. Particle size played an important role, since the more severely torrefied samples still

showed high rates of pressure rise and flame speeds at the most reactive mixtures which were possibly enhanced by the higher proportion of finer particles present, which indicated that these samples are still reactive. Therefore, the explosibility of torrefied samples appeared to decrease with increasing severity of torrefaction but this was somewhat counter-balanced by the higher proportion of smaller particles in these samples resulting from them being more brittle when more torrefied. Therefore, overall even the most severely torrefied samples remained very reactive and therefore potentially hazardous. The results showed a behaviour more similar to raw biomass than to coal. Samples containing bigger particles (<500 μm) had their lean limits at mixtures between Ø=0.24-0.27 and narrow size distributions (63-500 μm), where the finer particles had been removed, reacted between Ø=0.29-0.34. This shows that torrefied biomass samples, as well as raw biomass samples containing big particles can cause explosions at much lower concentrations than other combustible dusts such as polyethylene or coal.

Chapter 5 EXPLOSION CHARACTERISTICS OF TORREFIED BIOMASS AND THEIR CORRESPONDING UNTREATED BIOMASS

CONTENTS

5.1. Introduction

As discussed in Chapters 1 and 2 torrefied biomass fuels are upgraded renewable fuels with higher calorific values and better grindability than untreated biomass [16, 123, 124, 139, 142, 145, 146]. Their similarity to low rank coals facilitates replacing coal with minimal changes in combustion technology systems.

Torrefaction technologies, however, have not yet been scaled up suitably to offer sufficient amounts of fuel for power generation. In the meantime, the demand of torrefied fuels for domestic scale is growing, and this could help break down the technical and economic barriers for torrefied biomass to become a steady and reliable fuel source.

Some of the technical concerns of torrefaction relate to safety during handling and storage. For example torrefaction results in a biomass fuel with much better grindability, which however means that it is prone to dust cloud formation and therefore presents an explosion hazard which might be different to coal. The explosibility characteristics of coal are fairly well understood, and despite the testing difficulties data also exist on raw biomass [82, 86]. The explosion characteristics of **torrefied** biomass are however unknown, with no data in the

public domain (to the Author's knowledge). The large variation in the source fuels and also in the changes resulting from the non-standardised torrefaction process would reasonably lead to variable final fuel properties which would result in uncertainty in the safety protection systems but also in the combustion characteristics and hence in the design/adaptation of burner and heat exchange systems.

The objective of the work presented in this chapter was to measure explosion and combustion characteristics (K_{St}, P_{max}, MEC, flame speeds, burning velocities, heat release rates) of torrefied fuels and investigate the effect of torrefaction on the reactivity of biomass by comparing them to the same characteristics of their corresponding untreated biomass. Comparisons to two different coal samples were also revised.

5.2. Procured fuels and their characteristics

5.2.1. Materials

Six torrefied biomass materials, stemming from four different untreated biomass materials, were sourced for this study. Details are given in Table 5-1. Due to commercial sensitivities the torrefaction technologies and conditions used on the samples were not always disclosed by the suppliers (details are listed where available). For this reason all the samples were fully characterised (elemental and proximate analyses as well as other physical properties) and from this information it was possible to deduce how severely the samples were torrefied (discussed later).

Torrefied biomass samples were supplied in enough quantities for explosion characterisation according to the European standards [30, 73, 74]. In some cases it was not possible to fully characterise the explosibility of some of the untreated counterparts as less material was supplied, however it was possible to establish trends for comparison. It was not possible to supply other torrefied biomass types (such as energy crops or agricultural residues), as these were not available in the quantities needed. The samples tested were therefore representative of materials that are torrefied in larger amounts these days.

The samples were provided either in chips or pellets, and were milled according to the procedures stated in Chapter 3, section 3.1.

Table 5-1. Torrefied biomass and corresponding untreated biomass tested

Specifications	Sample Name	Supplier
Raw "whole tree" wood supplied in chips (ca. 3 cm x 3 cm)	ECNR	ECN
Torrefied (T=250 °C) "whole tree" wood supplied in chips (ca. 3 cm x 3 cm)	ECNT	ECN
Raw wood supplied in chips (ca. 2 cm x 1 cm)	RWER	RWE
Off specification torrefied wood supplied in pellets	RWET	RWE
Raw Norway spruce wood supplied in chips (ca. 2 cm x 2 cm)	S2SR	Sea2Sky Energy UK Ltd.
Torrefied Norway spruce (T=260 °C, t=13 min). Supplied in chips (ca. 2 cm x 2 cm) Milled to <75 μm (ABT Reactor, Gotland, Sweden)	S2STS	Sea2Sky Energy UK Ltd.
Torrefied Norway spruce (T=260 °C, t=13 min). (ca. 2 cm x 2 cm) Milled to <60 μm (ABT Reactor, Gotland, Sweden)	S2STA	Sea2Sky Energy UK Ltd.
Torrefied Norway spruce. (ca. 2 cm x 2 cm). Milled to <60 μm (River Basin Energy Reactor, Wyoming, USA)	S2STB	Sea2Sky Energy UK Ltd.
Southern pine harvested in Mississippi (USA)	NBER	New Biomass Energy (USA)
Torrefied wood pellets. Torrefaction details not disclosed by supplier.	NBET	New Biomass Energy (USA)

5.2.2. Fuel characterisation

The characterisation of fuels was conducted as described in Chapter 3, section 3.2 for all the samples in their final milled size. The composition of Kellingley and Colombian coal is also given here for comparison.

5.2.2.1. Composition, heating value, stoichiometric fuel to air ratios and bulk density.

Table 5-2 contains the elemental and proximate composition of all fuels used for the present study. Typical differences between raw and torrefied samples and their comparison with coal are shown. As a consequence of torrefaction all samples lost moisture and volatiles, except in the case of ECNR and ECNT, which underwent a very mild pyrolysis.

The contents of carbon and fixed carbon also increased during torrefaction. However in comparison to coal the carbon content of biomass samples was 25% lower on average. On the other hand biomass and torrefied biomass contained an average of 80% more oxygen than coal. Also, more severely torrefied samples and coal contained more ash. The gross calorific value (GCV) of torrefied samples improved after torrefaction, but remained lower than that of coal. The bulk density of biomass varies widely, all the raw samples supplied had low bulk densities around 200 kg/m^3. Torrefaction had an effect over the bulk densities, generally increasing, except on the case of ECNT, where the mild torrefaction conditions did not change this property of the sample. The bulk density of two of the pairs RWER-RWET and NBER-NBET increased by 80% and 55% respectively, reaching values similar to that of coal. RWET and NBET were supplied as pellets. The great increase in bulk density could be a result of pelletisation rather than torrefaction.

Figure 5-1 is a Van Krevelen diagram (analogous to Figure 2-10) and shows the atomic hydrogen to carbon ratio as a function of the oxygen to carbon ratio, for the present fuels. The torrefied samples occupy a region between coals and biomass where low rank coals are usually positioned. Torrefaction results in a material with lower H/C and O/C ratios, through mainly the loss of volatiles. The severity of the torrefaction process is represented by the relative displacement along the dotted line. On this basis the ECNT sample underwent a very mild torrefaction since both the raw and torrefied samples appear superimposed in the diagram. S2STS and S2STA were the same material torrefied to the same conditions; however, they were milled to different final sizes. This suggests that the degree of milling (and possibly the method of milling) can also change the chemical composition of the final fuel again most likely through the loss of moisture and perhaps volatiles during comminution [198].

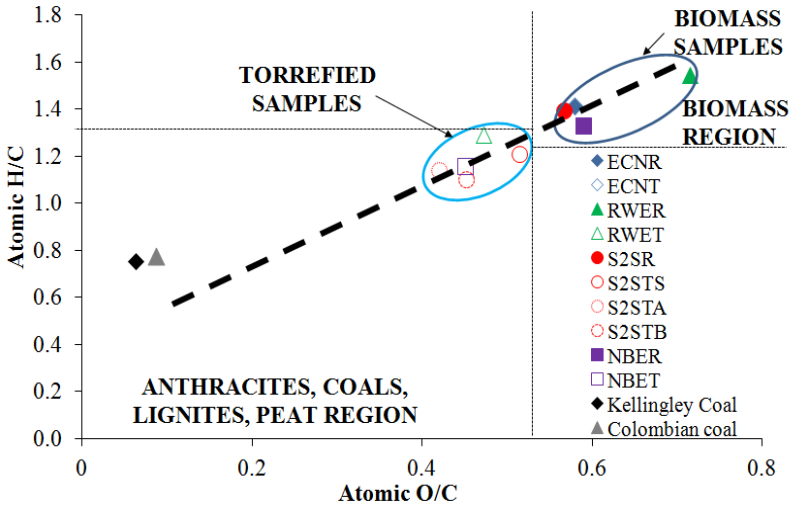

Figure 5-1. Van Krevelen diagram containing tested samples

Table 5-2. Fuel characterisation

	Elemental Analysis (wt%)[1]	C	H	O*	N	S	Proximate Analysis (wt%)[1]	Moisture	VM	FC	Ash*	VM/FC	y=H/C**	z=O/C**	A/F	A/F[2] (g/m^3)	GCV[2] (MJ/kg)	Bulk density (kg/m^3)
ECNR		48.0	5.7	37.1	0.0	0.0		5.3	78.0	12.8	3.9	6.1	1.41	0.58	6.5	185	20.8	212.1
ECNT		49.9	5.9	38.6	0.3	0.0		2.0	78.2	16.5	3.3	4.7	1.42	0.58	6.5	185	21.2	208.0
RWER		42.4	5.5	40.4	2.0	0.0		4.6	83.4	6.8	5.1	12.3	1.55	0.71	5.8	208	20.3	237.4
RWET		49.1	5.3	30.9	2.4	0.0		3.9	68.9	18.8	8.4	3.7	1.29	0.47	7.3	165	22.8	427.5
S2SR		48.1	5.6	36.3	0.0	0.0		5.8	79.0	11.1	4.1	7.1	1.39	0.57	6.5	184	21.3	175.6
S2STS		51.6	5.2	35.4	0.7	0.0		2.8	77.0	15.9	4.2	4.8	1.21	0.51	6.7	178	23.4	235.0
S2STA		54.8	5.2	30.7	0.7	0.0		2.7	69.4	22.1	5.8	3.1	1.14	0.42	7.5	160	22.5	236.2
S2STB		50.6	4.6	30.5	0.6	0.0		3.4	63.6	22.8	10.2	2.8	1.10	0.45	7.1	168	23.1	254.2
NBER		48.4	5.4	38.1	0.6	0.0		5.0	78.5	14.0	2.5	5.6	1.33	0.59	6.3	190	21.0	268.4
NBET		54.0	5.2	32.5	0.7	0.0		3.3	70.3	22.1	4.3	3.2	1.16	0.45	7.2	166	23.4	415.4
Kellingley Coal		65.0	4.1	5.5	2.4	2.2		1.7	29.2	50.0	19.1	0.6	0.75	0.06	11.3	106	33.8	443.0
Colombian coal		66.6	4.3	7.8	2.1	0.7		3.2	33.7	47.8	15.3	0.7	0.77	0.09	11.1	108	33.5	407.4

*calculated by difference, **molar ratio, [1]As received basis, [2]Dry, ash free basis

The RWET sample underwent the biggest relative change (compared to the raw parent sample RWER) probably through more severe torrefaction conditions (undisclosed by the supplier). This is also supported by the results of volatility (VM/FC) in Table 5-2. The volatility decreased 70% with torrefaction, which was significantly bigger reduction than for the other samples.

Figure 5-2 plots the percentage of mass loss during pyrolysis normalised for the loss of volatiles. All treated and untreated biomass samples had almost completely lost all volatiles before reaching the temperature at which Kellingley coal started to lose volatiles. Also, the volatiles were released at a faster rate for biomass compared to coal.

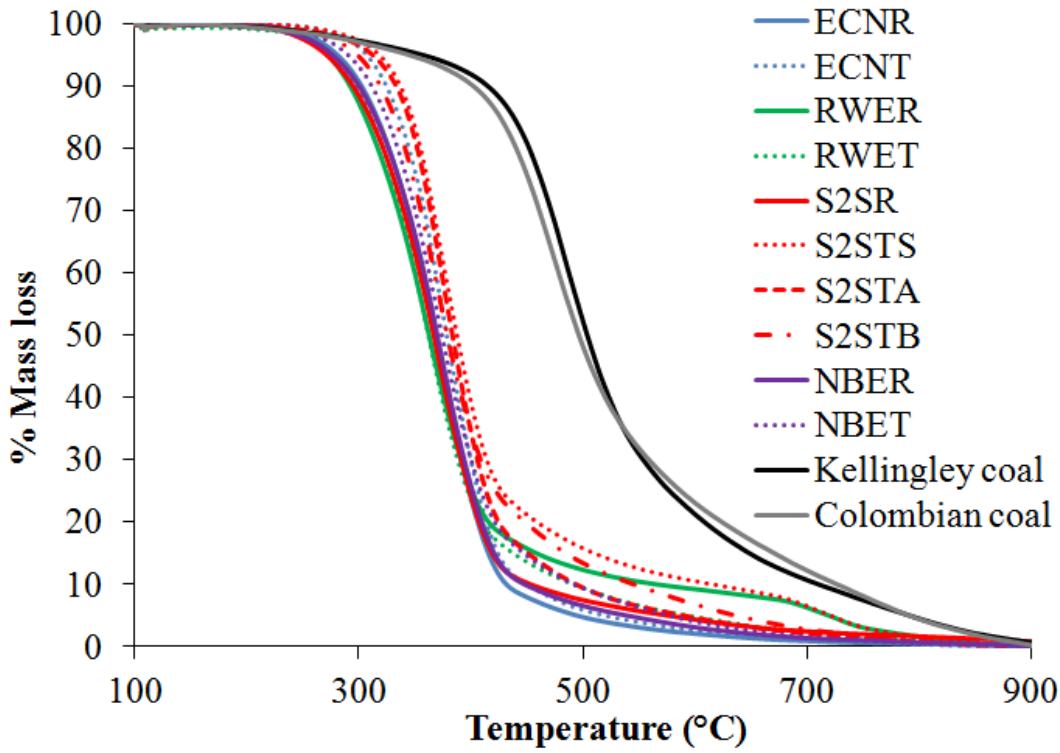

Figure 5-2. Volatile matter mass loss as a function of temperature

This is confirmed in Figure 5-3 and summarised in Table 5-3. The rate of mass loss was higher for biomass samples and the temperature at which maximum rate of mass lost was achieved (T_{max}) was lower for biomass and torrefied biomass samples. T_{max} is often used in reactivity assessments through pyrolysis as an indicator of reactivity, being a lower T_{max} indicative of higher reactivity [169]. Most of such studies used to compare the reactivity of biomass and their torrefied counterparts have indicated that although the change is small, torrefied biomass was less reactive than the untreated counterparts due to the loss of volatiles. Temperatures and heating rates in TGA conditions are lower than those encountered in an explosion event. In addition samples in a TGA react in a packed bed rather than as suspended particles. Therefore no conclusions should be drawn on the relative explosion reactivity of

torrefied and untreated biomass purely based on the TGA analysis. However, the TGA results indicate clear differences in the devolatilisation behaviour of coal and biomass (raw and torrefied).

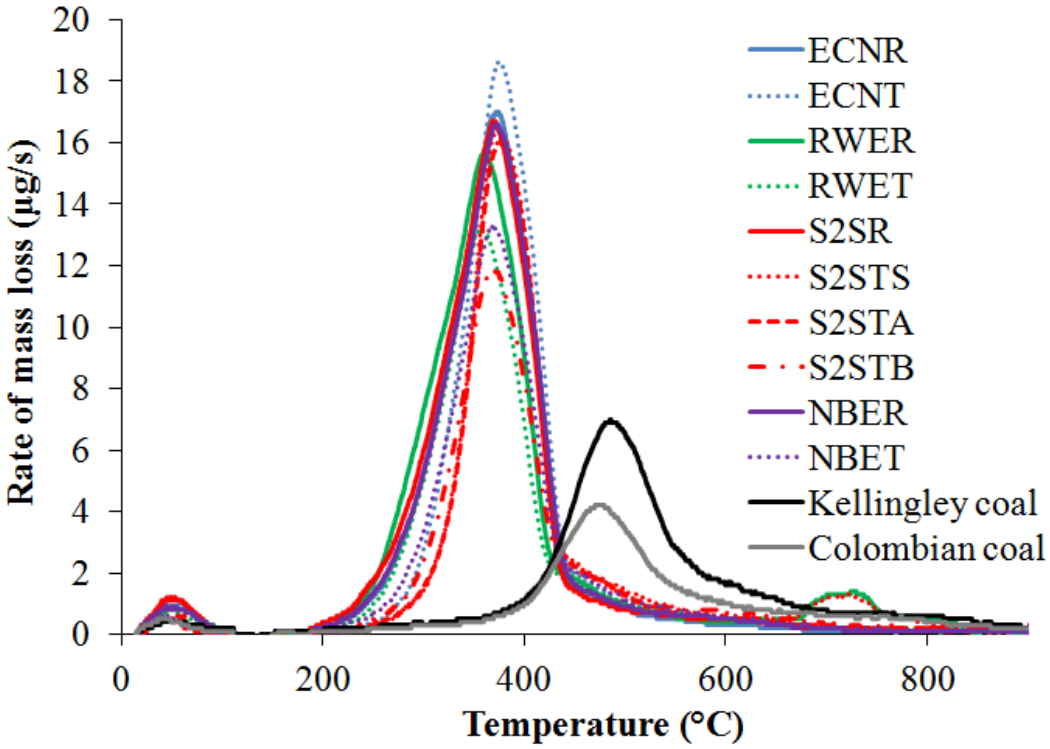

Figure 5-3. Rate of mass loss as a function of temperature

Table 5-3. Temperature of maximum rate of mass loss and maximum rates of mass loss

	Tmax (°C)	Maximum rate of mass loss (µg/s)
ECNR	372	17.0
ECNT	374	18.6
RWER	359	15.7
RWET	355	13.2
S2SR	368	16.7
S2STS	372	16.4
S2STA	373	16.0
S2STB	368	11.9
NBER	370	16.6
NBET	367	13.3
Kellingley coal	486	7.0
Colombian coal	472	4.2

Gross calorific values (GCV) included in Table 5-2 were measured through bomb calorimetry. However calorific values can be calculated through a number of equations using the elemental composition or proximate analysis of samples. Many correlations exist in the literature. In Figure 5-4 the calculated calorific values are compared to the measured values showing good agreement. All samples are within

5% difference, except for Kellingley and Colombian coal which, being coal samples, do not suit the biomass correlation used here, given by Friedl et al [119]. There are similar correlations for coal.

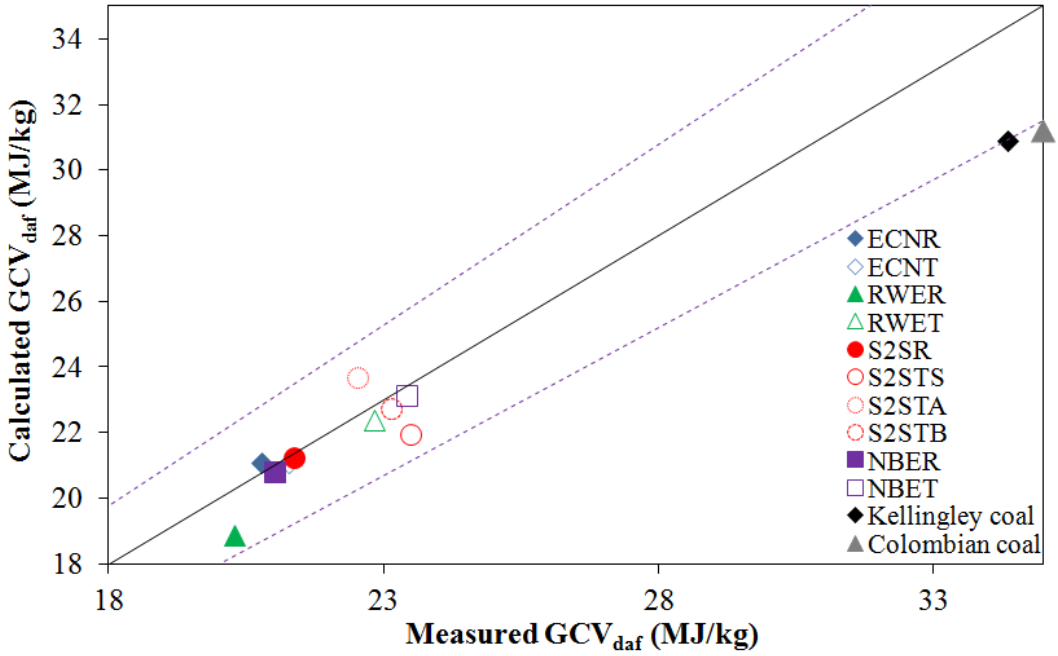

Figure 5-4. Comparison of calculated and measured calorific values for biomass

The typical formula for calculation of calorific values of coal is the Dulong formula (Eq.(3.3)). Using this specific formula for example with Kellingley coal the calculated GCV is 33.8 MJ/kg which is only 1.5% deviation from the measured value of 34.3 MJ/kg. It can be concluded that the calorific values measured were correct and that the corresponding correlations used fit the results well.

5.2.2.2. Particle characteristics (density, size distribution, morphology)

The cell wall density (true density) of common wood is typically 1530 kg/m^3 [214]. For coal, values range from 1550 kg/m^3 for anthracite to 1350 kg/m^3 for bituminous coal to 1250 kg/m^3 for lignite [215]. These values are in good agreement with the results shown in Table 5-4. The density of particles seemed to decrease slightly or remain unchanged after torrefaction.

The surface area is an important parameter in heterogeneous combustion since the rate of reaction increases when the surface area available for the reaction to occur is high. Surface area therefore can affect K_{St} in great measure. The variation of surface area with torrefaction did not follow a trend; it was increased in some cases and decreased in others. Researchers have suggested that after torrefaction the surface area could either increase or decrease depending on the torrefaction conditions. Low torrefaction temperatures lead to opening of pores for the release of volatiles and

subsequent increase in surface area. Conversely, at high torrefaction temperatures pores can soften and undergo plastic deformation, decreasing the surface area of the product material. These theories are in agreement with the present results and although the exact torrefaction temperatures were not known, samples that appeared more severely torrefied (RWER-RWET and NBER-NBET) showed a decrease in surface area. On the other hand the more mildly torrefied samples showed an increase. Coal had a significantly higher surface area than any of the biomass or torrefied biomass samples.

Table 5-4. Particle characteristics: particle density and surface area

	Particle Density(kg/m^3)	BET Surface Area (m^2/g)	Surface weighted mean D[3,2]	Volume weighted mean D[4,3]	d_{10}	d_{50}	d_{90}
ECNR	1505	1.66	46.7	152.0	19.3	78.9	401.0
ECNT	1494	2.08	39.1	87.7	17.3	57.7	187.4
RWER	1510	1.18	39.9	267.3	23.5	176.5	671.8
RWET	1476	1.09	22.4	237.3	11.1	125.2	663.3
S2SR	1546	0.65	70.7	238.7	28.4	148.5	602.7
S2STS	1496	0.69	25.8	117.7	14.5	66.5	280.7
S2STA	1494	2.10	28.5	59.2	13.1	38.5	128.2
S2STB	1549	1.50	30.6	49.3	15.3	39.5	97.8
NBER	1491	1.71	72.3	293.7	25.5	189.8	739.4
NBET	1454	1.47	35.2	80.6	16.5	45.1	145.2
Kellingley coal	1484	3.69	12.0	30.9	5.0	25.5	65.3
Colombian coal	1446	15.8	14.7	40.1	6.8	28.1	85.2

All samples were milled following the same process; torrefied samples were easier to grind than untreated biomass and therefore torrefied biomass samples contained finer particles. This is depicted in Figure 5-5, where the cumulative volume distribution for all torrefied samples is compared to their raw counterparts. In all cases, the raw biomass contained larger particles. During an explosion, large particles could burn as a result of smaller particles enhancing the reaction or else they could act as a heat sink or fall by the action of gravity, therefore not participating in the combustion reaction. If larger particles did not participate in the reaction the residue found in the explosion chamber after an explosion should contain bigger particles. It will be shown in section 5.5 that this was actually not the case, and it is believed that large particles (that is long but thin enough particles) burnt equally well during the explosion. In comparison to coal (see Figure 5-6), all biomass samples contained larger particles than typical pulverised coal used in power stations.

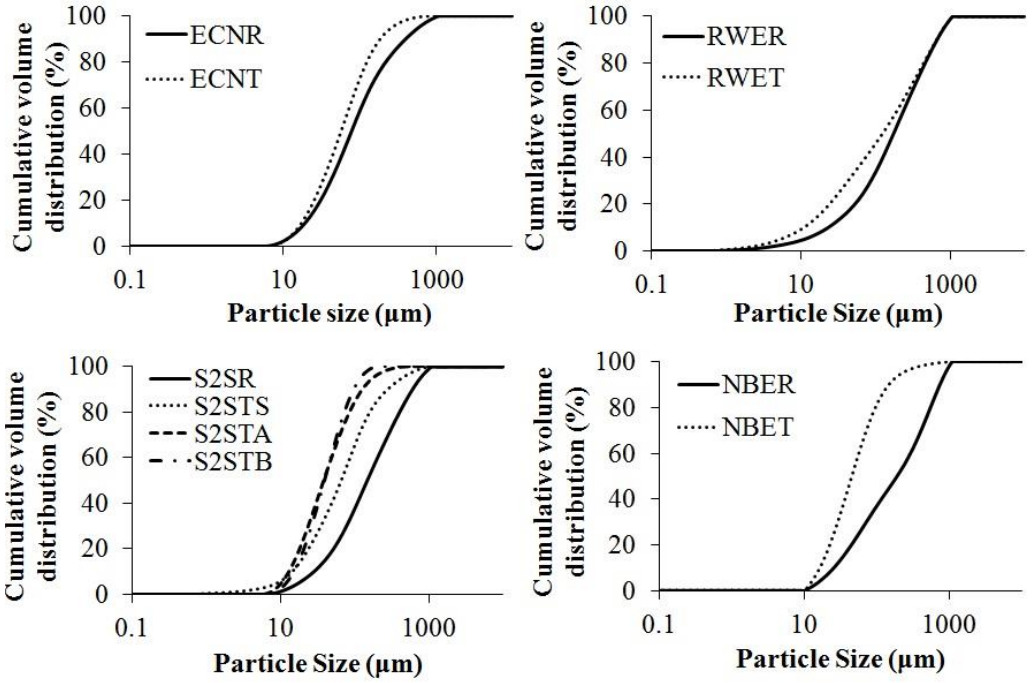

Figure 5-5. Cumulative volume distribution. Comparison of particle size distribution before and after torrefaction

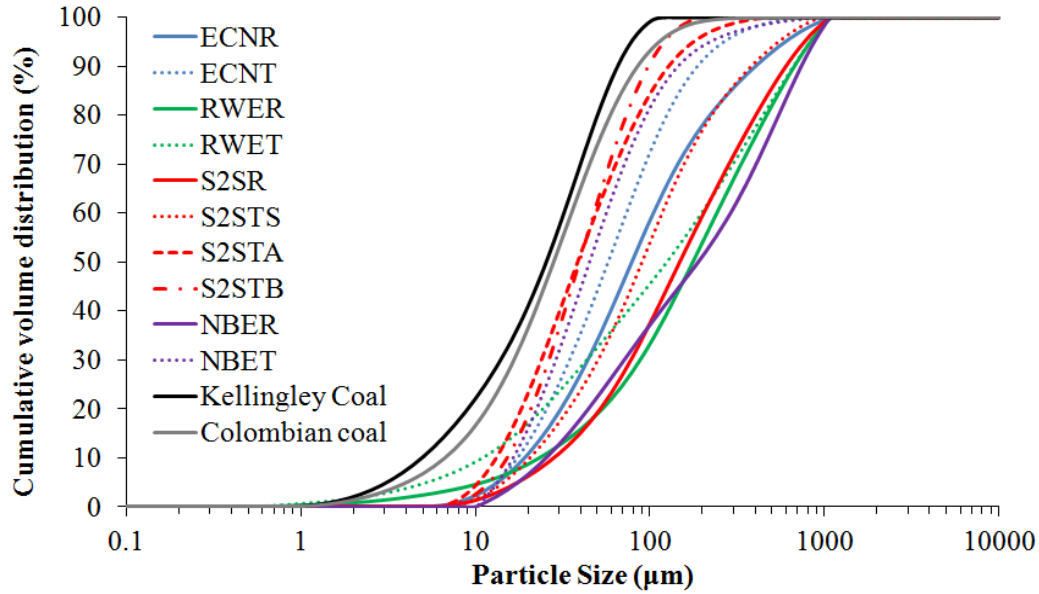

Figure 5-6. Size distribution. Comparison of biomass and torrefied biomass samples with coal

Typically, for particles of regular shapes, as particle size decreases, surface area increases. However particles used in this study have intricate pores that add surface area to the particle. Eckhoff [58] pointed out that if particles are fibrous, with large length to diameter ratio, the specific surface area is related to the particle diameter as follows:

$$Specific\ surface\ area\ (m^2/m^3) = \frac{4}{Particle\ diameter} \tag{5.1}$$

Since particles are not perfect spheres or cubes, they cannot be described by a single dimension. The measurement of particle size can be defined by the diameter of an equivalent sphere having the same property as the actual particle such as volume or mass for example. This method is not very appropriate when dealing with particles that differ significantly in one dimension relative to the others, such as needles. Any size parameter used here for biomass samples should be regarded as approximate. The surface weighted mean diameter is most appropriate when monitoring the proportion of fines present.

All of the biomass samples used were woody and fibrous. As shown in Figure 5-7 for both the pairs ECNR-ECNT and RWER-RWET, particles were cylindrical with variable width. Cellular surfaces can be appreciated in the non-treated samples. Big pores can be observed in ECNT sample. These pores might have been formed during the release of volatiles, which is confirmed by the increase in surface area. RWET, however, does not present such large pores, confirming that the loss of volatiles did not increase the surface area, and on the contrary, pores suffered a plastic deformation and carbonisation due to high torrefaction temperature. The same effect is found with the other biomass-torrefied biomass groups, see Figure 5-9. All samples torrefied from S2SR saw an increase in surface area and consequently pores can be appreciated, this indicates that the temperatures of torrefaction were likely to be lower. However, NBET shows no such pores and its surface area decreased after torrefaction. This indicates torrefaction temperatures close to 300°C. In comparison to all biomass samples, the coal samples (Figure 5-8) contained particles with softer surfaces; particles were smaller, rounder and edgier.

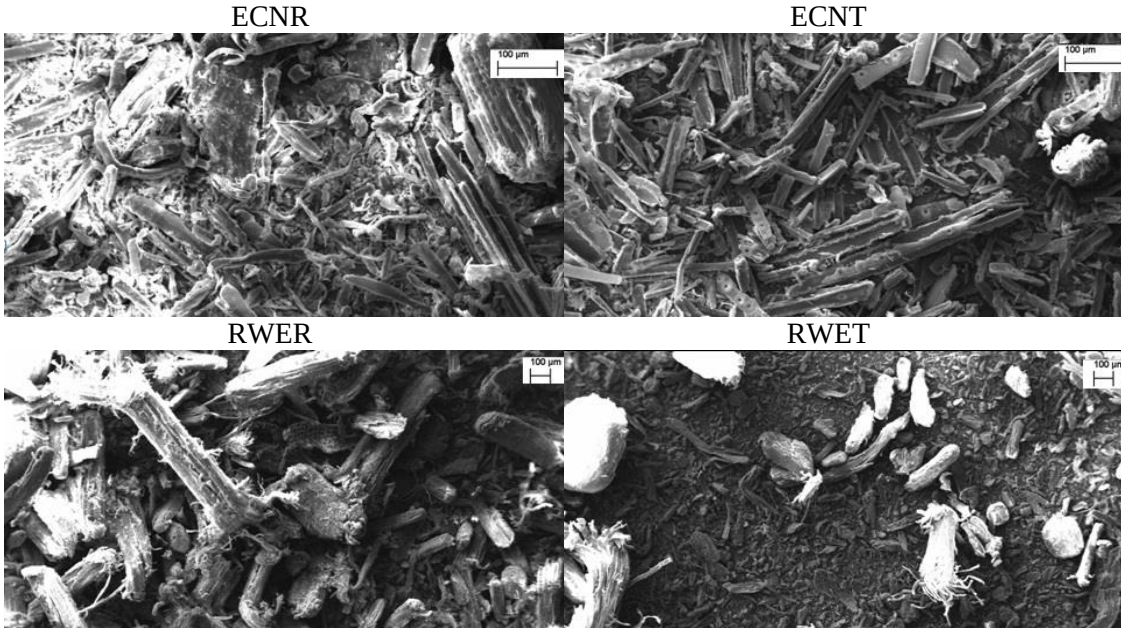

Figure 5-7. SEM images of ECNR (x300), ECNT (x300), RWER (x100) and RWET (x100)

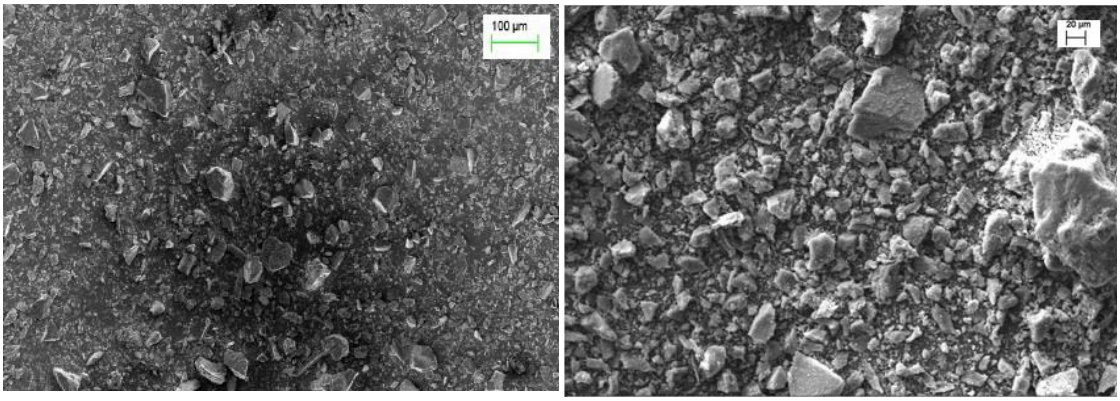

Figure 5-8. SEM images of Kellingley coal (left: x300) and Colombian coal (right: x500)

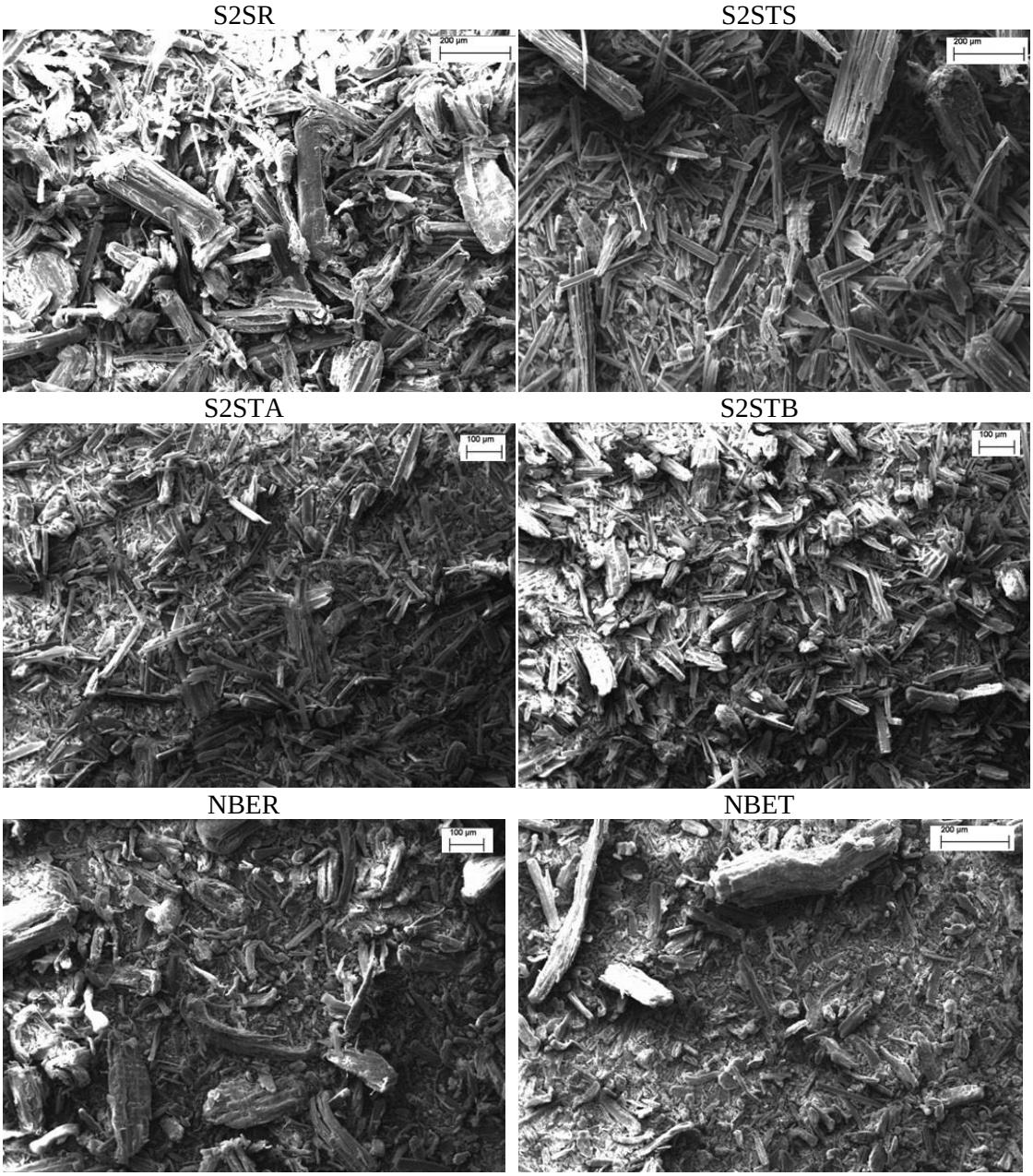

Figure 5-9. SEM images (x200) of S2SR, S2STS, S2STA, S2STB, NBER AND NBET

5.3. Explosion characterisation

All samples were tested to measure the explosion characteristics (K_{St}, P_{max} and MEC) according to the European standards [30, 73, 74]. Therefore starting with a concentration of 500 g/m^3 and moving both ways of the flammable range (including tests at 750 g/m^3, 1000 g/m^3, 1250 g/m^3) until two lower values of K_{St} and P_{max} had been measured either side of the highest K_{St} and P_{max} values. In the lean side of the flammable range after testing 250 g/m^3, the concentrations tested were halved until a concentration of dust is found not to explode (MEC).

5.3.1. Deflagration index and maximum pressure

The reactivity plots in terms of K_{St} and pressure ratios (P_{max}/P_i) are shown in Figure 5-10 and Figure 5-11 respectively.

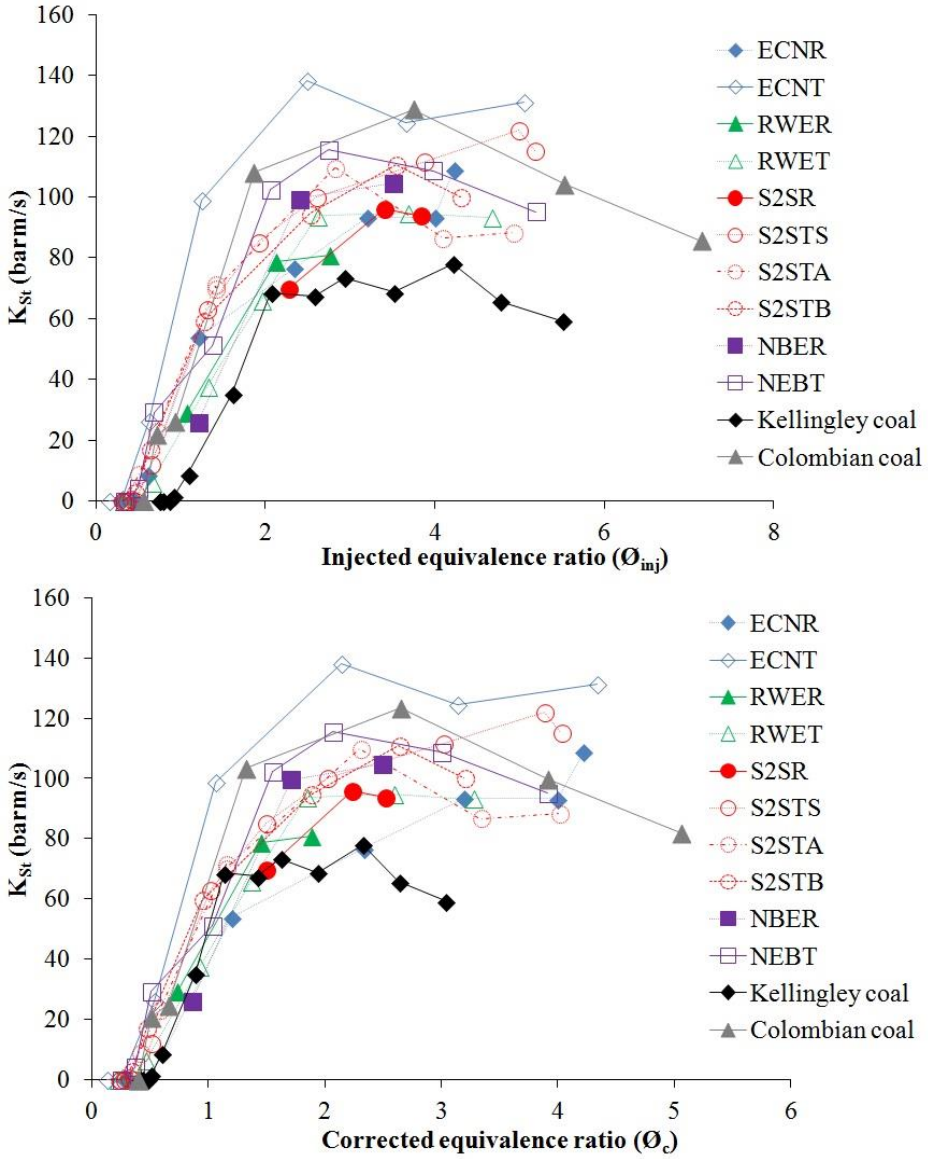

Figure 5-10. K_{St} as a function of the injected equivalence ratio (top) and the corrected equivalence ratio (bottom)

Two graphs are included in both figures. One corresponds to the K_{St} or pressure ratio measured as a function of the injected concentration, and the other as a function of the concentrations corrected for maximum percentage of mass burnt according to the residues found inside the explosion chamber after explosion. In addition, instead of concentrations, equivalence ratios are used to account for the variable composition of the samples. Torrefied materials appear with open symbols.

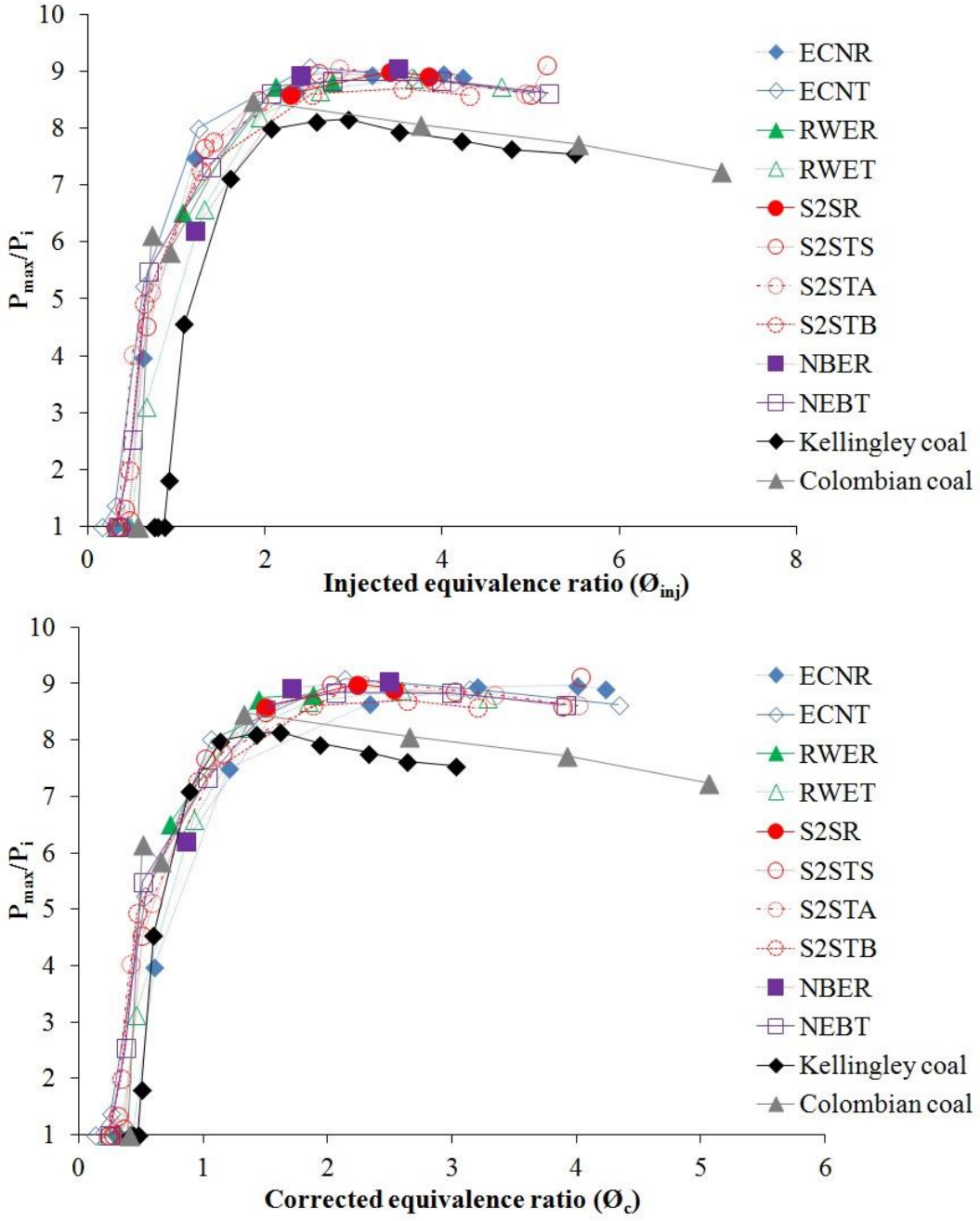

Figure 5-11. Pressure ratio as a function of injected equivalence ratio (top) and corrected equivalence ratio (bottom)

The K_{St} and pressure ratios are also given for Kellingley and Colombian coal. Kellingley coal presented lower K_{St} and pressure ratios than any of the biomass and

torrefied biomass fuels. But Colombian coal presented similar values to biomass and torrefied biomass. In every case torrefied fuels presented higher K_{St} values than their untreated counteraparts. The most reactive of all torrefied materials was the very mildly torrefied ECNT.

Regarding pressure ratios, all biomass and torrefied materials reached very similar values, whereas Kellingley and Colombian coal presented about 1 bar lower values.

Maximum explosion pressures are typically affected by parameters that can have an effect over the flame temperature or the amount of mass burnt, like composition, moisture or ash content. Kellingley and Colombian coal contained more ash than the biomass samples, which could be reducing the flame temperature and therefore the maximum pressure. S2STB is the biomass sample containing more ash and is also found in the low part of the pressure ratio range. Nevertheless, it is clear that particle size (which is one of the main differences between torrefied and raw biomass samples) did not have a big effect on maximum pressures. It is also noteworthy that whilst for K_{St} a reduction in reactivity was generally found for mixtures richer than the most reactive mixture, the pressure ratio remained fairly constant. The maximum pressure decreased more rapidly for coal samples than for biomass samples. It is likely that the high ash content of coal contributed to this effect.

Most reactive mixtures were found for injected mixtures around 3 times richer than the stoichiometric mixture. For biomass and torrefied biomass samples, even though the correction shifted all curves towards leaner mixtures (see Figure 5-10 and Figure 5-11), most reactive mixtures were still found for mixtures Ø~2. It should be noted that the calculation of the equivalence ratio is based on the stoichiometry resulting from the chemical composition of the solid sample. In reality the solid sample decomposes before burning and therefore the combustion stoichiometry should be based on the gas phase pyrolysis products. As these are not available and difficult to determine theoretically or measure experimentally the solid sample stoichiometry was used instead.

Figure 5-12 shows that depending on the dust used and the concentration tested, a lot of residue was left undelivered in the dust holder. This is dust that, unequivocally, did not participate in the reaction. In the specific case of the samples tested for this project at high dust loadings (>500 g/m^3) some samples left undelivered more than 10% of the initial mass of sample placed in the dust holder. Untreated biomass presented poor flowing characteristics as did some torrefied fuels. Coal samples and both Southern pine (NBER) and its torrefied version (NBET) presented best flowing properties.

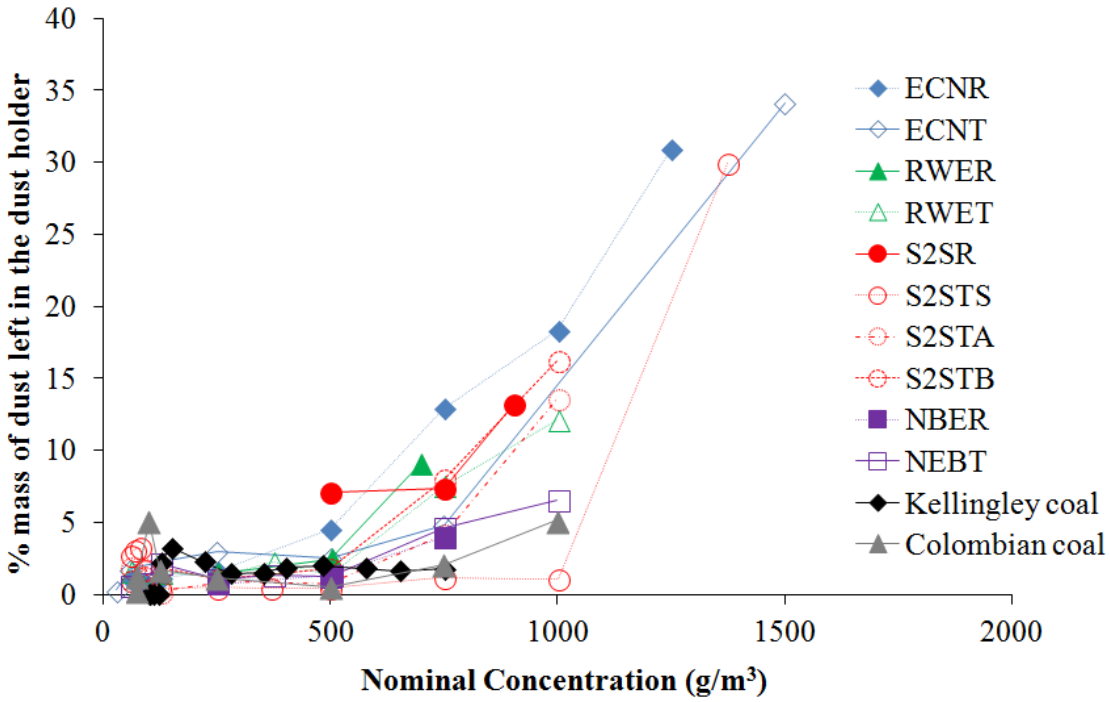

Figure 5-12. Percentage of initial mass placed in dust holder left undelivered as a function of the nominal concentration

It has also been discussed that large residues of dust were found inside the explosion vessel after an explosion test in the 1m^3 vessel. Figure 5-13 shows the percentage of mass burnt as a function of the injected concentration (essentially, the combustion efficiency). The calculation of the % of mass burnt assumed that the mass of residue found inside the vessel following an explosion test did not participate in the explosion, and therefore it is calculated as the mass of residue subtracted from the total mass injected and divided by the injected mass (Eq.(3.9)) . It will be shown later that this assumption is valid as residue samples appeared not to participate in the combustion reaction. In Figure 5-13 the percentage of mass burnt varies with concentration, in all cases the % of mass burnt reached a peak and then steadily decreased as more mass was injected. It is noteworthy that biomass and torrefied biomass samples seemed to have better combustion efficiency than Kellingley coal. At equal values of injected concentration, a lower mass of Kellingley coal burned. It should be noted that all biomass samples were tested using the spherical nozzle injector whereas the tests with Kellingley coal were performed using the standard C-ring injector. However, the calibration work undertaken by Sattar [187, 194] confirmed that the % of mass burnt with different dusts (walnut shells, pistachio nut shells and corn flour) and different dispersers remained fairly constant. In the cases where the combustion efficiency was slightly different, the combustion efficiency was better with the C-ring disperser.

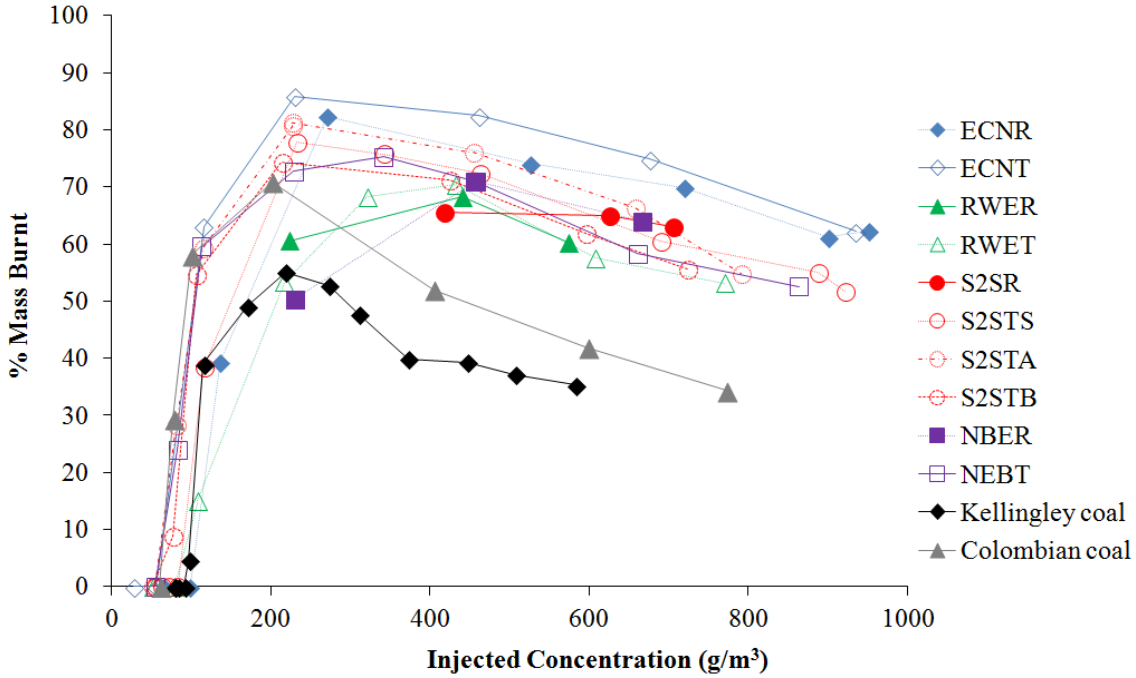

Figure 5-13. Percentage of mass burnt as a function of injected concentration

5.3.2. Minimum Explosible Concentrations

The minimum explosible concentrations were measured for all samples following the procedure recommended by the European standard, that is, by halving concentrations consecutively until one concentration did not ignite. No repeats and no refining between concentrations are required. Following this procedure the results for MEC are presented in Table 5-5. Minimum explosible concentrations are expressed as "corrected" concentrations. Expressing the MEC's as equivalence ratios indicated that torrefied biomass samples burnt at leaner mixtures than coal samples. Only ECNR was supplied in enough quantity to measure the MEC therefore it is unclear how torrefaction affected the MEC for the rest of the samples. According to the result for these pair of samples (ECNR-ECNT) the torrefied sample burned at a leaner mixture, and therefore it was more reactive. This is in agreement with the K_{St} result.

An additional test conducted which was not required according to the standard procedure, indicated that the procedure for MEC measurement predicted values which might be too small. The MEC for ECNR was found for a corrected concentration of 54 g/m^3 (nominal concentration=60 g/m^3). The previous test with a nominal concentration of 125 g/m^3 showed a clear pressure rise (3 bar overpressure). An additional test in between 60 g/m^3 and 125 g/m^3, with a nominal concentration of 90 g/m^3, did not ignite and therefore it would be more accurate to take this value as the MEC. This concentration corresponded to a corrected MEC of 81g/m^3 (Ø=0.44). The method recommended in the standard could be leading to conservative MEC values. As a result it is recommendable to express the lean limits as a range between

a concentration at which explosion takes place and a concentration at which it does not. This is included in the fourth column of Table 5-5.

Table 5-5. Minimum Explosible Concentration measured according to European standard

	MEC (g/m^3) Corrected Concentration	$Ø_{corrected\ MEC}$	MEC as range, corrected ($Ø_0$-$Ø_{100}$)
ECNR	54	0.29	81-112(0.44-0.60)
ECNT	24	0.13	24-48 (0.13-0.26)
RWER	-	-	-
RWET	36	0.21	55-76 (0.32-0.44)
S2SR	-	-	-
S2STS	49	0.27	49-56 (0.27-0.31)
S2STA	44	0.27	44-66 (0.27-0.40)
S2STB	38	0.22	38-57 (0.22-0.34)
NBER	-	-	-
NBET	41	0.25	41-62 (0.25-0.37)
Kellingley coal	50	0.45	50-53 (0.45-0.48)
Colombian coal	43	0.39	43-55 (0.39-0.51)

The MEC found for ECNR was high, however it should be reminded that, of all the samples for which it was possible to measure the minimum explosive concentration, ECNR contained larger particles. Despite containing much larger particles the MEC for ECNR was similar to that found for coal. This highlights again the high reactivity of biomass regardless of particle size in comparison to other dusts.

5.3.3. Combustion properties: flame speeds, burning velocities and heat release rates

Flame position, measured at constant pressure (as shown in Figure 3-34) could be mapped out using arrays of thermocouples in three directions: horizontal right and left, and vertical downwards. The time of flame arrival to the thermocouples was marked by a sudden increase in the thermocouple signal. The slope of the linear fit to the times of flame arrival for a given direction provides the average flame speed in such direction. The average radial flame speed is calculated as the average of flame speeds in each direction. This is depicted for the most reactive concentrations of all the samples in Figure 5-14 to Figure 5-17.

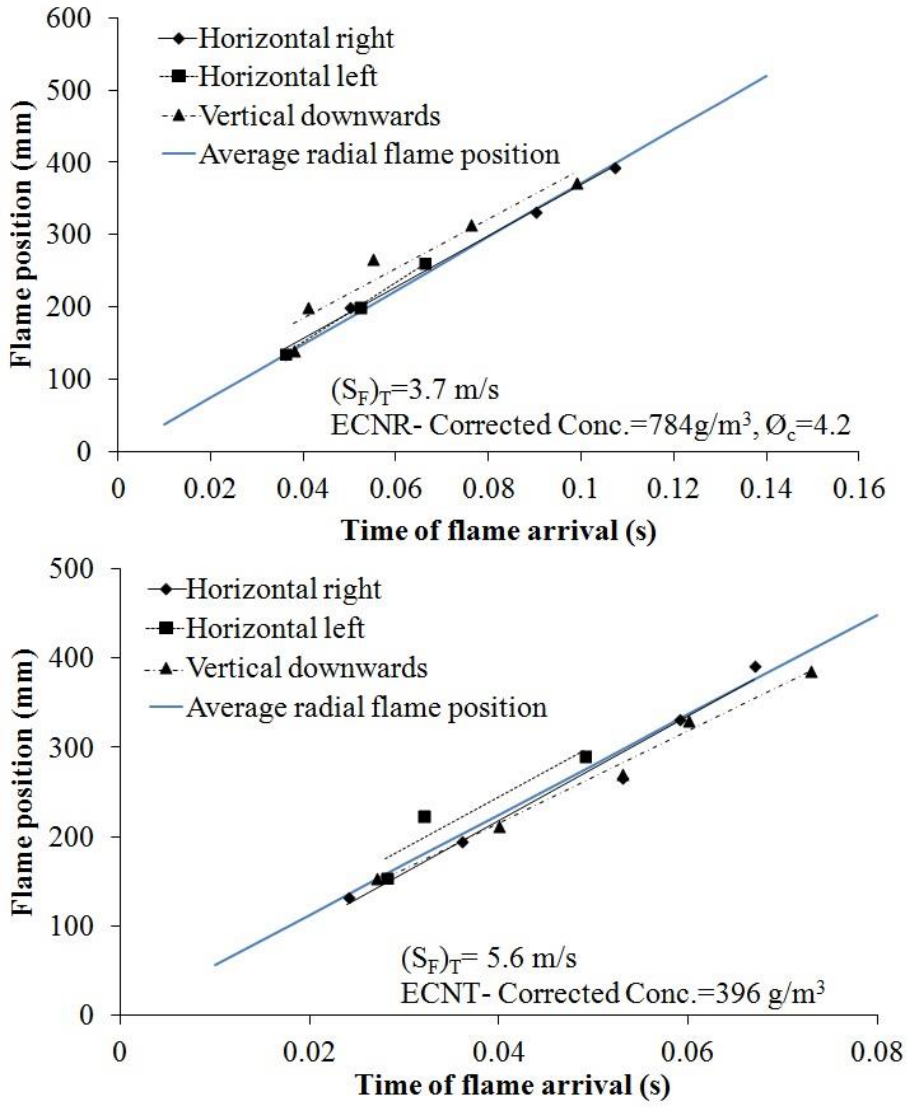

Figure 5-14. Flame speed position as a function of time for most reactive concentrations of ECNR (top) and ECNT (bottom)

Parallel linear fits in every direction denoted spherical flame propagation. It can be observed that turbulent flame speeds are higher for torrefied samples than for the untreated counterparts. Laminar flame speeds have been measured before in closed vessels by increasing the ignition delay and therefore decreasing the turbulence [93]. However, it was observed that at high ignition delays particles would fall out of dispersion due to gravity. By knowing the turbulence factor of the vessel used, it is possible to calculate the laminar flame speeds. For the specific case of the Leeds ISO 1 m^3 vessel the turbulence factor β was 4.03, dividing the turbulent flame speed by the turbulence factor results in laminar flame speeds for the present samples of around 1 m/s.

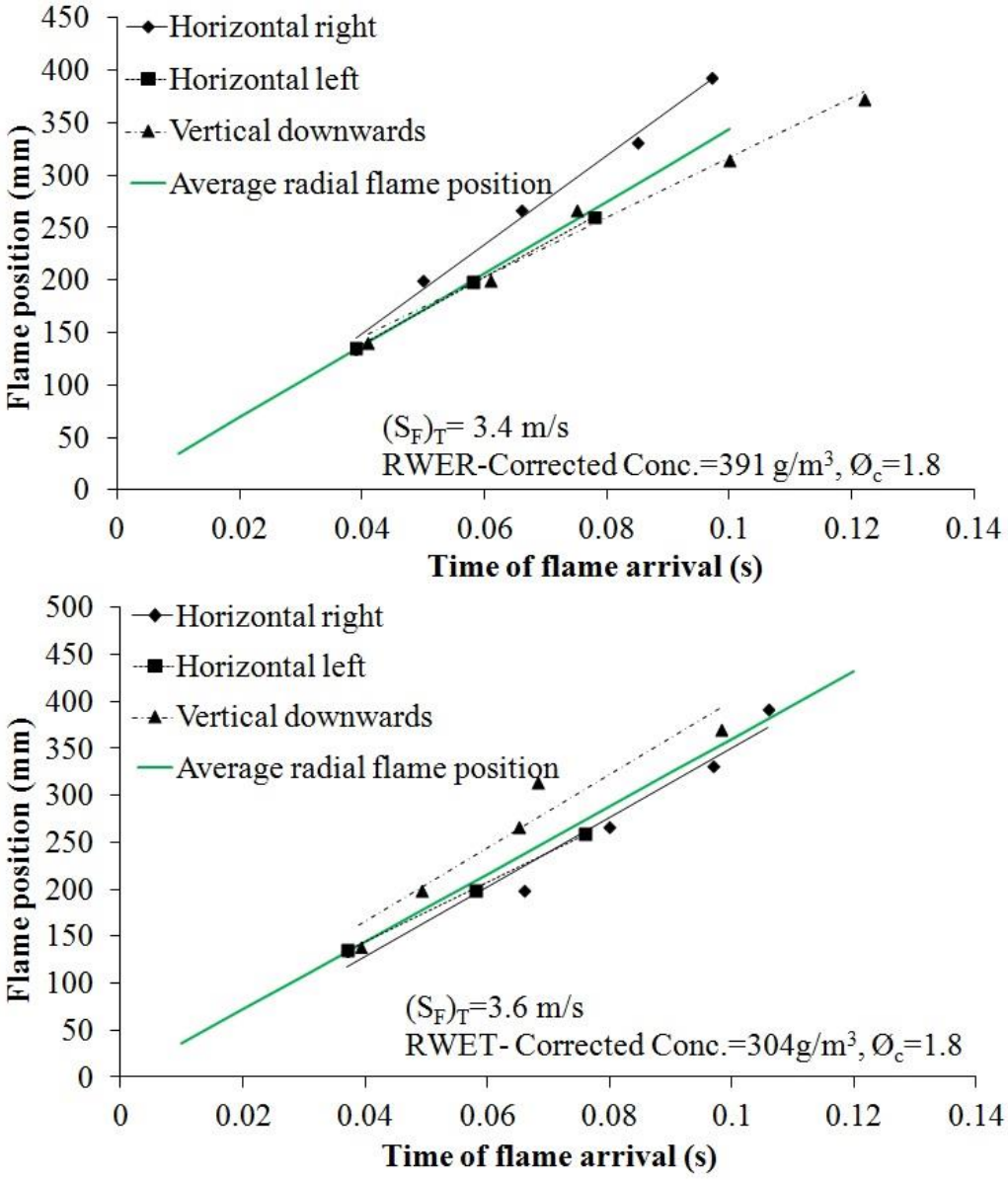

Figure 5-15. Flame speed position as a function of time for most reactive concentrations of RWER AND RWET

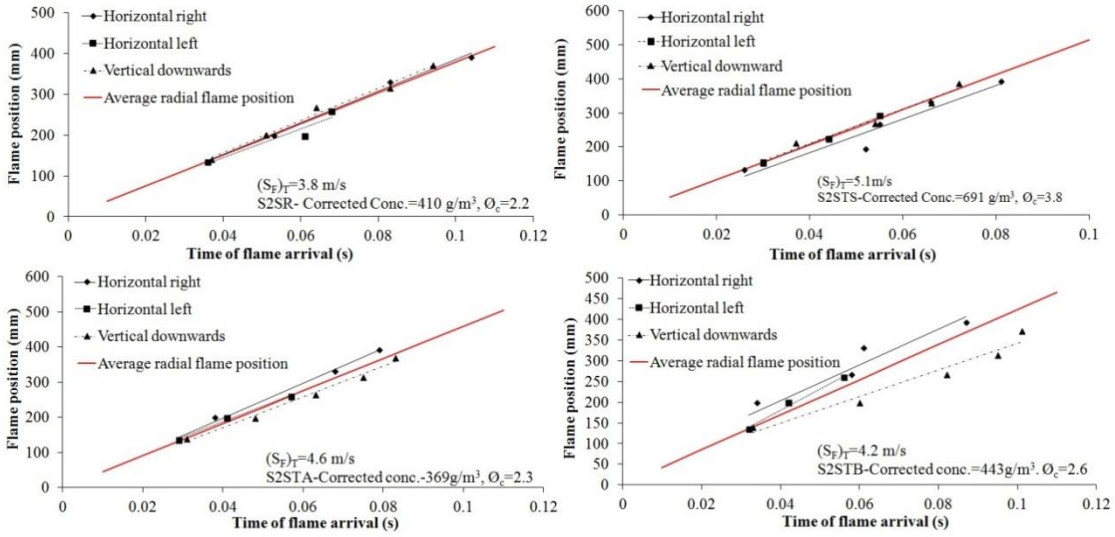

Figure 5-16. Flame speed position as a function of time for most reactive concentrations of S2SR, S2STS, S2STA and S2STB

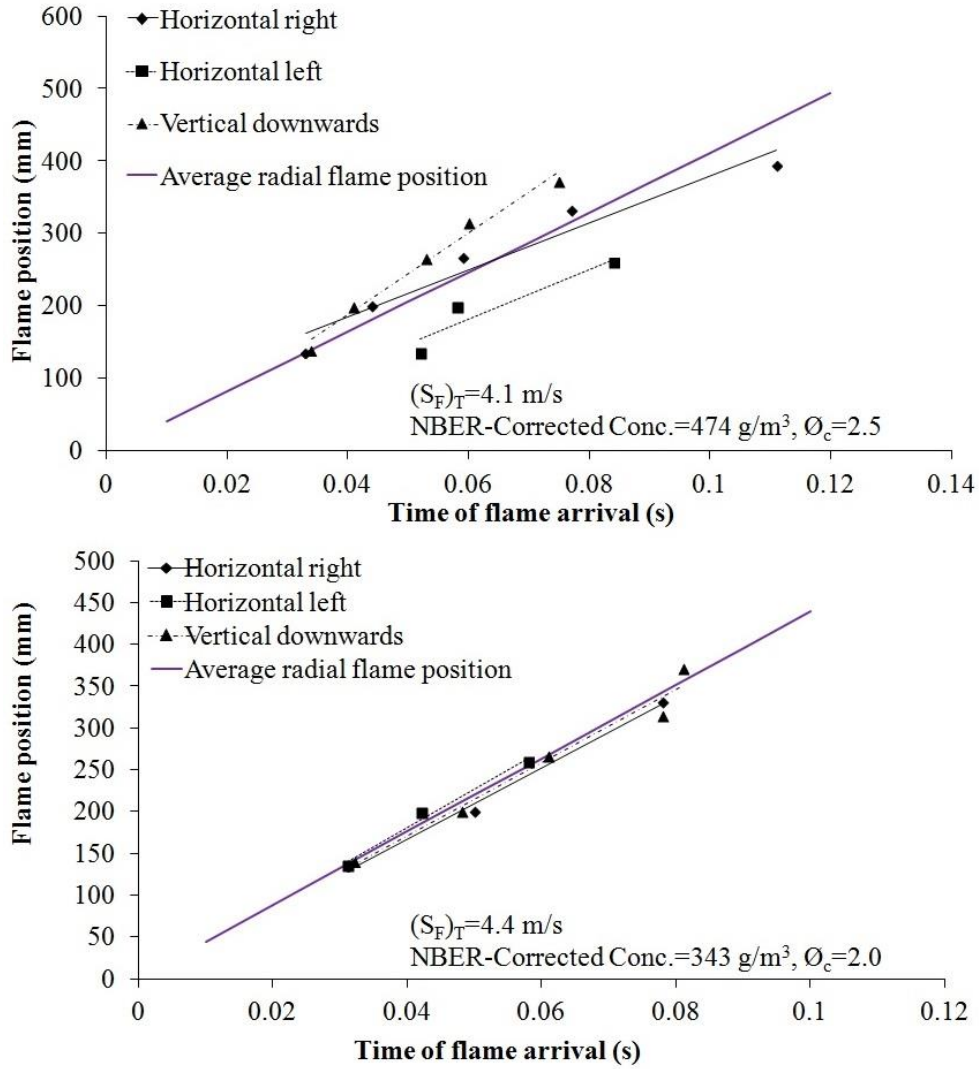

Figure 5-17. Flame speed position as a function of time for most reactive concentrations of NBER and NBET

Figure 5-18 plots maximum K_{St} values as a function of maximum turbulent flame speeds. There was a linear relationship between flame speeds and K_{St}, which confirms that either of the parameters could be used to measure the reactivity of dusts.

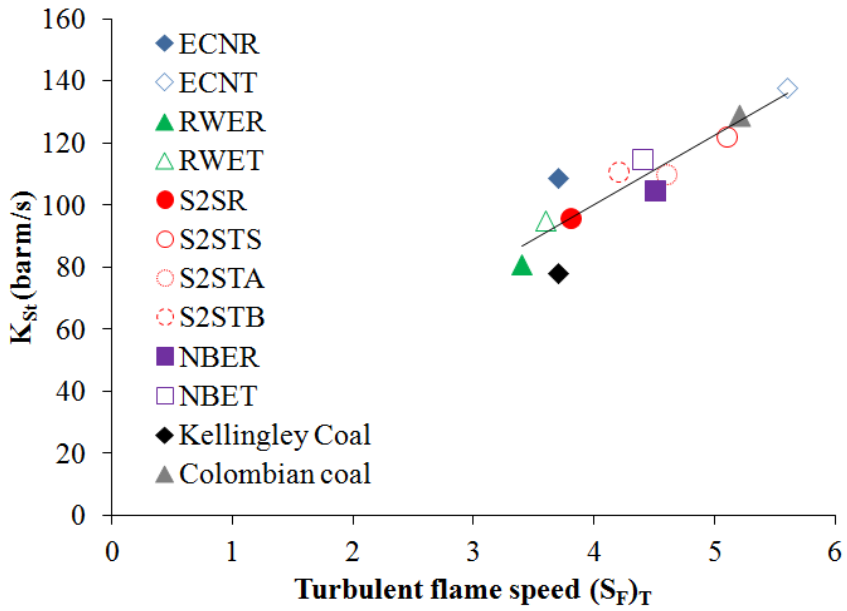

Figure 5-18. Correlation between K_{St} and turbulent flame speeds.

Flame speeds were measured in the constant pressure period of flame propagation. In order to derive laminar burning velocities the expansion ratio used in Eq.(2.8) should be the expansion ratio at constant pressure; however the constant pressure ratio produces burning velocities about 2.5 times higher than burning velocities calculated using the peak pressure [194]. Therefore the experimentally measured pressure ratio P_{max}/P_i was used as the expansion ratio. This procedure was previously adopted by Zabetakis, and Hertzberg et al. [208, 216] and showed comparable results with laminar burning velocities found in the literature review for gases [217]. However, the burning velocities derived using Eq.(3.20) are an approximation and could be therefore slightly low.

Table 5-6 summarises the main explosion and combustion characteristics of all samples. In every case it has been found that the torrefied samples were more reactive than the untreated biomass and Kellingley coal but similar to Colombian coal. All K_{St} values are between 0 and 200 barm/s, which classifies them as St-1 dusts (moderately explosible). Maximum explosion pressures were similar for all biomass samples and higher than for Kellingley coal. Burning velocity values are comparable to the order of magnitude found by other researchers for corn flour (similar composition to biomass) which is typically about 0.27 m/s [218]. Using the same method as in the present study Sattar [194] derived the laminar burning velocity of 0.30 m/s for cornflour.

Table 5-6. Summary of explosion and combustion characteristics of torrefied biomass samples and corresponding untreated biomass

	K_{St} (barm/s)	P_{max}/P_i	$(S_F)_T$ (m/s)	S_F (m/s)	S_L (m/s)
ECNR	109	9.0	3.7	0.9	0.1
ECNT	138	9.1	5.6	1.4	0.15
RWER	81	8.8	3.4	0.8	0.1
RWET	95	8.9	3.6	0.9	0.1
S2SR	96	9.0	3.8	0.9	0.1
S2STS	122	9.0	5.1	1.3	0.15
S2STA	110	9.1	4.6	1.1	0.12
S2STB	111	8.7	4.2	1.0	0.12
NBER	105	9.0	4.5	1.1	0.12
NBET	115	8.8	4.4	1.1	0.12
Kellingley Coal	78	8.2	3.7	0.9	0.12
Colombian coal	129	8.5	5.2	1.3	0.16

K_{St} and flame speeds not only had a linear relationship for the most reactive concentration. Figure 5-19 to Figure 5-22 show the relationship between K_{St} and flame speeds for all tests performed.

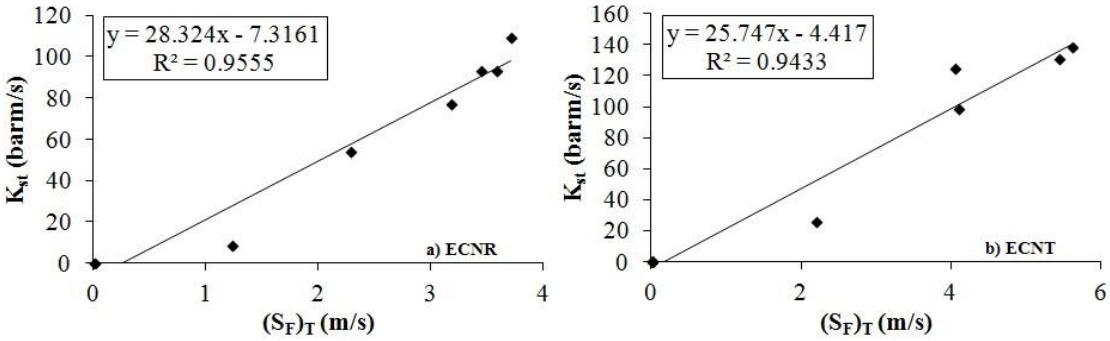

Figure 5-19. Correlation between K_{St} and turbulent flame speed for ECN samples

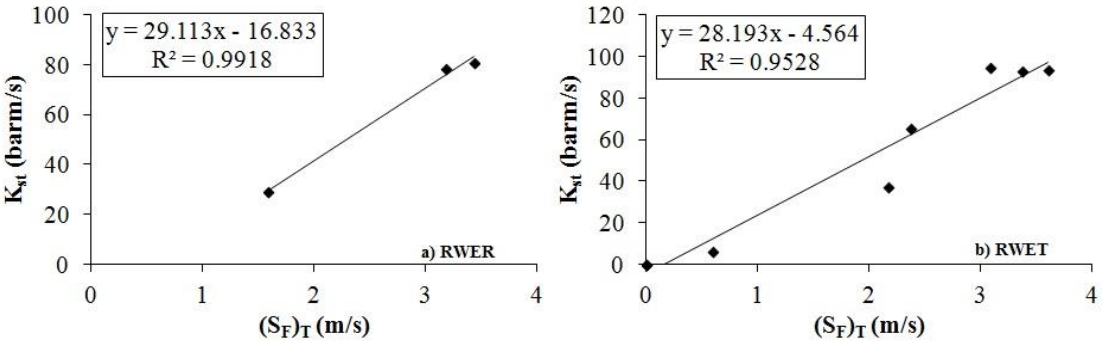

Figure 5-20. Correlation between K_{St} and turbulent flame speed for RWE samples

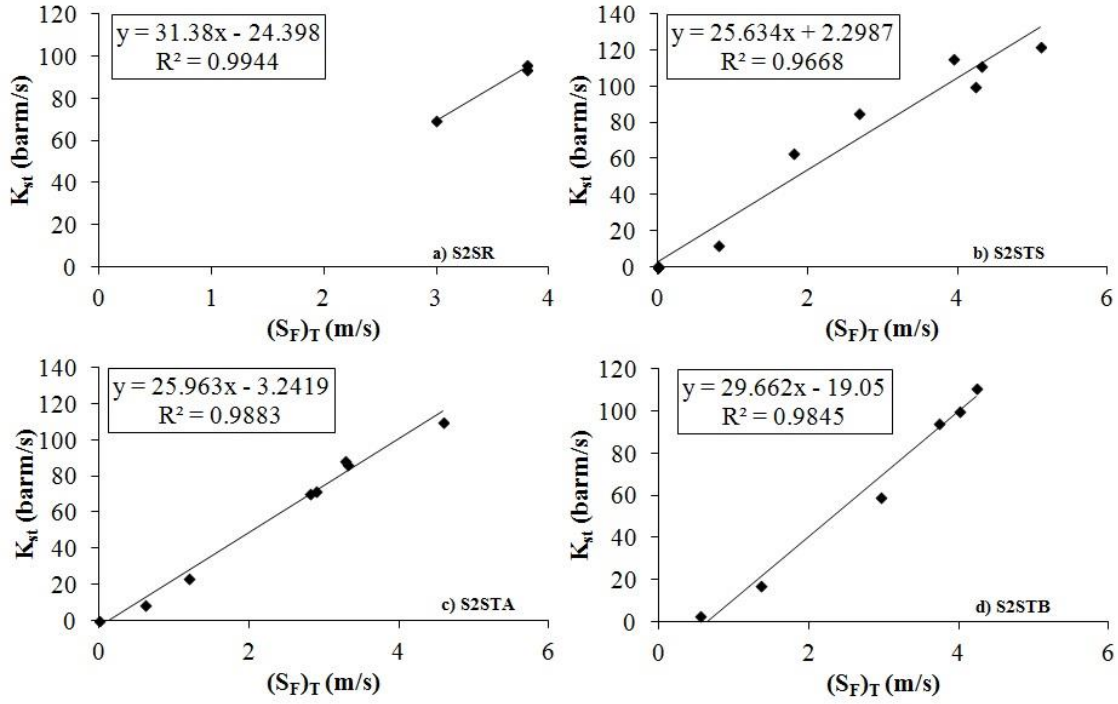

Figure 5-21. Correlation between K_{St} and turbulent flame speed for S2S samples

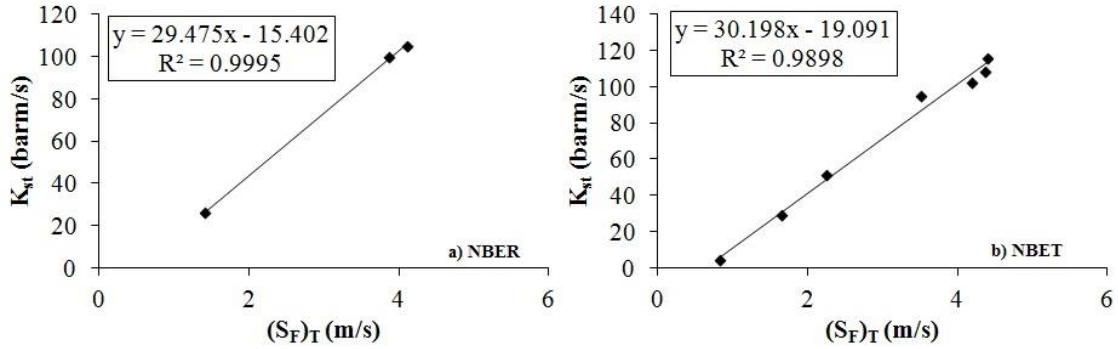

Figure 5-22. Correlation between K_{St} and turbulent flame speed for NBE samples

The NFPA68 recommends the use of laminar burning velocity in the venting correlations as a measure of gas reactivity, although the method for measurement of burning velocities is not agreed on. Similar situation occurs with dusts; however, in the case of dusts K_{St} values are still used as the reactivity parameter. Laminar burning velocities were derived in this study. As shown in Table 5-6, maximum laminar burning velocities ranged from 0.1 to 0.16 m/s for all the samples considered in this work. However, burning velocities varied with dust concentration, as shown in Figure 5-23. In addition, using the turbulent flame speeds measured, global heat release rates were calculated and these are shown in Figure 5-24 as a function of corrected equivalence ratio.

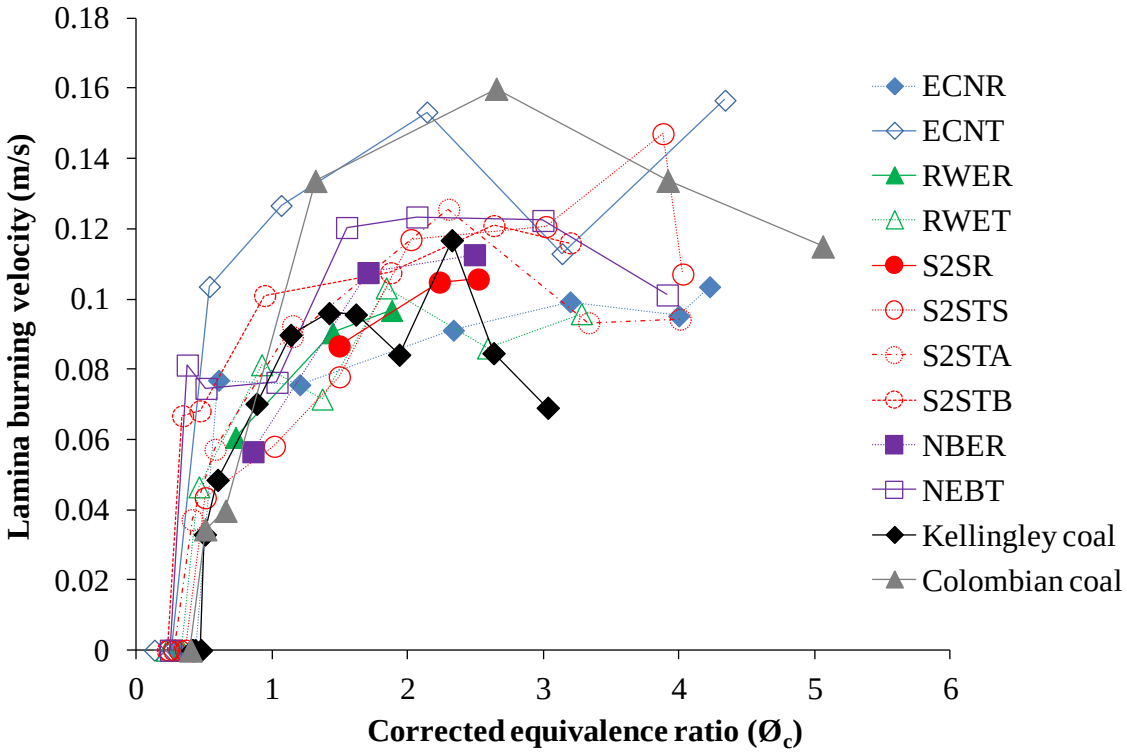

Figure 5-23. Laminar burning velocity as a function of corrected equivalence ratio

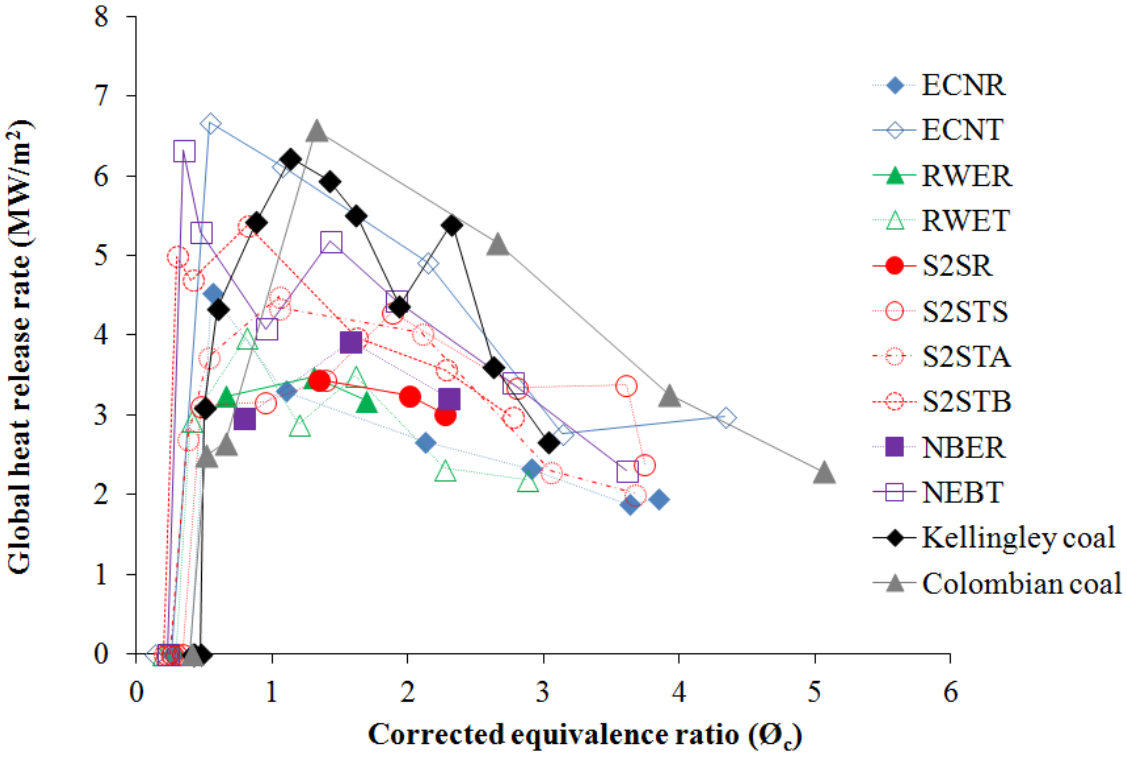

Figure 5-24. Global heat release rates as a function of corrected equivalence ratio

The measured global heat release rates at typical burner conditions of 15-20 % excess air for these specific samples range from 3 to 6 MW/m^2. These values are

comparable to values quoted in the literature for actual burners (3 to 4.5 MW/m^2 [219], 3.8 MW/m^2 [220]). Therefore, flame speed and burning velocity data produced in the 1 m^3 explosion rig is relevant for burner design and flame stability issues.

5.4. Factors affecting the reactivity of biomass and torrefied biomass

As discussed in Chapter 2 there are a number of parameters that affect the reactivity of dusts. These are experimental conditions (such as pressure, temperature, turbulence) and dust properties (composition, particle size). For all tests performed as part of this work the experimental conditions were kept constant, thus, the differences in explosion reactivity were due to the properties of each dust. The lowest K_{St} found for any of the biomass samples (untreated or torrefied) was 81 barm/s and the highest 138 barm/s. The range widens if Kellingley coal is considered with 78 barm/s. All dusts were C-H-O type dusts. Despite being composed by the same elements these were bound differently and, as discussed in Chapter 2, coals tend to be formed by bonded aromatic structures more difficult to break unlike biomass bonds. Biomass, having non-aromatic bonds and a higher volatile matter content was more reactive than Kellingley coal, as confirmed by the explosion characteristics measured. However it was similar in reactivity to Colombian coal. Torrefied biomass showed higher reactivity than the untreated counterparts despite having a lower volatile content. Moisture has been known for affecting the explosibility of dusts. All fuels used in this study were tested "as received" and as shown in Table 5-2 the moisture content was smaller than 10% for all samples. Moisture typically affects reactivity when it is present in larger measure. Due to the small variability of moisture for the samples tested in this work, other literature values were also considered. Figure 5-25 compiles data available in the literature [82, 86, 194] and from this work. Despite the scatter, moisture seems to have a tendency to decrease K_{St}. All torrefied samples, marked in Figure 5-25 with a letter "T" above or below their corresponding symbols, contained less moisture than their parent material and appeared on the low moisture range with higher K_{St} values.

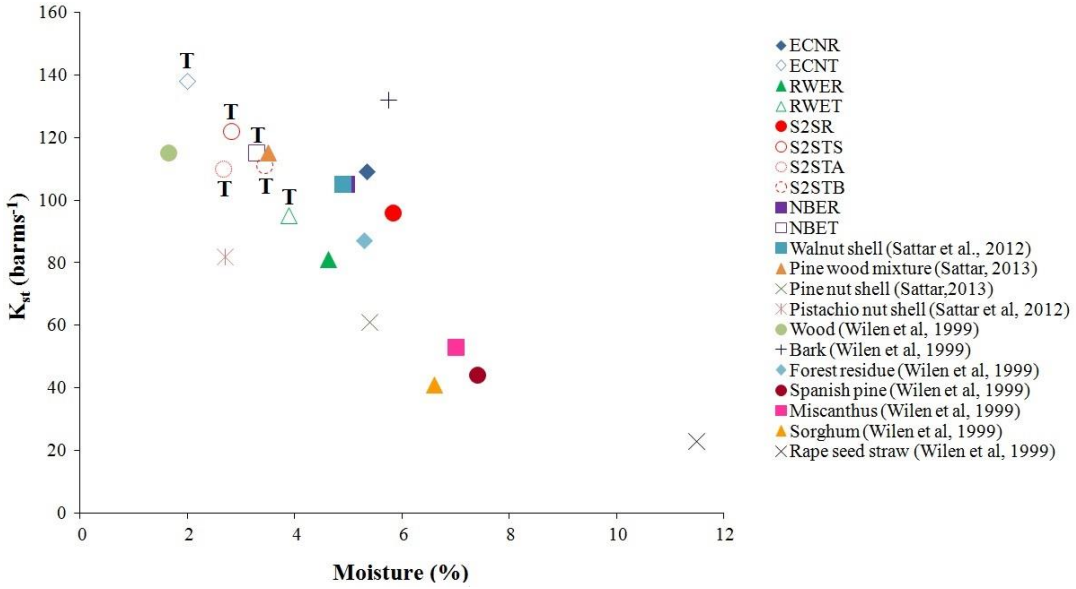

Figure 5-25. Effect of moisture on K_{St}

Similarly, the minimum explosible concentrations, expressed in Figure 5-26 as equivalence ratios, increase with moisture content. Torrefied samples, marked also with a letter T in the graph, appear on the lower range of moisture content burning at leaner mixtures, which indicates that the low moisture levels promote leaner flammability limits for these samples.

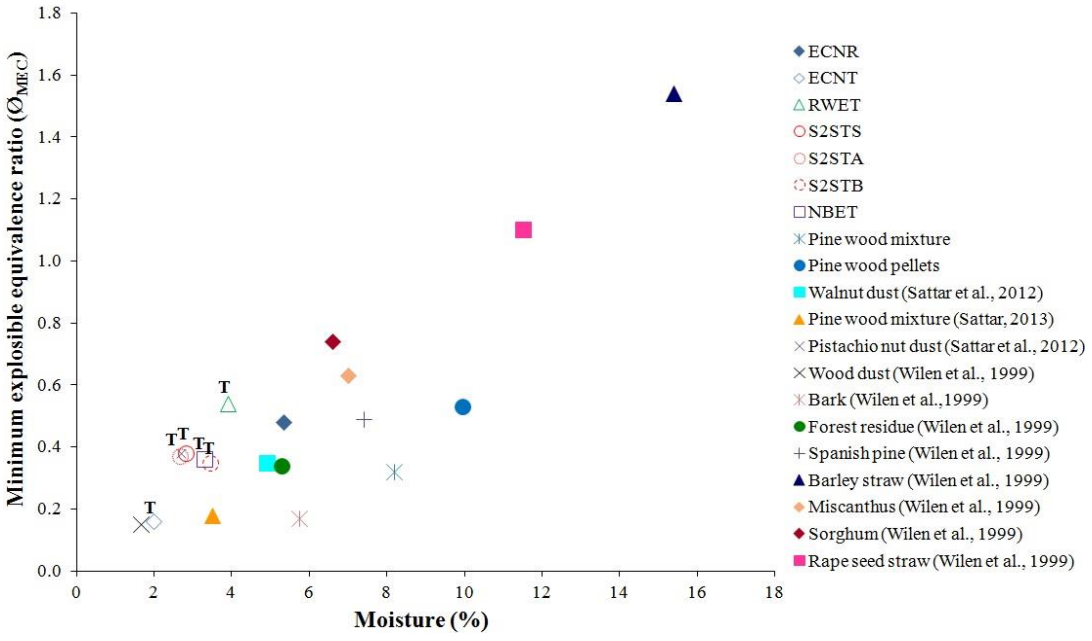

Figure 5-26. Effect of moisture on the minimum explosible mixtures ($Ø_{MEC}$)

When the combustion reaction takes place at the surface of the particle between the solid and air, surface area is often a parameter to take into account. In dust explosions heterogeneous combustion typically takes place with metal dusts, and K_{St} is largely affected by surface area [221]. As depicted in Figure 5-27 there is no correlation between K_{St} and surface area for biomass samples. This could be an

indication that reactions are not taking place at the surface of the particles but in the gas phase, however, there is not enough data and variability of surface area in this set to draw definite conclusions.

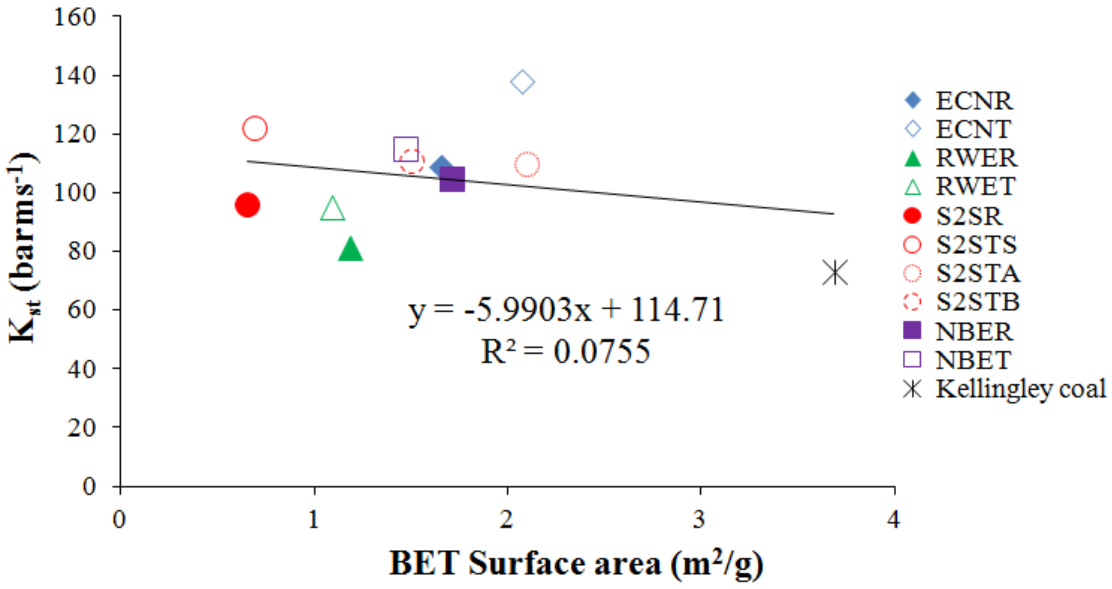

Figure 5-27. Effect of surface area on K_{St}

However, particle size is a key parameter, not only in heterogeneous but also in homogeneous combustion, as it has an effect over the rate at which volatiles are released. The amount of samples tested was not enough to define an exact trend, as the variability of particle size was not too large. In Figure 5-28 a number of results for other biomass samples has been added to the results of the samples tested in this study and shows that a large proportion of fines can have an effect over K_{St}, increasing the reactivity of samples.

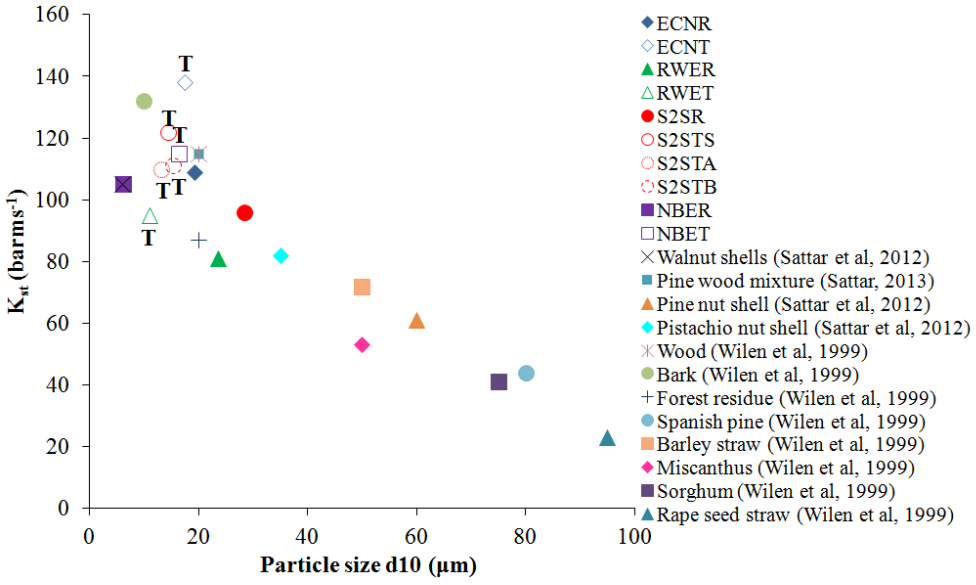

Figure 5-28. Effect of fine particles presence on K_{St}

5.5. Analysis of explosion residue

Residual dust was systematically found inside the explosion chamber after an explosion test. This is an issue that has been rarely reported by researchers but as explained in Chapter 2 some studies on the morphology of the residual particles and postulations on the reasons why these residues are created are available in the literature.

Residues were collected and weighted and the composition of the residue for the most reactive concentration test was further analysed. The amount of residue was collected and corrected assuming a collection efficiency of 95%. As shown in Figure 5-29, the higher the mass injected, the higher the vessel residue. The proportion was fairly constant for biomass and torrefied samples, whereas it is clear that tests performed with coal created a larger amount of residual dust, which resulted in the lower combustion efficiency of coal samples observed in Figure 5-13.

The elemental and proximate analysis shown in Table 5-7 to Table 5-11 correspond to the original samples and the explosion test residue for the most reactive concentration test. Explosion events reach temperatures at which both biomass and coal should fully devolatilise leaving only ash as residue. However, the analysis of the residues collected showed that the amount of volatiles lost was not higher than 31% for any of the samples, and in many cases the loss of volatiles was much lower. This suggested that residues were not only left-over ash formed as a result of combustion in the explosion flame front.

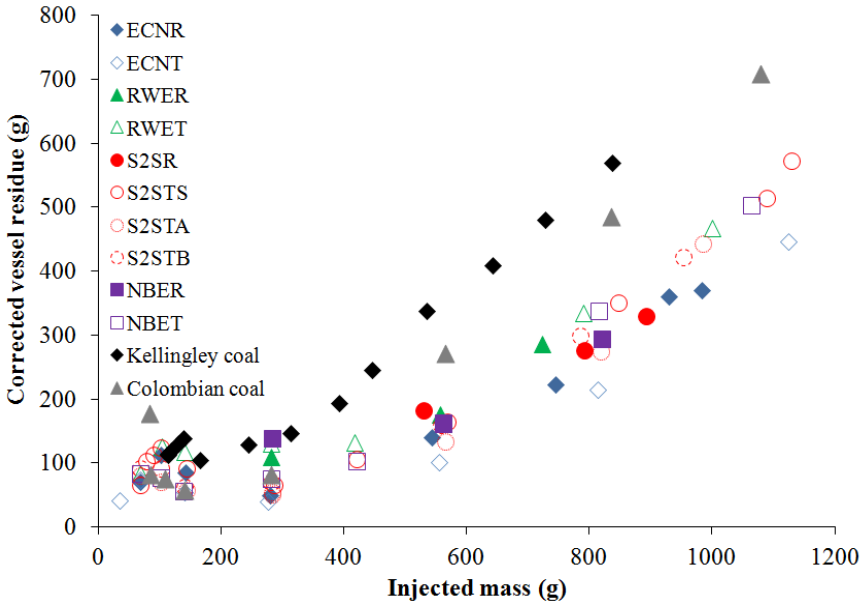

Figure 5-29. Vessel residue as a function of injected mass

The elemental composition of the residues indicates that oxygen, nitrogen and

hydrogen contents were generally decreased as a result of devolatilisation. Residues appeared carbonized. This can be observed in Figure 5-30 where the comparison between Van Krevelen plots of original samples and residues is shown.

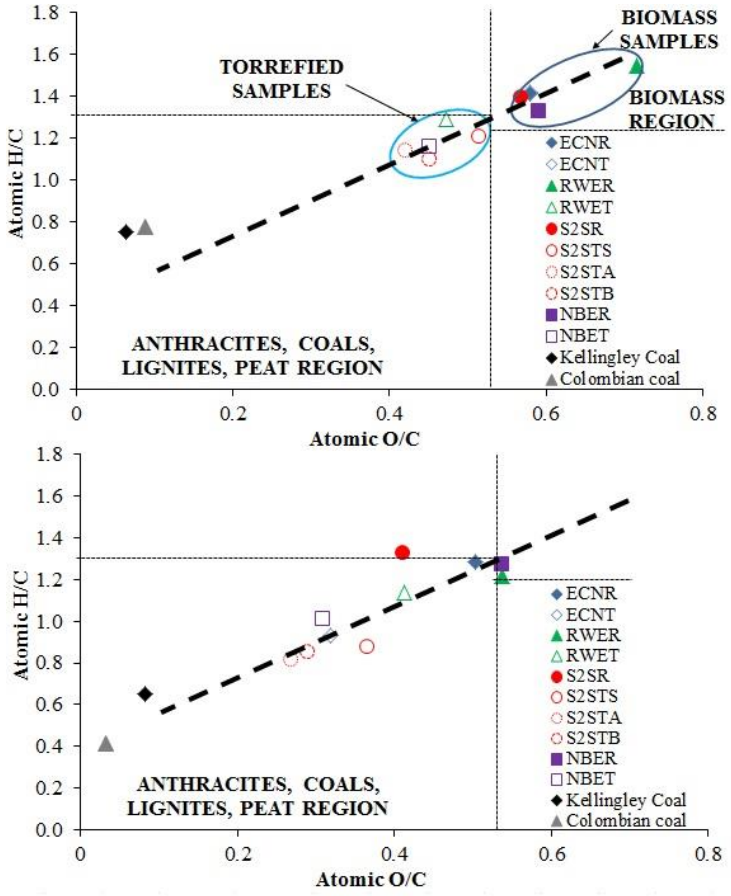

Figure 5-30. Van Krevelen plots for all original samples (left) and explosion residues (right)

Table 5-7. Most reactive mixture residue analysis for ECN samples

	Pre-Explosion		Post-Explosion	
Fuel Sample	**ECNR**	**ECNT**	**ECNR (Change %)**	**ECNT (Change %)**
Elemental analysis (wt%)				
C	48.0	49.9	50.7 (+5)	55.4 (+11)
H	5.7	5.9	5.4 (-5)	4.3 (-27)
O	37.1	38.6	34.0 (-8)	23.6 (-39)
N	0.0	0.3	0.5 (+)	1.2 (+)
S	0.0	0.0	0.0	0.0
TGA-Proximate (wt%)				
Moisture	5.3	2.0	3.6 (-32)	3.5 (+75)
Ash	3.9	3.3	5.7 (+46)	12.0 (+73)
Volatile Matter	78.0	78.2	76.8 (-1.5)	55.9 (-29)
Fixed Carbon	12.8	16.5	13.9 (+8)	28.7 (+43)
True Density (kg/m^3)	1.51	1.49	1.52 (+0.6)	1.62 (+8)
Mass burnt (%)	62.3	82.0	-	

Table 5-8. Most reactive mixture residue analysis for RWE samples

	Pre-Explosion		Post-Explosion	
Fuel Sample	**RWER**	**RWET**	**RWER (Change %)**	**RWET (Change %)**
Elemental analysis (wt%)				
C	42.4	49.1	49.3 (+16)	51.3 (+4)
H	5.5	5.3	5.0 (-9)	4.9 (-8)
O	40.4	30.9	35.3 (-13)	28.2 (-9)
N	2.0	2.4	0.9 (-55)	1.2 (-50)
S	0.0	0.0	0.0	0.0
TGA-Proximate (wt%)				
Moisture	4.6	3.9	4.0 (-13)	3.6 (-8)
Ash	5.1	8.4	5.6 (+10)	10.8 (+29)
Volatile Matter	83.4	68.9	72.6 (-13)	60.6 (-12)
Fixed Carbon	6.8	18.8	17.8 (+162)	25.0 (+33)
True Density (kg/m^3)	1.51	1.48	1.53 (+1)	1.54 (+4)
Mass burnt (%)	60.2	57.5	-	

The proximate analysis of residues corroborated that the volatile matter was consistently decreased. In addition, residues showed an overall increase in ash and fixed carbon. Such characteristics are distinctive of biomass and coal behaviour when subjected to high temperature in the absence of oxygen or air, that is, pyrolysis.

Table 5-9. Most reactive mixture residue analysis for S2S samples

	Pre-Explosion				Post-Explosion			
Fuel Sample	**S2SR**	**S2STS**	**S2STA**	**S2STB**	**S2SR (Change %)**	**S2STS (Change %)**	**S2STA (Change %)**	**S2STB (Change %)**
Elemental analysis (wt%)								
C	48.1	51.6	54.8	50.6	48.4 (+0.6)	55.4 (+7)	60.6 (+11)	57.4 (+13)
H	5.6	5.2	5.2	4.6	5.4 (-4)	4.1(-21)	4.1(-21)	4.1(-11)
O	36.3	35.4	30.7	30.5	26.6 (-27)	27.1 (-23)	21.7 (-29)	22.2(-27)
N	0.0	0.7	0.7	0.6	0.0	1.4 (+50)	1.2 (+71)	1.1 (+83)
S	0.0	0.0	0.0	0.0	0.0	0.0	0.0	0.0
TGA-Proximate (wt%)								
Moisture	5.8	2.8	2.7	3.4	3.1 (-47)	3.6 (+29)	2.9 (+7)	3.3 (-3)
Ash	4.1	4.2	5.8	10.2	16.6 (+305)	8.5 (+102)	9.5 (+64)	12.0 (+18)
Volatile Matter	79.0	77.0	69.4	63.6	66.5 (-16)	53.4 (-31)	48.8 (-30)	52.5 (-17)
Fixed Carbon	11.1	15.9	22.1	22.8	13.8 (+24)	34.5 (+117)	38.8 (+76)	32.2 (+41)
True Density	1.41	1.50	1.49	1.55	1.54 (+9)	1.59 (+6)	1.57 (+5)	1.56 (+0.6)
Mass burnt (%)	65.0	55.0	76.1	61.8	-			

Table 5-10. Most reactive mixture residue analysis for NBE samples

	Pre-Explosion		Post-Explosion	
Fuel Sample	**NBER**	**NBET**	**NBER (Change %)**	**NBET (Change %)**
Elemental analysis (wt%)				
C	48.4	54.0	50.9 (+5)	58.3 (+8)
H	5.4	5.2	5.4	4.9 (-6)
O	38.1	32.5	36.5 (-4)	24.0 (-26)
N	0.6	0.7	0.6	1.3 (+86)
S	0.0	0.0	0.0	0.0
TGA-Proximate (wt%)				
Moisture	5.0	3.3	3.7 (-13)	2.4 (-27)
Ash	2.5	4.3	2.9 (+10)	8.9 (+107)
Volatile Matter	78.5	70.3	72.9 (-13)	54.8 (-22)
Fixed Carbon	14.0	22.1	20.5 (+162)	33.8 (+53)
True Density (kg/m^3)	1.49	1.45	1.50 (+0.7)	1.50 (+3)
Mass burnt (%)	64.0	71.0	-	

Table 5-11. Most reactive mixture residue analysis for Kellingley coal

	Pre-Explosion		Post-Explosion	
Fuel Sample	**Kellingley coal**	**Colombian coal**	**Kellingley coal (Change %)**	**Colombian coal (Change %)**
Elemental analysis (wt%)				
C	65.0	66.6	64.3 (-1)	61.8 (-7.2)
H	4.1	4.3	3.5 (-15)	2.1 (-51)
O	5.5	7.8	7.1 (+29)	2.7 (-65)
N	2.4	2.1	1.4 (-42)	1.7 (-19)
S	2.2	0.7	2.2	0.9 (+28)
TGA-Proximate (wt%)				
Moisture	1.7	3.2	1.6 (-6)	2.2 (-31)
Ash	19.1	15.3	19.9 (+4)	28.5 (+86)
Volatile Matter	29.2	33.7	25.0 (-14)	14.4 (-57)
Fixed Carbon	50.0	47.8	53.5 (+7)	54.9 (+15)
True Density (kg/m^3)	1.48	1.45	1.64 (+11)	1.81 (+25)
Mass burnt (%)	39.3	51.9	-	

Residues true density measurements are also presented in Table 5-7 to Table 5-11. Particle density was found to change in a small measure for all samples, however, if

there was a change this was always to increase the density of the particle. The biggest increase was experienced by Kellingley coal (11%) and Colombian coal (25%), virtually no change was generally found for untreated biomass samples.

Slatter et al. [35] postulated that residues were a proportion of the injected dust which was pushed by the explosion wind towards the vessel wall. This was proven by measuring the rates of pressure loss in gas and dust tests. The rate of pressure loss in gas tests was much faster than with dusts, where a layer of dust acted as insulator. At the wall, the flame front impinged in the outer layer of dust momentarily as the flame was quenched by conduction through the walls.

In view of the resulting residue composition, it is likely that as the flame front quenched at the vessel wall, particles closer to the flame front were pyrolysed whereas particles close to the wall remained largely unchanged resulting in the slight changes in composition shown in previous tables.

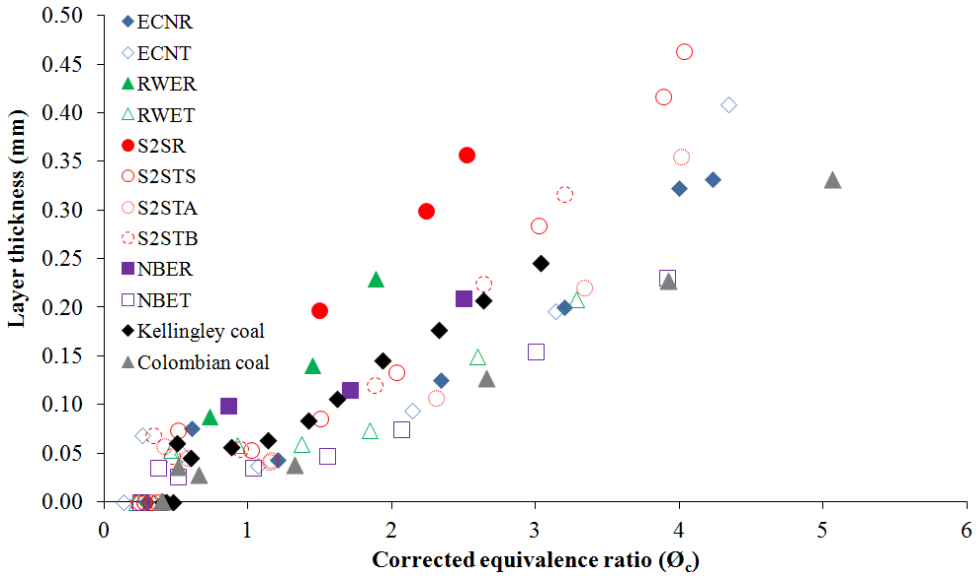

Figure 5-31. Theoretical thickness of residue layer in vessel walls

In Figure 5-31, it is shown that the thickness of a uniformly formed layer in the vessel wall increases as more mass is present in the vessel. Although the amount of deposits was larger after coal dust explosions (see Figure 5-13), as coal samples presented much higher bulk density, the layer thickness was similar to that of biomass and torrefied biomass explosion deposits.

As pointed out in [35], the layer of dust is believed to act as an insulation during the dust explosion, therefore, decreasing the rate of mass loss. The rate of mass loss not only depended on the layer of dust but on the maximum flame temperature. According to the maximum explosion pressure ratio results (see Figure 5-11), the maximum flame temperature remained fairly constant for $Ø_c$>2.For mixtures richer

than $Ø_c$=2 the rate of pressure loss decreased as the dust layer thickness increased (see Figure 5-32). All this data corroborates the existence of an insulation layer in dust explosion tests and supports actual observations following explosion tests in which layers of compressed powder were found when opening the vessel.

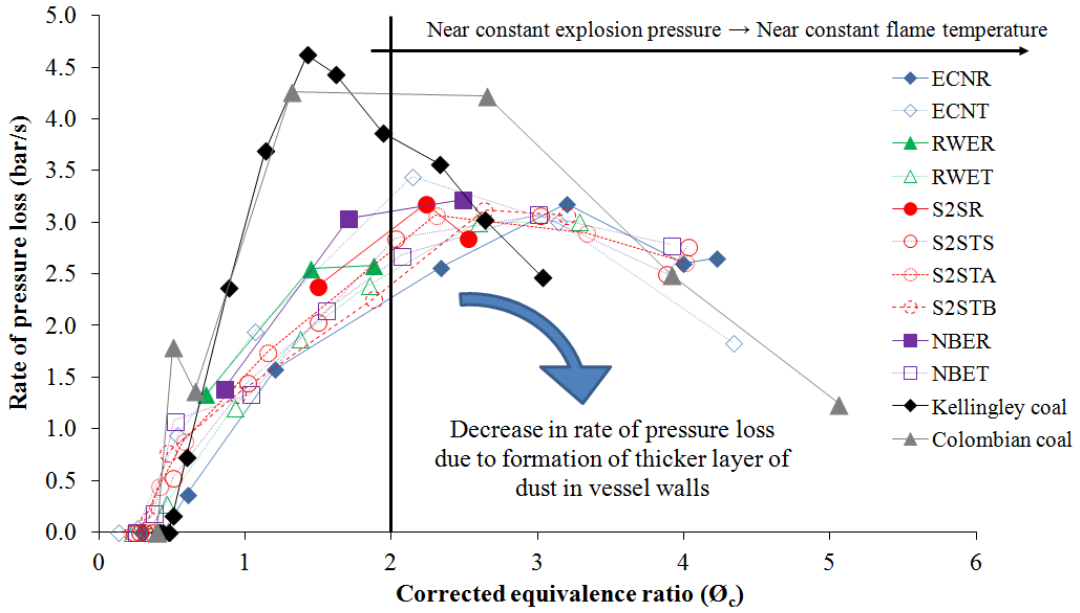

Figure 5-32. Rate of pressure loss as a function of corrected equivalence ratio

Further studies on the morphology of residual particles and particle size distribution were undertaken in order to corroborate and understand these findings.

The particle size distribution of residues found after explosion tests were compared to the size distribution of the original samples in Figure 5-33 to Figure 5-37. It can be observed that generally, the residue contained bigger particles than the original samples more notably in torrefied and coal samples.

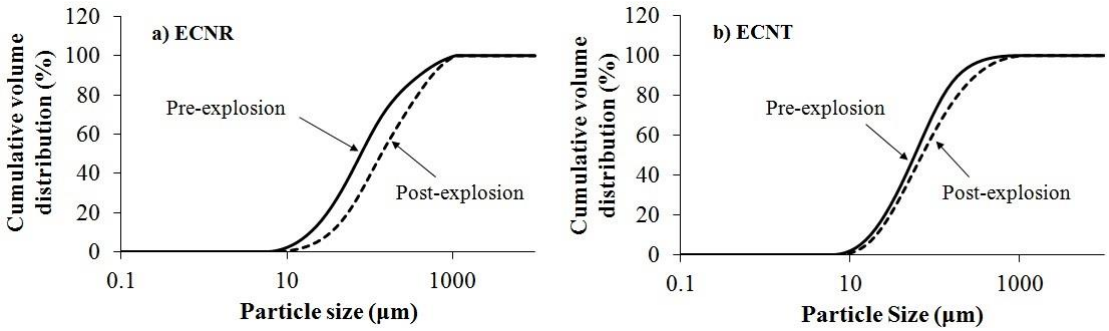

Figure 5-33. Cumulative volume size distribution of ECN samples before and after explosion

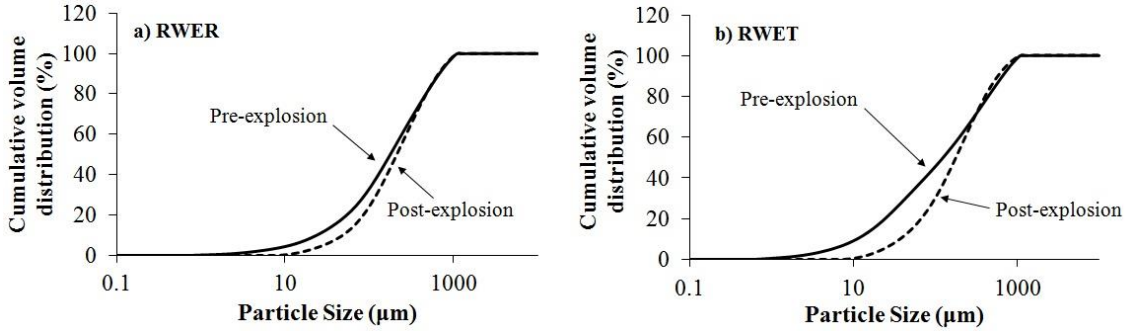

Figure 5-34. Cumulative volume size distribution of RWE samples before and after explosion

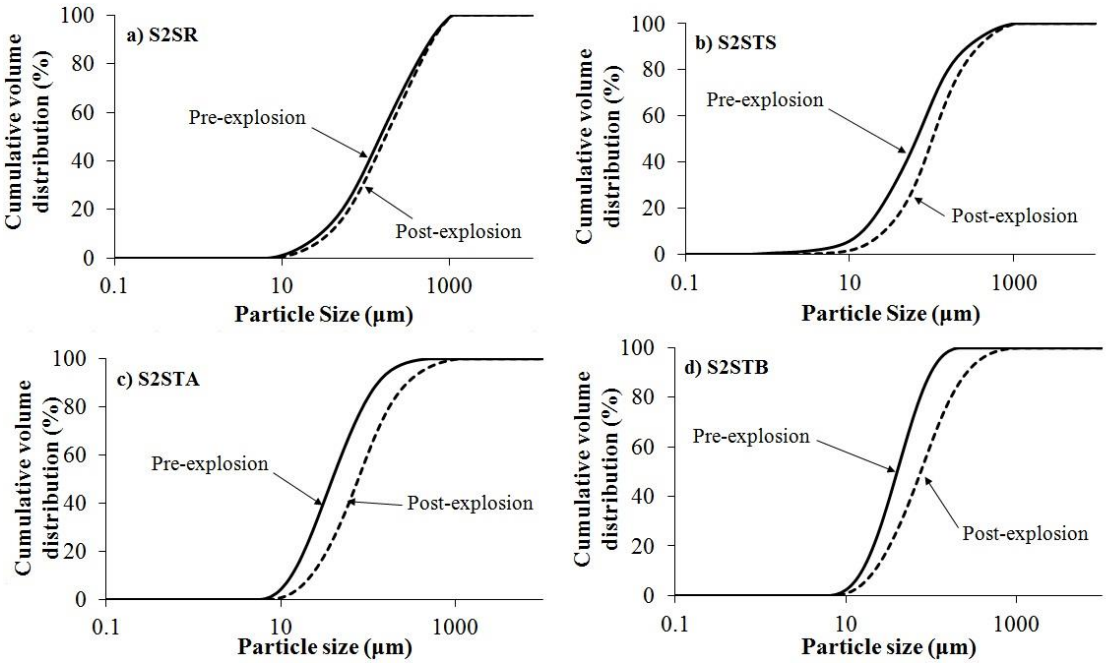

Figure 5-35. Cumulative volume size distribution of S2S samples before and after explosion

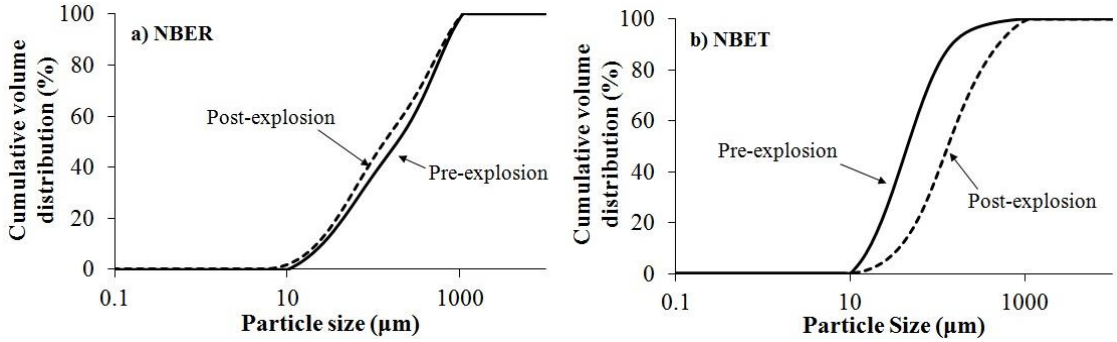

Figure 5-36. Cumulative volume size distribution of NBE samples before and after explosion

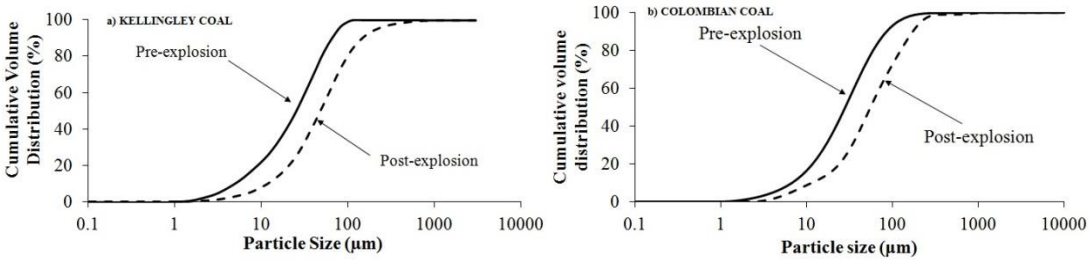

Figure 5-37. Cumulative volume size distribution of Kellingley coal before and after explosion

SEM images of all samples are presented in Table 5-12 to Table 5-17. These images clearly show clusters of char particles present in torrefied biomass and Kellingley coal post-explosion residues. These char clusters presented blow out holes that confirmed that certain degree of devolatilisation occurred. Mixed with them appear particles similar to those found in the original samples which remain unaffected. In the case of untreated biomass residues, much fewer char structures can be observed; most of the particles retained the original particle shape.

Table 5-12. SEM images of the original samples and the residue for most reactive concentration of ECN samples

ECNR	ECNT
BEFORE EXPLOSION (x300)	
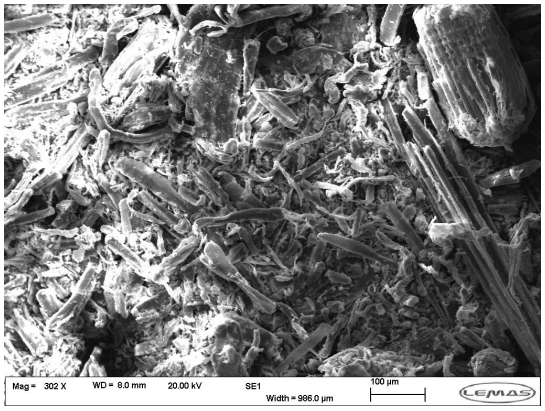	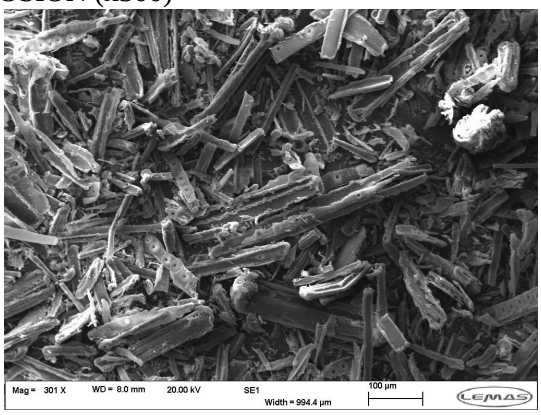
AFTER EXPLOSION (x300)	
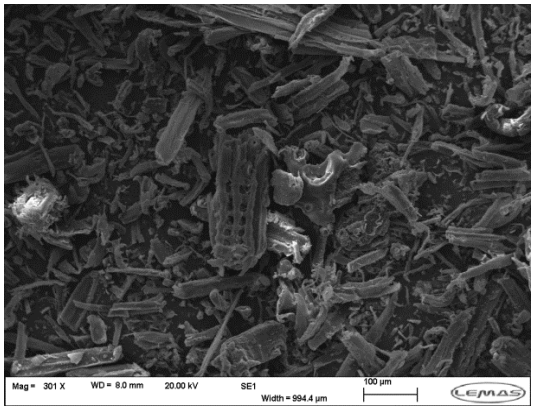	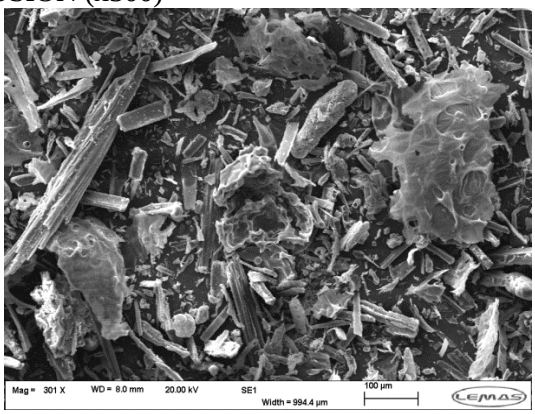

These findings support the theory that the differences in particle size distribution between original samples and post-explosion residues are due to the formation of char structures: in the case of raw biomass samples, very few char structures are formed and the size distribution remains the same as the original sample. On the contrary, for torrefied samples and coal, more char structures were formed, and as these fuse together to create clusters of bigger diameter, the size distribution of the residue contained larger particles.

Table 5-13. SEM images of the original samples and the residue for most reactive concentration of RWE samples

RWER	RWET
BEFORE EXPLOSION (x100)	
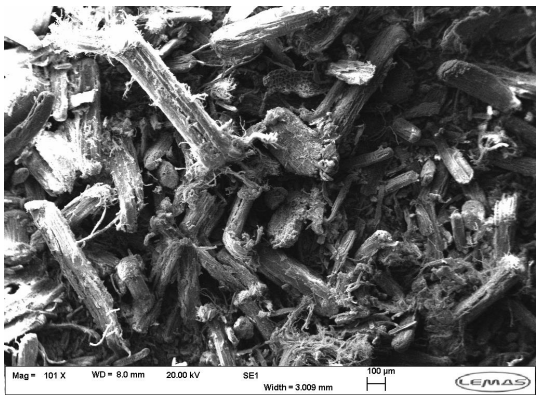	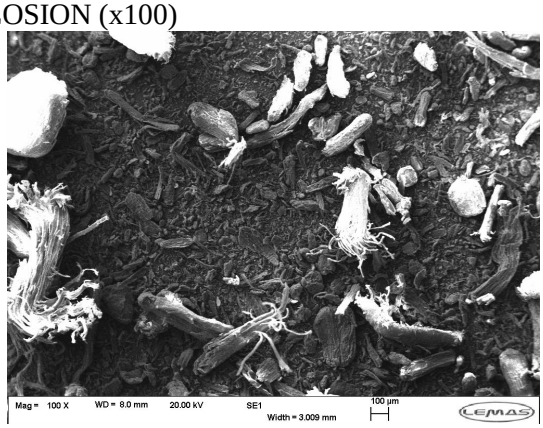
AFTER EXPLOSION (x100)	
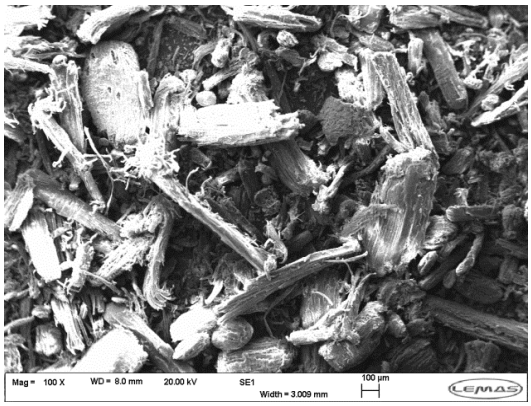	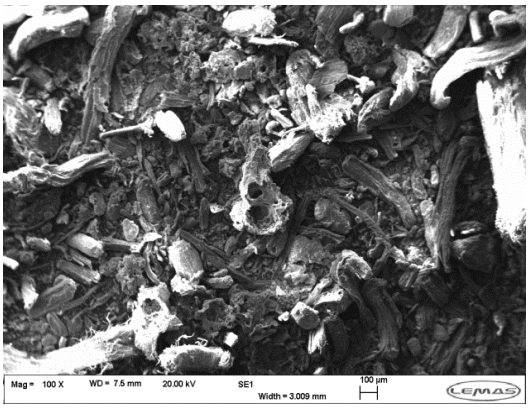

It has been previously found in the literature that heating rates have a large effect in pyrolysis and formation of char. For biomass samples at high heating rates char formation is lower whereas gas formation is higher. This behaviour has been attributed to the high cellulose content of biomass. At temperatures <300°C, cellulose dehydrates to a more stable anhydrocellulose which gives higher yields of char. However at high heating rates the rate of cracking of primary products is higher, and therefore cracking happens in preference to condensation [222].

In the case of torrefied biomass, part of the cellulose content decomposed during the torrefaction process, therefore there was more condensation and formation of char than in raw biomass samples.

Table 5-14. SEM images of the original samples and the residue for most reactive concentration of S2SR and S2STS samples

S2SR	S2STS
BEFORE EXPLOSION (x200)	
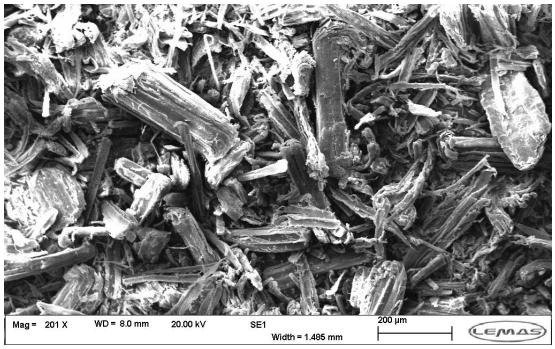	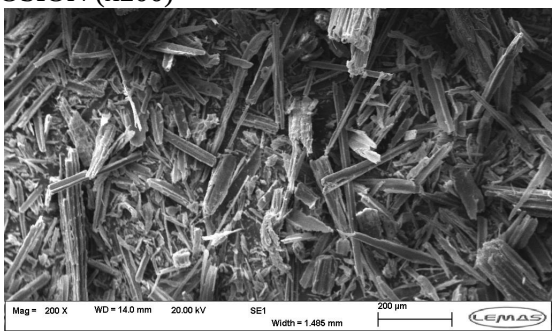
AFTER EXPLOSION (x200)	
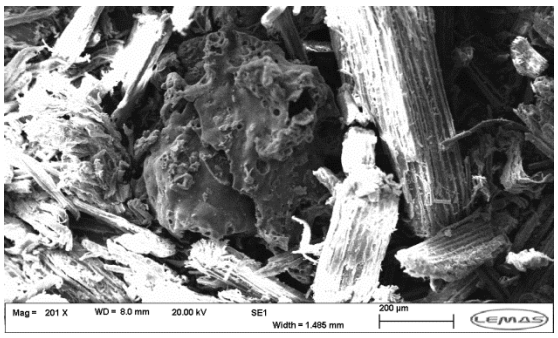	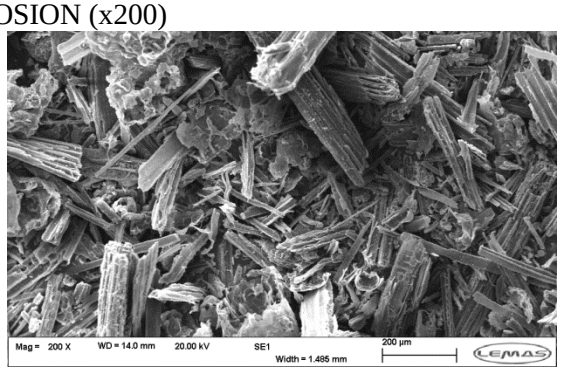

Table 5-15. SEM images of the original samples and the residue for most reactive concentration of S2STA and S2STB samples

S2STA	S2STB
BEFORE EXPLOSION (x200)	
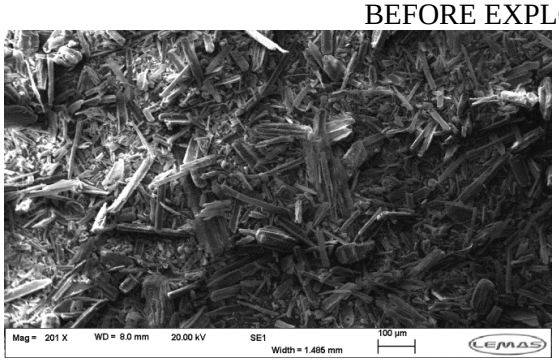	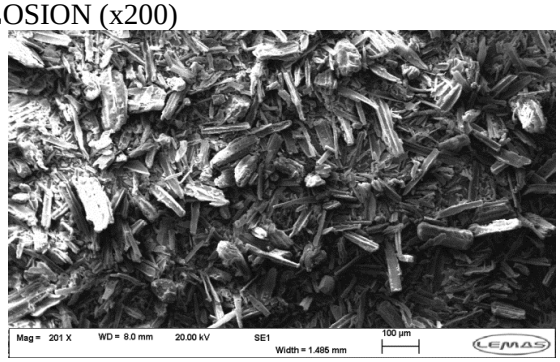
AFTER EXPLOSION (x200)	
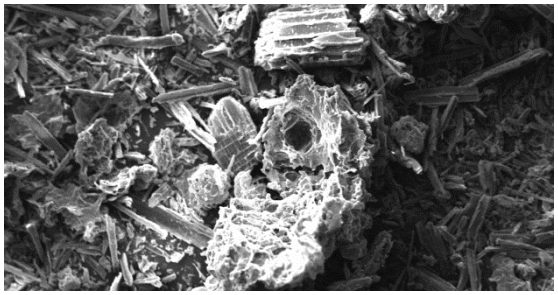	

Table 5-16. SEM images of the original samples and the residue for most reactive concentration of NBE samples

NBER NBET

BEFORE EXPLOSION (x200)

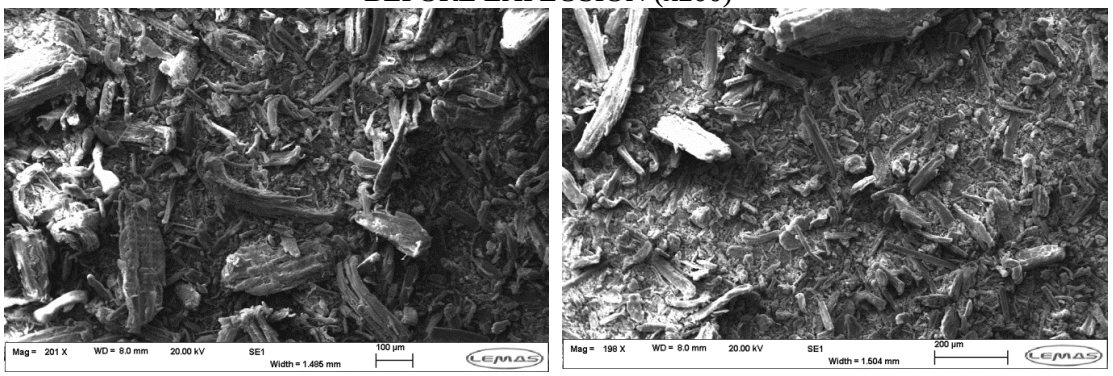

AFTER EXPLOSION (x200)

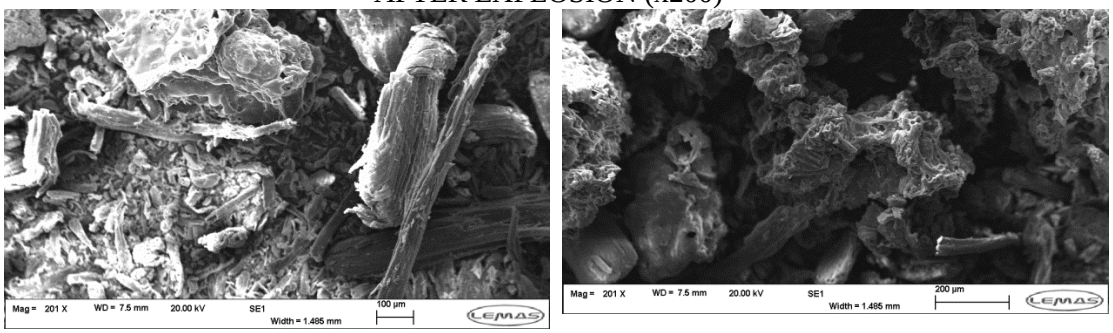

Table 5-17. SEM images of the original samples and the residue for most reactive concentration of Colombian coal and Kellingley coal samples

BEFORE EXPLOSION AFTER EXPLOSION

Colombian coal (x500)

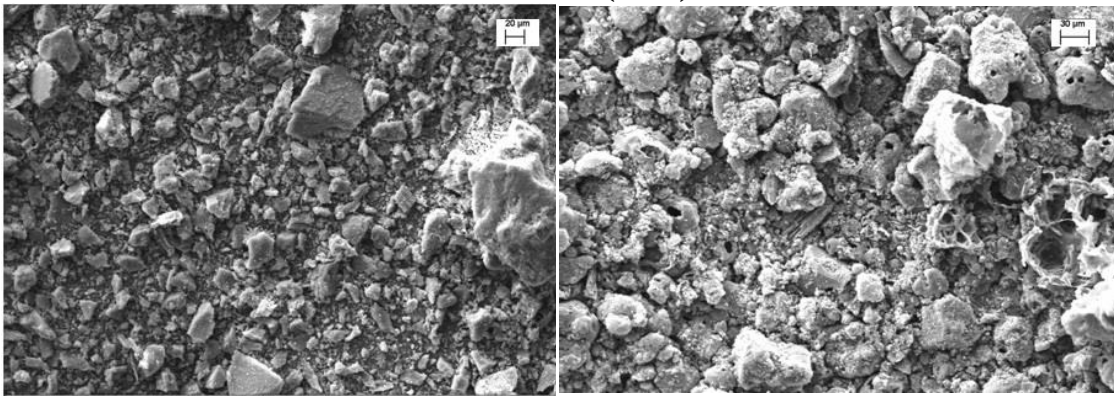

Kellingley coal (x300)

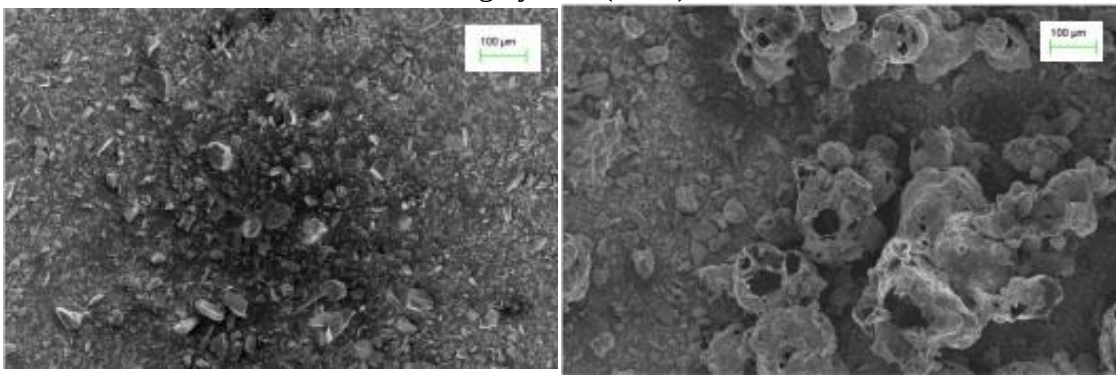

5.6. Conclusions

A number of torrefied woody biomass samples, ranging from mild to severe torrefaction conditions, were used in the present study. The composition and physical properties of the samples were presented and typical differences between raw and torrefied biomass were shown: increase in carbon and fixed carbon contents, as well as increases in high heating values and in some cases an improvement in bulk density were observed. At the same time these properties could be compared to those of bituminous coal that still presents much higher carbon and fixed carbon contents than any of the torrefied samples, as well as heating value. Bulk density is also much higher than for raw biomass samples. This property appears to improve in some cases with torrefaction. The oxygen content of both biomass and torrefied biomass is significantly higher than for coal, as well as the volatile matter.

The thermogravimetric analysis showed that biomass (raw and torrefied) are more reactive than coal due to the higher volatile content. The density of the particles is similar for all biomass samples and the samples of coal tested. The surface area of the particles however was bigger for coal. The surface area of torrefied samples depends on the torrefaction conditions: increasing when torrefaction conditions are milder and decreasing when torrefaction conditions are severe.

Using the same milling procedures, torrefied samples presented a larger fraction of fines in comparison to the raw biomass samples. However pf coal typical of power stations, like Kellingley coal, contain finer particles and also have a narrower particle size distribution, unlike biomass and torrefied biomass samples.

Explosion characteristics were measured using the modified and calibrated 1 m^3 vessel arrangement for fibrous powders. Although this system allowed testing fibrous biomass milled to <60 μm, dusts containing bigger particles are likely to choke the delivery system. It is recommended that in order to test coarser samples of fibrous dusts (more representative of the sizes used in the industry) other dispersion system, preferably an in-vessel design is used.

For every pair of torrefied and their corresponding raw materials K_{St} was higher for the torrefied biomass. The sample of Kellingley coal had lower K_{St} value but Colombian coal had similar K_{St} as the torrefied biomass samples. Correspondingly, the MEC for torrefied samples were lower than for coal. However, the explosion pressures, normalised for the initial pressure (P_{max}/P_i) were very similar for all biomass samples regardless of being torrefied. Explosion pressures for all biomass samples reached around 9 bar, 1 bar higher than the values found for Kellingley coal. This suggests that torrefaction has little effect over the flame temperature, but

it does affect properties that have an effect over the rate of reaction, namely particle size. Additional data available from the literature was used to assess the effect of various parameters over K_{St}, and those which appeared to produce an increase in K_{St} value included moisture content and particle size. A relationship between the calculated volatile yield at high temperature, using the elemental composition and K_{St} was also found. On the other hand, surface area did not show a relationship with K_{St}, This implies that it is likely that the reactions during explosion occur homogeneously between gases.

The vessel used also allowed derivation of turbulent flame speeds using arrays of thermocouples in various directions. It was confirmed that flames are relatively spherical. Flame speeds and K_{St} have a linear relationship and therefore either parameter could be used as a reactivity parameter. Derivation of approximate laminar burning velocities was also possible using the measurements of turbulent flame speeds. These were found to be between 10-15 cm/s for biomass. These approximated values are however likely to be a bit low.

Residual masses of dust were found at the bottom and around the vessel walls after explosion tests. These residues were collected and quantified and the residue found at the most reactive concentration test was further analysed, following the same analysis techniques as for the original samples. The proximate analysis of the residues revealed that residues had undergone very small devolatilisation, and therefore it was concluded that this proportion of dust could not have taken part in the explosion reaction. It is believed that the explosion induces wind ahead of the flame pushing a proportion of dust towards the walls of the vessel. Particles closer to the flame front were affected by the impinging flame front, as it cooled down by heat transfer to the walls of the vessel, undergoing pyrolysis by the action of hot temperature at the flame front and absence of air (or oxygen). As a result residues showed typical signs of pyrolysis: decrease in oxygen, hydrogen and volatile matter, and increase in fixed carbon and ash. Further studies into the morphology of the particles in the residues showed that char structures are present in coal and torrefied biomass explosion tests residues. These char structures fused together forming big clusters, which was reflected in the particle size distribution of the residues. Conversely, the residues found after raw biomass tests showed very few char structures and therefore hardly no change in the particle size distribution. It is believed that this effect is due to raw biomass giving lower char yield at high heating rates than torrefied and coal samples.

Chapter 6 EXPLOSION CHARACTERISTICS OF MIXTURES OF COAL AND BIOMASS

CONTENTS

6.1. Introduction

As discussed in Chapter 1 and 2, co-firing of coal and biomass is an attractive way of introducing renewable fuels in power generation. In these plants dust explosion hazards are associated both to the mixtures and to the individual fuels co-fired.

The objective of the present study was to measure the explosion (K_{St}, P_{max}, MEC) and combustion (flame speed, burning velocity) properties of coal and biomass blended in a range of ratios containing low to medium proportions of biomass. A blend of torrefied wood and coal was also tested. Results were compared to the biomass and coal samples alone.

6.2. Fuels and their characteristics

6.2.1. Elemental and proximate analysis

Pulverised pine wood pellets (pine sawdust and chips without bark) were blended in a range of ratios with a sample of Colombian coal from the “El Cerrejón” mine supplied by Moneypoint power station (ESB). The blends with Colombian coal contained: 5%, 15%, 20% and 40% (by mass) pulverised Pine wood pellets. The blend of torrefied biomass and coal was prepared from torrefied Norway spruce pulverised to <75 μm (S2STS) and Kellingley coal, containing 50% torrefied biomass, by mass. Coal samples were supplied in pulverised form from power stations and thus were representative of the fuels and particle size used in these plants. The sample of torrefied wood was pulverised following the procedures detailed in Chapter 3. However 30 kg of Pine wood pellets were already pulverised

when supplied using a different procedure: the pellets were initially broken up in a Holmes LC-401 hammer mill crusher by passing the sample three times. Following this, the samples were fed to a Holmes LC-501X rotor and hammer pulveriser with a 60 μm bottom sieve. All samples were stored in sealed containers. Mixtures of biomass and coal were blended through manual shaking and stirring. Evidence of good mixing was obtained from repeatable elemental analysis results.

All samples were individually characterised for elemental and proximate compositions as well as for other physical properties such as density or particle size as detailed in Chapter 3. Results of elemental and proximate compositions and other properties are given in Table 6-1 and Table 6-2.

Table 6-1. Fuel characteristics of Pine wood pellets, Colombian coal and their mixtures

	Pine wood pellets	Colombian coal	Mixture (5/95)	Mixture (15/85)	Mixture (20/80)	Mixture (40/60)
Elemental Analysis (wt%)[1]						
C	46.8	66.6	64.9	64.0	59.2	57.5
H	5.7	4.3	4.8	4.0	4.4	4.8
O*	37.0	7.8	7.5	9.8	20.1	21.5
N	0.0	2.1	2.0	2.2	1.9	1.3
S	0.0	0.7	0.5	0.5	0.2	0.2
Proximate Analysis (wt%)[1]						
Moisture	9.9	3.2	3.0	3.5	4.0	5.0
VM	77.1	33.7	34.8	38.6	50.3	51.1
FC	12.4	47.8	44.9	41.9	35.4	34.2
Ash*	0.6	15.3	17.3	16.1	10.2	9.7
Volatility (VM/FC)	6.2	0.7	0.8	0.9	1.4	1.3
y=H/C**	1.4	0.8	0.9	0.7	0.9	1.0
z=O/C**	0.6	0.1	0.1	0.1	0.3	0.3
Stoichiometric Air/Fuel Ratio	6.4	10.7	10.9	10.2	8.6	8.6
Stoichiometric concentration[2] (g/m^3)	187	112	110	117	139	140
GCV[2] (MJ/kg)	21.1	33.5	34.3	31.8	26.3	22.5
Bulk density (kg/m^3)	220.6	407.4	492.9	453.6	449.1	423.9

*calculated by difference, **molar ratio, [1]As received basis, [2]Calculated, dry, ash free basis

The analysis was done for the actual mixtures; however, theoretical values could be calculated for the mixtures. Experimental and theoretical values were compared. Most properties were measured within 10% difference from the theoretical values, however, other properties differed for every mixture, and these were the oxygen content, the volatility of the mixtures and the bulk density. The discrepancies could be due to the small quantities used in both the elemental and proximate analysis, however for elemental composition duplicate measurements were taken and results were found to be within 10% of each other.

Table 6-2. Fuel characteristics of Kellingley coal, torrefied Norway spruce and their 50/50 mixture (by mass)

	S2STS	Kellingley coal	Mixture (50/50)
Elemental Analysis (wt%)[1]			
C	51.6	65.0	59.7
H	5.2	4.1	5.0
O*	35.4	5.5	21.0
N	0.7	2.4	1.8
S	0.0	2.2	0.1
Proximate Analysis (wt%)[1]			
Moisture	2.8	1.7	2.4
VM	77.0	29.2	55.5
FC	15.9	50.0	32.0
Ash*	4.2	19.1	10.0
Volatility (VM/FC)	4.8	0.6	1.7
y=H/C**	1.2	0.8	1.0
z=O/C**	0.5	0.1	0.3
Stoichiometric Air/Fuel Ratio	6.6	10.8	8.7
Stoichiometric concentration[2] (g/m^3)	180	111	138
GCV[2] (MJ/kg)	21.9	33.8	26.9
Bulk density (kg/m^3)	235.0	443.0	302.8

*calculated by difference, **molar ratio, [1]As received basis, [2]Calculated, dry, ash free basis

Measured bulk densities were higher than expected (more coal like) in the mixtures with Colombian coal. Zulfiqar [223] reported a linear change in bulk density for a coal/sawdust blend containing 10% biomass, this differs from the present results which suggests that the effect could be sample dependent. In the particular case of the blends with Colombian coal, mixtures had higher bulk density. It is likely that the gaps between biomass particles were filled with coal particles. In the mixture of 50% torrefied material biomass and 50% Kellingley coal the bulk density of the mixture was only 10% smaller than the theoretical value.

The oxygen content for the Colombian coal blends was also different than the theoretically determined values, for mixtures with low proportion of biomass (5% and 15%) the measured values were smaller than expected (more coal like). When the proportion of biomass was increased the oxygen content measured was higher than the additive calculated value. The measured volatility was for all mixtures lower than the theoretical value (more coal like). This suggests that interactions between the fuels took place during combustion. These interactions seemed to be related to the devolatilisation step.

In Figure 6-1, the position of all samples in the Van Krevelen diagram is shown. Blends containing low proportion of biomass were situated in the typical coal region of the diagram. The 50/50 mixture of torrefied biomass and coal is situated equidistant to the fuels.

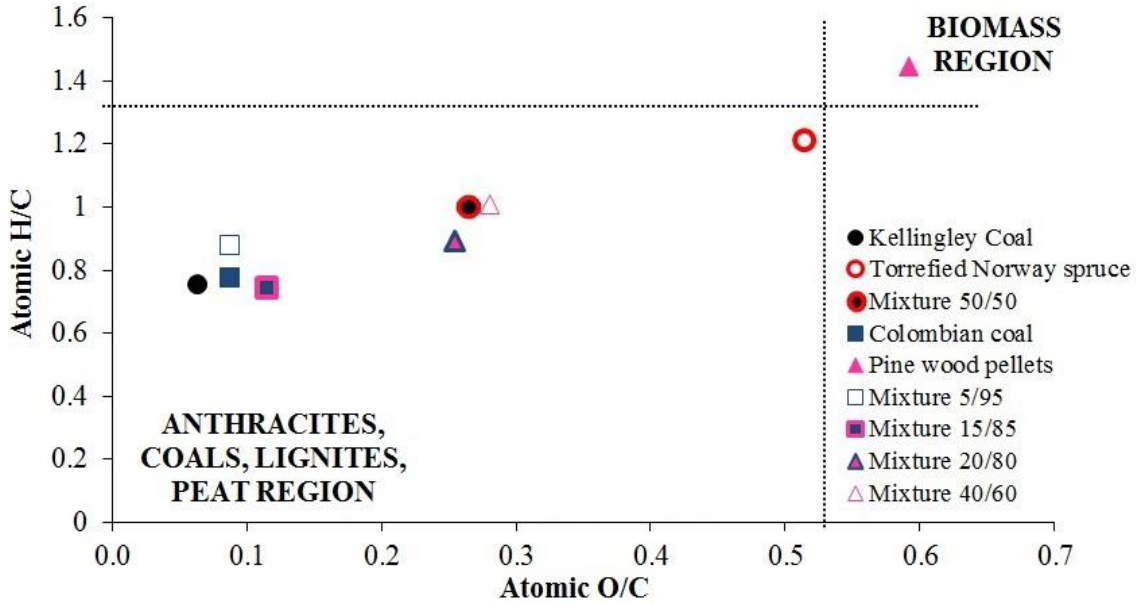

Figure 6-1. Van Krevelen diagram of biomass and coal samples and their mixtures

All samples were further analysed using thermogravimetric techniques. The behaviour of coal and biomass blends has been previously studied by many

researchers through TGA techniques [151, 152, 176, 178, 181, 224-226]. Figure 6-2 and Figure 6-3 show the weight loss normalised only for the volatiles release and fixed carbon burn out respectively for Colombian coal, pine wood pellets and their mixtures and similar graphs for Kellingley coal and torrefied Norway spruce (S2STS) and their mixture are presented in Figure 6-4 and Figure 6-5.

Colombian coal and pine wood pellets decomposition curves presented the typical characteristics for a coal and a biomass respectively. The devolatilisation of mixtures containing a smaller proportion of biomass remained similar to coal, but it is clear that the addition of biomass to the blend had an effect by which devolatilisation of the bulk started at lower temperatures and at a faster rate.

The burnout of fixed carbon also occurred at a faster rate for 100% biomass sample than for Colombian coal and again, the addition of biomass increased the rate of fixed carbon burnout of the blends.

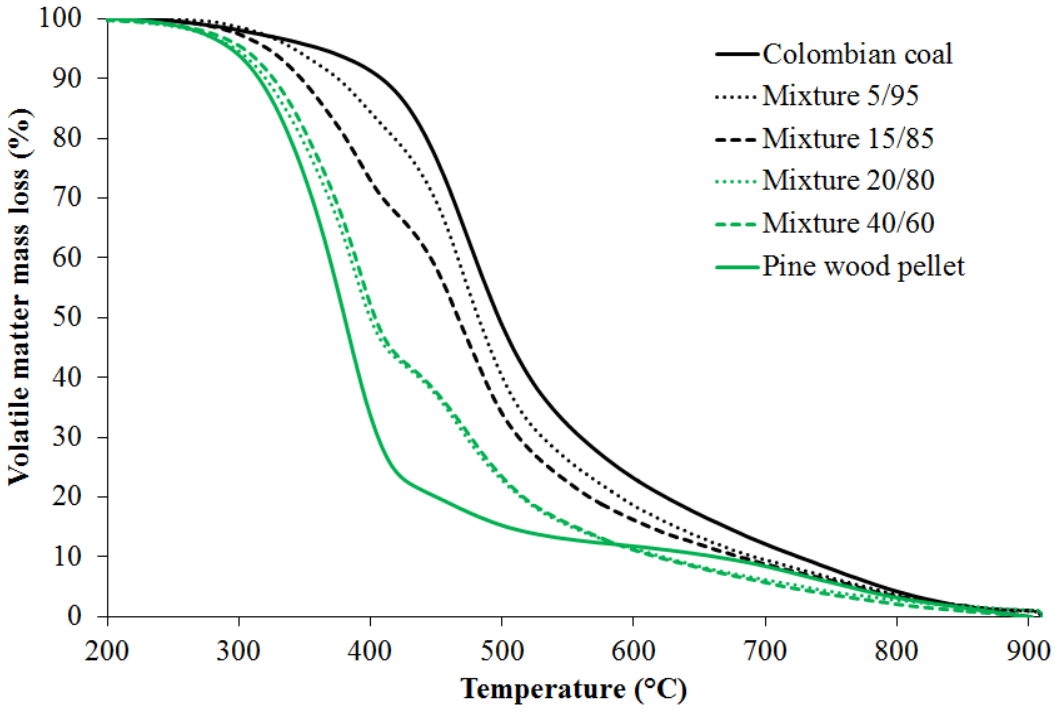

Figure 6-2. Volatile matter mass loss (%) for Colombian coal, pine wood pellet and their mixtures

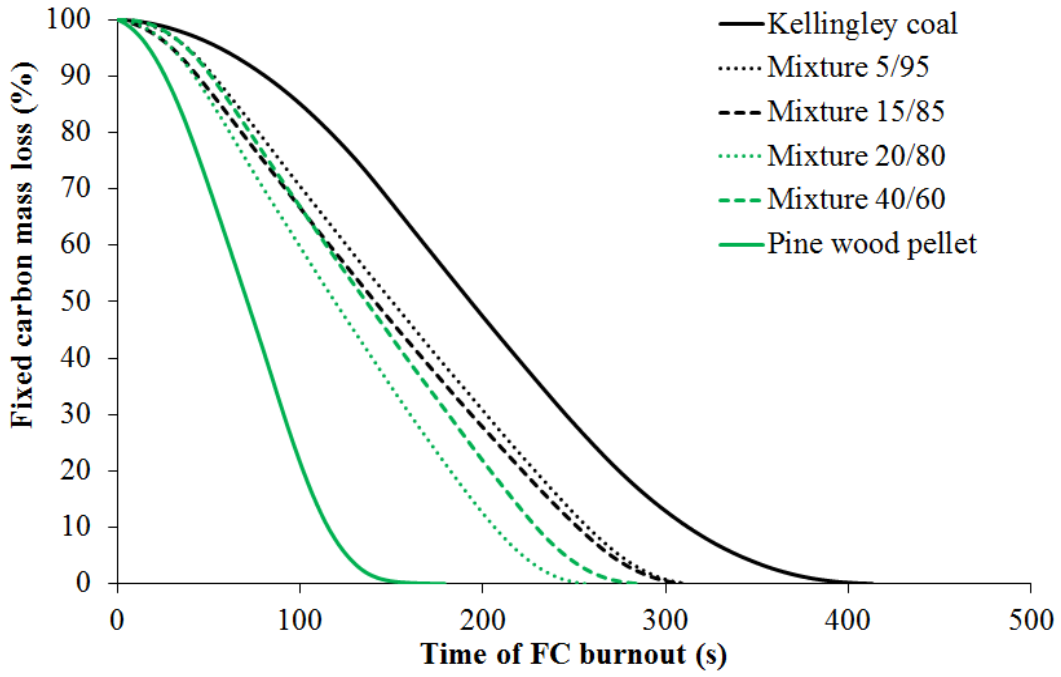

Figure 6-3. Fixed carbon mass loss (%) for Colombian coal, pine wood pellet and their mixtures

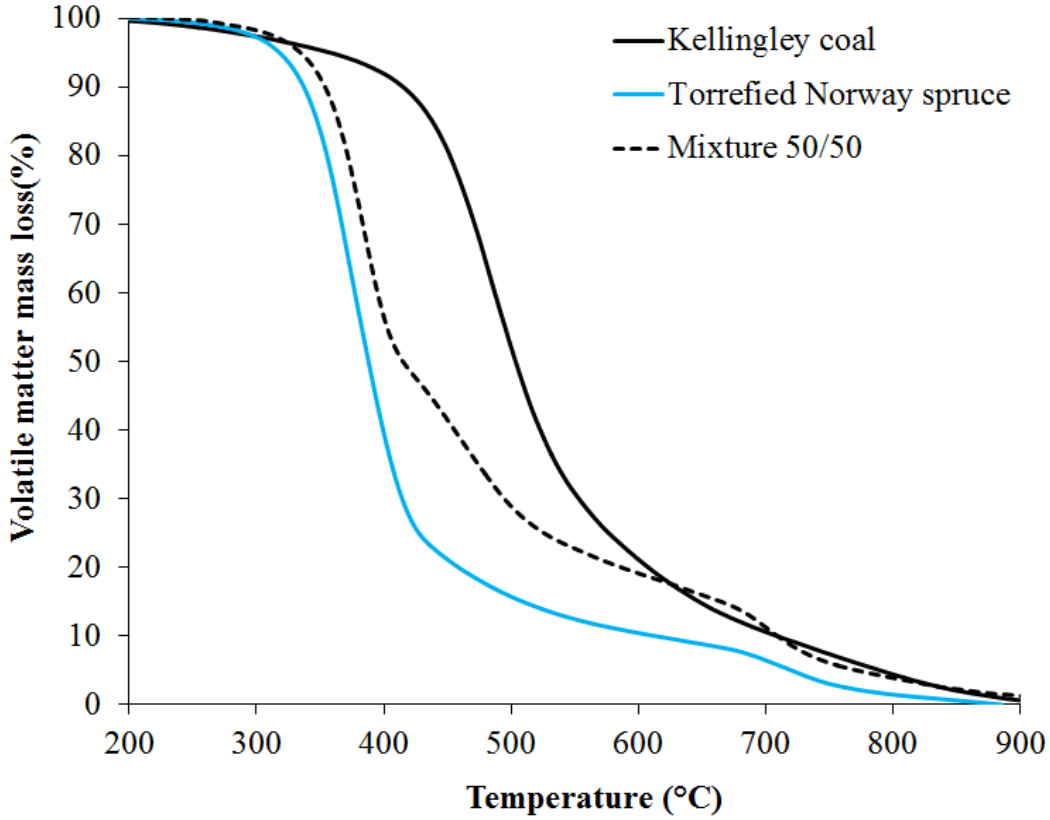

Figure 6-4. Volatile matter mass loss (%) for Kellingley coal, torrefied Norway spruce and their mixture (50%/50%)

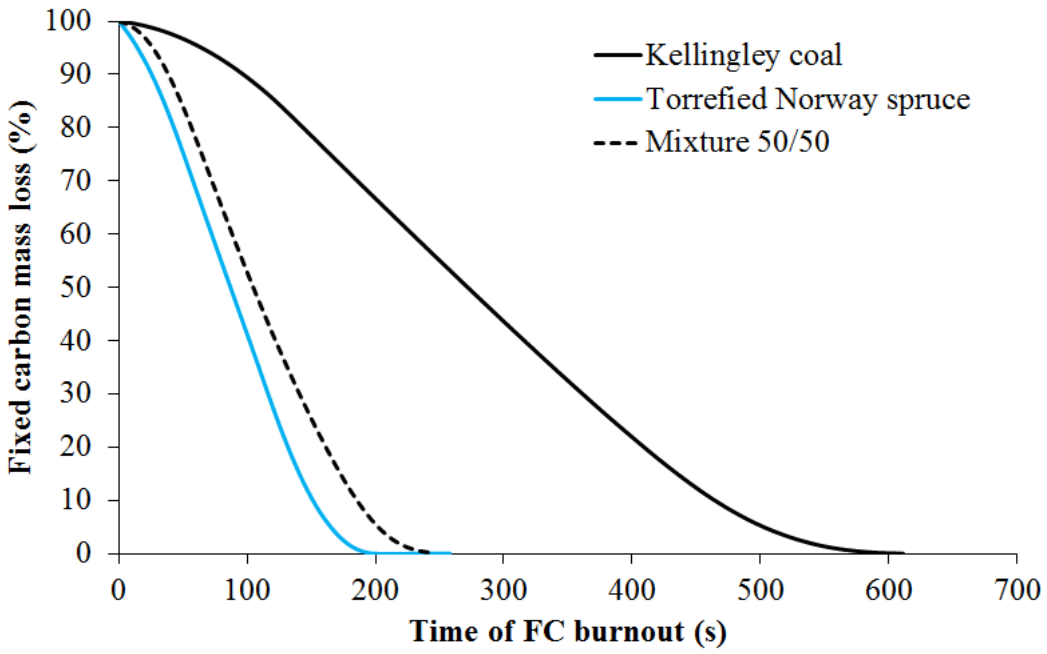

Figure 6-5. Fixed carbon mass loss (%) for Kellingley coal, torrefied Norway spruce and their mixture (50%/50%)

The observed behaviour of the mixtures of raw biomass (pine wood pellets) and Colombian coal was also found with the mixture of torrefied biomass and Kellingley coal.

Table 6-3 shows the devolatilisation and char burnout rates for the individual fuels and the blends obtained from the curves in Figure 6-2 to Figure 6-5.

Table 6-3. Maximum devolatilisation and fixed carbon burnout rates

	Devolatilisation rate (%/s)	Char burnout rate (%/s)
Colombian coal	0.25	0.39
Mixture 5/95	0.28	0.40
Mixture 15/85	0.22	0.39
Mixture 20/80	0.27	0.50
Mixture 40/60	0.27	0.46
Pine wood pellet	0.38	0.98
Kellingley coal	0.27	0.22
Mixture 50/50	0.38	0.58
Torrefied Norway spruce	0.41	0.68

Previous studies assessing the kinetics during co-combustion or co-pyrolysis also studied possible interactions between the fuels contained in biomass-coal blends using the TGA curves. In this respect, studies yield contradictive results and it appears that certain fuels, at certain blend ratios and experimental conditions can present interaction between the fuels, often referred to as “synergistic” effects [180, 227, 228], however there are other studies where such effects were not observed [226]. In principle, it is considered that no interactions take place if the pyrolysis

characteristics of the blends are a direct consequence of the addition of the characteristics of the parent materials [181]. This is often represented as follows:

$$Z_{blend} = x_{coal} \cdot Z_{coal} + x_{biomass} \cdot Z_{biomass} \quad (6.1)$$

Where Z can be either the weight loss or the rate of mass loss of the blend, coal or biomass, and x_{coal} and $x_{biomass}$ are the proportions of coal and biomass in the blend [176, 181, 225, 229]. Following this procedure, theoretical curves can be obtained for the blends and these can be compared to the experimentally obtained curves. Researchers concluded that if the difference between calculated and experimental curves were smaller than 4-6% then no significant synergistic effects were considered [181, 229]. Figure 6-6 and Figure 6-7 show the comparison between the experimental and calculated TG and DTG curves for all the mixtures. Figure 6-7 also show the TG and DTG curves for the torrefied biomass and the coal alone for comparison. Visually it can be observed that major differences between experimental and calculated curves appear for Colombian coal and pine wood pellet dust for mixtures with higher proportion of biomass present (20/80 and 40/60).

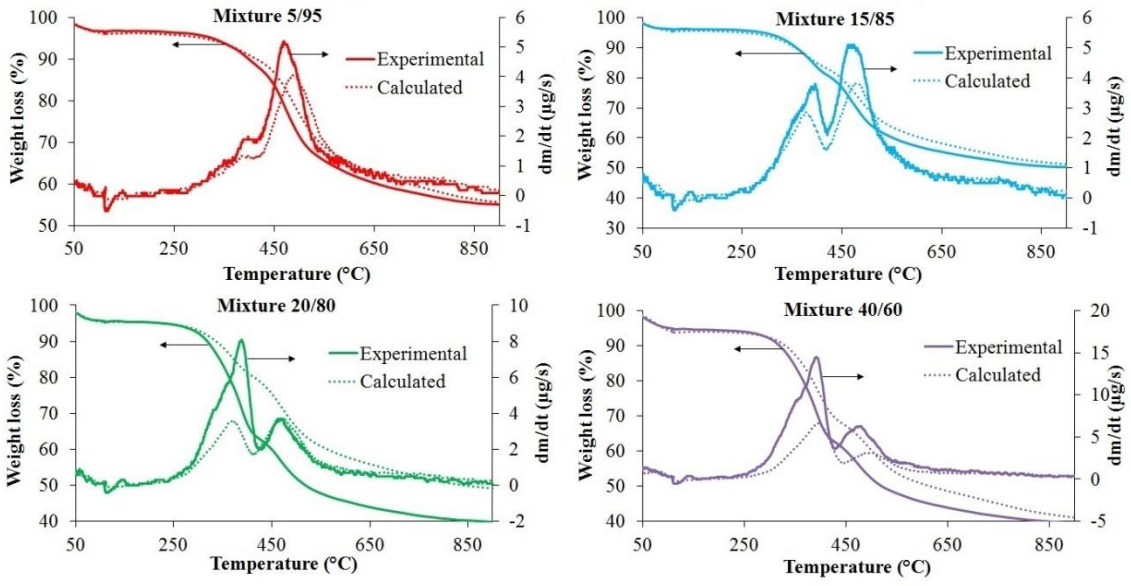

Figure 6-6. Comparison of experimental and calculated TG and DTG for mixtures of Colombian coal and pine wood pellet dust

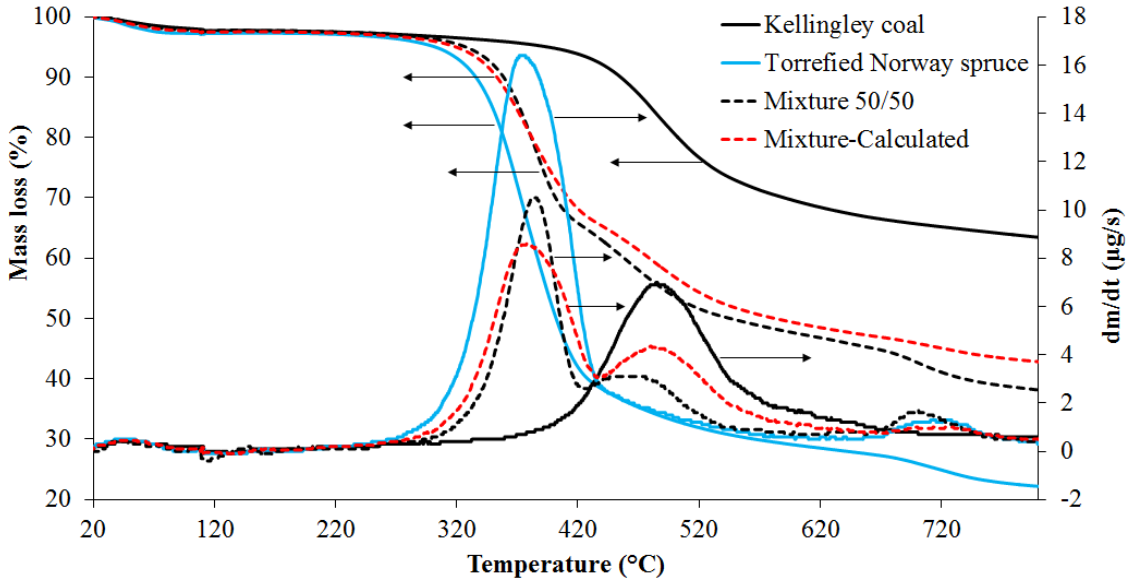

Figure 6-7. Comparison of experimental and calculated TG and DTG for a 50/50 mixture of torrefied Norway spruce and Kellingley coal.

Adopting the criteria used by other researchers mentioned above, the difference between calculated and experimental TG curves is graphically showed in Figure 6-8. Using ±5% difference as the limits, it is confirmed that there is a significant synergistic effect for the mixtures containing a higher proportion of pine wood pellet dusts (20/80 and 40/60) in Colombian coal. In contrast no synergistic effects are observed in the mixture of torrefied biomass and Kellingley coal.

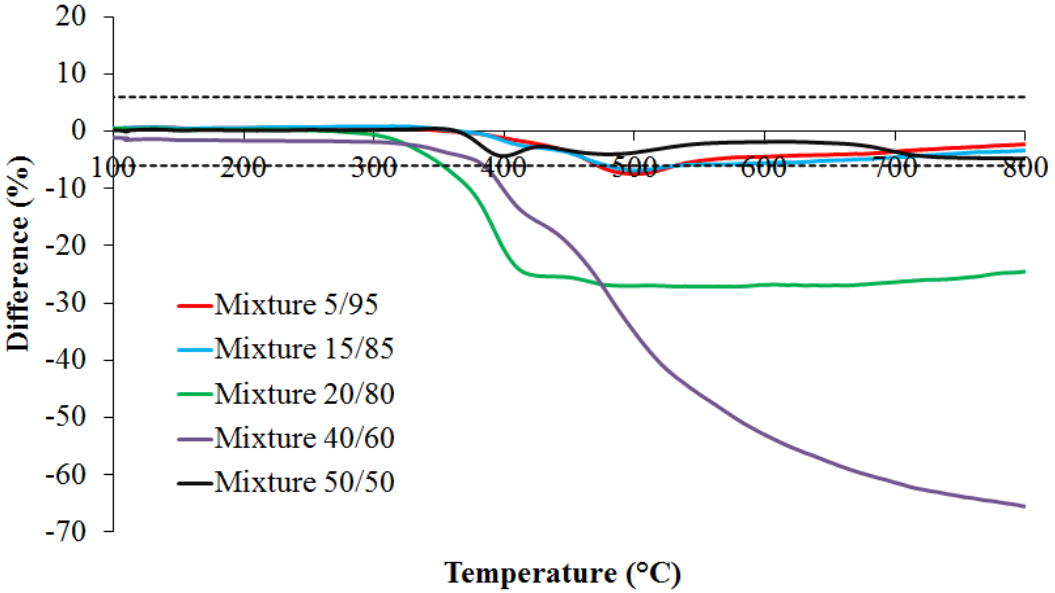

Figure 6-8. Difference between calculated and experimental TG curves of all mixtures

The results also show that interactions occur under pyrolysis conditions between 350 °C and 600°C. This temperature range corresponds to the stage where volatiles are

released. Therefore, the interactions between fuels in the blend could also have an effect over the rate of volatile release during an explosion and consequently on K_{St}.

6.2.2. Particle characteristics

Particle characteristics, such as true density, surface area and size distributions are presented in Table 6-4.

The variability in particle density is very small and there is not a clear trend on how it is affected by the mixing of fuels overall. The biomass samples, pine wood pellet dust and torrefied Norway spruce, present slightly higher particle density than coal. Particles of the mixtures formed by Colombian coal and pine wood pellets seem to have an overall particle density that increases with an increasing biomass proportion, as would be expected. However, the mixture of Kellingley coal and torrefied spruce had an overall particle density smaller than both of the fuels alone. Particle density values presented are the average of three measurements, in the particular case of the Mixture 50/50 the variation coefficient was 0.03%, therefore the result was considered valid. The theoretical value calculated for the mixture was 1471 kg/m^3. The experimental result is 2% different to the theoretical.

Table 6-4. Particle characteristics of fuels and their mixtures

	Particle Density (kg/m^3)	BET Surface Area (m^2/g)	Surface weighted mean D[3,2]	Volume weighted mean D[4,3]	d_{10}	d_{50}	d_{90}
Colombian coal	1446	15.8	14.7	40.1	6.8	28.1	85.2
Mixture 5/15	1431	18.0	15.1	71.6	6.8	31.5	139.8
Mixture 15/85	1435	13.1	17.2	110.3	7.5	40.1	319.8
Mixture 20/80	1446	4.9	25.1	180.1	10.9	78.9	529.4
Mixture 40/60	1448	6.8	22.3	159.6	9.7	64.4	480.2
Pine wood pellets	1493	0.4	51.1	267.2	29.3	178.2	652.8
Kellingley coal	1484	3.7	12.0	30.9	5.0	25.5	65.3
Mixture 50/50	1439	2.0	32.1	117.2	15.3	74.7	263.9
S2STS	1458	0.7	51.1	151.2	20.4	90.0	378.6

Surface areas of both coal samples were higher than those of biomass samples. The surface area of the mixtures was decreased when the proportion of biomass in the sample increased.

Particle size distribution data are detailed in Table 6-4, and also Figure 6-9 and Figure 6-10. The biomass samples, both pine wood pellet dust and torrefied Norway spruce, contained larger amounts of big particles than coal samples. As could be expected, the addition of biomass to the blends affected the overall particle distribution by also increasing the presence of bigger particles in the bulk.

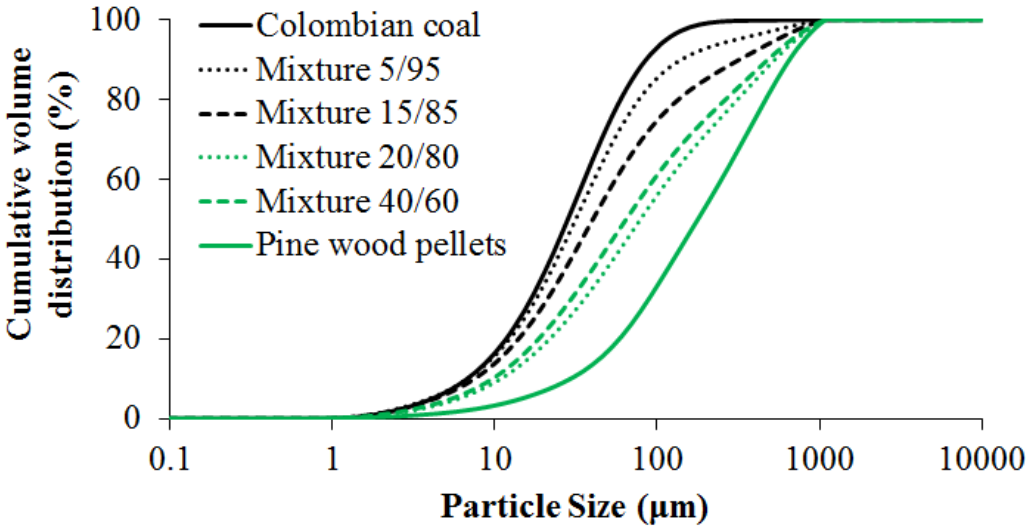

Figure 6-9. Particle size distribution of Colombian coal, Pine wood pellet dust and their mixtures

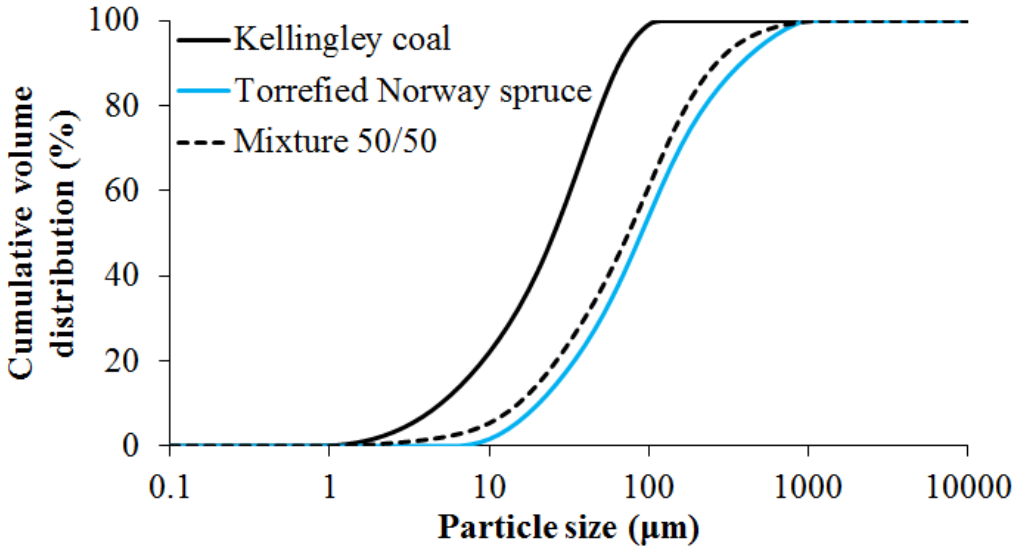

Figure 6-10. Particle size distribution of Kellingley coal, torrefied Norway spruce and their mixture

The morphology of individual particles in the bulk were analysed through SEM images, examples of which are shown in Figure 6-11 and Figure 6-12. As expected

the mixtures containing coal and biomass or torrefied biomass are a mixture of coal particles and flock-type particles of biomass. Comparatively there were biomass particles of much larger size than coal particles which resulted in the shifting of particle size distributions of mixtures to larger particle sizes as more biomass is added to the blend. This corroborates the particle size distribution measurements.

Contrary to the pine wood pellet particles, the particles of torrefied Norway spruce sample appear more homogeneous and needle-like. Both coal samples had particles of similar size and shape.

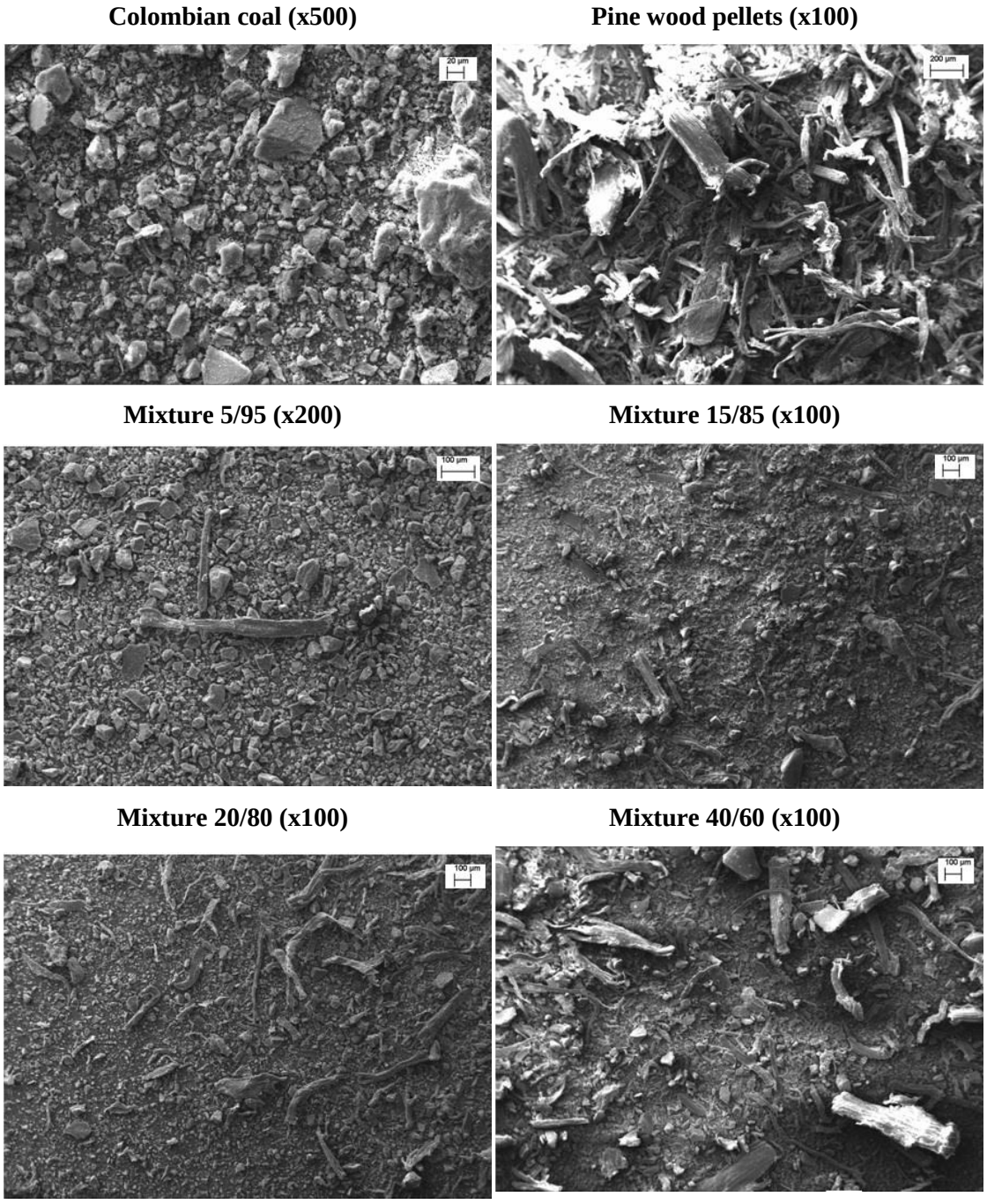

Figure 6-11. SEM images of Colombian coal, Pine wood pellet dust and their mixtures

Kellingley coal (x300)

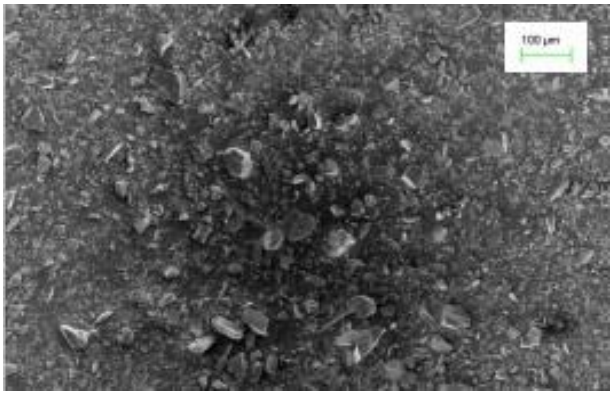

Torrefied Norway spruce (x200)

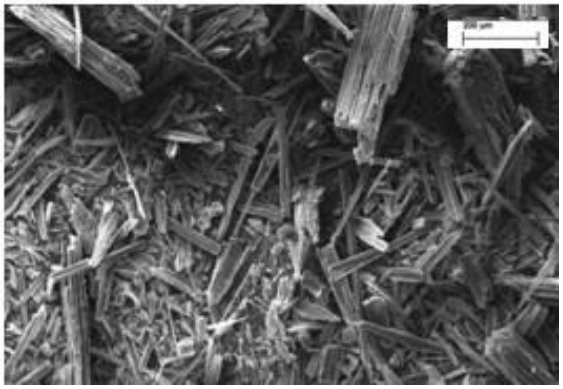

Mixture 50/50 (x200)

Figure 6-12. SEM images of Kellingley coal, torrefied Norway spruce and their mixture

6.3. Explosion characteristics

All samples were tested in the 1 m^3 ISO vessel using the calibrated modifications available to ensure acceptable flow of dust through the delivery system and good pressurisation of low bulk density dusts in the dust holder. Table 6-5 shows the settings used for all the samples tested for the present study. In general, to ease the experimental process all samples were tested using the extended 10 L dust holder pressurised to 10 bar. Kellingley coal was tested using both systems and the results obtained in terms of explosion characteristics, mass burnt and flame speeds were within the experimental variability [194].

Where the proportion of biomass in the blend was small (less than 50%) the C-tube was used with the standard 0.6 s ignition delay. For the mixture of torrefied Norway spruce made up of 50% biomass the spherical nozzle was used with the calibrated ignition delay of 0.5 s. Where 100% biomass or torrefied biomass was tested the settings used were those of fibrous dust with the extended dust holder and spherical nozzle.

Table 6-5. 1 m^3 calibrated settings for testing of mixtures

	Dust holder volume (L)	Dust holder pressure (bar)	Disperser	Ignition delay (s)
Colombian coal	10	10	C-tube	0.6
Pine wood pellet	10	10	Spherical nozzle	0.5
Mixtures	**10**	**10**	**C-tube**	**0.6**
Kellingley coal	5	20	C-tube	0.6
Torrefied Norway spruce	10	10	Spherical nozzle	0.5
Mixture (50/50)	**10**	**10**	**Spherical nozzle**	**0.5**

Colombian coal, pine wood pellet and the mixture containing high proportion of biomass (Mixture 40/60) were tested along the flammable range from the lean flammability to at least two richer concentrations than the most reactive concentration. Similarly all three: Kellingley coal, torrefied Norway spruce and their 50/50 mixture by mass were tested in this way. On the other hand Mixtures 5/95, 15/85 and 20/80 were tested only for nominal concentrations of 250 g/m^3, 500 g/m^3, 750 g/m^3 and 1000 g/m^3. Therefore results for MEC of these samples are not provided.

Explosion characteristics (K_{St} and P_{max}/P_i) of Colombian coal, Pine wood pellets and their mixtures are presented in Figure 6-13 and Figure 6-14.

All samples were St-1 dusts. Pine wood pellet dust presented the lowest K_{St} value. This is attributable to the bigger amount of large particles present in the sample. The Colombian coal sample was therefore the more reactive of the fuels in the blends. Mixtures 5/95 and 15/85 containing low proportion of biomass had very similar reactivity as the coal sample, and presented a very small reduction in K_{St} due to the presence of biomass. However, Mixtures 20/80 and 40/60 had an increased reactivity surpassing the rates of pressure rise found for the most reactive of the fuels in the blend (Colombian coal). Therefore these fuels, at these particular blend ratios, presented a synergistic effect (coincidental with the trends observed through TGA techniques) on their reactivity; reaching K_{St} values ca. 150 barm/s, higher K_{St} values than any other biomass or torrefied material tested as part of this research. Most reactive mixtures are found for injected concentrations equivalent to around Ø=3-4.

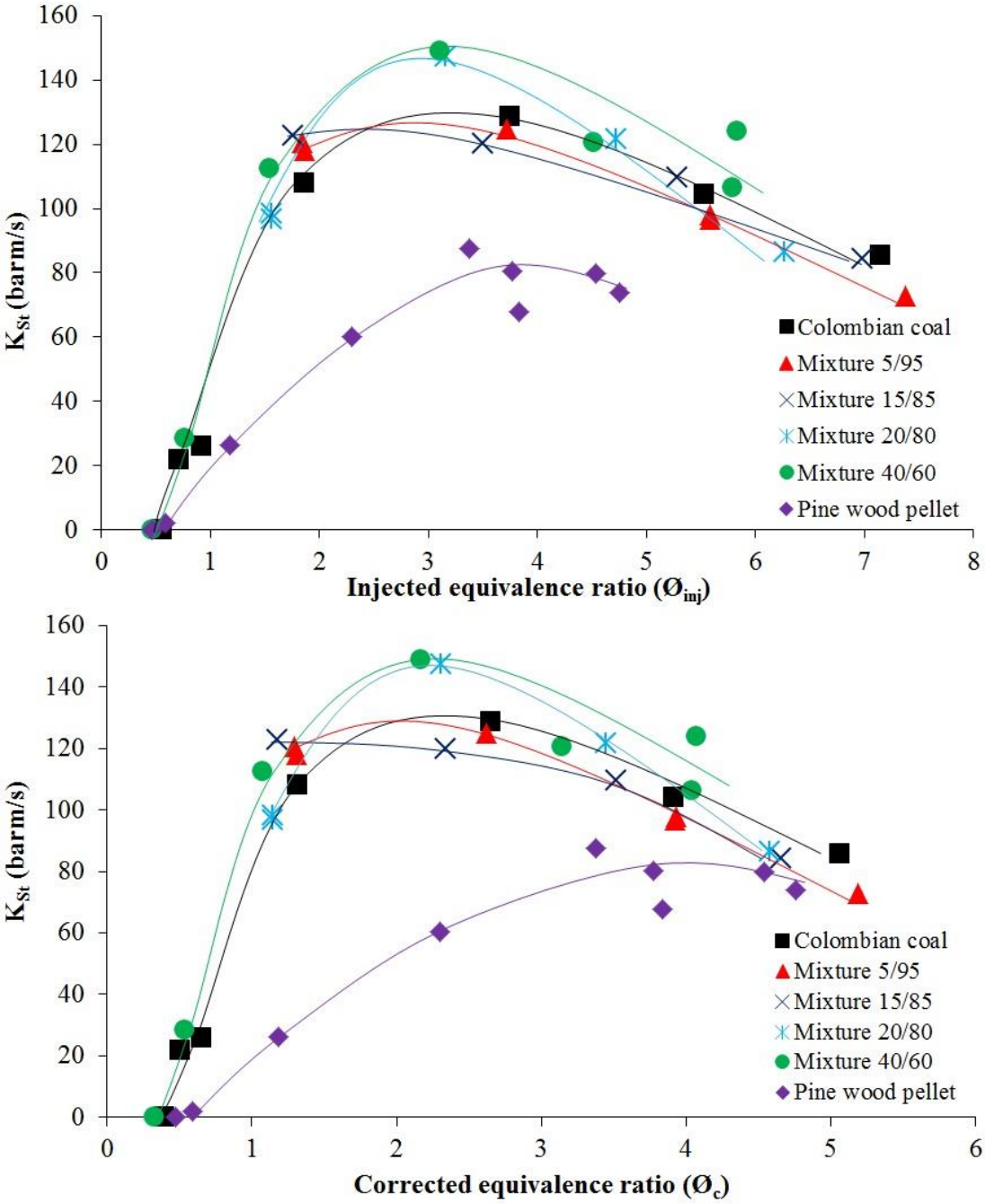

Figure 6-13. K_{St} of Colombian coal, pine wood pellets and their mixtures as a function of the injected (top) and corrected equivalence ratio (bottom)

Maximum explosion pressures are shown in Figure 6-14. Maximum pressures were ca. 9 bar for all samples. The maximum pressure of the least reactive sample in terms of K_{St}, Pine wood pellets, is comparable to that of the other samples despite containing much bigger particles.

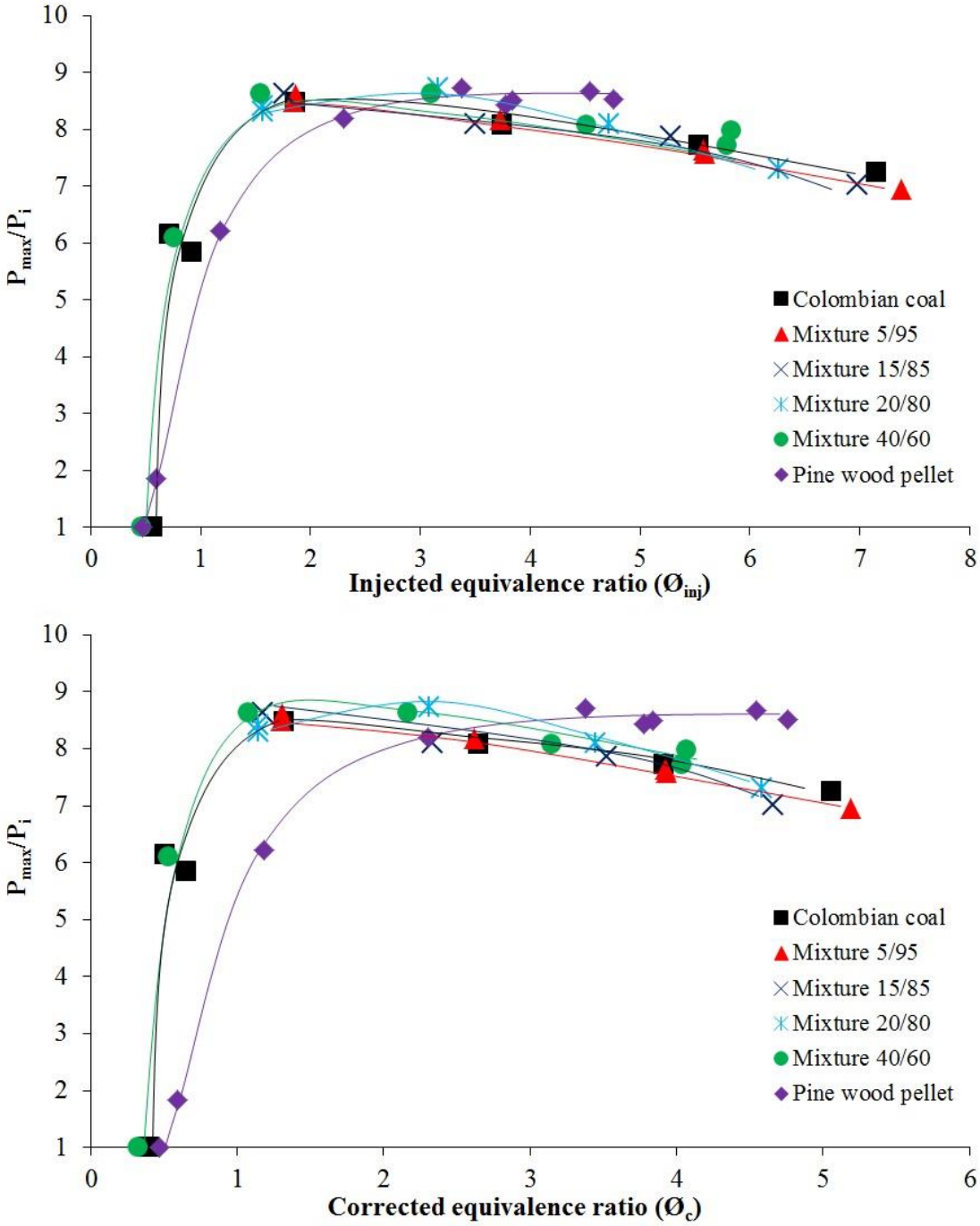

Figure 6-14. P_{max}/P_i of Colombian coal, pine wood pellets and their mixtures as a function of the injected (top) and corrected equivalence ratio (bottom)

Figure 6-15 shows how as the nominal mass placed into the dust holder increased there was an increasing residue of dust left in the dust holder after dispersion. For biomass samples, the mass of residual dust remaining in the dust holder was bigger than for the mixtures and the coal sample.

Furthermore, it is shown in Figure 6-16, that for rich mixtures around 50% of the mass that was injected remained in the explosion chamber after an explosion test.

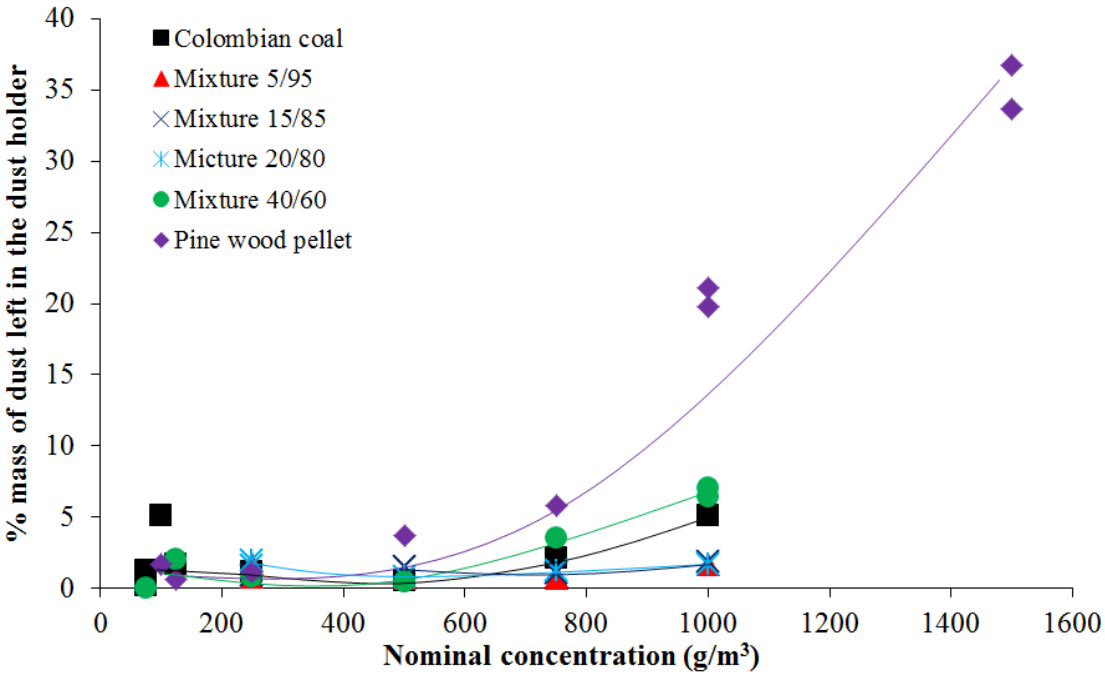

Figure 6-15. % Mass left in dust holder after dispersion as a function of nominal concentration for Colombian coal, pine wood pellet dust and their mixtures

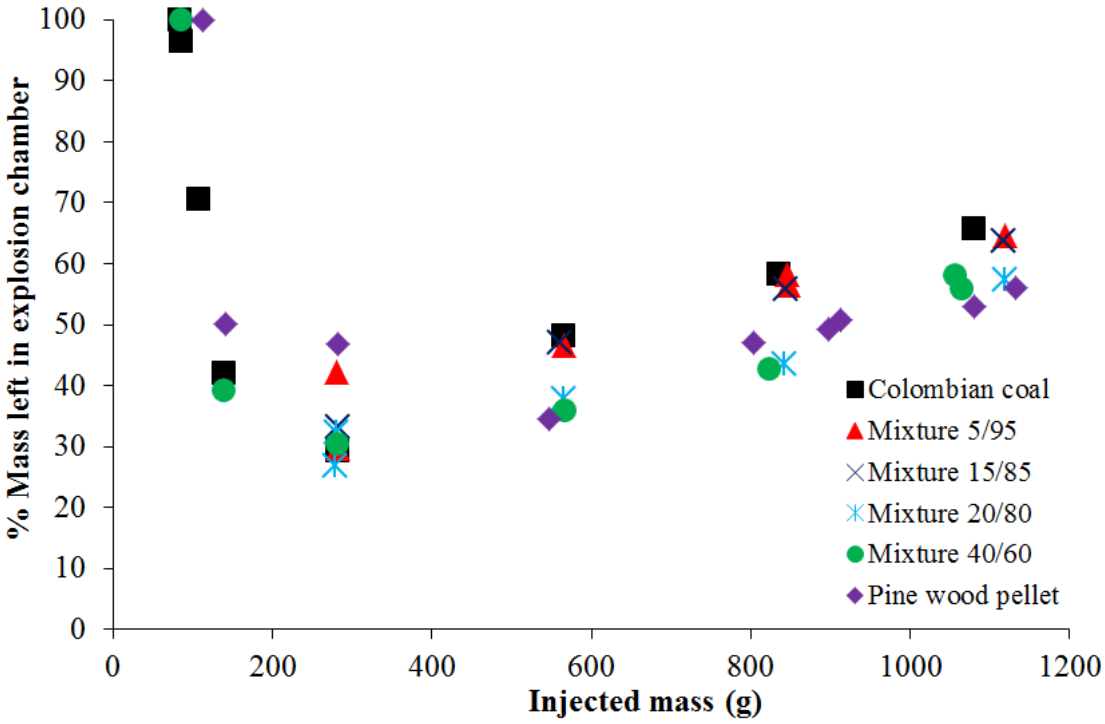

Figure 6-16. % Mass left in explosion chamber as a function of the injected concentration for Colombian coal, pine wood pellet dust and their mixtures

The results for Kellingley coal, torrefied Norway spruce and their 50/50 (by mass) mixture are presented in the following figures. In this case, the torrefied biomass

sample was more reactive than the coal sample used in the blend. The 50/50 mixture did not present a synergistic effect on its reactivity and remained lower than the most reactive sample (torrefied wood sample) but more reactive than the least reactive sample (Kellingley coal) for this particular blend ratio.

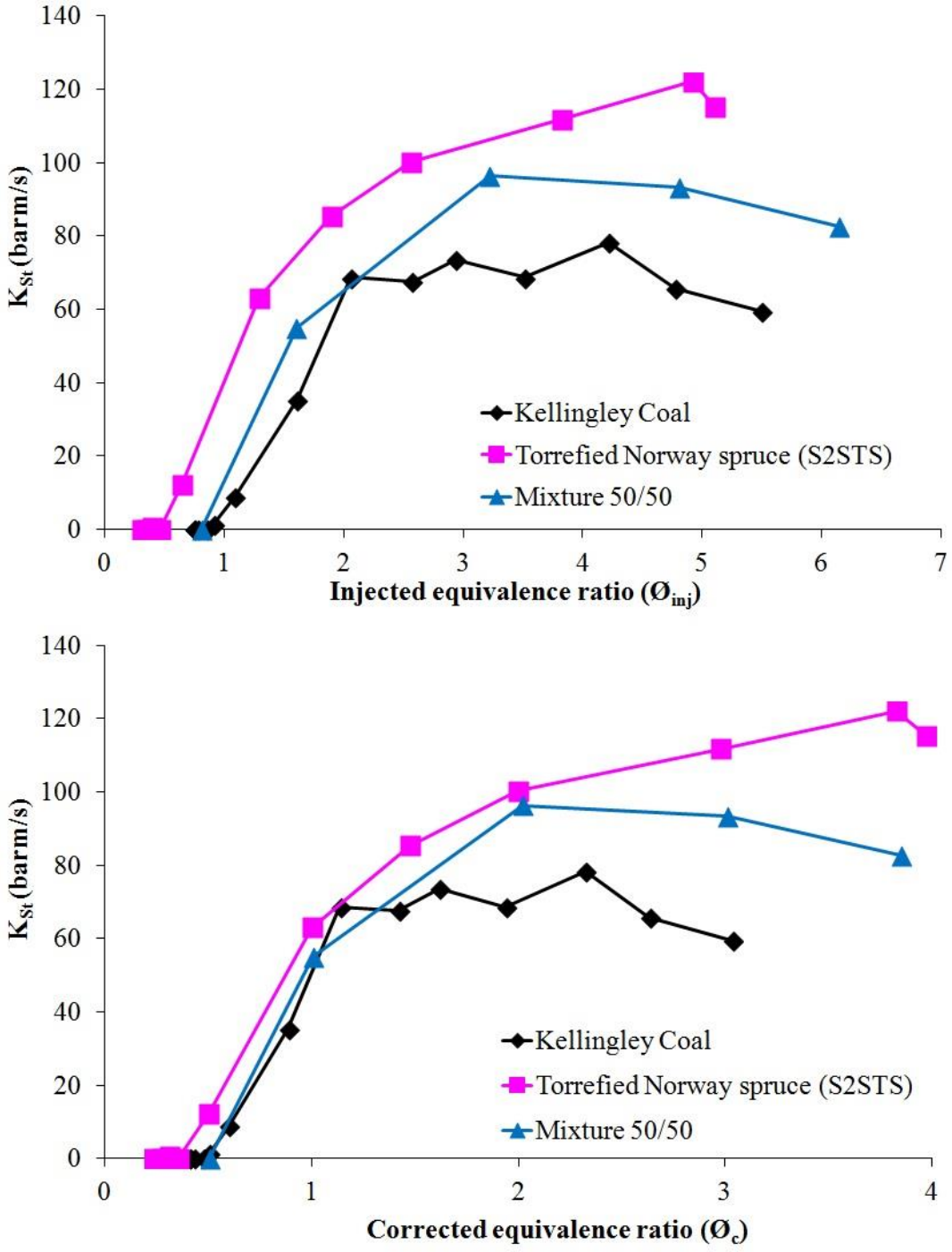

Figure 6-17. K_{St} of Kellingley coal, torrefied Norway spruce and their mixture as a function of the injected (top) and corrected equivalence ratio (bottom)

In terms of the maximum explosion pressure the same trend was found, where the maximum explosion pressure of torrefied biomass alone is higher than that of the

mixture and Kellingley coal, which presents the lowest maximum explosion pressure.

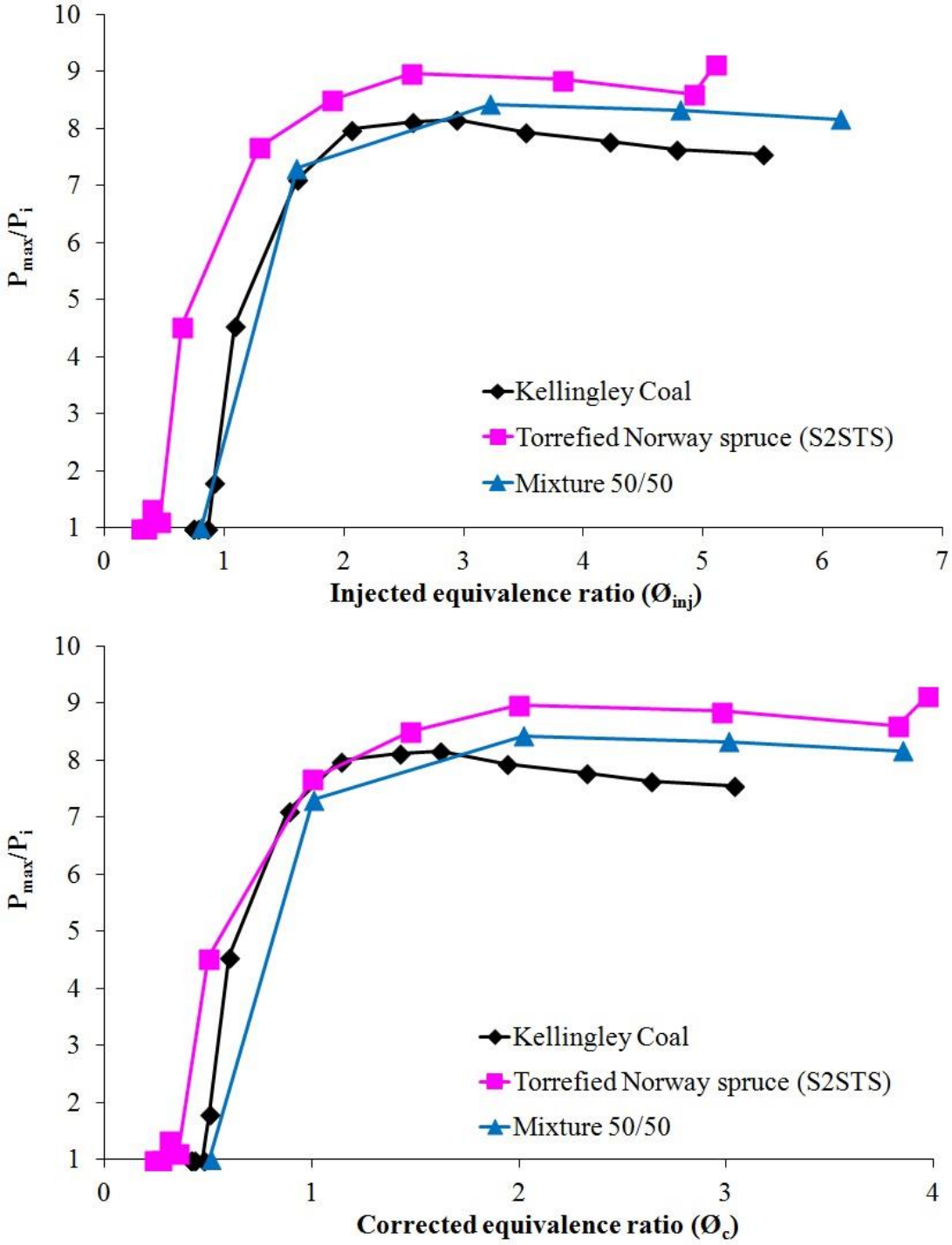

Figure 6-18. P_{max}/P_i of Kellingley coal, torrefied Norway spruce and their mixture as a function of the injected (top) and corrected equivalence ratio (bottom)

Although the torrefied biomass sample initially passed through the delivery system satisfactorily and, as shown in Figure 6-19, no significantly large quantities of dust remained undelivered in the dust holder, it was not possible to find a second less

reactive mixture richer than the most reactive mixture, since, when placing more than 1000 g/m^3 in the dust holder a large fraction of the dust remained in the dust holder preventing the injection of more dust into the vessel.

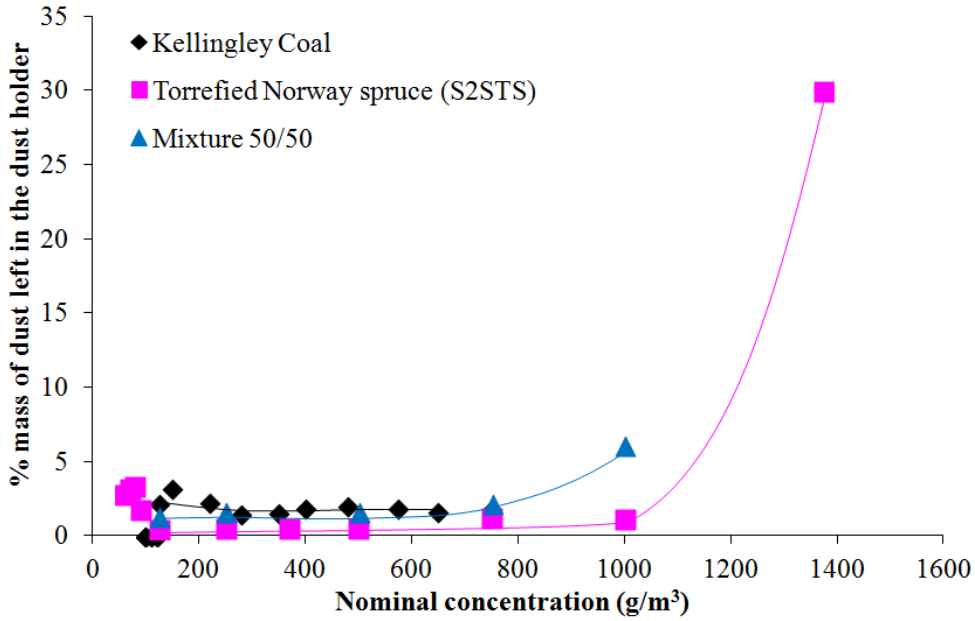

Figure 6-19. % Mass left in dust holder after dispersion as a function of nominal concentration for Kellingley coal, torrefied Norway spruce and their mixture

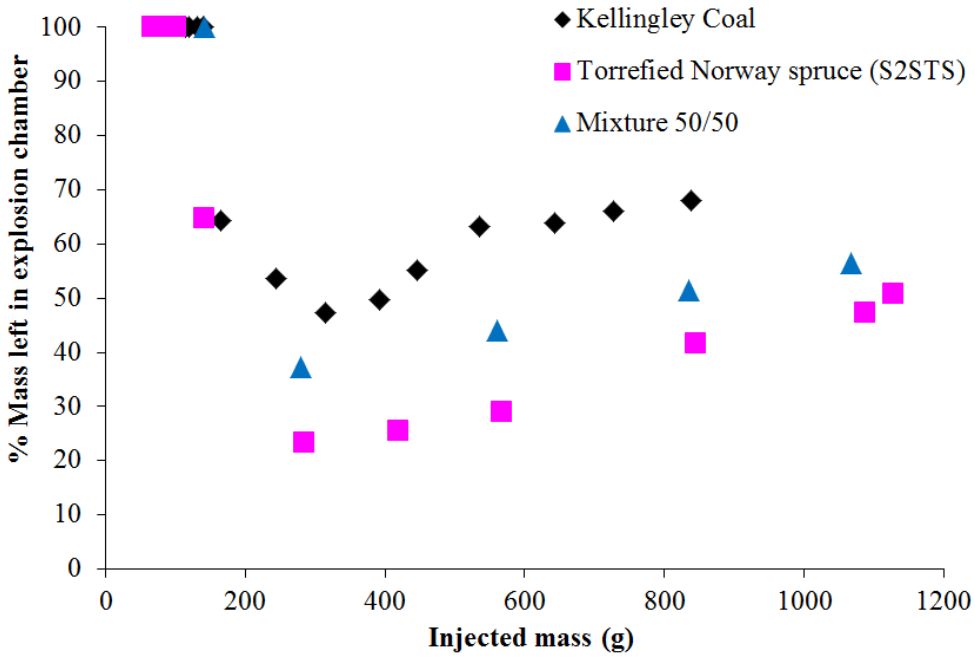

Figure 6-20. % Mass of residual dust remaining in the explosion chamber as a function of the injected mass for Kellingley coal, torrefied Norway spruce and their 50/50 mixture

For these three samples it was also found that, for richer mixtures, around 50% of the mass that was injected into the vessel remained in the explosion chamber after an explosion test (Figure 6-20)

Table 6-6 shows the available MEC results of the mixtures compared to the individual fuels used in the blend. The mixture containing 40% pine wood pellet dust and 60% Colombian coal, which showed an increased reactivity in terms of K_{St}, had a MEC similar to that of Colombian coal, which was the most reactive of the fuels in the blend and was present in a higher proportion.

Table 6-6. Minimum Explosible Concentration of fuels and their blends

	MEC_0-MEC_{100} (g/m^3) Corrected concentration	Corrected equivalence ratio ($Ø_0$-$Ø_{100}$)
Colombian coal	42-55	0.38-0.55
Mixture (40/60)	45-74	0.32-0.53
Pine wood pellets	88-110	0.47-0.59
Kellingley coal	50-53	0.47-0.50
Mixture (50/50)	68-135	0.49-0.98
Torrefied Norway spruce	49-56	0.27-0.31

On the contrary the blend with Kellingley coal and torrefied biomass had a lean limit similar to that of the least reactive sample, Kellingley coal in this case. In this case, the reactivity was brought down by the presence of the less reactive Kellingley coal which is also reflected by the MEC measurement. It appears that MEC was sample dependent and was most likely affected by the blend ratio and the fuels used in the blend.

Turbulent flame speeds were derived for all tests and the maximum average turbulent and laminar flame speeds are shown in Table 6-7, as well as the laminar burning velocity.

Table 6-7. Summary of explosion and combustion properties of coal and biomass (raw and torrefied) mixtures

	K_{St} (barm/s)	P_{max}/P_i	$(S_F)_T$ (m/s)	S_F (m/s)	S_L (m/s)
Colombian coal	129	8.5	5.8	1.4	0.17
Mixture 5/95	125	8.2	5.6	1.4	0.17
Mixture 15/85	123	8.6	5.3	1.3	0.15
Mixture 20/80	147	8.7	6.3	1.6	0.18
Mixture 40/60	149	8.6	6.3	1.6	0.19
Pine wood pellet	87	8.7	3.3	0.8	0.09
Kellingley coal	78	8.2	3.6	0.9	0.12
Mixture 50/50	96	8.4	4.1	1.0	0.12
Torrefied Norway spruce	122	9.0	5.1	1.3	0.15

Overall there was a good correlation between K_{St} and turbulent flame speeds as is shown for Colombian coal, pine wood pellets and their mixtures in Figure 6-21.

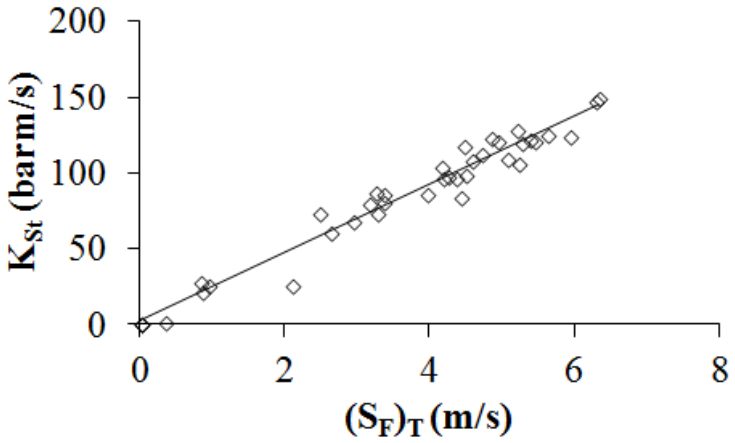

Figure 6-21. Relationship between K_{St} and turbulent flame speed for Colombian coal and pine wood pellets and their mixtures

6.4. Analysis of explosion residues

In the same way as with the samples used in Chapter 5, residual deposits of dust were collected from the dust vessel after each explosion test. The residue collected corresponded to the most reactive concentration. In the case of biomass-coal mixtures the residue collected consisted of black coal-like powder where it was difficult to identify burnt, unburnt or partially burnt particles. The residue was further studied by completing elemental and proximate analysis of the bulk, as well as by determining particle density, morphology and size distribution. Table 6-8 and Table 6-9 present the elemental and proximate analysis as well as the true density measurements of the original samples for Colombian coal, pine wood pellets and their mixtures and these can be compared to the analysis of the bulk residue corresponding to the most reactive concentration for each of the samples. The percentage of change between the original samples and the residues are presented in brackets.

Previously, in Chapter 5, it was found that all residues showed clear signs of undergoing mild pyrolysis inside the vessel, as residues were only partially devolatilised and carbonised and fixed carbon and ash contents were significantly increased. Also there was an increase in particles density which was much higher for coal and torrefied samples.

Consequently it is believed that residues were a proportion of dust that on initiation of flame propagation was pushed by the explosion wind towards the vessel wall, forming a layer where the particles closest to the flame front were subjected to decreasing flame temperatures (as the flame touched the wall) in the absence of oxygen (which was consumed in the explosion flame front).

Table 6-8. Post-explosion residue analysis for Colombian coal and its mixtures with pine wood pellet dust containing 5% and 15% biomass respectively.

	Pre-Explosion			Post-Explosion		
Fuel Sample	**Colombian coal**	**Mixture 5/95**	**Mixture 15/85**	**Colombian coal (Change %)**	**Mixture 5/95 (Change %)**	**Mixture 15/85 (Change %)**
Elemental analysis (wt%)						
C	66.6	64.9	64.0	61.8 (-7.2)	62.2 (-4)	55.5 (-13)
H	4.3	4.8	4.0	2.1 (-51)	3.0 (-38)	2.8 (-30)
O	7.8	7.5	9.8	2.7 (-65)	2.4 (-68)	4.8 (-51)
N	2.1	2.0	2.2	1.7 (-19)	2.1 (+5)	2.1 (-5)
S	0.7	0.5	0.5	0.9 (+29)	0.6 (+20)	0.5
TGA-Proximate (wt%)						
Moisture	3.2	3.0	3.5	2.2 (-31)	1.9 (-37)	2.1 (-40)
Ash	15.3	17.3	16.1	28.5 (+86)	27.9 (+61)	32.3 (+101)
Volatile Matter	33.7	34.8	38.6	14.4 (-57)	15.7 (-55)	19.6 (-49)
Fixed Carbon	47.8	44.9	41.9	54.9 (+15)	54.5 (+21)	46.1 (+10)
True Density (kg/m^3)	1.45	1.43	1.44	1.81 (+25)	1.74 (+22)	1.72 (+19)
Mass burnt (%)	51.9	53.3	66.7	-		

Table 6-9. Post-explosion residue analysis for mixtures of Colombian coal and pine wood pellet dust containing 20% and 40% biomass respectively, and pine wood pellet dust alone

	Pre-Explosion			Post-Explosion		
Fuel Sample	**Mixture 20/80**	**Mixture 40/60**	**Pine wood pellet**	**Mixture 20/80 (Change %)**	**Mixture 40/60 (Change %)**	**Pine wood pellet (Change %)**
Elemental analysis (wt%)						
C	59.2	57.5	46.8	61.2 (+3)	61.6 (+7)	48.6 (+4)
H	4.4	4.8	5.7	3.7 (-16)	2.6 (-46)	5.3 (-7)
O	20.1	21.5	37.0	6.5 (-68)	8.0 (-63)	33.7 (-9)
N	1.9	1.3	0.0	2.0 (+5)	2.1 (+62)	0.5
S	0.2	0.2	0.0	0.3 (+50)	0.4 (+100)	0.0
TGA-Proximate (wt%)						
Moisture	4.0	5.0	9.9	2.4 (-40)	1.4 (-72)	5.0 (-49)
Ash	10.2	9.7	0.6	23.9 (+134)	24.0 (+147)	6.9 (+1050)
Volatile Matter	50.3	51.1	77.1	28.4 (-44)	26.4 (-48)	74.3 (-4)
Fixed Carbon	35.4	34.2	12.4	45.3 (+28)	48.3 (+41)	13.8 (+11)
True Density (kg/m^3)	1.45	1.45	1.49	1.69 (+17)	1.73 (+19)	1.48 (-0.6)
Mass burnt (%)	62.1	64.2	53.0	-		

The results coincide with those found in Chapter 5 for various other biomass and torrefied materials and further corroborates the theories there explained. Van Krevelen plots of the original mixtures and the residues found after explosions were compared in Figure 6-22. All mixtures were carbonised as previously found for all samples studied in Chapter 5.

For further confirmation of these trends, the particle size distribution and particles morphology of the residues have also been studied for the blends and the individual fuels.

Table 6-10. Post-explosion residue analysis of Kellingley coal, Torrefied Norway spruce and their 50/50 mixture (by mass)

	Pre-Explosion			Post-Explosion		
Fuel Sample	**Kellingley coal**	**Mixture (50/50)**	**Torrefied Norway spruce**	**Kellingley coal (Change %)**	**Mixture 50/50 (Change %)**	**Torrefied Norway spruce (Change %)**
Elemental analysis (wt%)						
C	65.0	59.7	51.6	64.3 (-1)	62.0 (+4)	55.4 (+7)
H	4.1	5.0	5.2	3.5 (-15)	4.9 (-2)	4.1(-21)
O	5.5	21.0	35.4	7.1 (+29)	10.4 (-50)	27.1 (-23)
N	2.4	1.8	0.7	1.4 (-42)	2.0 (+11)	1.4 (+50)
S	2.2	0.1	0.0	2.2	0.2 (+100)	0.0
TGA-Proximate (wt%)						
Moisture	1.7	2.4	2.8	1.6 (-6)	3.0 (+25)	3.6 (+29)
Ash	19.1	10.0	4.2	19.9 (+4)	17.6 (+76)	8.5 (+102)
Volatile Matter	29.2	55.5	77.0	25.0 (-14)	34.0 (-39)	53.4 (-31)
Fixed Carbon	50.0	32.0	15.9	53.5 (+7)	45.4 (+42)	34.5 (+117)
True Density (kg/m^3)	1.48	1.44	1.50	1.64 (+11)	1.57 (+9)	1.59 (+6)
Mass burnt (%)	39.3	56.0	55.0	-		

In Chapter 5, it was shown that the size distribution of residues for coal and torrefied biomass samples contained larger particles, whereas the size distribution of residues of explosion tests where raw biomass was used remained virtually equal to the original sample. It was later found, by the assessment of particles morphology, that this was due to creation of char structures with coal and torrefied biomass samples

that fused together forming clusters of bigger size. This pointed out to differences in the way particles of biomass behave during pyrolysis, as such char structures were very few in comparison to coal and torrefied samples.

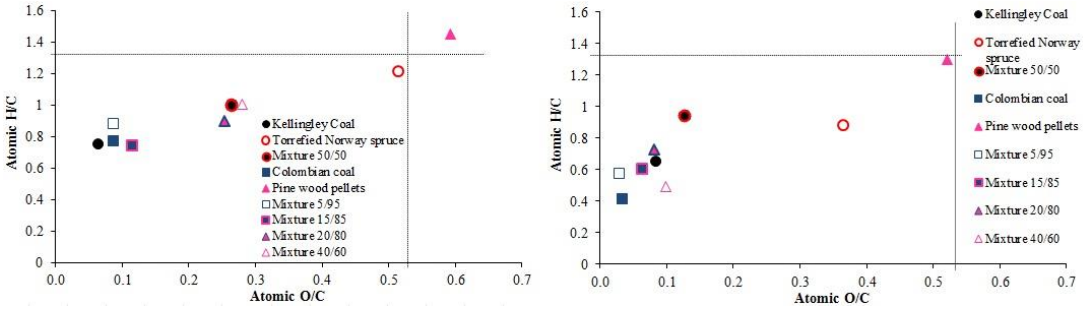

Figure 6-22. Van Krevelen plots for original mixtures and post explosion residues

Figure 6-23 and Figure 6-24 present the results of the size distribution analysis of the blends and individual fuels followed by the particles morphology studies using SEM images in Figure 6-25, Figure 6-26 and Figure 6-27. In summary results corroborate the previous findings.

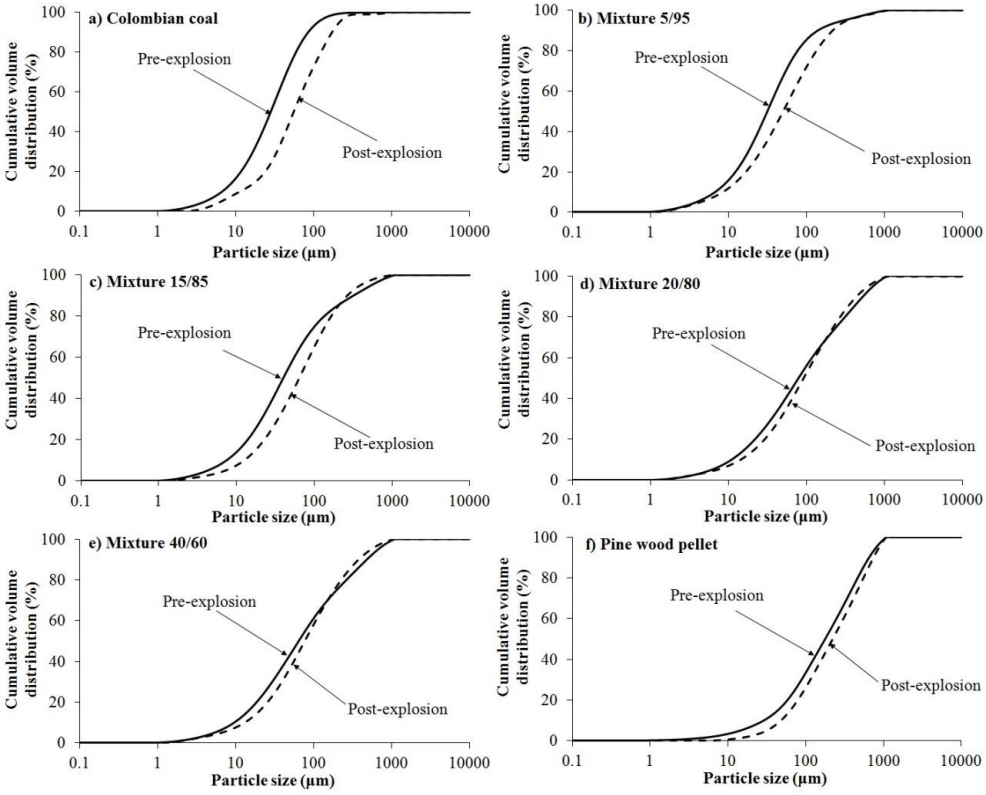

Figure 6-23. Comparison of particle size distribution of the post explosion residue and original samples of Colombian coal, pine wood pellet and their mixtures

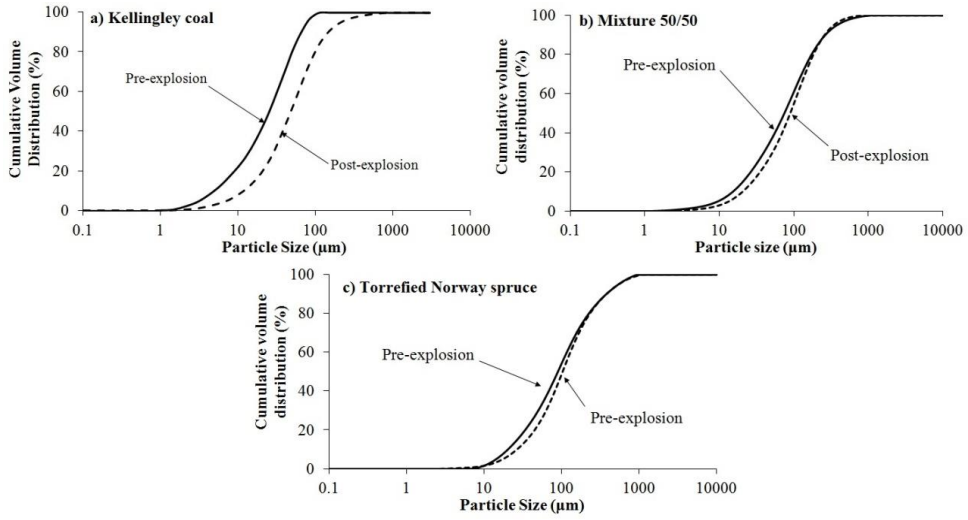

Figure 6-24. Comparison of particle size distribution of the post explosion residue and original samples of Kellingley coal, torrefied Norway spruce wood and their mixture

BEFORE EXPLOSION AFTER EXPLOSION

Colombian coal (x500)

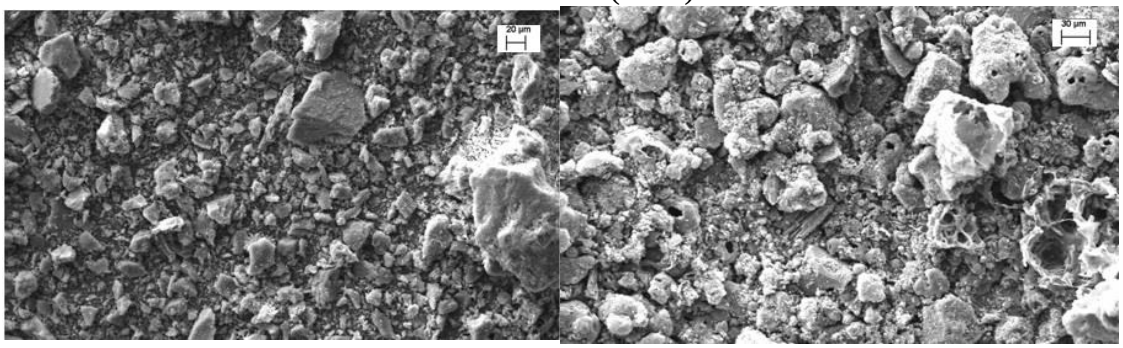

Mixture 5/95 (x200)

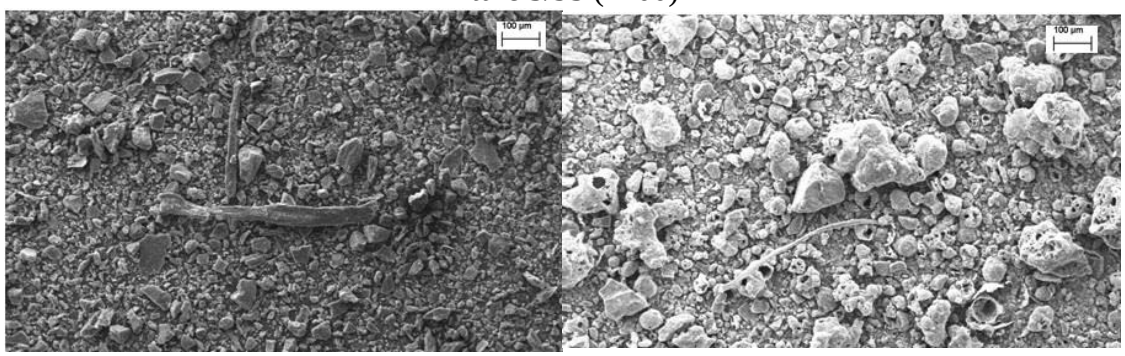

Mixture 15/85 (x100)

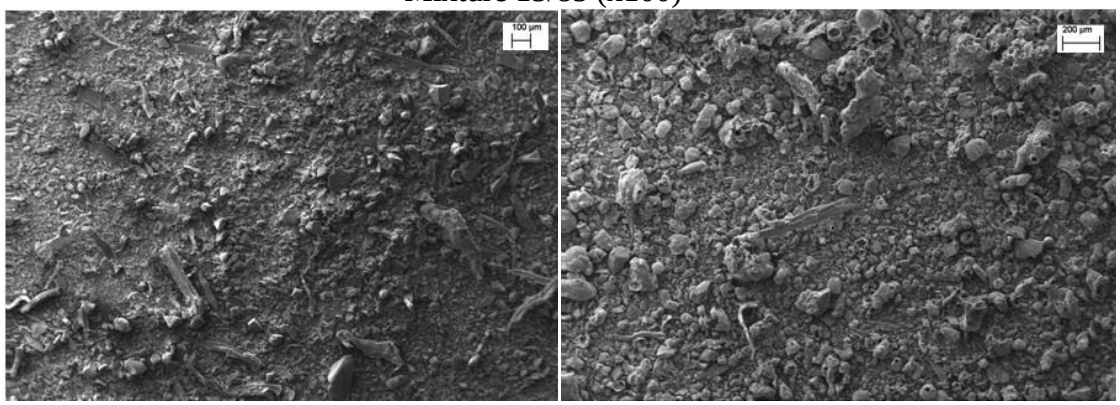

Mixture 20/80 (x100)

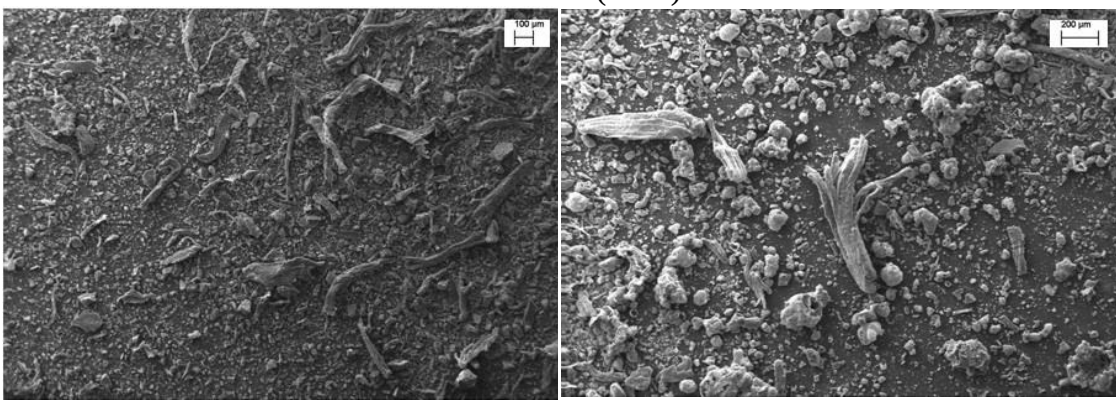

Figure 6-25. SEM images of Colombian coal and its blend with 5%, 15% and 20% pine wood pellets before and after an explosion test

Mixture 40/60 (x100)

Pine wood pellet (x100)

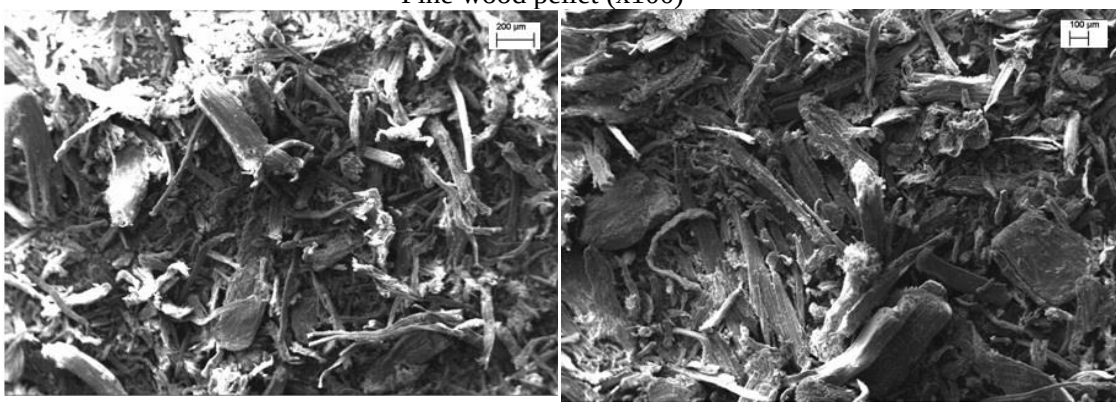

Figure 6-26. SEM images of Colombian coal mixed with 40% pine wood pellets and pine wood pellets alone before and after an explosion test

Mixtures containing larger proportions of coal produced explosion residues where char structures were common, while where biomass had been present in the original blend sample biomass flock-like biomass particles remained unchanged which resulted in more similar size distributions of the residues. In the specific case of pine wood pellets alone most of the particles remain as in the original sample, only small char structures could be found.

The residue corresponding to the most reactive explosion test of the blend with Kellingley coal and torrefied Norway spruce also showed the presence of char structures mixed with unchanged torrefied biomass particles and also a few original coal particles but the overall particle size distribution did not change in great measure.

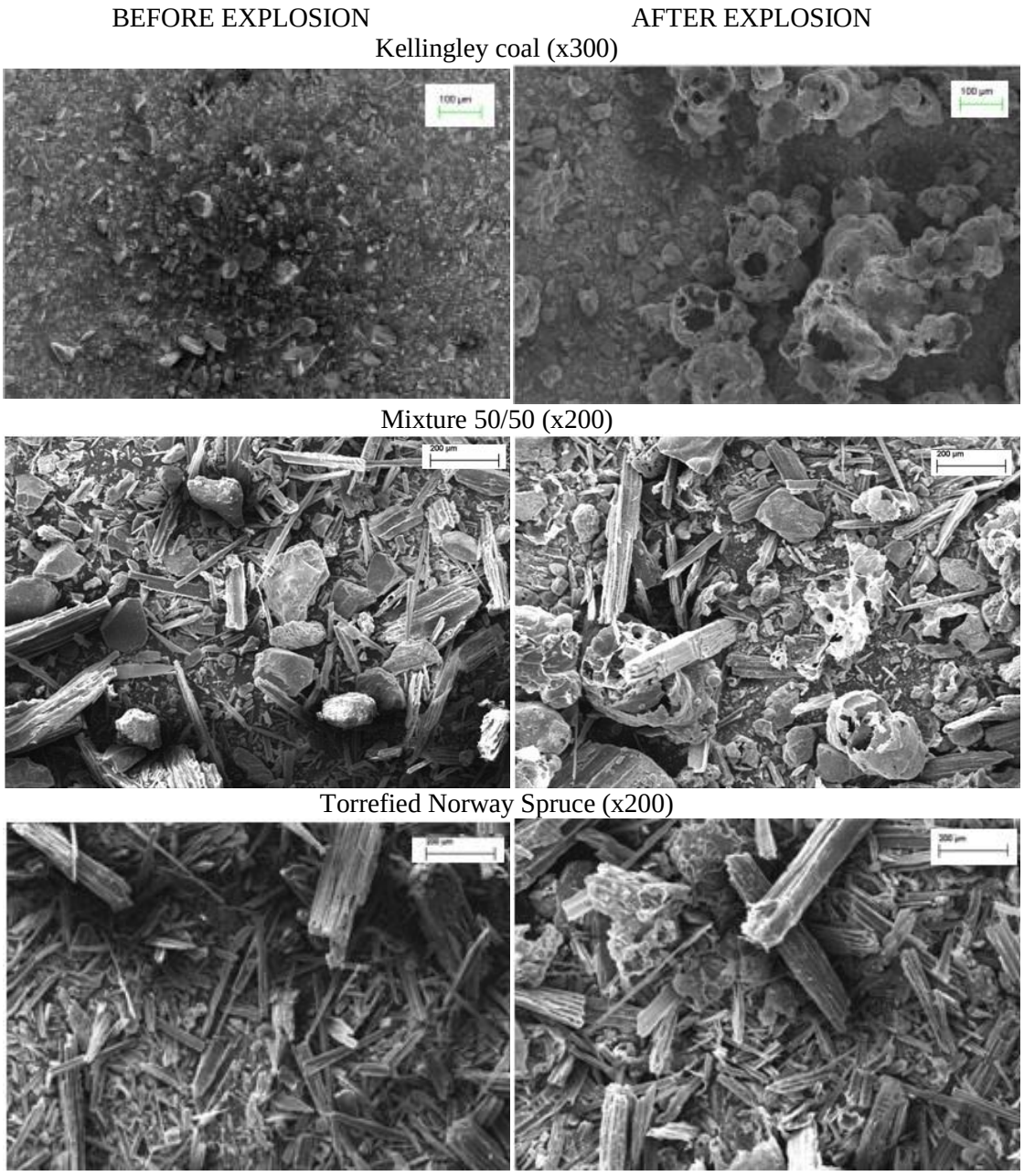

Figure 6-27. SEM images of Kellingley coal and torrefied Norway spruce and their 50/50 blend before and after an explosion test

6.5. Note on Colombian and Kellingley coal explosibility

Colombian and Kellingley coal are both bituminous coals, and as shown in Table 6-1 and Table 6-2, had similar elemental composition. Also there were not

significant differences in the proximate analysis. Surprisingly in terms of their explosion characteristics these apparently similar fuels showed different behaviour: The K_{St} for Colombian coal was almost double the K_{St} found for Kellingley coal, and burned much faster and at leaner mixtures. However, in terms of maximum explosion pressure the results were comparable, 8.2 bar and 8.5 bar for Kellingley and Colombian coal respectively (see Figure 6-28).

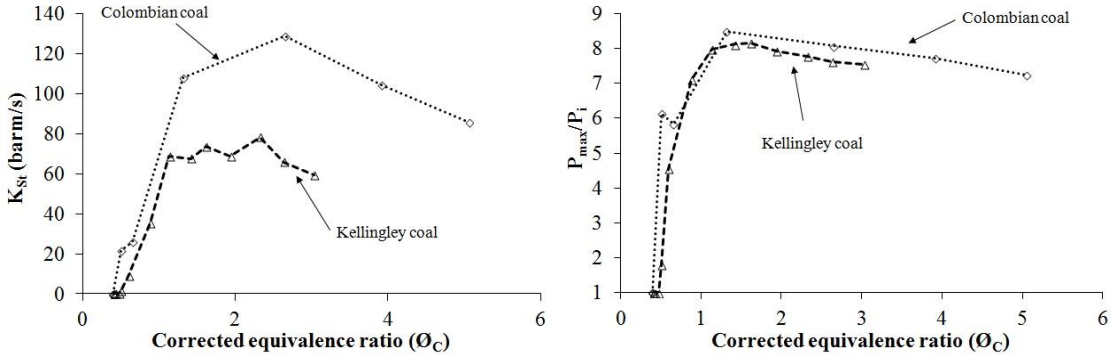

Figure 6-28. Comparison of explosion characteristics of coal samples

Therefore, due to the similarity in composition and maximum explosion pressure results, the difference in explosion reactivity could not lay on the heat available for the reaction, which will be comparable for both coal, but on the rate of mass burning. Therefore, particle size and surface area, as well as the amount and rate of volatile released were investigated as the reason for the higher reactivity of Colombian coal.

Particle size distributions proved to be also very similar, as can be seen in Figure 6-29. Although the samples were supplied from different power stations, it is likely that they were milled to a similar specification in similar mills, which resulted in similar size pulverised products.

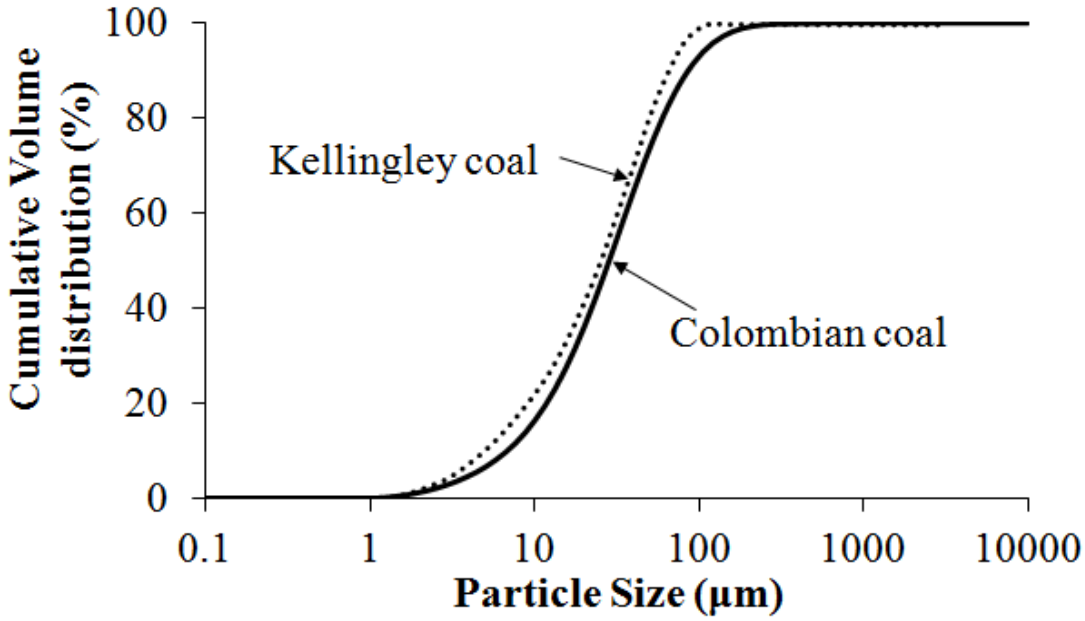

Figure 6-29. Comparison of size distribution of Colombian and Kellingley coal

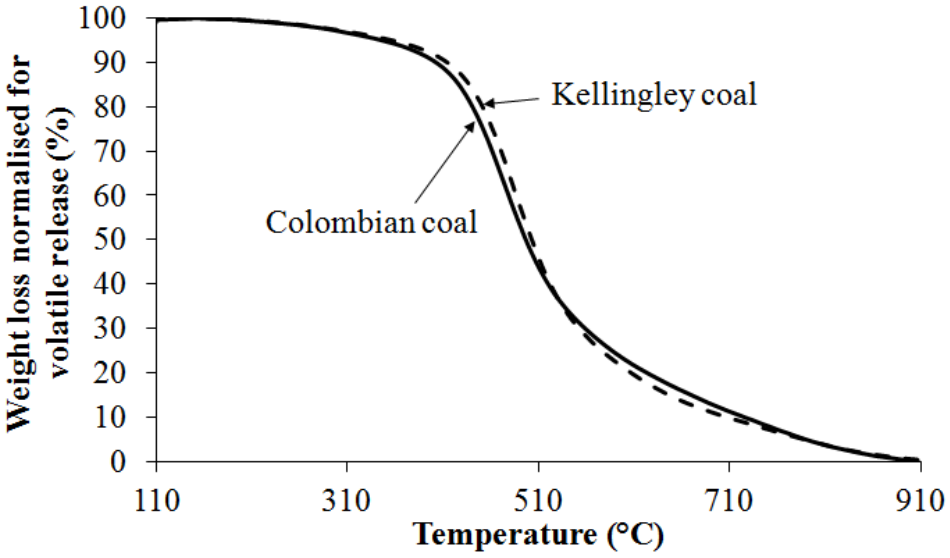

Figure 6-30. Comparison of volatile mass loss (%) for Colombian and Kellingley coal

The weight loss curve for both coals normalised for volatiles release is shown in Figure 6-30. Curves were very similar as it was the rate of volatile release, which differed by only 7%. The temperatures of maximum rate of volatile release were also similar, 485°C and 474 °C for Kellingley coal and Colombian coal respectively. Therefore under pyrolysis conditions the devolatilisation process for both coals was virtually equal

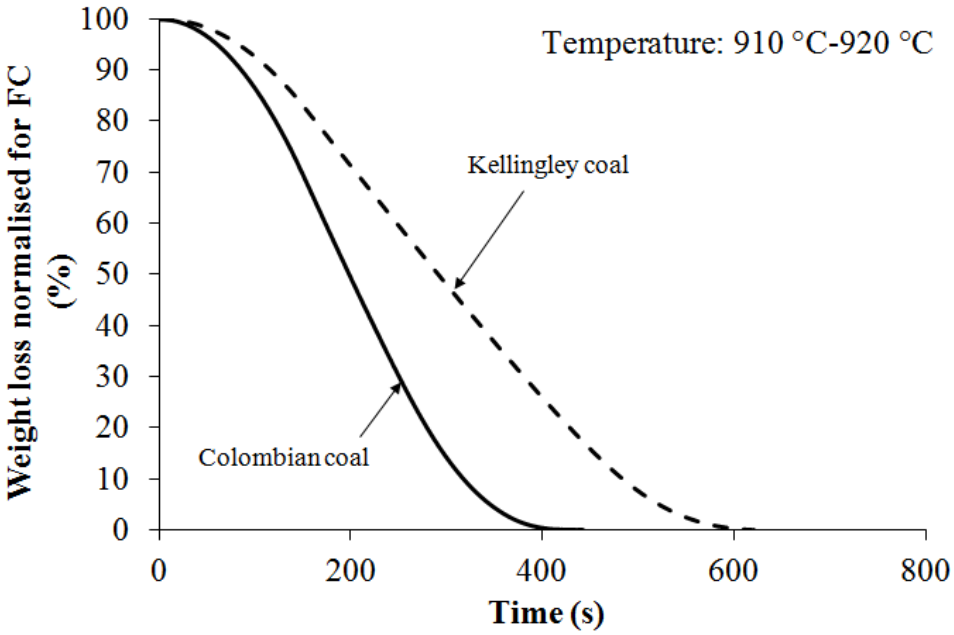

Figure 6-31. Comparison of fixed carbon mass loss (%) for Colombian coal and Kellingley coal

However, differences between coals were detected in the rate of char burnout. This was already shown earlier in Table 6-3, and is graphically depicted in Figure 6-31. Char burnout is almost two times faster for Colombian coal than for Kellingley coal. Therefore, the faster rate of char burnout presented by Colombian coal could be enhancing the overall rate of mass burning and therefore increasing the K_{St} parameter. According to researchers, char burnout is the limiting step during solid fuel combustion [230, 231]. In Table 6-3, char burnout rates were faster than devolatilisation rates due to devolatilisation taking place in an inert atmosphere, the rates of devolatilisation are usually faster in oxidative atmospheres [232], such as those encountered in the explosion tests.

Although it is generally accepted that the combustion of coal consists of two phases (devolatilisation and consumption of volatiles followed by combustion of solid residue i.e. char) [233], studies [234, 235] usually proposed models for coal dust flame propagation by which only the devolatilisation and their consumption are dominant in the combustion process whereas the char is proposed to act as a heat sink. However, Woskoboenko et al. [236] pointed out that such models ignore the importance of particle's structure and concluded that char oxidation could significantly contribute to the explosibility of coal fuels.

The char burnout rate is affected by properties of the particles such as surface area or porosity. It was already shown (Table 6-3) that coal samples had much higher surface area than biomass samples, and in the particular case of Colombian and Kellingley coal the surface area of Colombian coal was 4 times larger than that of

Kellingley coal. Also the pore volume of Colombian coal was 2 times higher than Kellingley coal's (Table 6-11).

Table 6-11. Surface area and pore volume of Colombian and Kellingley coal

	BET Surface area (m^2/g)	Pore volume (cm^3/g)
Kellingley coal	3.7	0.014
Colombian coal	15.8	0.032

In summary, it appears that for samples of coal of similar composition, size distribution, and volatile content, surface area and porosity can play an important role on the rate of char burnout and consequently in the overall rate of mass burning and therefore on K_{St}. Additionally this confirms that, contrary to the behaviour observed for biomass dusts, heterogeneous combustion process took place in coal dust flames, which led to increased reactivity (K_{St}) of Colombian coal.

6.6. Conclusions

The explosion characteristics of coal-biomass and coal-torrefied biomass blends were investigated. Four mixtures of Colombian coal and Pine wood pellets containing 5%, 15%, 20% and 40% Pine wood pellets were tested. Additionally a blend containing 50% torrefied Norway spruce and Kellingley coal was also tested.

The composition of fuels and blends of fuels were measured. Values measured for blends were generally comparable to values expected through calculations from the fuels used in the blend. However, some properties such as bulk density were similar to the fuel present in larger proportion.

The physical characteristics of particles were also measured. The overall surface area of blends decreased with increasing biomass proportions whereas the presence of larger particles increased. The morphology of particles was similar to other coal and biomass samples with biomass consisting of fibrous long particles of variable width. Particles of torrefied biomass appeared straighter and less intricate than raw biomass.

The rates of devolatilisation under relatively slow pyrolysis conditions were increased by the presence of biomass or torrefied biomass in the blend. The same effect was observed with char burnout rates.

Pine wood pellets presented the lowest K_{St} values most likely due to the presence of much bigger particles. Maximum explosion pressures were similar for both the fuels and all the mixtures.

Coinciding with synergistic effects observed through TGA techniques, K_{St} values of samples complaining 20% and 40% biomass blended with Colombian coal presented

values of K_{St} which were higher than any of the fuels used in the blend. These K_{St} values reached ca. 150 barm/s, 16% higher than the K_{St} value of the most reactive fuel in the blend: Colombian coal (129 barm/s). However, the mixture of torrefied biomass and Kellingley coal presented an additive behaviour both in K_{St} and maximum explosion pressure. Synergistic effect can appear depending on blending ratios and the fuels blended. Considering the limited range of the present study, further testing of different blend ratios and fuels is necessary in order to better understand the explosibility of torrefied biomass and coal blends.

The analysis of residues supported the findings highlighted in Chapter 5. All residues showed signs of undergoing mild pyrolysis (loss of volatiles and oxygen, and increase in fixed carbon and ash). Where the presence of char particles was considerable (for coal, torrefied biomass and blends of the two) the size distribution of the residues presented larger particles due to this char structures fusing together. The residues found in raw biomass explosion tests however, contained particles which were virtually identical to the original sample.

Aside from the explosibility of biomass and torrefied biomass blends with coal, it was observed that the reactivity of Colombian coal and Kellingley coal, despite having very similar composition and particle size distribution, differed largely on their K_{St} values. Colombian coal was more reactive (129 barm/s) than Kellingley coal (73 barm/s).

Devolatilisation rates were found to be similar, however variations were observed in char burnout rates. These differences were likely to be due to Colombian coal having a larger surface area (15 m^2/g), 4 times higher than that of Kellingley coal, and doubling Kellingley coal's pore volume.

Contrary to traditional assumptions in the literature, the structure of the coal particle and its effect over the stage of char combustion appeared to play a key role in the reactivity of these coal samples.

Chapter 7 MAIN FINDINGS AND RECOMMENDATIONS

CONTENTS

The major objective of the present research project was to provide data on the explosion and combustion characteristics of torrefied biomass powders which can be potentially used in power generation. Additional data for raw biomass and for mixtures with coal were produced. Fuel characteristics were compared in order to assess the most influential parameters on the reactivity of torrefied and raw biomass. Flame propagation mechanisms and the nature and formation of deposits after explosion tests were investigated.

7.1. Explosion characteristics of torrefied biomass

Torrefied biomass powders tested as part of this research were representative of the few materials that are being torrefied in large enough quantities (to use in the 1 m^3). For some, the exact torrefaction conditions were not known. Nevertheless, all torrefied fuels presented similar characteristics in comparison to the parent biomass material: torrefied fuels had a higher content of carbon, fixed carbon and ash; lower volatile mater and oxygen; improved calorific value, bulk density and grindability, which inevitably led to higher presence of fine particles upon comminution.

Particle size distributions were obtained for each sample. In the derivation of mean size parameters particles were assumed to be spheres which can be misleading when considering long and thin particles characteristic of biomass. The use of alternative size parameters is advised.

Characterisation of dusts and subsequent calculation of stoichiometric concentrations allowed direct comparison between samples with diverse stoichiometry by expressing concentrations as equivalence ratios. This was a feature of this work, however, it is not common in the literature despite being more

informative, especially when measuring MEC or establishing the most reactive mixture of dusts.

Furthermore, most studies available in the literature use nominal concentration values. An increasing number of publications mention inefficiencies in dust dispersion and the presence of residual dust in the explosion chamber, yet corrections to concentrations or further enquiry about the nature and reason for this occurrence are rare. In the present project corrections to concentrations were applied and residues were further analysed.

7.1.1. Deflagration index (K_{St}) and maximum explosion pressure

Investigations into the deflagration index of torrefied fuels using the modified and calibrated 1 m^3 Leeds ISO vessel for fibrous and low bulk density fuels showed that the deflagration index of all torrefied fuels tested was higher than the deflagration index of the corresponding raw biomass fuel. All fuels, torrefied and raw biomass, were St-1 fuels (moderately explosible). In all cases the biomass deflagration index was higher than Kellingley coal and lower or comparable to Colombian coal. It is therefore not possible to conclude that torrefied biomass fuels are more or less reactive than coal due to the variability of coal and biomass reactivity. The maximum K_{St} values of torrefied biomass samples were found to occur at very rich mixtures, as is common in dust explosions.

Particle size had the greatest influence on K_{St} values of biomass and it was also the cause of higher K_{St} values for torrefied mass compared to the parent material.

Maximum explosion pressures were around 9 bar for all biomass samples, and were similar or higher than for both the Kellingley and Colombian coal samples. The similarity in maximum explosion pressure indicated that the energy content of the mix and heat losses were similar regardless of composition, particle size or whether the biomass was thermally treated. Kellingley coal in particular appeared to produce slightly lower flame temperatures due to its high ash content.

7.1.2. Minimum Explosible Concentrations

The European standard recommends that MEC of dust clouds are determined using either the 1 m^3 ISO vessel or the 20 L sphere, however these methods appear to overpredict the limits. Due to the presence of dust deposits following explosion tests and the difficulty in delivering fibrous dusts, the exact concentration burnt is unknown. Also, the ignition energy is too large for the smaller 20 L sphere vessel. A method similar to the one used for the determination of LFL of gases using a Hartmann tube was developed as part of this research project which proved to be fast and repeatable, however dust dispersion was poor and it is believed that the

system could benefit from adding an ignition delay. Due to time constrains in the project this improvement is now underway by other researchers in Leeds.

Using both methods of MEC determination (modified Hartmann and 1 m^3 vessel) it was found that torrefied biomass samples presented leaner MEC values than coal when MEC was expressed as an equivalence ratio based on the chemical formula of the solid. This behaviour was similar to that of raw biomass. The effect of torrefaction on the MEC was studied only for one pair of samples where the raw biomass was available in enough quantities for the 1 m^3 vessel. The torrefied sample burnt at a leaner mixture. Particle size was also likely to be the reason for torrefied biomass presenting lower MEC than raw biomass.

7.1.3. Flame speeds and burning velocity

Turbulent flame speeds, measured in the constant pressure period of the explosion, for the torrefied fuels tested, ranged from 3 to 6 m/s and presented reasonable (given the small variability of K_{St} values measured) linear correlation with K_{St} (measured in the pressure rise period). Approximate calculated laminar burning velocities ranged 0.1-0.15 m/s. These values were comparable to those obtained from Colombian coal and Kellingley coal.

Calculated global heat release rates were comparable to actual coal burner values. The combustion data produced in the 1 m^3 explosion vessel are relevant to understanding the mechanism of turbulent flame propagation in power station burners, which is related to the problem of flame flash back and blow-off.

7.1.4. Explosibility of mixtures of biomass and torrefied biomass and coal

Mixtures of biomass and coal have shown synergistic effects on K_{St} at certain blend ratios where the proportion of biomass was increased. These effects depend on the feedstocks used and the blend ratio. TGA techniques gave indication of such synergistic effects which are likely to occur due to interaction of the fuels during the devolatilisation step.

One mixture of torrefied biomass and coal (containing 50% torrefied biomass by mass) was tested in this work. In this case, the reactivity of the mixture had an additive effect, increasing due to the presence of the more reactive torrefied biomass.

It is clear that the reactivity of a mixture changes depending on the fuels that form the blend and in some cases synergistic effects were evident, which highlights the necessity of testing the exact mixtures used on site to obtain suitable safety data.

7.2. Dust flame propagation mechanisms

Results have shown that on average 50% of the mass injected into the vessel stays in the explosion vessel after a test was performed. Analysis of the composition and physical properties of these residues led to the conclusion that, the dust remaining after the explosion is a proportion of dust that, upon dispersion and initiation of flame propagation is pushed by the explosion wind ahead of the flame towards the vessel walls. This proportion of dust pushed by the explosion wind was found to be larger in coal explosions than in torrefied or raw biomass explosion tests. Particles closest to the flame front are consumed until the flame front reaches the wall, where the remaining dust forms a cake. The outer layer of dust is believed to be scorched by the flame front as heat is lost through the wall. At this time the concentration of oxygen is reduced. As a result, the bulk of dust collected after the explosion test presents changes such as consumption of volatiles, with a significant reduction in oxygen, as well as an increase in fixed carbon and ash. This was generally the case for all biomass, torrefied biomass and coal samples. However a few differences suggest that raw biomass behaved in a different way to coal. The differences are related to: size distribution, particle density and morphology. The size distribution of raw biomass explosion residues was virtually identical to the size distribution of the original samples, in addition the density of the particle was unchanged as well as the shape. Only very few small char structures were perceptible under the scanning electron microscope. On the other hand, the residues from coal dust explosions presented a size distribution where larger particles were present, the density of the particles increased considerably and SEM images showed major presence of char structures fused together with blow out holes. These were mixed with a small number of unchanged particles. This implies that coal was prone to char formation whereas with biomass, char formation was inhibited. The increased presence of large particles in coal explosion residues is due to char particles merging together forming clusters rather than preferential burning of fines or particle agglomeration, as was initially suggested.

For biomass tests the residue consisted of ash originating from the complete combustion of particles, completely unreacted biomass and evidence of partial pyrolysis on some particles. There was no evidence of significant char residue. Judging by the results from the analysis of residues, biomass samples fully devolatilised with little char formation, which has been already proposed by researchers working on fast pyrolysis of biomass studies. Char formation is lower with biomass due to the high content of cellulose, resulting in an homogeneous gas flame propagation mechanism. This is also supported by the inexistent relationship between explosion reactivity and surface area of biomass particles.

On the other hand the mechanism for coal consists on devolatilisation and combustion of volatiles followed by the combustion of the char. The importance of the later step has been overlooked in many explosion flame propagation models as the devolatilisation and combustion of volatiles step is likely to be more dominant. However, it has been shown in this work with Colombian coal and Kellingley coal that the step of char combustion and the physical characteristics of the surface of the particle can considerably affect the reactivity of coal samples.

For all the torrefied biomass fuels tested in this work, the analysis of residues pointed at similar behaviour to that of coal, that is, presence of char in the residue and bigger particles in the size distribution and increase in particle density. However, a lot of particles still appeared unchanged in the same way as raw biomass. The presence of char structures was not as prevalent as for coal samples. Therefore a torrefied biomass flame could have some degree of heterogeneous combustion as the torrefied fuel is already carbonised and has a greater propensity for char production. It has not been possible to identify a dependence of particle surface area with K_{St} in the case of torrefied fuels due to the small variability in surface area for the samples tested.

7.3. Future work

Due to the limited availability of torrefied fuels in large quantities for the present work, testing of a diverse range of torrefied fuels including agricultural residues and energy crops is required. In addition, the effect of torrefaction severity on reactivity should be further investigated in order to corroborate the findings of this research. The effect of particle size and testing of size distributions representative of those used in the industry is highly recommended as the results point to an explosibility of samples containing larger particles that has not been found before with traditional dusts.

The moisture content of samples tested here ranged through very similar values, never higher than 10%, therefore the effect of moisture could also be the object of future studies.

The effect of torrefaction and particle size over MEC should also be further investigated.

The modified Hartmann method developed here could be used but the addition of a suitable ignition delay is recommended to allow for adequate dust dispersion before ignition. In addition detailed high speed video studies could assist on getting:

a) better understanding of flame propagation

b) flame speed measurements for comparison and improvement of the technique

c) confirmation of acceptable dust dispersion throughout volume of the tube

Improvement to the laminar burning velocities derived in this work would be possible if expansion factors at constant pressure and volume or else adiabatic flame temperatures were predicted. This would require the use of an equilibrium chemical code.

Further work on mixtures of coal and biomass and torrefied biomass is required, in order to confirm whether mixing coal and torrefied biomass poses a more or less severe hazard than coal-biomass mixtures or vice versa.

Further confirmation of the postulations regarding the different flame propagation mechanism for biomass, torrefied biomass and coal could be achieved by testing a diverse range of fuels. In addition the determination of cellulose, hemicellulose and lignin for all biomass and torrefied biomass samples could help verify if effectively it is the quantity of any of these components and in particular cellulose that determines whether the propagation mechanism is heterogeneous or homogeneous.

The analysis of residues of all mixtures, not only for the most reactive mixture, could also give valuable information.

Additional studies related to protection against explosions in the power generation industries where biomass, torrefied biomass and coal are used should include studies on suppressants or venting efficiency and whether results are relevant to large scale applications.

References

[1] DECC, UK Energy in Brief 2013. 2013.

[2] DECC, Digest of UK energy statistics (DUKES). 2013, The Stationery Office: Norwich.

[3] International Energy Agency, World Energy Outlook Special Report. 2013: Paris, France.

[4] Great Britain, Climate Change Act 2008: Elizabeth II. Chapter 27. 2008, The Stationery Office: London.

[5] Davey, E, Jones, C, Foster, A, and Ewing, F, UK Renewable Energy Roadmap, Department of Energy and Climate Change, Editor. 2011: London.

[6] DEFRA (2007) UK Biomass Strategy.

[7] Haberl, H, Sprinz, D, Bonazountas, M, Cocco, P, Desaubies, Y, Henze, M, Hertel, O, Johnson, RK, Kastrup, U, Laconte, P, Lange, E, Novak, P, Paavola, J, Reenberg, A, van den Hove, S, Vermeire, T, Wadhams, P, and Searchinger, T, Correcting a fundamental error in greenhouse gas accounting related to bioenergy. Energy Policy, 2012. **45**(0): 18-23.

[8] Lamers, P, Thiffault, E, Paré, D, and Junginger, M, Feedstock specific environmental risk levels related to biomass extraction for energy from boreal and temperate forests. Biomass and Bioenergy, 2013. **55**(0): 212-226.

[9] Ofgem, Annual sustainability report 2011-2012, in https://www.ofgem.gov.uk/publications-and-updates/annual-sustainability-report-2011-2012. 2012: London.

[10] Woods, J, Tipper, R, Brown, G, Diaz-Chavez, R, Lovell, J, and de Groot, P, Evaluating the Sustainability of Co-firing in the UK. 2006, Themba Technology Ltd and The Edinburgh Centre for Carbon Management: London. p.68.

[11] DECC and Ofgem, Renewables Obligation banding levels: 2013-2017. 2013.

[12] Macalister, T, New biomass plants shelved as Drax and Centrica blame lack of support, in The Guardian. 2012.

[13] Demirbas, A, Combustion characteristics of different biomass fuels. Progress in Energy and Combustion Science, 2004. **30**(2): 219-230.

[14] Tumuluru, JS, Wright, CT, Hess, JR, and Kenney, KL, A review of biomass densification systems to develop uniform feedstock commodities for bioenergy application. Biofuels, Bioproducts and Biorefining, 2011. **5**(6): 683-707.

[15] Evans, G, Techno-economic assessment of biomass "densification" technologies. 2008, NNFCC. 140pp.

[16] Bergman, PCA and Kiel, JHA. Torrefaction for biomass upgrading. in 14th European Biomass Conference & Exhibition. 2005. Paris, France: ETA Renewable Energies.

[17] Batidzirai, B, Mignot, APR, Schakel, WB, Junginger, HM, and Faaij, APC, Biomass torrefaction technology: Techno-economic status and future prospects. Energy, 2013. **62**: 196-214.

[18] Health and Safety Executive, The health and safety risks and regulatory strategy related to energy developments. 2006: London.

[19] Oveisi, E, Lau, A, Sokhansanj, S, Jim Lin, C, Bi, X, Larsson, SH, and Melin, S, Breakage behaviour of wood pellets due to free fall. Powder Technology, 2013. **235**(0): 493-499.

[20] Grossel, SS, Safety considerations in conveying of bulk solids and powders. Journal of Loss Prevention in the Process Industries, 1988. **1**(2): 62-74.

[21] Gummer, J and Lunn, GA, Ignitions of explosive dust clouds by smouldering and flaming agglomerates. Journal of Loss Prevention in the Process Industries, 2003. **16**(1): 27-32.

[22] Malmgren, A and Riley, J, Biomass Power Generation. Reference module in Earth Systems and Environmental Sciences Comprehensive Renewable Energy, 2012. **5**(0): 27-53.

[23] García-Torrent, J, Ramírez-Gómez, Á, Querol-Aragón, E, Grima-Olmedo, C, and Medic-Pejic, L, Determination of the risk of self-ignition of coals and biomass materials. Journal of Hazardous materials, 2012. **213–214**(0): 230-235.

[24] Ramírez, Á, García-Torrent, J, and Tascón, A, Experimental determination of self-heating and self-ignition risks associated with the dusts of agricultural materials commonly stored in silos. Journal of Hazardous materials, 2010. **175**(1–3): 920-927.

[25] Abbasi, T and Abbasi, SA, Dust explosions–Cases, causes, consequences, and control. J Hazard Mater, 2007. **140**(1-2): 44.

[26] European Parliament, Directive 99/92/EC. On minimum requirements for improving the safety and health protection of workers potentially at risk from explosive atmospheres. 15th individual Directive within the meaning of Article 16(1) of Directive 89/391/EEC. 1999. 34.

[27] European Parliament, Directive 94/9/EC. On the approximation of the laws of the Member States concerning equipment and protective systems intended for use in potentially explosive atmospheres and ammending and subsequently repealing Directives 76/117/EEC and 82/130/EEC. 1994. 33.

[28] Versloot, NHA, Klein, AJJ, and De Maaijer, M, Summary of European directives for explosion safety. Process Safety Progress, 2008. **27**(1): 80-85.

[29] Eckhoff, RK, Differences and similarities of gas and dust explosions: A critical evaluation of the European 'ATEX' directives in relation to dusts. Journal of Loss Prevention in the Process Industries, 2006. **19**(6): 553-560.

[30] BSI, BS EN 14034-1: Determination of explosion characteristics of dust clouds Part 1: Determination of maximum pressure Pmax of dust clouds. 2004, BSI: London.

[31] International Organization of Standardization, ISO-6184/1 Explosion Protection Systems- Part 1: Determination of Explosion Indices of Combustible Dusts in Air. 1985: Geneva.

[32] van der Wel, PGJ, Ignition and propagation of dust explosions, in Applied Sciences. 1993, Delft University: Delft.

[33] Coward, HF and Jones, GW, Limits of flammability of gases and vapors. 1952: Washington D.C.

[34] Sattar, H, Phylaktou, HN, Andrews, GE, and Gibbs, BM, Pulverised biomass explosions: Investigation of the ultra rich mixtures that give peak

reactivity, in IX International Symposium on Hazard, Prevention and Mitigation of Industrial Explosions. 2012: Cracow, Poland.

[35] Slatter, DJF, Huescar Medina, C, Sattar, H, Andrews, G, Phylaktou, HN, and Gibbs, BM, Biomass explosion residue analysis, in X International Symposium on Hazards, Prevention and Mitigation of Industrial Explosions. 2014: Bergen, Norway.

[36] Hertzberg, M, Zlochower, IA, and Cashdollar, KL, Volatility model for coal dust flame propagation and extinguishment. Symposium (International) on Combustion, 1988. **21**(1): 325-333.

[37] National Fire Protection Association, NFPA 68 standard on Explosion Protection by Deflagration Venting and supersedes all previous editions. 2007, Standards Council.

[38] British Standards Institution, BS EN 14034-4:2004+A1:2011 Determination of explosion characteristics of dust clouds. Part 4: Determination of the limiting oxygen concentration (LOC) of dust clouds. 2011, BSI: London.

[39] Pu, YK, Jia, F, Wang, SF, and Skjold, T, Determination of the maximum effective burning velocity of dust–air mixtures in constant volume combustion. Journal of Loss Prevention in the Process Industries, 2007. **20**(4–6): 462-469.

[40] Bidabadi, M, Montazerinejad, S, and Fanaee, SA, The influence of radiation on the flame propagation through micro organic dust particles with non-unity Lewis number. Journal of the Energy Institute, 2014(0).

[41] Haghiri, A and Bidabadi, M, Modeling of laminar flame propagation through organic dust cloud with thermal radiation effect. International Journal of Thermal Sciences, 2010. **49**(8): 1446-1456.

[42] Bidabadi, M, Haghiri, A, and Rahbari, A, The effect of Lewis and Damköhler numbers on the flame propagation through micro-organic dust particles. International Journal of Thermal Sciences, 2010. **49**(3): 534-542.

[43] Dahoe, AE, Hanjalic, K, and Scarlett, B, Determination of the laminar burning velocity and the Markstein length of powder-air flames. Powder Technology, 2002. **122**: 222-238.

[44] Goroshin, S, Fomenko, I, and Lee, JHS, Burning velocities in fuel-rich aluminum dust clouds. Symposium (International) on Combustion, 1996. **26**(2): 1961-1967.

[45] Silvestrini, M, Genova, B, and Leon Trujillo, FJ, Correlations for flame speed and explosion overpressure of dust clouds inside industrial enclosures. Journal of Loss Prevention in the Process Industries, 2008. **21**(4): 374-392.

[46] Harris, RJ, The investigation and control of gas explosions and heating plant. 1983, London: E&FN Spon in association with the British Gas Corporation.

[47] Cassel, HM, Das Gupta, AK, and Guruswamy, S, Factors affecting flame propagation through dust clouds. Symposium on Combustion and Flame, and Explosion Phenomena, 1949. **3**(1): 185-190.

[48] Dahoe, AE, Zevenbergen, JF, Lemkowitz, SM, and Scarlett, B, Dust explosions in spherical vessels: The role of flame thickness in the validity of the ‘cube-root law’. Journal of Loss Prevention in the Process Industries, 1996. **9**(1): 33-44.

[49] Kumar, RK and Bowles, EM, Large Scale Dust Explosion Experiments to Determine the Effects of Scaling on Explosion Parameters. Combustion and Flame, 1992. **89**: 320-332.

[50] Han, O-S, Yashima, M, Matsuda, T, Matsui, H, Miyake, A, and Ogawa, T, A study of flame propagation mechanisms in lycopodium dust clouds based on dust particles' behavior. Journal of Loss Prevention in the Process Industries, 2001. **14**(3): 153-160.

[51] Proust, C, A few fundamental aspects about ignition and flame propagation in dust clouds. Journal of Loss Prevention in the Process Industries, 2005. **19**(2-3): 104-120.

[52] Proust, C, Flame propagation and combustion in some dust-air mixtures. Journal of Loss Prevention in the Process Industries, 2006. **19**(1): 89-100.

[53] Dorsett, HG, Jacobson, M, Nagy, J, and Williams, RP, Laboratory equipment and test procedures for evaluating explosibility of dusts. 1960: Washington, D.C. 21 p.

[54] Jacobson, M, Nagy, J, Cooper, AR, and Ball, FJ, Explosibility of agricultural dusts. 1961: Washington, D.C. 23p.

[55] Dorsett, HG and Nagy, J, Dust explosibility of chemicals, drugs, dyes, and pesticides. 1968: Washington, D.C. 23 p.

[56] Nagy, J, Cooper, AR, and Dorsett, HG, Explosibility of miscellaneous dusts. 1968: Washington, D.C. 31p.

[57] Nagy, J, Dorsett, HG, and Cooper, AR, Explosibility of carbonaceous dusts, in R.I. 6597. 1965: Washington, D.C. 30 p.

[58] Eckhoff, RK, Dust Explosions in the Process Industries. 3rd ed. 2003, USA: Gulf Professional Publishing. 719.

[59] Amyotte, PR and Pegg, MJ, Lycopodium Dust Explosions in a Hartmann Bomb: Effects of Turbulence. Journal of Loss Prevention in the Process Industries, 1989. **2**.

[60] Field, P, Explosibility assessment of industrial powders and dusts. 1983, London: Her Majesty's Stationary Office. 52.

[61] Maisey, HR, Gaseous and Dust Explosion Venting. Chemical and Process Engineering, 1965. **46**(3): 685.

[62] British Standards Institution, BS EN 13821:2002: Potentially explosive atmospheres-Explosion prevention and protection-Determination of minimum ignition energy of dust/air mixtures. 2002, BSI: London.

[63] Trostel, LJ and Frevert, HW, The lower limits of concentration for explosion of dusts in air. Chemical and Metallurgical Engineering, 1924. **30**(4): 141-146.

[64] Eggleston, LA and Pryor, AJ, The limits of dust explosibility. Fire Technology, 1967. **3**: 77-89.

[65] Wolanski, P, Dust explosion research in Poland. Powder Technology, 1992. **71**(2): 197-206.

[66] Lee, RS, Aldis, DF, Garret, DW, and Lai, FS, Improved diagnostics for determination of Minimum Explosive Concentration, Ignition Energy and Ignition Temperature of dusts. Powder Technology, 1982. **31**: 51-62.

[67] Makris, A and Lee, JHS, Lean flammability limits of dust-air mixtures. Archivum Combustionis, 1989. **9**: 43-64.

[68] Lovachev, LA, Babkin, VS, Bunev, VA, V'Yun, AV, Kirivulin, VN, and Baratov, AN, Flammability limits: An invited review. Combustion and Flame, 1973. **20**: 259-289.

[69] Janes, A, Chaineaux, J, Carson, D, and Le Lore, PA, MIKE 3 versus HARTMANN apparatus: Comparison of measured minimum ignition energy (MIE). Journal of Hazardous Materials, 2008. **152**(1): 32-39.

[70] Wu, HC, Chang, RC, and Hsiao, HC, Research of minimum ignition energy for nano Titanium powder and nano Iron powder. Journal of Loss Prevention in the Process Industries, 2009. **22**(1): 21-24.

[71] Kalejaiye, O, Amyotte, PR, Pegg, MJ, and Cashdollar, KL, Effectiveness of dust dispersion in the 20-L Siwek chamber. Journal of Loss Prevention in the Process Industries, 2010. **23**(1): 46-59.

[72] Bartknecht, W, Dust Explosions: Course, prevention, protection. 1989, London: Springer London. 270.

[73] British Standards Institution, BS EN 14034-2: Determination of explosion characteristics of dust clouds Part 2: Determination of the maximum rate of explosion pressure rise of dust clouds. 2006, BSI: London.

[74] British Standards Institution, BS EN 14034-3: Determination of explosion characteristics of dust clouds Part 3: Determination of the lower explosion limit LEL of dust clouds. 2006, BSI: London.

[75] Siwek, R, Determination of technical safety indices and factors influencing hazard evaluation of dusts. Journal of Loss Prevention in the Process Industries, 1996. **9**(1): 21-31.

[76] Proust, C, Accorsi, A, and Dupont, L, Measuring the violence of dust explosions with the “20l sphere” and with the standard “ISO 1m3 vessel” Systematic comparison and analysis of the discrepancies. Journal of Loss Prevention in the Process Industries, 2007. **20**(4-6): 599-606.

[77] Going, JE, Chatrathi, K, and Cashdollar, KL, Flammability limit measurements for dusts in 20-L and 1-m3 vessels. Journal of Loss Prevention in the Process Industries, 2000. **13**(3–5): 209-219.

[78] Chawla, N, Amyotte, PR, and Pegg, MJ, A comparison of experimental methods to determine the minimum explosible concentration of dusts. Fuel, 1996. **75**(6): 654-658.

[79] Cashdollar, KL and Chatrathi, K, Minimum Explosible Dust Concentrations Measured in 20-L and 1-M3 Chambers. Combustion Science and Technology, 1993. **87**(1): 157-171.

[80] Bartknecht, W, Explosionsschutz-Grundlagen und Anwendung, ed. Springer-Verlag. 1993, Berlin: Springer Verlag. 906.

[81] Cashdollar, KL and Hertzberg, M. Industrial Dust Explosions. in Symposium on Industrial Dust Explosions. 1986. Pittsburgh: ASTM.

[82] Wilén, C, Moilanen, A, Rautalin, A, Torrent, J, Conde, E, Lödel, R, Carlson, D, Timmers, P, and Brehm, K, Safe handling of renewable fuels and fuel mixtures. 1999, VTT Technical Research Cenre of Finland: Espoo. 117 p.+app. 8p.

[83] Di Benedetto, A, Russo, P, Sanchirico, R, and Di Sarli, V, CFD simulations of turbulent fluid flow and dust dispersion in the 20 liter explosion vessel. AIChE Journal, 2013. **59**(7): 2485-2496.

[84] Di Sarli, V, Russo, P, Sanchirico, R, and Di Benedetto, A, CFD simulations of the effect of dust diameter on the dispersion in the 20L bomb. Chemical Engineering Transactions, 2013. **31**(0): 727-732.

[85] Di Sarli, V, Russo, P, Sanchirico, R, and Di Benedetto, A, CFD simulations of dust dispersion in the 20 L vessel: Effect of nominal dust concentration. Journal of Loss Prevention in the Process Industries, 2014. **27**(0): 8-12.

[86] Sattar, H, Phylaktou, HN, Andrews, GE, and Gibbs, BM, Explosions and flame propagation in nut-shell biomass powders, in IX International Symposium on Hazards, Prevention and Mitigation of Industrial Explosions. 2012: Cracow, Poland.

[87] Pilão, R, Ramalho, E, and Pinho, C, Overall characterization of cork dust explosion. Journal of Hazardous Materials, 2006. **133**(1-3): 183-195.

[88] Ng, DL, Cashdollar, KL, Hertzberg, M, and Lazzara, CP, Electron Microscopy Studies of Explosion and Fires Residues, in IC 8936. 1983, Dept. of the Interior, Bureau of Mines: Washington D.C.

[89] Garcia-Torrent, J, Conde-Lazaro, E, Wilen, C, and Rautalin, A, Biomass dust explosibility at elevated initial pressures. Fuel, 1998. **77**(9/10): 97.

[90] Eckhoff, RK, Prevention and mitigation of dust explosions in the process industries: A survey of recent research and development. Journal of Loss Prevention in the Process Industries, 1996. **9**(1): 3-20.

[91] Skjold, T, Selected aspects of turbulence and combustion in 20 litre explosion vessels, in Department of Physics. 2003, University of Bergen: Bergen.

[92] Amyotte, PR, Chippett, S, and Pegg, MJ, Effects of turbulence on dust explosions. Progress in Energy and Combustion Science, 1988. **14**(4): 293-310.

[93] Phylaktou, HN, Gardner, CL, and Andrews, GE. Flame speed measurements in dust explosions. in 6th International Seminar on Fire and Explosion Hazards. 2010. Leeds: Research Publishing.

[94] Alexiou, A, Phylaktou, HN, and Andrews, GE. Vented gas explosions in a long vessel with obstacles. in Major Hazards Onshore and Offshore II. 1995: IChemE.

[95] Zhen, G and Leuckel, W, Effects of ignitors and turbulence on dust explosions. Journal of Loss Prevention in the Process Industries, 1997. **10**(5–6): 317-324.

[96] Amyotte, PR, Baxter, BK, and Pegg, MJ, Influence of initial pressure on spark-ignited dust explosions. Journal of Loss Prevention in the Process Industries, 1990. **3**(2): 261-263.

[97] Cashdollar, KL, Overview of Dust Explosibility Characteristics. Journal of Loss Prevention in the Process Industries, 2000. **13**: 183-199.

[98] Wiemann, W, Influence of temperature and pressure on the explosion characteristics of dust/air and dust/air/inert gas mixtures, in Industrial dust explosions, K.L. Cashdollar and M. Hertzberg, Editors. 1987, ASTM Special Technical Publication 958: Philadelphia. 202-216.

[99] Siwek, in First International Specialist Meeting of the Combustion Institute. Seminar on Fire and Explosion Hazards. 1995: Moscow. 329.

[100] Traore, M, Dufaud, O, Perrin, L, Chazelet, S, and Thomas, D, Dust explosions: how should the influence of humidity be taken into account? Process Safety and Environmental Protection, 2009. **87**(0): 14-20.

[101] Gao, W, Dobashi, R, Mogi, T, Sun, J, and Shen, X, Effects of particle characteristics on flame propagation behavior during organic dust explosions in a half-closed chamber. Journal of Loss Prevention in the Process Industries, 2012. **25**(6): 993-999.

[102] Amyotte, PR, Cloney, CT, Kahn, FI, and Ripley, RC, Dust explosion risk moderation for flocculent dusts. Journal of Loss Prevention in the Process Industries, 2012. **25**(0): 862-869.

[103] Hartmann, I, Dust Explosions in Coal Mines and industry. The Scientific Monthly, 1954. **79**(2): 97-108.

[104] Man, CK and Harris, ML, Participation of large particles in coal dust explosions. Journal of Loss Prevention in the Process Industries, 2014. **27**(0): 49-54.

[105] Hertzberg, M, Cashdollar, KL, Ng, DL, and Conti, RS, Domains of flammability and thermal ignitability for pulverized coals and other dusts: Particle size dependences and microscopic residue analyses. Symposium (International) on Combustion, 1982. **19**(1): 1169-1180.

[106] Kuai, N, Li, J, Chen, Z, Huang, W, Yuan, J, and Xu, W, Experiment-based investigations of magnesium dust explosion characteristics. Journal of Loss Prevention in the Process Industries, 2011. **24**(0): 302-313.

[107] Cashdollar, KL, Coal dust explosibility. Journal of Loss Prevention in the Process Industries, 1996. **9**(1): 65-76.

[108] Gao, W, Mogi, T, Sun, J, Yu, J, and Dobashi, R, Effects of particle size distributions on flame propagation mechanism during octadecanol dust explosions. Powder Technology, 2013. **249**(0): 168-174.

[109] Holbrow, P, Wall, M, Sanderson, E, Bennet, D, Rattigan, W, Bettis, R, and Gregory, D, Fire and explosion properties of nanopowders, HSE Books, Editor. 2010, HSE: Buxton. 76 p.

[110] Green, HL and Lane, WR, Particulate clouds: Dusts smokes and mists. 2nd ed. 1964, London: E. & FN. Spon Ltd.

[111] Eckhoff, R, Does the dust explosion risk increase when moving from micron particle powders to powders of nano particles? Journal of Loss Prevention in the Process Industries, 2011. **25**(0): 448-459.

[112] Hedlund, FH, Astad, J, and Nichols, J, Inherent hazards, poor reporting and limited learning in the solid biomass energy sector: A case study of a wheel loader igniting wood dust, leading to fatal explosion at wood pellet manufacturer. Biomass and Bioenergy, 2014. **in press**.

[113] Nordin, A, Chemical elemental characteristics of biomass fuels. Biomass and Bioenergy, 1994. **6**(5): 339-347.

[114] Vassilev, SV, Baxter, D, Andersen, LK, and Vassileva, CG, An overview of the chemical composition of biomass. Fuel, 2010. **89**(5): 913-933.

[115] Vassilev, SV, Baxter, D, Andersen, LK, Vassileva, CG, and Morgan, TJ, An overview of the organic and inorganic phase composition of biomass. Fuel, 2012. **94**(0): 1-33.

[116] Telmo, C and Lousada, J, Heating values of wood pellets from different species. Biomass and Bioenergy, 2011. **35**(7): 2634-2639.

[117] Garcia, R, Pizarro, C, Lavin, AG, and Bueno, JL, Spanish biofuels heating value estimation. Part II: Proximate analysis data. Fuel, 2014. **117**(0): 1139-1147.

[118] Erol, M, Haykiri-Acma, H, and Küçükbayrak, S, Calorific value estimation of biomass from their proximate analyses data. Renewable Energy, 2010. **35**(1): 170-173.

[119] Friedl, A, Padouvas, E, Rotter, H, and Varmuza, K, Prediction of heating values of biomass fuel from elemental composition. Analytica Chimica Acta, 2005. **544**(1-2): 191-198.

[120] Mason, DM and Gandhi, KN, Formulas for calculating the calorific value of coal and coal chars: Development, tests, and uses. Fuel Processing Technology, 1983. **7**(1): 11-22.

[121] Yin, C-Y, Prediction of higher heating values of biomass from proximate and ultimate analyses. Fuel, 2011. **90**(3): 1128-1132.

[122] Sheng, C and Azevedo, JLT, Estimating the higher heating value of biomass fuels from basic analysis data. Biomass and Bioenergy, 2005. **28**(5): 499-507.

[123] Bridgeman, T, Jones, J, Shield, I, and Williams, P, Torrefaction of reed canary grass, wheat straw and willow to enhance solid fuel qualities and combustion properties. Fuel, 2008. **87**(6): 844-856.

[124] Kongkeaw, N and Patumsawad, S. Thermal upgrading of biomass as a fuel by torrefaction. in 2nd International Conference on Environmental Engineering and Applications. 2011. Shanghai, China: IACSIT Press.

[125] van Loo, S and Koppejan, J, The handbook of biomass combustion and co-firing, ed. S. van Loo and J. Koppejan. 2008, London: Earthscan.

[126] Darvell, LI and Straker, P.Email to Huescar Medina C., 4th of March, 2014

[127] British Standards Institution, BS EN 14961-2:2011 Solid biofuels. Fuel specifications and classes. Wood pellets for non-industrial use. 2011, BSI: London.

[128] McKendry, P, Energy production from biomass (part 1): overview of biomass. Bioresource Technol, 2002. **83**(1): 46.

[129] Tillman, DA, Biomass cofiring: the technology, the experience, the combustion consequences. Biomass and Bioenergy, 2000. **19**(6): 365-384.

[130] van den Broek, R, Faaij, A, and van Wijk, A, Biomass combustion for power generation. Biomass and Bioenergy, 1996. **11**(4): 81.

[131] Bedane, AH, Afzal, MT, and Sokhansanj, S, Simulation of temperature and moisture changes during storage of woody biomass owing to weather variability. Biomass and Bioenergy, 2011. **35**(7): 3147-3151.

[132] Barontini, M, Scarfone, A, Spinelli, R, Gallucci, F, Santangelo, E, Acampora, A, Jirjis, R, Civitarese, V, and Pari, L, Storage dynamics and fuel quality of poplar chips. Biomass and Bioenergy, 2014. **62**(0): 17-25.

[133] Ramírez, Á, García-Torrent, J, and Aguado, PJ, Determination of parameters used to prevent ignition of stored materials and to protect against explosions in food industries. Journal of Hazardous Materials, 2009. **168**(1): 115-120.

[134] Deguingand, B and Galant, S, Upper flammability limits of coal dust-AIR mixtures. Symposium (International) on Combustion, 1981. **18**(1): 705-715.

[135] Smoot, LD, Horton, MD, and Williams, GA, Propagation of laminar pulverized coal-air flames. Symposium (International) on Combustion, 1977. **16**(1): 375-387.

[136] Jensen, B and Gillies, A. Review of coal dust explosibility research. in Australasian Institute of Mining and Metallurgy. 1994: AusIMM.

[137] Antal, MJ, Biomass pyrolysis:a review of the literature. Part I ecarbonydrate pyrolysis. Adv Sol Energy, 1983. **11**: 61-111.

[138] Mansaray, KG and Ghaly, AE, Thermal Degradation of Rice Husks in Nitrogen Atmosphere. Bioresource Technol, 1998. **65**: 13-20.

[139] Chen, W-H, Cheng, W-Y, Lu, K-M, and Huang, Y-P, An evaluation on improvement of pulverized biomass property for solid fuel through torrefaction. Applied Energy, 2011.

[140] Bridgeman, TG, Jones, JM, Williams, A, and Waldron, DJ, An investigation of the grindability of two torrefied energy crops. Fuel, 2010. **89**(12): 3911-3918.

[141] Repellin, V, Govin, A, Rolland, M, and Guyonnet, R, Energy requirement for fine grinding of torrefied wood. Biomass and Bioenergy, 2010. **34**(7): 923-930.

[142] Arias, B, Pevida, C, Fermoso, J, Plaza, MG, Rubiera, F, and Pis, JJ, Influence of torrefaction on the grindability and reactivity of woody biomass. Fuel Process Technology, 2008. **89**(2): 75.

[143] Broström, M, Nordin, A, Pommer, L, Branca, C, and Di Blasi, C, Influence of torrefaction on the devolatilization and oxidation kinetics of wood. Journal of Analytical and Applied Pyrolysis, 2012. **96**(0): 100-109.

[144] Ibrahim, RHH, Darvell, LI, Jones, JM, and Williams, A, Physicochemical characterisation of torrefied biomass. Journal of Analytical and Applied Pyrolysis, 2013. **103**(0): 21-30.

[145] Phanphanich, M and Mani, S, Impact of torrefaction on the grindability and fuel characteristics of forest biomass. Bioresource Technology, 2011. **102**(2): 1246-1253.

[146] van der Stelt, MJC, Gerhauser, H, Kiel, JHA, and Ptasinski, KJ, Biomass upgrading by torrefaction for the production of biofuels: A review. Biomass and Bioenergy, 2011. **35**(9): 3748-3762.

[147] Keipi, T, Tolvanen, H, Kokko, L, and Raiko, R, The effect of torrefaction on chlorine content and heating value of eight woody biomass samples. Biomass and Bioenergy, 2014. **In press, available March 2014**.

[148] Xue, G, Kwapinska, M, Kwapinski, W, Czajka, KM, Kennedy, J, and Leahy, JJ, Impact of torrefaction on properties of Miscanthus x giganteus relevant to gasification. Fuel, 2014. **121**(0): 189-197.

[149] Agar, D and Wihersaari, M, Bio-coal, torrefied lignocellulosic resources – Key properties for its use in co-firing with fossil coal – Their status. Biomass and Bioenergy, 2012. **44**(0): 107-111.

[150] Li, J, Brzdekiewicz, A, Yang, W, and Blasiak, W, Co-firing based on biomass torrefaction in a pulverized coal boiler with aim of 100% fuel switching. Applied Energy, 2012. **99**(0): 344-354.

[151] Haykiri-Acma, H and Yaman, S, Effect of co-combustion on the burnout of lignite/biomass blends: A Turkish case study. Waste Management, 2008. **28**(11): 2077-2084.

[152] Sami, M, Annamalai, K, and Wooldridge, M, Co-firing of coal and biomass fuel blends. Progress in Energy and Combustion Science, 2001. **27**(2): 214.

[153] Colechin, M, Best practice brouchure: Co-firing of biomass, Department for Trade and Industry, Editor. 2005, The National Archives: Surrey.

[154] Di Nola, G, de Jong, W, and Spliethoff, H, The fate of main gaseous and nitrogen species during fast heating rate devolatilization of coal and

secondary fuels using a heated wire mesh reactor. Fuel Processing Technology, 2009. **90**(3): 388-395.

[155] Skreiberg, A, Skreiberg, Ø, Sandquist, J, and Sørum, L, TGA and macro-TGA characterisation of biomass fuels and fuel mixtures. Fuel, 2011. **90**(6): 2182-2197.

[156] Wang, Q, Zhao, W, Liu, H, Jia, C, and Xu, H, Reactivity and Kinetic Analysis of Biomass during Combustion. Energy Procedia, 2012. **17, Part A**(0): 869-875.

[157] Keown, DM, Hayashi, J-i, and Li, C-Z, Effects of volatile–char interactions on the volatilisation of alkali and alkaline earth metallic species during the pyrolysis of biomass. Fuel, 2008. **87**(7): 1187-1194.

[158] Di Blasi, C, Combustion and gasification rates of lignocellulosic chars. Progress in Energy and Combustion Science, 2009. **35**(2): 121-140.

[159] Li, S, Chen, X, Wang, L, Liu, A, and Yu, G, Co-pyrolysis behaviors of saw dust and Shenfu coal in drop tube furnace and fixed bed reactor. Bioresource Technology, 2013. **148**(0): 24-29.

[160] Lewellen, PC, Peters, WA, and Howard, JB, Cellulose pyrolysis kinetics and char formation mechanism. Symposium (International) on Combustion, 1977. **16**(1): 1471-1480.

[161] Palmer, KN, Dust explosions and fire. 1973, London: Chapman & Hall.

[162] Yan, B-H, Cao, C-X, Cheng, Y, Jin, Y, and Cheng, Y, Experimental investigation on coal devolatilization at high temperatures with different heating rates. Fuel, 2014. **117, Part B**(0): 1215-1222.

[163] Desypris, J, Murdoch, P, and Williams, A, Investigation of the flash pyrolysis of some coals. Fuel, 1982. **61**(9): 807-816.

[164] Krazinski, JL, Buckius, RO, and Krier, H, Coal dust flames: A review and development of a model for flame propagation. Progress in Energy and Combustion Science, 1979. **5**(1): 31-71.

[165] Tolvanen, H, Kokko, L, and Raiko, R, Fast pyrolysis of coal, peat, and torrefied wood: Mass loss study with a drop-tube reactor, particle geometry analysis, and kinetics modeling. Fuel, 2013. **111**(0): 148-156.

[166] Continillo, G, Crescitelli, S, Furno, E, Napolitano, F, and Russo, G, Coal dust explosions in a spherical bomb. Journal of Loss Prevention in the Process Industries, 1991. **4**: 223-229.

[167] Neoh, KG and Gannon, RE, Coal volatile yield and element partition in rapid pyrolysis. Fuel, 1984. **63**(10): 1347-1352.

[168] Di Benedetto, A and Russo, P, Thermo-kinetic modelling of dust explosions. Journal of Loss Prevention in the Process Industries, 2007. **20**(4-6): 303-309.

[169] Darvell, LI, Jones, JM, Gudka, B, Baxter, XC, Saddawi, A, Williams, A, and Malmgren, A, Combustion properties of some power station biomass fuels. Fuel, 2010. **89**(10): 90.

[170] Li, J, Bonvicini, G, Tognotti, L, Yang, W, and Blasiak, W, High-temperature rapid devolatilization of biomasses with varying degrees of torrefaction. Fuel, 2014. **122**(0): 261-269.

[171] Neves, D, Thunman, H, Matos, A, Tarelho, L, and Gómez-Barea, A, Characterization and prediction of biomass pyrolysis products. Progress in Energy and Combustion Science, 2011. **37**(5): 611-630.

[172] Granger, AF and Ladner, WR, The flash heating of pulverized coal. Fuel, 1970. **49**(1): 17-25.

[173] Biagini, E, Narducci, P, and Tognotti, L, Size and structural characterization of lignin-cellulosic fuels after the rapid devolatilization. Fuel, 2008. **87**(2): 177-186.

[174] Wornat, MJ, Hurt, RH, Yang, NYC, and Headley, TJ, Structural and compositional transformations of biomass chars during combustion. Combustion and Flame, 1995. **100**(1–2): 131-143.

[175] Lu, H, Ip, E, Scott, J, Foster, P, Vickers, M, and Baxter, LL, Effects of particle shape and size on devolatilization of biomass particle. Fuel, 2010. **89**(5): 1156-1168.

[176] Gil, MV, Casal, D, Pevida, C, Pis, JJ, and Rubiera, F, Thermal behaviour and kinetics of coal/biomass blends during co-combustion. Bioresource Technology, 2010. **101**(14): 5601-5608.

[177] Munir, S, Daood, SS, Nimmo, W, Cunliffe, AM, and Gibbs, BM, Thermal analysis and devolatilization kinetics of cotton stalk, sugar cane bagasse and shea meal under nitrogen and air atmospheres. Bioresource Technology, 2009. **100**(3): 1413-1418.

[178] Vamvuka, D and Sfakiotakis, S, Combustion behaviour of biomass fuels and their blends with lignite. Thermochimica Acta, 2011. **526**(1–2): 192-199.

[179] Tillman, DA, Duong, DNB, and Harding, NS, Chapter 4 - Blending Coal with Biomass: Cofiring Biomass with Coal, in Solid Fuel Blending, D.A. Tillman, D.N.B. Duong, and N.S. Harding, Editors. 2012, Butterworth-Heinemann: Boston. 125-200.

[180] Haykiri-Acma, H and Yaman, S, Synergy in devolatilization characteristics of lignite and hazelnut shell during co-pyrolysis. Fuel, 2007. **86**(3): 373-380.

[181] Lu, K-M, Lee, W-J, Chen, W-H, and Lin, T-C, Thermogravimetric analysis and kinetics of co-pyrolysis of raw/torrefied wood and coal blends. Applied Energy, 2013. **105**(0): 57-65.

[182] Goldfarb, JL and Liu, C, Impact of blend ratio on the co-firing of a commercial torrefied biomass and coal via analysis of oxidation kinetics. Bioresource Technology, 2013. **149**(0): 208-215.

[183] American Standard Test Method, ASTM E1226-12a Standard test method for explosibility of dust clouds. 2012, ASTM International: West Conshohocken, PA.

[184] Wilén, C and Rautalin, A. Safe handling of biomass fuels in IGCC power production. in 9th European Bioenergy Conference. 1996. Copenhagen.

[185] Iarossi, I, Amyotte, PR, Khan, FI, Marmo, L, Dastidar, AG, and Eckhoff, R, Explosibility of polyamide and polyester fibers, in IX International Symposium on Hazards, Prevention and Mitigation of Industrial Explosions. 2012: Cracow, Poland.

[186] Babrauskas, V, Ignition Handbook. 2003, Issaquah, USA: Fire Science Publishers.

[187] Sattar, H, Huescar Medina, C, Phylaktou, HN, Andrews, GE, and Gibbs, BM. Calibration of a 10L volume dust holding pot for the 1m3 standard vessel, for use in low bulk density biomass explosibility testing. in 7th International Seminar on Fire and Explosion Hazards. 2013. Providence, USA: Research publishing.

[188] Tobin, TW, Explosive and dangerous dusts. Journal of the Franklin Institute, 1882. **114**(6): 412-425.

[189] Brown, HH, Inflammability of carbonaceous dusts in air and in atmospheres of low oxygen content. Journal of the Franklin Institute, 1919. **187**(4): 504-506.

[190] Callé, S, Klaba, L, Thomas, D, Perrin, L, and Dufaud, O, Influence of the size distribution and concentration on wood dust explosion: Experiments and reaction modelling. Powder Technology, 2005. **157**(1–3): 144-148.

[191] Conde Lazaro, E and Garcia Torrent, J, Experimental research on explosibility at high initial pressure of combustible dusts. Journal of Loss Prevention in the Process Industries, 2000. **13**(0): 221-228.

[192] Melin, S, Determination of explosibility of dust layers in pellet manufacturing plants, in WPAC. 2012, Wood Pellet Association of Canada.

[193] Skjold, T, Arntzen, BJ, Hansen, OR, Taraldset, OJ, Storvik, IE, and Eckhoff, RK, Simulating dust explosions with the first version of DESC. Process Safety and Environment Protection, 2005. **83**(151-160).

[194] Sattar, H, Combustion and explosions of biomass, in School of Process, Environmental and Materials Engineering. 2013, University of Leeds: Leeds.

[195] Pilao, R, Ramalho, E, and Pinho, C, Influence of initial pressure on the explosibility of cork dust/air mixtures. Journal of Loss Prevention in the Process Industries, 2004. **17**(0): 87-96.

[196] British Standards Institution, BS EN 1839:2003 :Determination of explosion limits of gases and vapours. 2003, BSI: London.

[197] Kauffman, CW, Srinath, SR, and Tai, CS. Needs in dust explosion testing. in International Symposium on Explosion Hazard Classification of Vapors, Gases and Dusts. 1987: National Academy Press.

[198] Slatter, DJF, Huescar Medina, C, Sattar, H, Andrews, GE, Phylaktou, HN, and Gibbs, BM. The influence of particle size and volatile content on the reactivity of CH and CHO chemical and biomass dusts. in 7th International Seminar on Fire and Explosion Hazards. 2013. Providence, USA: Research Publishing.

[199] Polymeropoulos, CE, Flame propagation in aerosols of fuel droplets, fuel vapor and air. Combustion Science and Technology, 1984. **40**(0): 217-232.

[200] Huescar Medina, C, Phylaktou, HN, Andrews, GE, and Gibbs, BM, Determination of the minimum explosible and most reactive concentrations for pulverised biomass using a modified Hartmann apparatus, in IX International Symposium on Hazard, Prevention and Mitigation of Industrial Explosions. 2012: Cracow, Poland.

[201] Demirbaş, A, Calculation of higher heating values of biomass fuels. Fuel, 1997. **76**(5): 431-434.

[202] Frey, A, Das Brechungsvermögen der Zellulosefasern. Kolloidchemische Beihefte, 1927. **23**(1-9): 40.

[203] Speight, JG, The chemistry and technology of coal. 3rd ed. 2013, Boca Raton, Florida, USA: CRC Press Taylor and Francis Group.

[204] Webb, PA and Orr, C, Analytical methods in fine particle technology. 1997, Norcross, GA: Micrometrics Instrument Corporation.

[205] Braker, W and Mossman, AL, Matheson gas data book. 5th ed. 1971, East Rutherford, NJ: Matheson Gas Products.

[206] Phylaktou, HN and Andrews, GE, Gas explosions in linked vessels. Journal of Loss Prevention in the Process Industries, 1993. **6**(1): 15-19.

[207] Lewis, B and Von Elbe, G, Combustion, flames and explosions of gases. 1961, London: Academic Press.

[208] Zabetakis, MG, Flammability characteristics of combustible gases and vapors. 1965, Bureau of Mines: Washington DC.

[209] British Standards Institution, BS EN 15967:2011 Determination of maximum explosion pressure and the maximum rate of pressure rise of gases and vapours. 2011, BSI Standards Limited.

[210] American Society for Testing and Materials. E1515-07, Standard Test Method for Minimum Explosible Concentration of Combustible Dusts: West Conshohocken: ASTM, 2007.

[211] Brandes, E and Ural, EA. Towards a global standard for flammability determination. in Proceedings of the 42nd annual loss prevention symposium-Global safety congress. 2008. New Orleans: American Institute of Chemical Engineers.

[212] Zlochower, IA and Green, GM, The limiting oxygen concentration and flammability limits of gases and gas mixtures. Journal of Loss Prevention in the Process Industries, 2009. **22**(4): 499-505.

[213] Cashdollar, KL, Coal dust explosibility. Journal of Loss Prevention in the Process Industries, 1996. **9**: 65-76.

[214] Basu, P, Biomass gasification, pyrolysis and torrefaction: Practical design and theory. 2010, Amsterdam; London: Elsevier/Academic Press.

[215] Speight, JG, Handbook of coal analysis, ed. J.D. Winefordner. 2005, New Jersey: John Wiley & Sons.

[216] Hertzberg, M, Conti, RS, and Cashdollar, KL, Spark ignition energies for dust-air mixtures: Temperature and concentration dependences. Symposium (International) on Combustion, 1985. **20**(1): 1681-1690.

[217] Sattar, H, Andrews, G, Phylaktou, HN, and Gibbs, BM, Turbulent flame speeds and laminar burning velocities of dusts using the ISO 1m3 dust explosion method. Chemical Engineering Transactions, 2014. **36**(0): 157-162.

[218] Proust, C and Veyssiere, B, Fundamental Properties of Flames Propagating in Starch Dust-Air Mixtures. Combustion Science and Technology, 1988. **62**(4-6): 149-172.

[219] Basu, P, Combustion and gasification in fluidised beds. 2006, Boca Raton, FL: CRC Press Taylor & Francis Group.

[220] Kuprianov, VI and Tanetsakunvatana, V, Assessment of gaseous, PM and trace element emissions from a 300-MW lignite-fired boiler unit for various fuel qualities. Fuel, 2006. **85**(14–15): 2171-2179.

[221] Bartknecht, W and Kuhnen, G, Brenngas- und Staubexplosionen. Bundesinstitut für Arbeitsschutz. Forschungsbericht, F 45. 1971: Koblenz.

[222] Zanzi, R, Sjöström, K, and Björnbom, E, Rapid high-temperature pyrolysis of biomass in a free-fall reactor. Fuel, 1996. **75**(5): 545-550.

[223] Zulfiqar, M, Moghtaderi, B, and Wall, TF, Flow properties of biomass and coal blends. Fuel Processing Technology, 2006. **87**(4): 281-288.

[224] Moghtaderi, B, A study on the char burnout characteristics of coal and biomass blends. Fuel, 2007. **86**(15): 2431-2438.

[225] Zhou, L, Wang, Y, Huang, Q, and Cai, J, Thermogravimetric characteristics and kinetic of plastic and biomass blends co-pyrolysis. Fuel Processing Technology, 2006. **87**(11): 963-969.

[226] Meesri, C and Moghtaderi, B, Lack of synergetic effects in the pyrolytic characteristics of woody biomass/coal blends under low and high heating rate regimes. Biomass and Bioenergy, 2002. **23**(1): 55-66.

[227] Seo, MW, Goo, JH, Kim, SD, Lee, SH, and Choi, YC, Gasification Characteristics of Coal/Biomass Blend in a Dual Circulating Fluidized Bed Reactor. Energy & Fuels, 2010. **24**(5): 3108-3118.

[228] Zhang, L, Xu, S, Zhao, W, and Liu, S, Co-pyrolysis of biomass and coal in a free fall reactor. Fuel, 2007. **86**(3): 353-359.

[229] Delgado, R, Rosas, JG, Gómez, N, Martínez, O, Sanchez, ME, and Cara, J, Energy valorisation of crude glycerol and corn straw by means of slow co-pyrolysis: Production and characterisation of gas, char and bio-oil. Fuel, 2013. **112**(0): 31-37.

[230] Huey, SP, Davis, KA, Hurt, RH, and Wornat, MJ. Comparison of biomass and coal reactivities. in Biomass Fuels Symposium. 1995. Chicago, IL (USA).

[231] Smith, IW, The combustion rates of coal chars: A review. Symposium (International) on Combustion, 1982. **19**(1): 1045-1065.

[232] Gani, A and Naruse, I, Effect of cellulose and lignin content on pyrolysis and combustion characteristics for several types of biomass. Renewable Energy, 2007. **32**(4): 649-661.

[233] Bardon, MF and Fletcher, DE, Dust explosions. Science Progress, 1983. **68**(272): 459-473.

[234] Hertzberg, M, Cashdollar, KL, and Lazzara, CP, The limits of flammability of pulverized coals and other dusts. Symposium (International) on Combustion, 1981. **18**(1): 717-729.

[235] Rockwell, SR and Rangwala, AS, Modeling of dust air flames. Fire Safety Journal, 2013. **59**(0): 22-29.

[236] Woskoboenko, F, Explosibility of Victorian brown coal dust. Fuel, 1988. **67**(8): 1062-1068.

Appendix A

T_p [°C], t_r [min]	Untreated wood	A: 260, 8	B: 260, 25	C: 285, 16.5	D: 310, 8	E: 310, 25
Ash content %	0.23	0.3	0.4	0.4	0.4	0.7
Fixed carbon %	14.6	15.7	19.3	22.3	23.4	47.8
Volatiles %	85.4	84	80.3	77.3	76.2	51.5
C %	50.3	51.4	53.6	55.2	55.8	69.2
H %	6.2	5.9	5.9	5.6	5.8	5
O %	43.2	42.3	40	38.7	37.9	25
S %	<0.01	<0.01	<0.01	<0.01	<0.01	0.01
Cl %	<0.01	<0.01	<0.01	<0.01	<0.01	<0.01
N %	0.1	0.1	<0.1	0.1	0.1	0.1
Energy yield %	100	98.8	94.5	87.9	84.5	62.8
Mass yield %	100	97.1	89.2	80.3	76.5	45.9
HHV [MJ/kg]	20.3	20.6	21.5	22.2	22.4	27.8
LHV [MJ/kg]	19	19.4	20.2	21	21.1	26.7

Appendix B

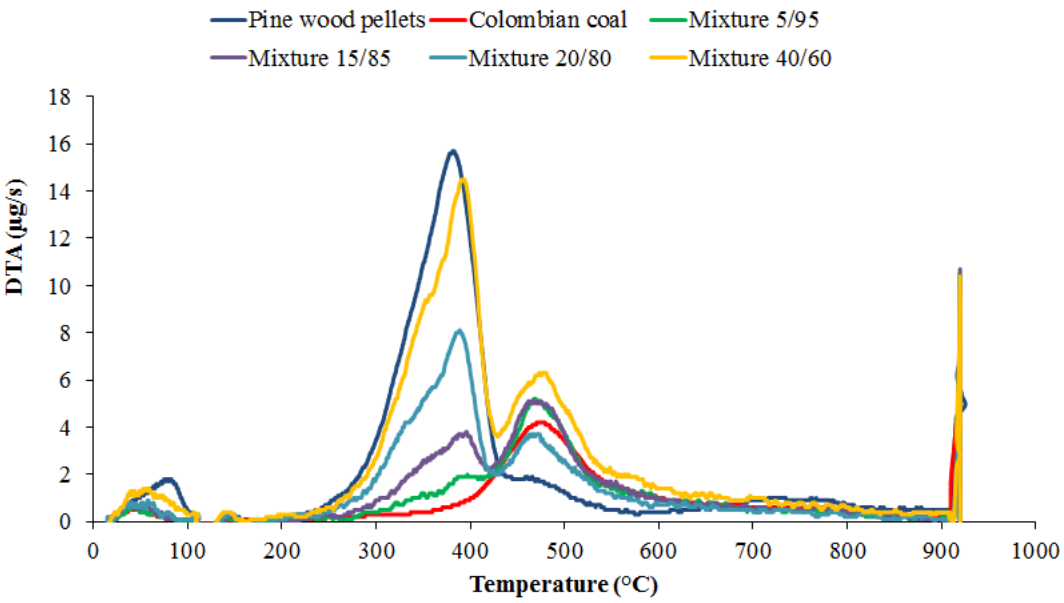
Pine wood pellets
Colombian coal
Mixture 5/95
Mixture 15/85
Mixture 20/80
Mixture 40/60
DTA (µg/s)
Temperature (°C)

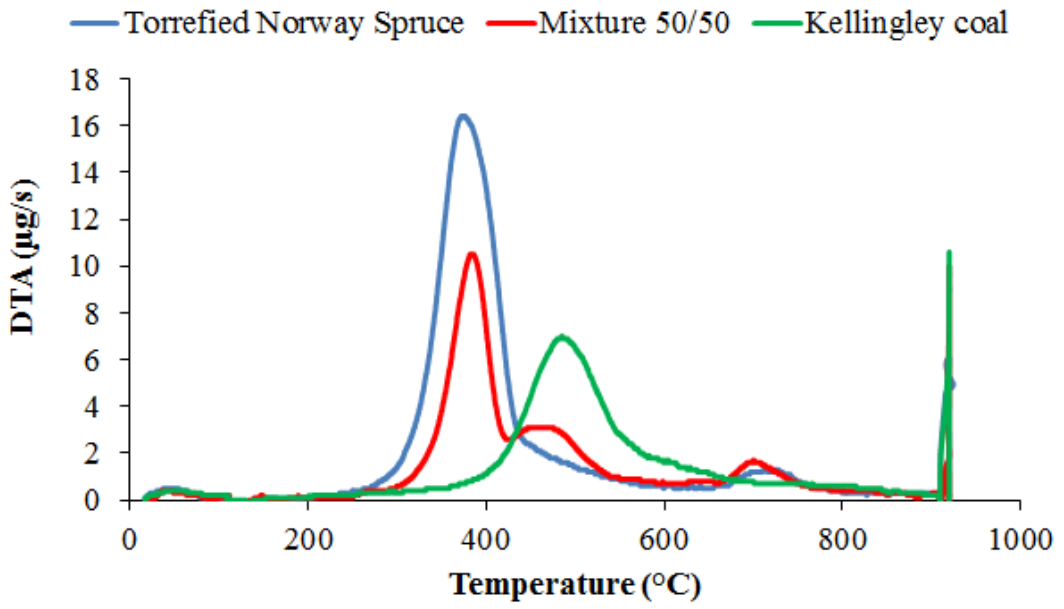
Torrefied Norway Spruce
Mixture 50/50
Kellingley coal
DTA (µg/s)
Temperature (°C)